Technical Report for
European Space Agency

# OPTIMISATION OF ROTATING, RANGE-GATED FANBEAM SCATTEROMETER FOR WIND RETRIEVAL

ESA CONTRACT NO. 14383/00/NL/DC

TASK 3B - REPORT

# Table of Contents

While preparing the final version of the accompanying Task-3a Report, a bug was discovered in the routine that was used to compute the quality index for a single node.

This bug has been corrected in the software delivered to ESA. However, all figures of this Task-3b Report are affected by this failure. Extensive tests have shown that the FoM, which is used as a measure of the instrument performance (Chapter 2.1), did not change significantly.

Details on this bug and its impact on the computation of the FoM are provided in the Task-3a Report.

# 1. Introduction

## 1.1. Scope

This document summarizes the results of the end-to-end performance evaluation of various instrumental settings for the rotating range-gated fanbeam scatterometer (RFSCAT). The goal of this evaluation is to compare different systems in order to study the impact of system parameters on the wind retrieval performance and to establish a way towards an optimized wind scatterometer on the basis of the rotating fanbeam concept.

The evaluation of the wind retrieval performance makes use of the concept of a figure of merit (FoM) which has been developed within this study. The details on this concept and on the wind retrieval in general are given in the Task 3a Report. All details of the computations of the measurement geometry and measurement error within the Pseudo-Level-1b-Generator were reported in the Task-2b Report. Descriptions of the various geophysical model functions (GMF) which relate the radar measurements including the measurement geometry to ocean surface winds were summarized in the Task-1 Report.

## 1.2. Structure of this Document

Section 1 summarizes briefly the background and principle idea of the rotating fanbeam scatterometer concept which is the basis of this study. In Section 2, the objectives of the simulations are provided together with the results of an impact evaluation for few general parameters which are important for all system simulations done later. A validation of the simulator has been performed, the details are provided in Section 3. All simulations are described in Section 4 while their results are summarized in Section 5. Conclusions and recommendations are given in Section 6.

## 1.3. Instrument Concept

The instrument being subject to this study is a spaceborne rotating range-gated fanbeam scatterometer on a polar orbiting platform. It will be addressed as RFSCAT in the rest of the document. The measurement geometry for RFSCAT is shown in Figure 1.

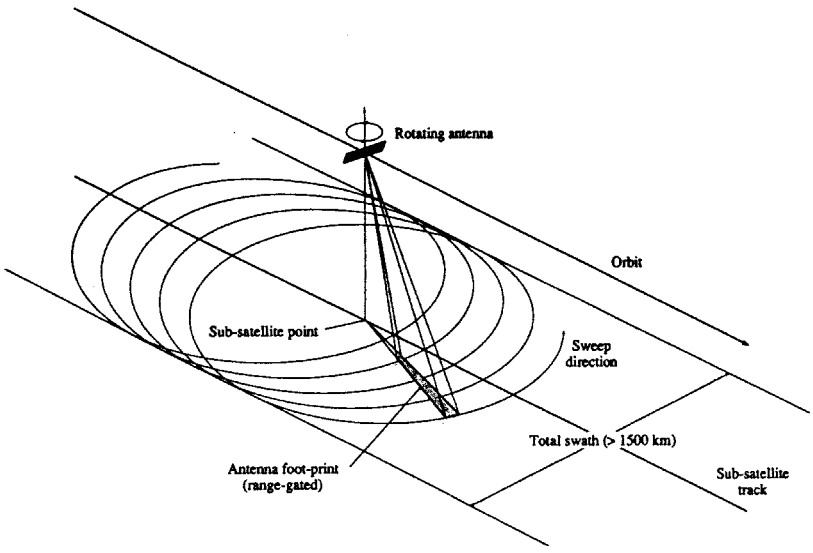


*Figure 1: Rotating fanbeam scatterometer concept*

In a basic configuration, the orbit height is 725 km and the antenna rotates at a rate of 0.35 rad/s while the satellite travels with a velocity of 7.49km/s. This results in an epicyclical footprint on the Earth's surface with a total swath width of 1500 km. The incidence angle varies from $28^0$ to $51^0$ within the fanbeam. The radar operates at C-band (5.3 GHz) and VV-polarization. Further options include a Ku-band channel (13.4 GHz) as well as horizontal polarization and the capability of polarimetric measurements. The radar operates in a pulsed mode and uses pulse compression in order to achieve the required spatial resolution in range direction. In azimuth direction, the spatial resolution is determined by the beam width of the antenna which requires a relatively large aperture. The instrument parameters of two options considered by ESA are listed in Table 1. The simulator allows to vary all the listed parameters within reasonable ranges.

| Parameter | Option 1 | Option 2 |
|---|---|---|
| Orbit / repeat cycle | 725 km / 2 day | 1075 km/2 days |
| Antenna scan rate | 0.35 rad/s (3.3 rpm) | 0.25 rad/s (2.4 rpm) |
| Swath width | 1500 km | 1600 km |
| Minimum wind speed | ≤ 4 m/s cross-wind | ≤ 4 m/s cross-wind |
| Incidence angle | $28^0$ - $51^0$ | $21^0$ – $42.5^0$ |
| Footprint length | 408.6 km | 450.5 km |
| Frequency | 5.3 GHz | 5.3 GHz |
| Polarization | VV | VV |
| Pulse bandwidth | 1.06 MHz | 1.39 MHz |
| Pulse compression ratio | 200 | 200 |
| PRF | 239 Hz | 179 |
| N range | 50 (HR) | 50 (HR) |
| N azimuth | 13.7 (HR) | 13.4 (HR) |
| Spatial resolution | 15 km × 15 km (HR)<br>50 km x 50 km (wind) | 15km x 15 km (HR)<br>50 km x 50 km (wind) |
| Radiometric resolution | ≤ 0.3 dB (HR)<br>≤ 0.09 dB (wind) | ≤ 0.3 dB (HR)<br>≤ 0.11 dB (wind) |
| Average RF power | 145 W | 83 W |
| Antenna size | 3.6 m × 0.4 m | 4.6 m x 0.4 m |

*Table 1: Parameter sets for RFSCAT Option 1 and Option 2*

The antenna dimensions indicated above are those from the previous study (Lin et al.,2000). However, ASCAT mid-beam antenna with a size of 2251 mm x 337 mm was used in the present simulation study.

### *1.4. Antenna Concepts*

In the standard RFSCAT configuration, a single, fanbeam, vertically polarized antenna is being used. More advanced concepts allow to combine measurements obtained at vertical and horizontal polarizations which further includes the capability of polarimetric measurements. It is expected that this will significantly improve the wind retrieval. Therefore, the following scenarios will be evaluated:

- Option A: either VV or HH, one beam
- Option B: alternating pulses HH and VV, one beam (the overall PRF is the same as for Option A).
- Option C: two beams with $180^0$ different azimuth look angle, one beam VV the other HH.
- Option D: dual beams, one for near swath, one for far swath.
- Option E: polarimetric measurements. In this option two scenarios are possible.
  First a semi-polarimetric mode in which only one transmitter sends a vertically polarized signal which is detected simultaneously by two separate receivers being vertically and horizontally polarized. Second, a fully polarimetric mode in which the transmitter also alternately uses both polarizations.

The rationale for Option D is that Option A produces many measurements with similar look-angles for regions in the middle of the right and left hand part of the swath. Thus Option D is supposed to reduce redundant information from this region and to allow at the same time better adaptation of the antenna to near and far swath geometry. The different antenna configurations are depicted in Figure 2.

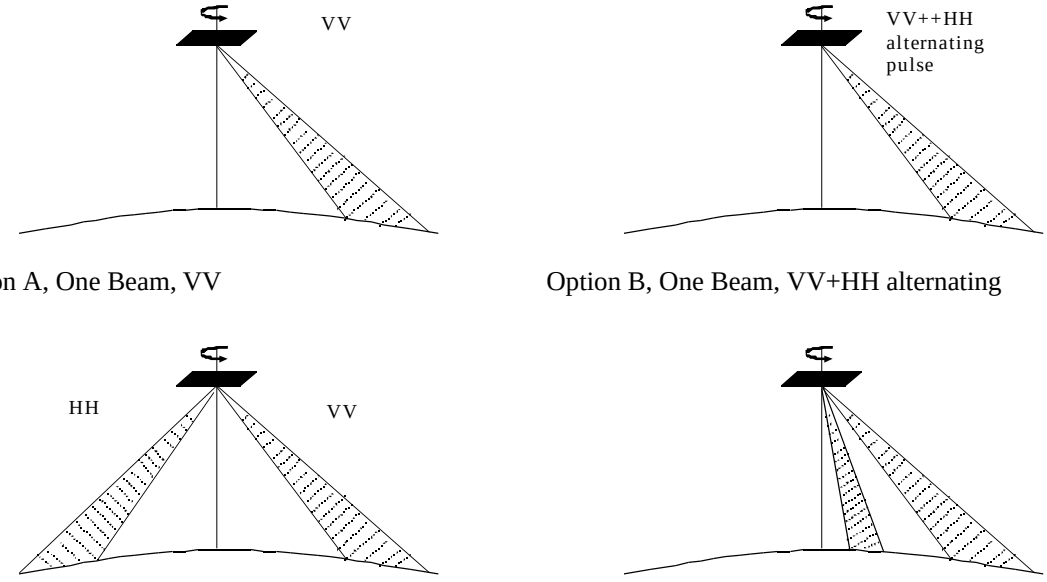


Option A, One Beam, VV

Option B, One Beam, VV+HH alternating

Option C, Two Beams, one VV one HH

Option D, Two Beams, One Near Swath, one far Swath

*Figure 2: Drawings of possible antenna beam modes for RFSCAT instruments.*

# 2. Simulation Considerations

The objective of this study is an end-to-end performance analysis of wind field retrieval based on the RFSCAT concept. In the simulation, an input wind field is being *observed* by various RFSCAT systems, which are defined by a set of radar system and processing parameters. The radar *measurements* including various errors and noise estimates are then used in a wind retrieval in order to compute the corresponding *measured* wind field. This retrieved wind field is being compared to the input wind field. Due to the ambiguous nature of the wind retrieval which typically provides more than one solution, a one-to-one comparison of input and output wind fields is not possible. In order to account for the ambiguities in the retrieved wind field and to take the ranking of solutions into consideration, the concept of the Figure-of-Merit (FoM) was developed for judging on the wind retrieval performance. Details on the FoM are provided in the Task-3a Report.

## *2.1. Application of the Figure of Merit Concept*

The wind retrieval performance of different realizations of RFSCAT instruments depends on the employed radar frequency and polarizations and thus on the respective GMF as well as on the measurement geometry. The latter varies considerably across the swath of the instrument. Therefore, the concept of the FoM was applied as follows: For each node across the swath, the FoM was computed from the data along one orbit resulting in a curve for the quality index as a function of node number. Node number denotes the coordinate of a resolution cell perpendicular to the satellite ground track. It counts from the left towards the right edge of the instrument swath. The quality index is computed as 1.0 minus the FoM as defined in Task 3a report. An example is depicted in Figure 3 for the reference system, which will be described later. The quality index is nearly symmetric around the center of the swath which is marked by the vertical line in the plot. The slight asymmetry is caused by different sampling on the right and left side of the swath caused by different ground speeds of the footprint. The FoM for an instrument is defined as the mean value of the quality index across the entire instrument swath. This mean value is indicated by the horizontal line in Figure 3 and is the metric being used for comparing various RFSCAT systems.

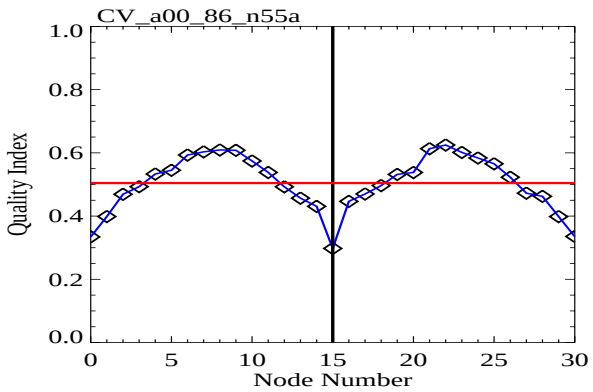


*Figure 3: Example of a quality index curve across the RFSCAT swath. The vertical line marks the centre of the swath below the satellite track. The horizontal line is the mean of the quality index across the swath and represents the figure of merit (FoM) used in all further graphs.*

### 2.2. Reference Wind Field

The reference wind field which is being used as the *target* for the radar *measurements* in the simulations should reflect the climatological behavior of the Earth's wind field, but also should allow to cover statistically all possible wind speeds and wind directions within a limited number of orbits. Details on the wind field are given in the Task-2a and Task-3a reports. The reference wind field has normal distributions for both u- and v-component with a width of 5.5 m/s. Typically one orbit is used which comprises approximately 25000 wind vector cells for a 1500 km wide swath with 50 km spatial resolution. Simulations were done for the reference system in order to check the impact of the number of wind vector cells on the analysis. Figure 4 depicts a comparison for satellite track lengths of 0.5, 1, and 3 orbits. The resulting FoM show no dependence on track length, however the graph for 0.5 orbit indicate slightly more small-scale variability across the swath due to poorer statistical coverage. In the subsequent simulations one orbit of data was used.

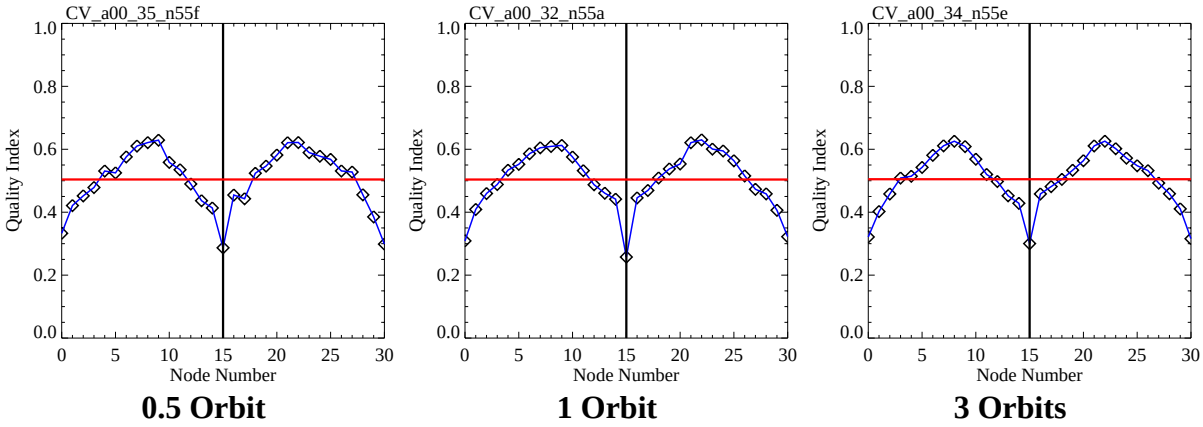


*Figure 4: Quality index curves for the reference system for different satellite track lengths of 0.5, 1, and 3 orbits. The number of wind vector cells are 12617, 25048, and 75702, while the resulting FoM are 0.50392, 0.50379, and 0.50482, respectively.*

### *2.3. Baseline Instrument*

A baseline, reference radar concept has been defined which allows a direct comparison with existing (ERS-AMI, SeaWinds) or soon to be flown instruments (ASCAT). As an antenna the mid-beam antenna of ASCAT was selected. Sufficient power in order to meet a signal to noise (SNR) for 4 m/s cross wind at high incidence angles will be provided by a traveling wave tube being also used on ERS which is capable to provide 5 KW radio frequency (RF) peak power. Further instrument settings of the reference system are given in Table 2 while the antenna pattern is shown in Figure 5.

| | |
|---|---|
| Radar Band: | C |
| Polarization: | VV |
| Antenna Pattern: | ASCAT mid-beam |
| Antenna Size (azi. / elev.): | 2251 mm / 337 mm |
| Scan Rate: | 3.3 rpm |
| PRF: | 239 Hz |
| Pulse Power: | 5 KW |
| Bandwidth: | 1 MHz |
| Pulse Duration: | 200 µs |
| Average RF Power: | 239 W |
| Resolution: | 50 Km |
| Swath Width: | 1500 Km |
| Orbit Height: | 725 Km |

*Table 2: Parameter set for the RFSCAT baseline (reference) instrument*

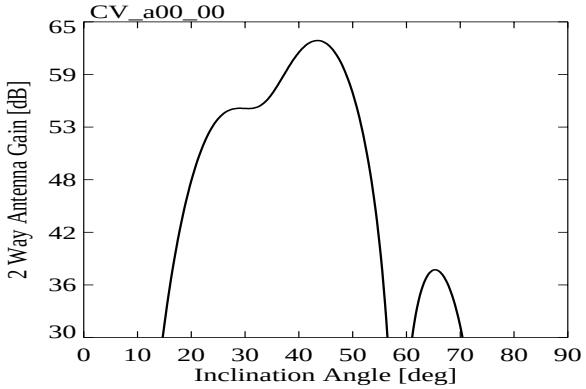


*Figure 5: Two way antenna pattern of the baseline instrument derived from the ASCAT mid-beam antenna.*

### 2.4. Simulator Runtime Optimization

The *Pseudolevel-1b-generator* requires considerable computation time which is about 9 hours for one orbit at 1500 km swath width on a present state-of-the-art PC. However it is possible to run the L1b-generator with poorer statistics but with a considerable gain in computation time. Two parameters are at disposal within the list of processing parameters for skipping computations of range bins (Range_Skip) and of pulses (Pulse_Skip). Internally, these loops need most of the computation time. The impact of these parameters on the results of the RFSCAT simulator was studied by simulating the baseline instrument with various settings of Range_Skip and Pulse_Skip. Neither from the graphs shown in Figure 6 (and those in the Annex) nor from the values of the FoM given in Table 3, it can be delineated that the poorer statistics within noise estimate provided by the L1b-generator has a considerable impact in the overall performance of the simulation. Thus in the following simulations, a Range_Skip and a Pulse_Skip of 10 was used. Table 4 indicates the gain in computation time when employing these parameters.

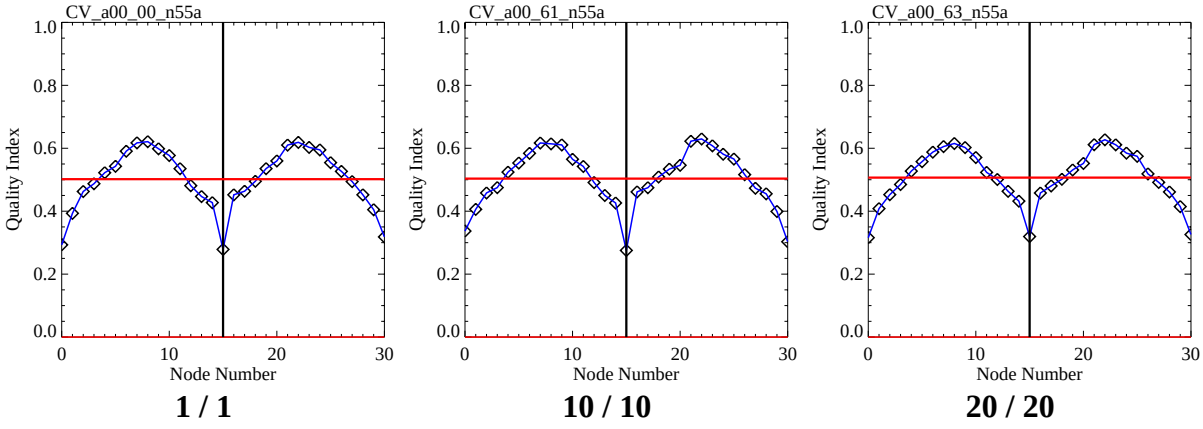


*Figure 6: Quality index curves for baseline instrument simulations with different settings for Range (first number) and Pulse Skip (second number), respectively. Further graphs are given in Annex A.*

| FoM | | Pulse Skip | | | | |
|---|---|---|---|---|---|---|
| | | 1 | 5 | 10 | 15 | 20 |
| Range Skip | 1 | 0.50183 | 0.50553 | 0.50531 | 0.50463 | 0.50720 |
| | 5 | 0.50415 | 0.50408 | | | |
| | 10 | 0.50289 | | 0.50347 | | 0.50434 |
| | 15 | 0.50350 | | | 0.50305 | |
| | 20 | 0.50302 | | 0.50119 | | 0.50679 |

*Table 3: Summary of derived FoM from simulations of the baseline system with various settings for Range Skip and Pulse Skip factors*

| Computation Time [min] | | Pulse Skip | | | | |
|---|---|---|---|---|---|---|
| | | 1 | 5 | 10 | 15 | 20 |
| Range Skip | 1 | 560 | 114 | 58 | 40 | 30 |
| | 5 | 114 | 58 | | | |
| | 10 | 58 | | 8 | | 6 |
| | 15 | 40 | | | 5 | |
| | 20 | 30 | | 6 | | 3 |

*Table 4: The computation time for simulations of one orbit of the baseline system for different settings of Range Skip and Pulse Skip (Values for a PC equipped with 1.5 GHz AMD processor).*

### 2.5. Impact of SNR on Retrieval Performance

The wind retrieval performance depends on the signal to noise ratio for the NRCS estimates. In the course of designing an instrument, an optimum SNR across the entire swath and for the wide range of wind speeds and directions has to be found. However, ambiguities in the wind retrieval due to the shape of the GMF will limit additionally the wind retrieval performance. Instead of varying the entire set of instrument parameters affecting the SNR of the instrument, e. g., antenna peak gain, bandwidths, pulse peak power, only the transmitted peak power has been varied as a representative measure of the SNR while all others were kept constant. This may lead to unreasonable high power values for pulse peak power, but considering the potential in other design parameters, these powers do not indicate an unrealistic instrument design. The SNR of the baseline system has been varied by increasing the transmitted peak power from 300 mW to 10 MW in steps of 3 dB in order to study the impact of the SNR on wind retrieval performance. Figure 7 depicts the evolution of the FoM with increasing pulse peak power. Further graphs are provided in Annex B.

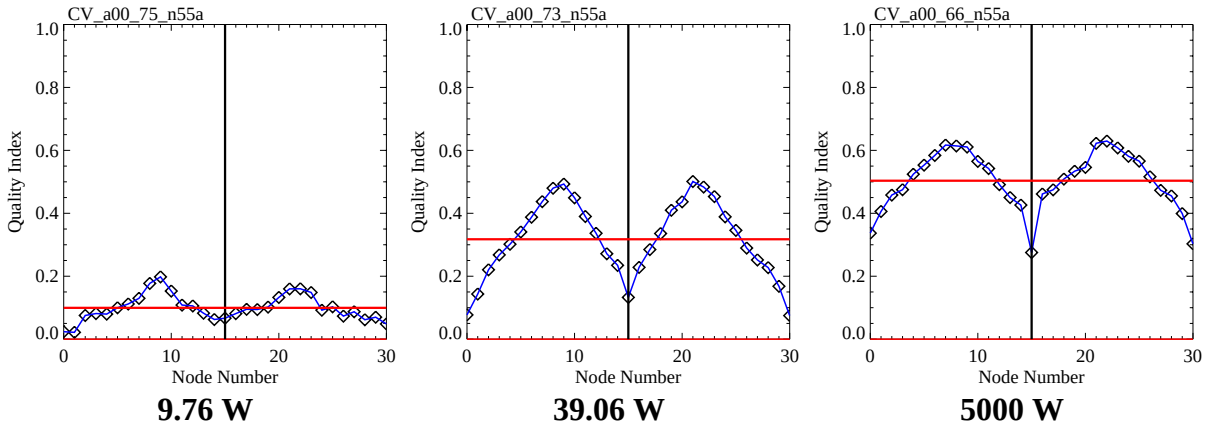


*Figure 7: Quality index curves as a function of transmitted power. The full set of graphs is shown in Annex B.*

The dependence of the FoM on pulse peak power (representing the SNR) is summarized in Figure 8. The quality of the retrieval increases significantly with SNR until a certain value and then reaches a saturation level. From this point on the FoM is entirely controlled by the inherent error of the wind retrieval method, which includes the corresponding geophysical model function (GMF) as well as the employed retrieval technique. From the technical and instrumental point of view, one would not want to operate the instrument in the region of the steep increase in FoM, but there is also no need for further improving the scatterometer beyond the point at which the FoM curves becomes saturated.

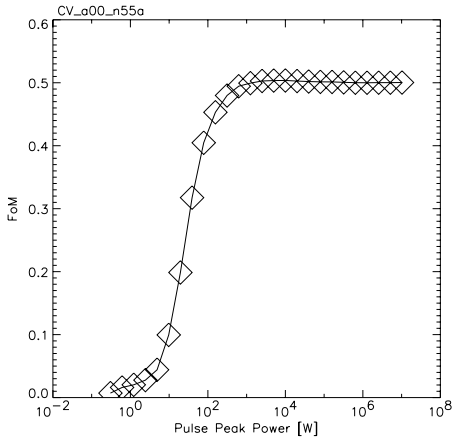


*Figure 8: FoM as a function of pulse peak power*

### *2.6. Impact of the Antenna Scan Rate on Retrieval Performance*

Beside the SNR of the instrument the "azimuthal sampling" of the NRCS measurements is affecting the wind retrieval performance. This sampling is being controlled by the antenna scan rate which directly influences the number of views per resolution cell (see Figure 9), and also has an impact on the measurement geometry for each node. For the baseline system with spatial resolution of 25 km and 50 km and various settings of pulse peak power, the antenna scan rate has been varied from 0.3 rpm to 17 rpm. Figure 10 depicts the evolution of the FoM with increasing antenna scan rate (further graphs are provided in Annex C). Especially at low scan rates the asymmetry between the left and right portion of the swath is obvious. This is caused by different sampling of the views due to the different effective ground speed of the footprint. Figure 11 summarizes the dependence of the FoM on antenna scan rate as a function of pulse peak power and spatial resolution.

In the case of sufficient radar power the radiometric properties do not affect the quality of the wind retrieval. Like for the SNR the FoM increases with scan rate due to the increased number of views for the wind retrieval and improved azimuthal separation between views. For scan rates higher than approximately 3 rpm only very little information is being added and "oversampling" starts. From the respective graphs of the quality index as a function of node, it can be seen that the further slight improvement is found only around the center of the swath. This indicates the impact of additional measurements at different incidence angles.

For lower pulse peak power a complex dependence of the FoM on kp, number of samples per view and views per node can be seen. Not only that the better spatial resolution of 25 km degrades the FoM as compared to the 50 km resolution instrument, also the reduced number of views at higher scan rates additionally reduces the quality of the wind retrieval.

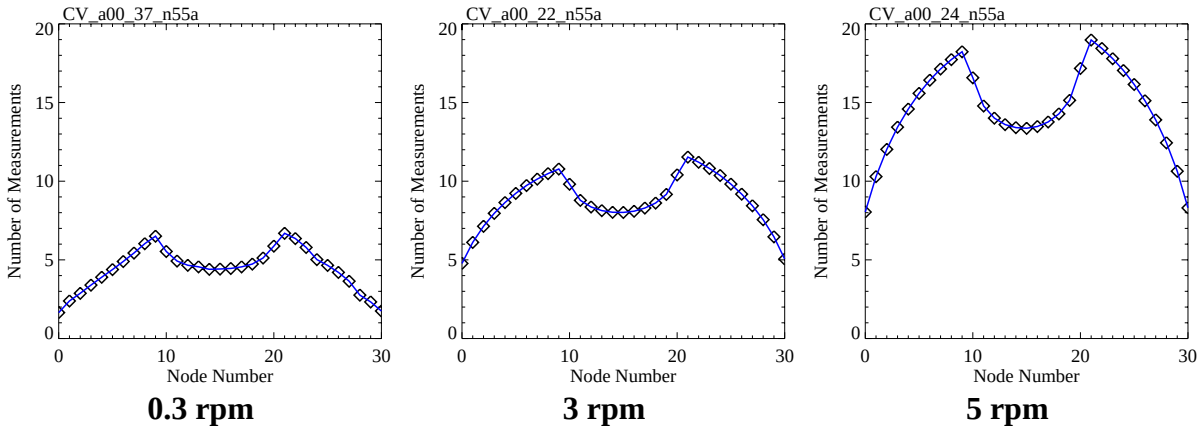


*Figure 9: Number of views (measurements) across the swath for various antenna scan rates. The instrument resolution is 50 km. Further graphs are given in Annex C.*

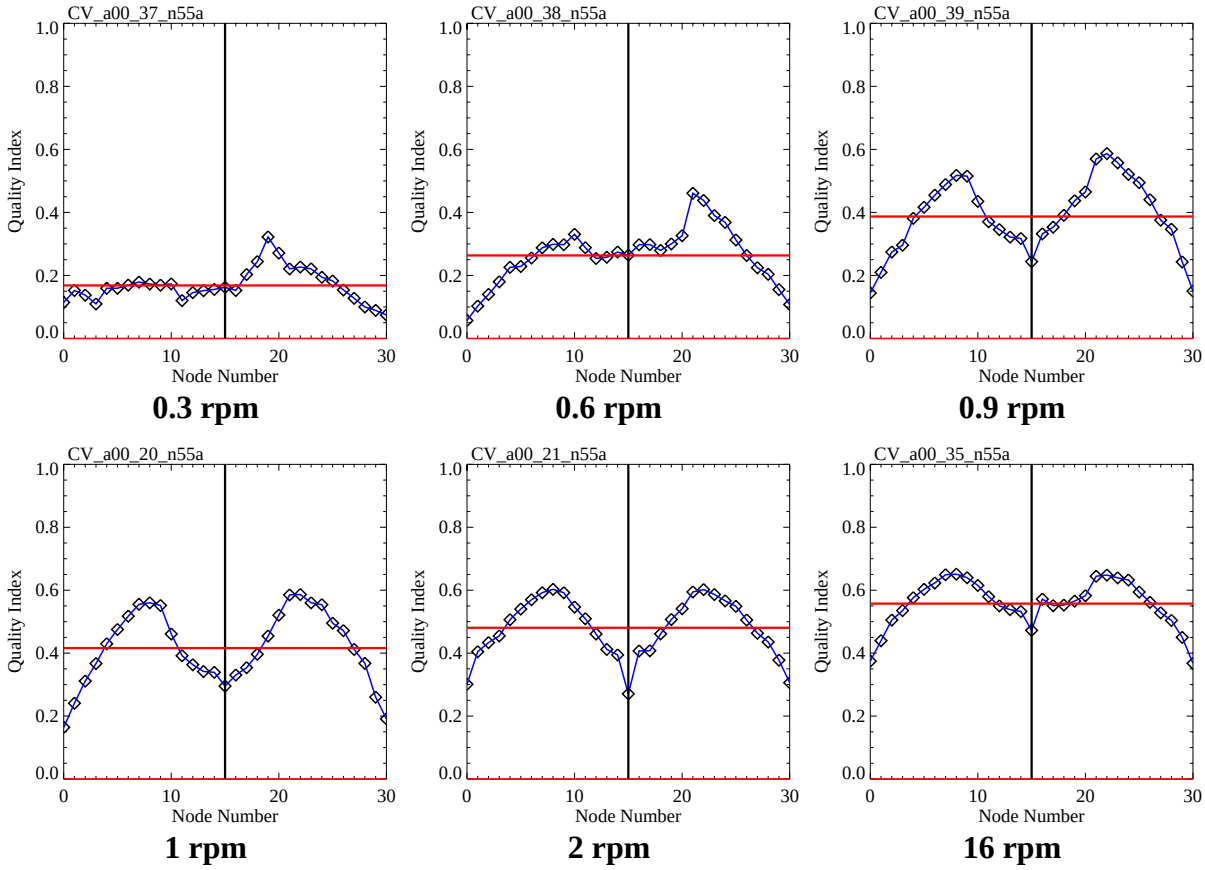


*Figure 10: Quality index curves as a function of antenna scan rate. The instrument resolution is 50 km. The full set of graphs is shown in Annex C.*

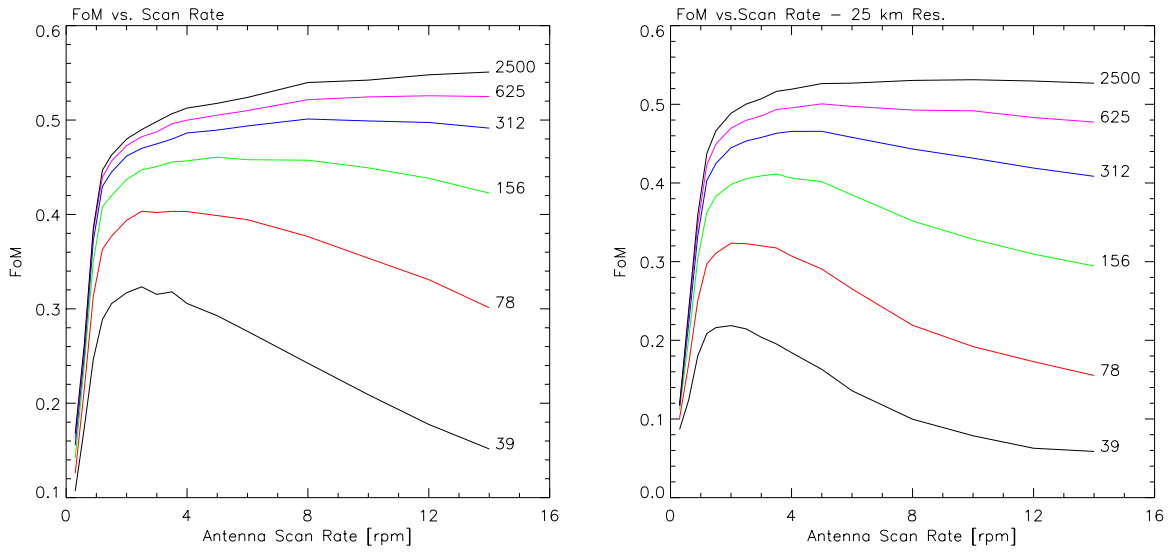


*Figure 11: FoM for the baseline instrument with 50 km and 25 km resolution as a function of antenna scan rate and pulse peak power (indicated in Watts at the curves).*

# 3. Simulator Validation

The simulation results for the general considerations in Section 2 indicate already that the simulator produces consistent results. As a validation of the simulator, existing windscatterometers were simulated and these result were compared to FoM obtained from wind measurements performed by the respective instruments.

## *3.1. Simulation of ERS and ASCAT*

For simplicity, the scatterometer mode of the Active Microwave Instrument (AMI) aboard ERS-1 and ERS-2 will be addressed as ERS in the following. ERS and ASCAT were simulated based on their technical parameters and their performance was evaluated. Only the right swath of ASCAT was considered because the left swath is symmetric with respect to the satellite ground track and is expected to perform equally. The RFSCAT simulator does not directly allow to include the antenna geometry of ERS and ASCAT. Therefore, the simulator was run three times with a non-rotating antenna fixed at the respective azimuth angles for fore-, mid-, and aft-beam while accounting for their different transmit/receive timings and antenna patterns. These three simulations were then combined to one data set for further evaluation. The simulation parameters for ERS and ASCAT are summarized in Table 5.

| **Instrument** | **ERS** | | **ASCAT** | |
|---|---|---|---|---|
| **Beam** | **mid** | **fore/aft** | **mid** | **fore/aft** |
| **Orbit** | 782 km | | 835 | |
| **Incidence** | 18-47 deg | 25-59 deg | 25-53 deg | 33-64 deg |
| **Peak Power** | 4.8 KW | | 120 W | |
| **PRF / per beam** | 32 Hz | | 28 Hz | |
| **Pulse duration** | 70 µs | 130 µs | 5.4 ms | 7.7 ms |
| **Average RF Power** | 50 W | | 34 W | |
| **System Bandwidth** | 100 KHz | | 1 MHz | |

*Table 5: Simulation parameters for ERS-AMI and ASCAT. Since ASCAT can be considered as an interrupted CW-FM system, the receiver integration time has been used instead of the transmitted pulse length.*

Although no data are available for ASCAT this system has been simulated as well for two reasons. First to check the consistency of the simulator - ERS differs significantly from ASCAT but for a portion of their swaths the measurement geometry is very similar. Consequently, the performance in this region should be similar as well. Second, the expected performance of ASCAT will be a reference for judging on the performance of the evaluated RFSCAT systems.

Figure 12 depicts the results of the simulation of ERS and ASCAT. For ASCAT only the right hand swath is shown. Although the system are quite different their results agree very well. Furthermore, real measurements of the ERS scatterometer are included in red color. These data were obtained between February 6 and 17, 1996, over an area which is extends from 30.65 to 50.00 degrees North and from 41.42 degrees West to 25.52 degrees East. The significant discrepancy between the simulation and these data points is caused by the error in the knowledge of the reference wind field. When simulating ERS and ASCAT with the RFSCAT simulator the reference wind field is well know, while for the real-world ERS data the quality index curve is based on a reference wind field from a numerical weather prediction model. The error of this model is of the order 1.5 m/s for the wind components and has to be considered in the simulation as well. When accounting for this error in the reference wind field the result of the simulation (red line in Figure 12) agrees very well with the ERS measurements. Further details on the ERS measurements and the error statistics of the reference wind field are provided in the Task-3a Report.

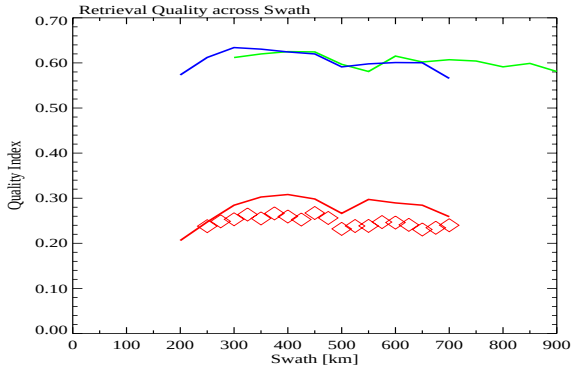


*Figure 12: Theoretical quality index curves as a function swath position for ERS (blue) and ASCAT (green). For ASCAT only the right hand swath is depicted. The red data points indicate ERS scatterometer measurements and the red line their simulation accounting for the error of the reference wind field.*

### *3.2. Simulation of SeaWinds*

The second instrument for validating the simulator software is the SeaWinds instrument aboard QuikSCAT. QuikSCAT measurements have been collected globally between February 2, 2002, 00:00 hrs and February 4, 2002, 24:00 hrs and were processed to 100 km spatial resolution. The outer cells of the swath which are known to provide winds of poor quality were excluded. In this case the error of the reference wind field was about 0.9 m/s for each wind component which is lower than for the simulation of ERS data. The details on the SeaWinds data as well as on the reference wind field are provided in the Task-3a Report. The simulation was also done at 100 km spatial resolution for the entire 1800 km swath and is based on the technical parameters of the SeaWinds instrument (see Table 6 and 7).

| | | | |
|---|---|---|---|
| Radar Frequency: | 13.4 GHz | Average RF Power | 30 W |
| Scan Rate: | 18 rpm | Resolution: | 50 Km |
| PRF / channel: | 92.5 Hz | Swath Width: | 1800 Km |
| Pulse Peak Power: | 110 W | Orbit Height: | 803 Km |
| Pulse Duration | 1.5 ms | Inclination: | 98.616 deg |

Table 6**:** Parameter set for the SeaWinds instrument (Lungu, 2001)

| | Inner beam | Outer beam |
|---|---|---|
| Polarization: | H | V |
| Elevation angle: | 40 ° | 46° |
| Incidence angle: | 46° | 52° |
| 3 dB beam width azi. / el. | 1.8° / 1.6° | 1.7° / 1.4° |
| Peak gain: | 38.5 dBi | 39 dBi |

Table 7**:** SeaWinds antenna parameter. The antenna pattern are plotted in Figure 13 (Spencer et al. 2000).

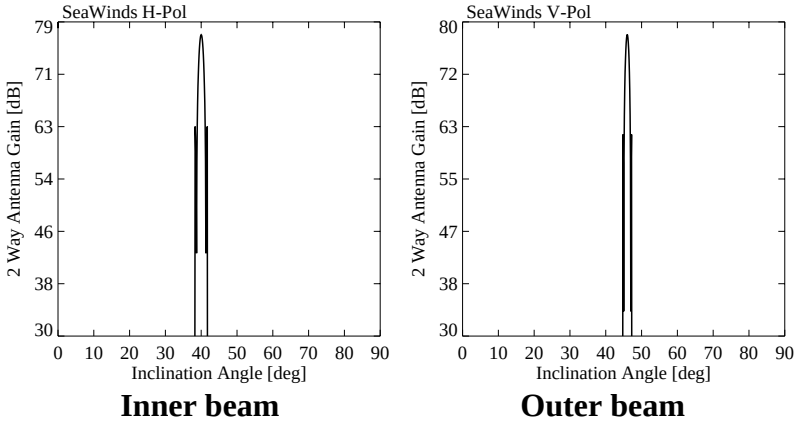


*Figure 13: Antenna pattern used in the SeaWinds simulation.*

The result of the simulation together with the measured data is shown in Figure 14. Except for the center node thee is a very good agreement between data and simulation.

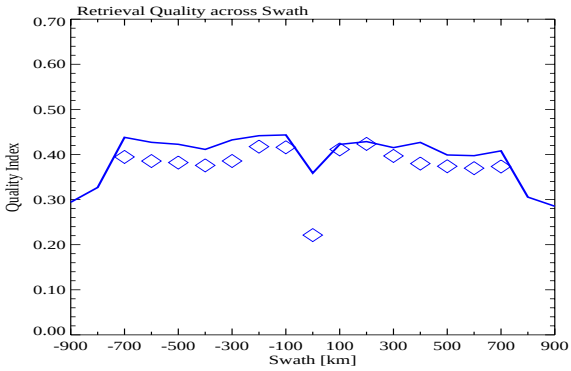


*Figure 14: Quality index across the SeaWinds swath. For comparison, data from an analysis of SeaWinds data are included.*

# 4. RFSCAT Simulations

This section provides an overview on the systems which have been analysed using the RFSCAT simulator. For each system, the pulse peak power has been varied over a wide range in order to find the optimum point of operation for each system. This point will be used at a later stage for the system comparison. In each sub-section, example plots are shown for the FoM vs node number and in summary the FoM vs average RF power. The full set of graphs for each set of simulations is provided in the corresponding annexes.

The baseline system has been described in the previous sections and as a reference, its performance curve is includes in those of the other systems. Therefore, the reference system is not further described in this section. The first step in improving the system is adding a HH polarized channel. This could be done either with a dual polarized antenna and alternating pulses (Option B in Figure 2) or by adding a second antenna (Option C in Figure 2). The performance of this system has been evaluated also for high (25 km) resolution mode as well as for a wide swath (1800 km) instrument. For the later, the antenna was tilted mechanically in its elevation plane by 4 degrees towards larger incidence angles. The Option D (see Figure 2) with a two (split) beam antenna was studied only for the normal orbit and 1500 km swath. The next step in complexity for improving the system is the operation in a polarimetric mode. This is a technically demanding solution since the signal level at cross-polarization is approximately 15 dB lower than at like-polarization, and it will be necessary to achieve a high isolation between the V- and H-channels even through a common rotary joint. However, it is not the purpose of the study to judge on these technical aspects. The above mentioned settings were repeated for the polarimetric system. The final step in complexity, although technically less challenging than the polarimetric capability, is the addition of an Ku-band channel.

The following table gives an overview on the simulated systems:

| Name | Antenna | Orbit [km] | Swath [km] | Resolution [km] | PRF [Hz] | Remarks |
|---|---|---|---|---|---|---|
| **cv** | ASCAT | 725 | 1500 | 50 | 239 | Baseline system |
| **cvch1** | ASCAT | 725 | 1500 | 50 | 119 | Dual-Pol. C-Band |
| **cvcp3** | ASCAT | 725 | 1500 | 25 | 239 | High Resolution |
| **cvcp4** | ASCAT-4 | 725 | 1800 | 50 | 228 | Wide Swath |
| **cvch6** | ASCAT-4 | 725 | 1800 | 25 | 228 | Wide Swath & High Resolution |
| **cvfp6** | ASCAT-4 | 725 | 1800 | 25 | 228 | Polarimetric Wide Swath & High Res. |
| **cvch2** | Split-Beam | 725 | 1500 | 50 | 119 | Split Beam Antenna |
| **cvcp5** | ASCAT-6 | 1075 | 1800 | 50 | | High Orbit |
| **cvcp1** | ASCAT | 725 | 1500 | 50 | 239 | Polarimetric |
| **cvcp2** | Split-Beam | 725 | 1500 | 50 | 239 | Polarimetric Split Beam |
| **kv** | ASCAT | 725 | 1500 | 50 | 239 | Ku-Band |
| **kvkh1** | ASCAT | 725 | 1500 | 50 | 119 | Dual-Pol. Ku-Band |
| **cvkv** | ASCAT | 725 | 1500 | 50 | 239 | Two Radar Frequencies |

*Table 8: Summary of the simulated systems.*

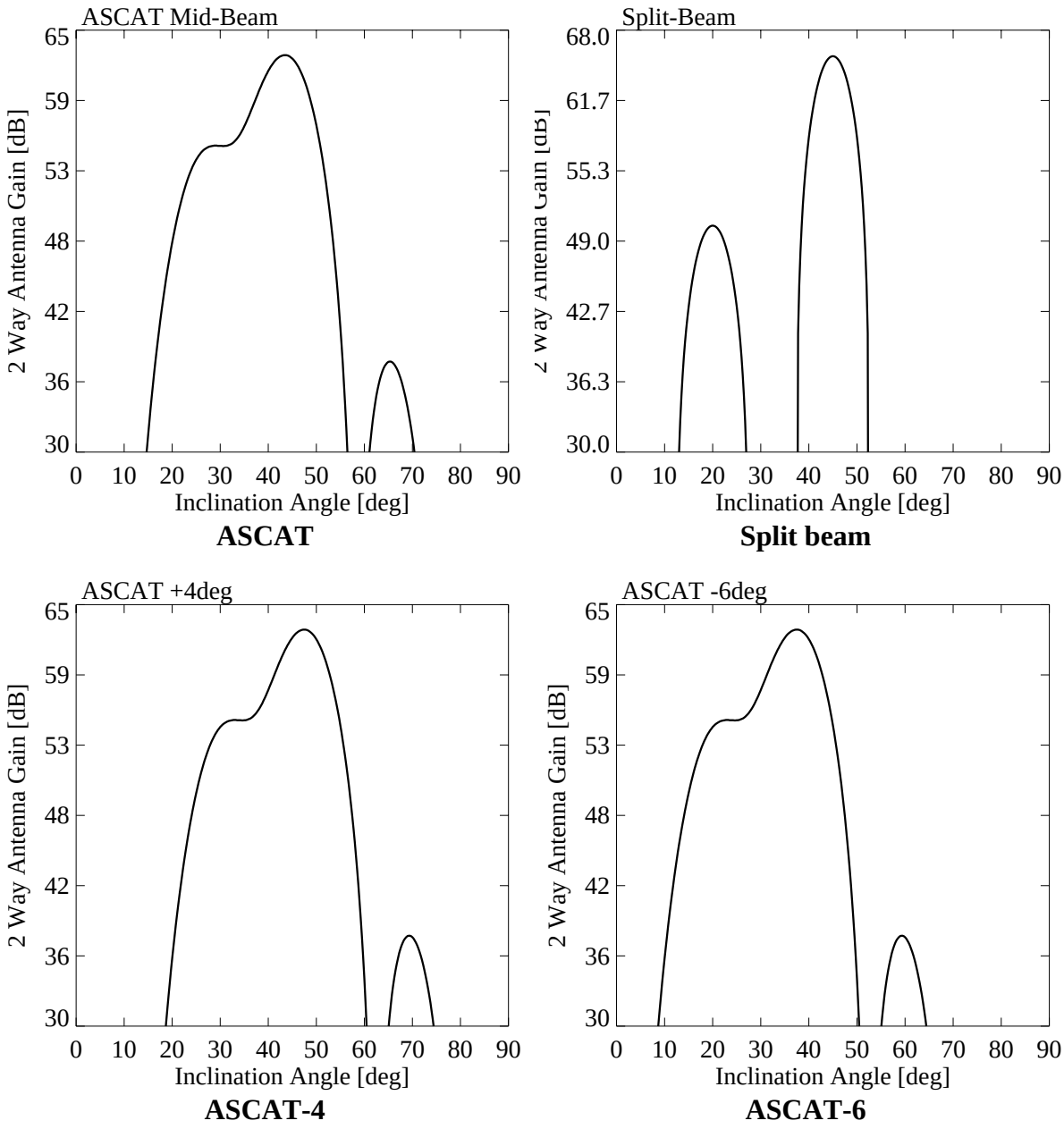


*Figure 15: Two way antenna gain pattern used for the various systems.*

### 4.0.1. Low Orbit and 25 km Spatial Resolution

The reference system has been simulated with higher spatial resolution while all other parameters were kept constant. The following Figure 16 shows the FoM for different settings of pulse peak power, while Figure 17 summarizes the results for this instrument.

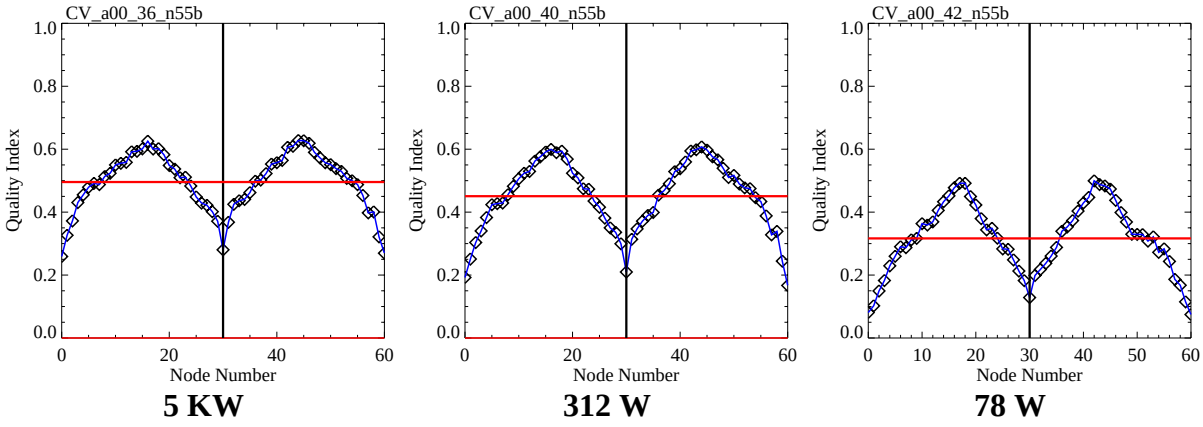


*Figure 16: Quality index curves for the high (25 km) resolution mode of a C-band VV-polarization system. Further graphs are provided in Annex E together with a polarimetric mode.*

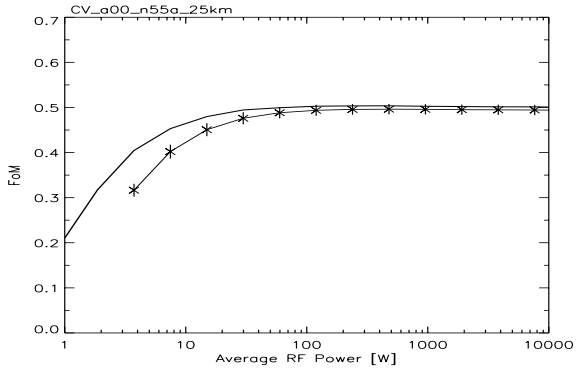


*Figure 17: FoM as a function of average RF power for a high resolution mode (25 km) together with the baseline system (thick solid line).*

At a higher resolution the system shows a slightly different and lower performance than the baseline system. For statistical reasons, a higher average power is needed at better spatial resolution in order to achieve the same SNR as for the baseline system. This explains the shift of the FoM curve towards higher pulse peak power, nevertheless a general lower performance is observed within the saturation part of the FoM curve. This is very likely due to the wind error statistics used in the retrieval which accounts for the larger variability within 50 km resolution cells. For very high power, the slight lower performance at 25 km is due to its lower radiometric resolution due to the lower number of averaged samples (¼ of the 50 km case as the radiometric resolution is given by the inverse of square-root of the number of samples).

### *4.1. C-Band Dual polarization*

This is an obvious extension of the system and the analysis of the GMF in the Task-1 report suggests that this additional channel will improve the wind retrieval considerably.

#### 4.1.1. Low Orbit and 1500 km Swath

These simulations comprise the Option B (a single dual polarized antenna and alternating pulses) and the Option C (two separate antennae looking left and right with either alternating pulses or simultaneous pulses and divided power). Figure 18 depicts the plots quality index vs. node number for two power settings for VV and HH polarization as well as for a combination of both channels. The strength of the radar backscatter is slightly lower for HH polarization than for VV. This difference causes the lower performance of the HH-pol channel for low pulse peak power. The entire set of graphs is provided in Annex D. From the plots shown there, it is obvious that there is no performance difference between the two options B and C, which is in line with the physics behind it.

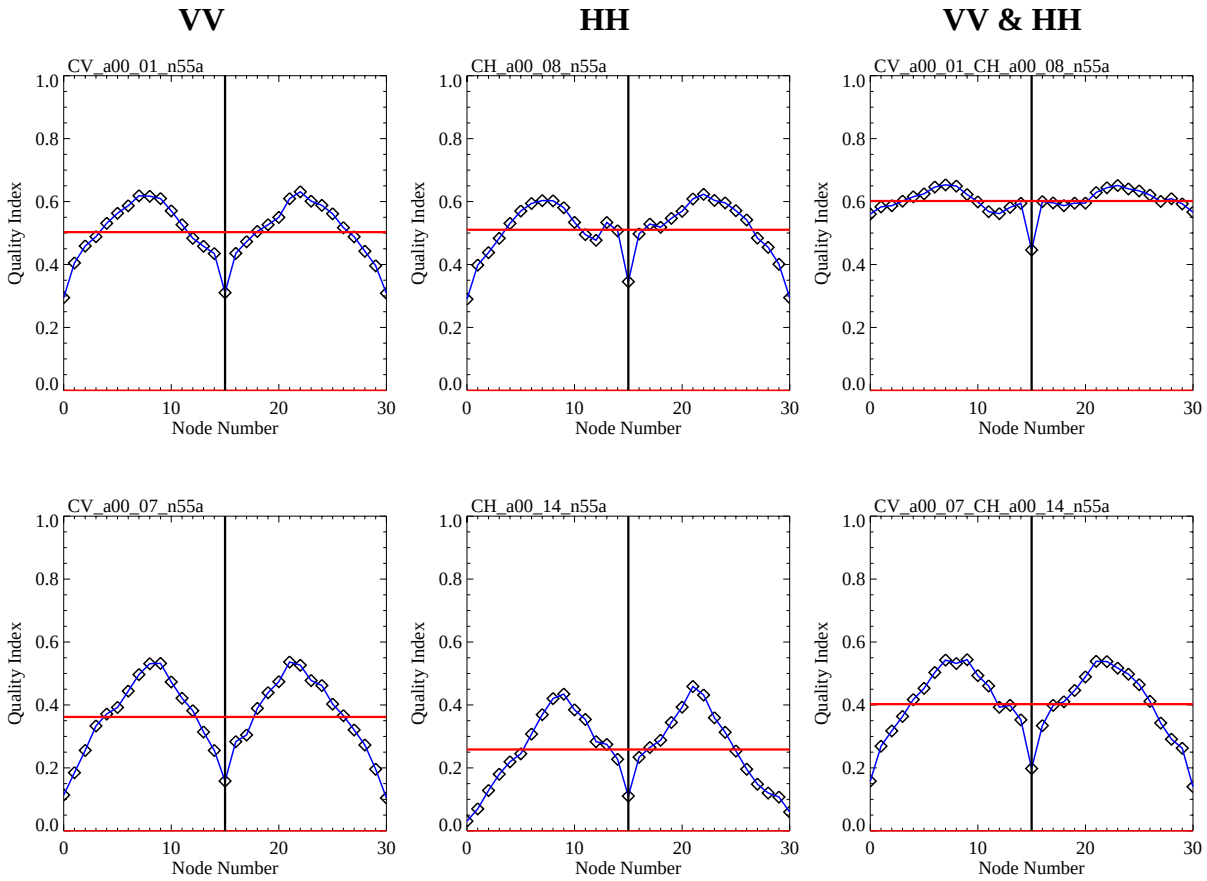


*Figure 18: Quality index curves for two different transmitter peak powers (5 KW top and 78 W bottom) for the VV and HH channel as well as a combination of VV & HH. The full set of plots for all power settings is shown in Annex-D.*

Although the performance of at VV- and HH-polarization is comparable across the swath for both level and shape of the quality index vs node number curve, there is a remarkable increase in wind retrieval performance when combining both data. The most significant improvement is encountered at the edges of the swath. Compared to the single polarization, performance across the swath is quite even, except for the center node.

The results for this system are summarized in Figure 19.

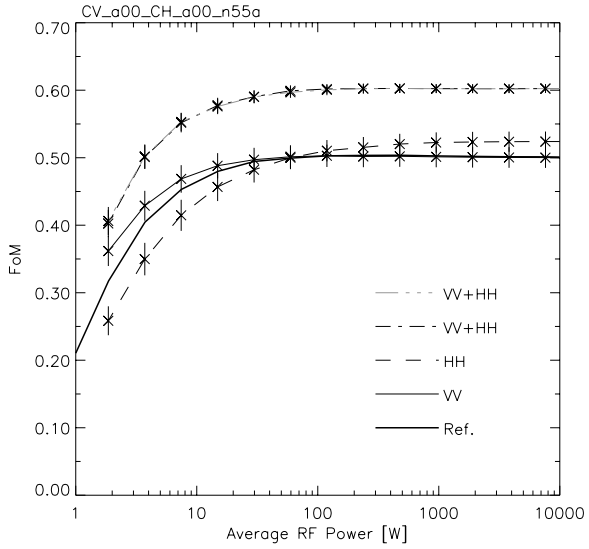


*Figure 19: FoM as a function of average RF power for the different channels of a dual polarized system. The thick solid line indicates the baseline (Ref.) system.*

### 4.1.2. Low Orbit and 1800 km Swath

A wider swath width is desirable in order to improve the temporal coverage within a global monitoring system. In order to achieve this, the antenna is being tilted by 4 degrees towards larger incidence angles. The advantage of larger incidence angles is that the wind retrieval will be improved due to the higher dynamic range of the azimuthal dependence of the NRCS. However, the disadvantage is that the signal level decrease significantly with incidence angle. Therefore, a higher pulse peak power will be needed in order to resolve low wind speeds at the outer swath.

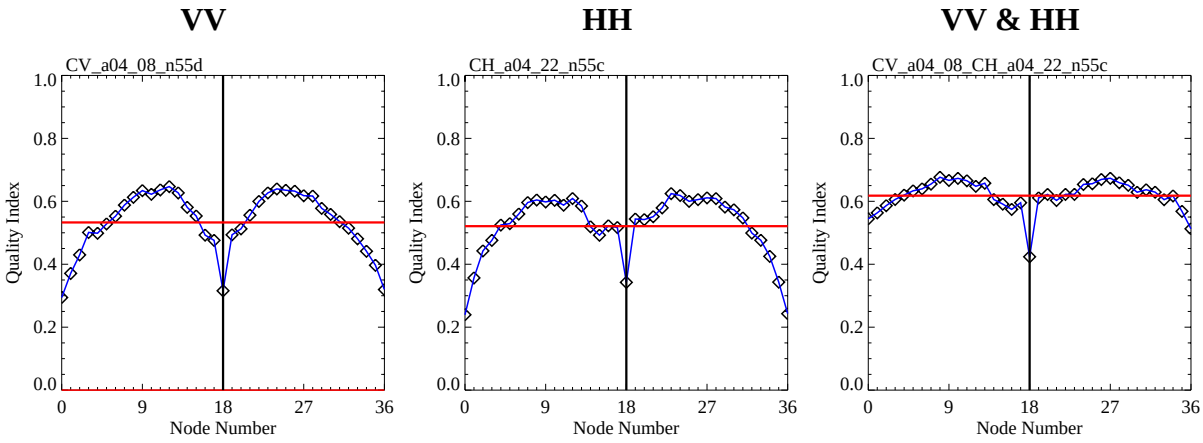


*Figure 20: Quality index curves for a dual polarized wide swath system with 5 KW pulse peak power. Further graphs are shown in Annex F.*

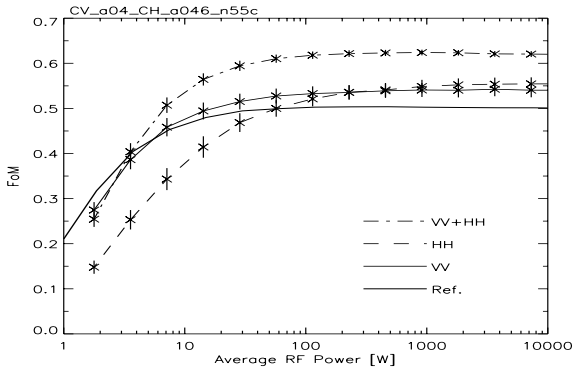


*Figure 21: FoM as a function of average RF power for a dual polarized system*

The FoM curve in Figure 21 depicts the expected result. Higher power is necessary to reach the saturation level, but even at relatively low average RF power a system operating only in VV-mode performs better than the reference system. The effect of the degradation in radiometric resolution is visible only at low RF power while the overall performance is still controlled by the wind retrieval method. Herein the larger incidence angle which is necessary for increasing the swath width has a positive impact on the wind retrieval due to the incidence angle dependence of the GMF. Again the lower backscatter at HH-polarization is reflected by the lower performance curve. However in the saturation region, a scatterometer operating at HH-polarization has a

slightly higher FoM than the corresponding VV-polarization instrument. The reason is the greater up-wind / down-wind ratio in the GMF for HH-polarization which reduces the number of ambiguous solutions. In a combination, a system that uses both channels is significantly better than the baseline system.

### 4.1.3. Low Orbit, 1800 km Swath and 25 km Resolution

This instrument is the higher resolution option of the previous system. The FoM is significant lower for low radar power as expected. However, already at reasonable average RF power the same performance can be achieved as for the 50 km resolution option.

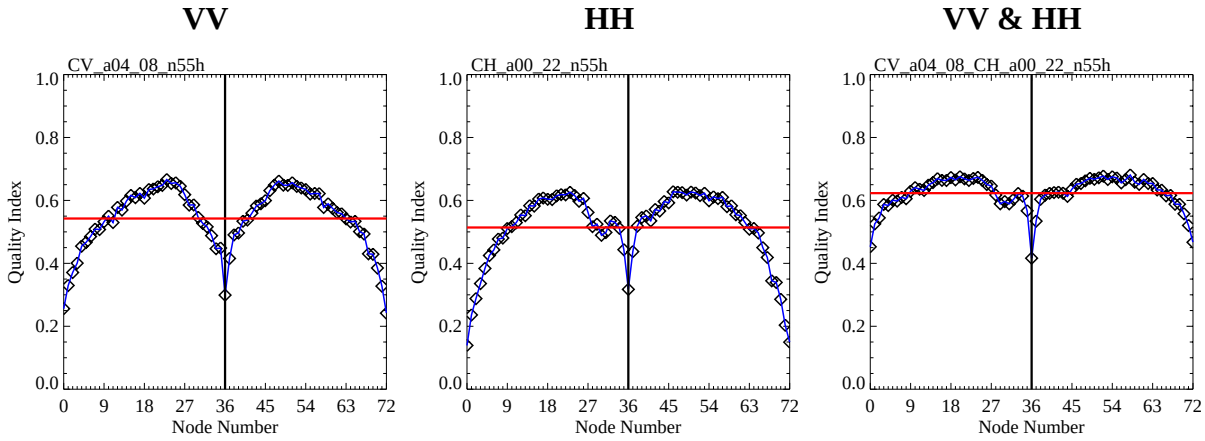


*Figure 22: Quality index curves for a dual polarized, wide swath, and high resolution (25 km) system with 5 KW pulse peak power. Further plots are shown in Annex G.*

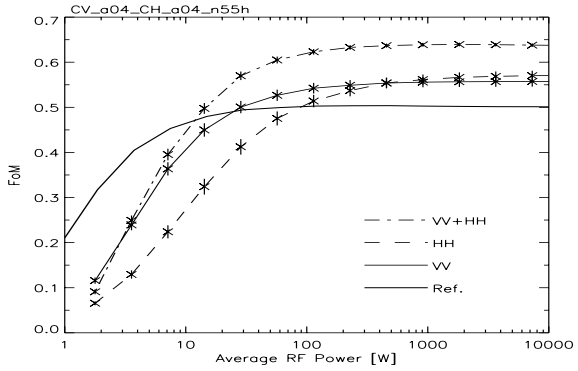


*Figure 23: FoM as a function of average RF power for a dual polarized wide swath and high resolution system.*

### 4.1.4. Split-Beam Antenna

Around the middle of each side of the swath the RFSCAT system will provide a relatively high number of views with similar look-angles (both in azimuth and incidence angle) and therefore "oversample" this region for wind retrieval. A way of reducing redundant information could be to split the wide antenna beam into two beams as depicted in Figure 2. This option also allows a better adaptation of the antenna gain to near and far swath geometry and better meets the SNR constraints. The resulting sampling pattern is depicted in Figure 24. It consists of the summation of the two pattern for each of the beams. Their contributions can easily be identified in the figure. For geometrical reasons it is not possible to achieve constant number of measurements across the swath.

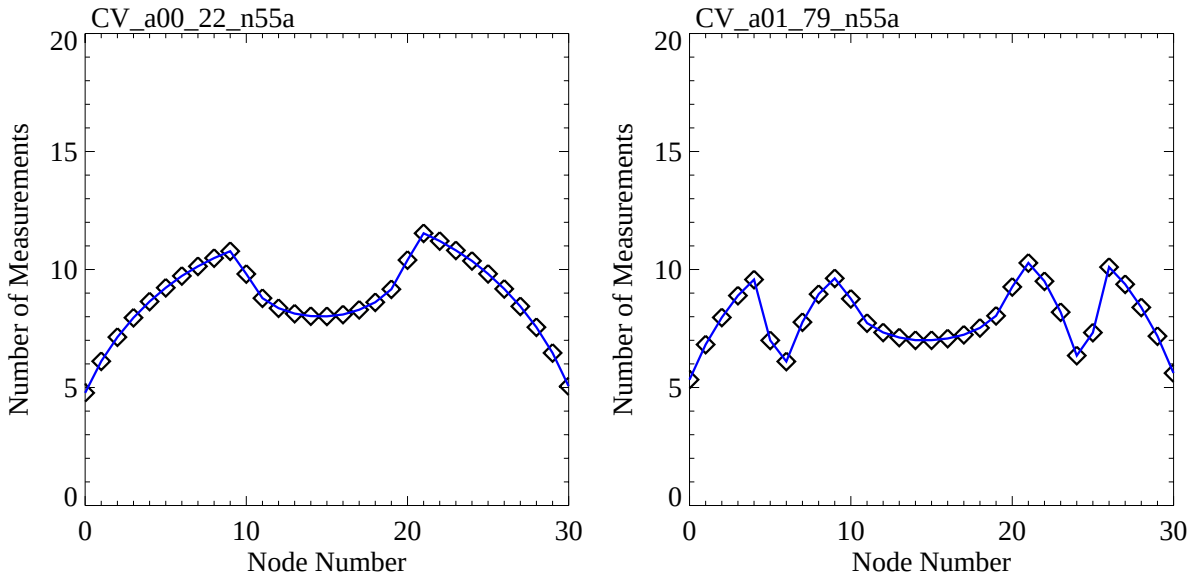


*Figure 24: Comparison of the sampling pattern across the swath of baseline wide beam antenna (left) and the two-pencil-beam (right). Their contributions to the pattern can easily be identified from its shape.*

Figure 25 depicts FoM curves for an alternating VV & HH polarization instrument (PRF=119 Hz) with 1500 km swath width. Around the center of the swath, the shape of the curve is comparable to the respective fan beam system. But at outer edge of the inner beam, the performance drops significantly. This is exactly where the fan beam system has its best performance. From an application point of view, e.g., data assimilation for numerical weather prediction models, such dramatic change in performance and thus in error statistic is not being appreciated.

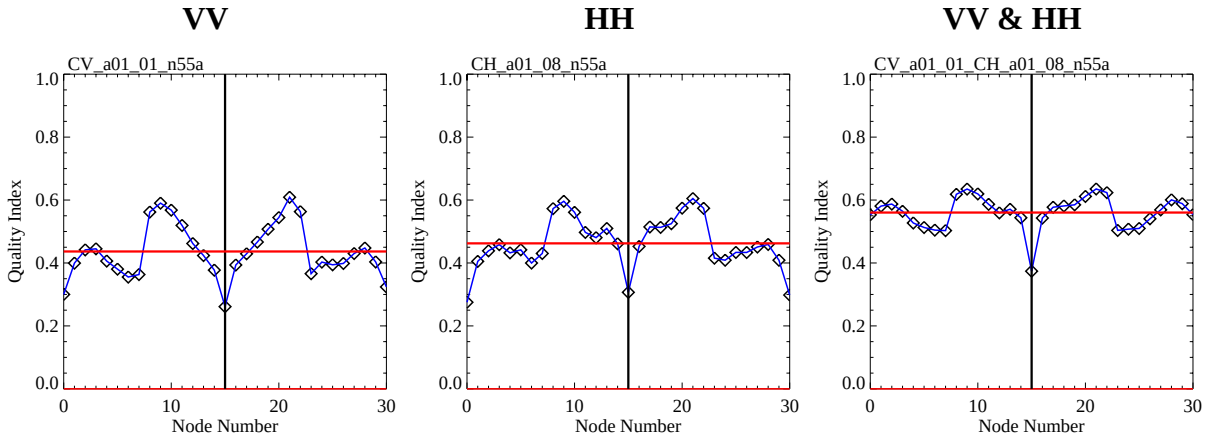


*Figure 25: Quality index curves for a split beam dual polarization system. The pulse peak power is 5 KW. Further graphs are depicted in Annex H.*

Figure 26 summarizes the results for the dual polarization split beam system. The performance for the single channels is significantly lower than for the reference system and also their combination does not perform as good for the corresponding full beam instrument (see Figure 19). The FoM increases monotonically with average RF power and does not saturate as observed for the other systems. The reason is that with increasing power more and more contributions from the edges of the main beam act as an effective widening of the single beams. Consequently, the effective gap in between the two beams decreases.

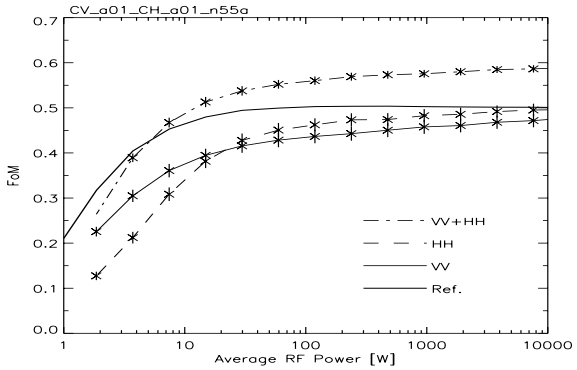


*Figure 26: FoM as a function of average RF power for a dual polarized split-beam system.*

### 4.1.5. High Orbit and 1800 km Swath

A higher orbit may be chosen for two reasons, either to save RF power or to increase the swath width. From a higher orbit the same swath can be observed at reduced incidence angle at the outer edges. Although the range to the target increases with orbit height, there is still a net saving in RF power because of the NRCS decreases with incidence angle is even larger. However, the simulation for the lower orbit showed already that it is desirable to use large incidence angle in order to improve the wind retrieval performance. Thus, it is inadvisable to simulate the performance across a 1500 km swath for a higher orbit. In order to cover an 1800 km swath from orbit at 1075 km, the antenna has to be tilted already by 6 degrees towards steeper incidence angles.

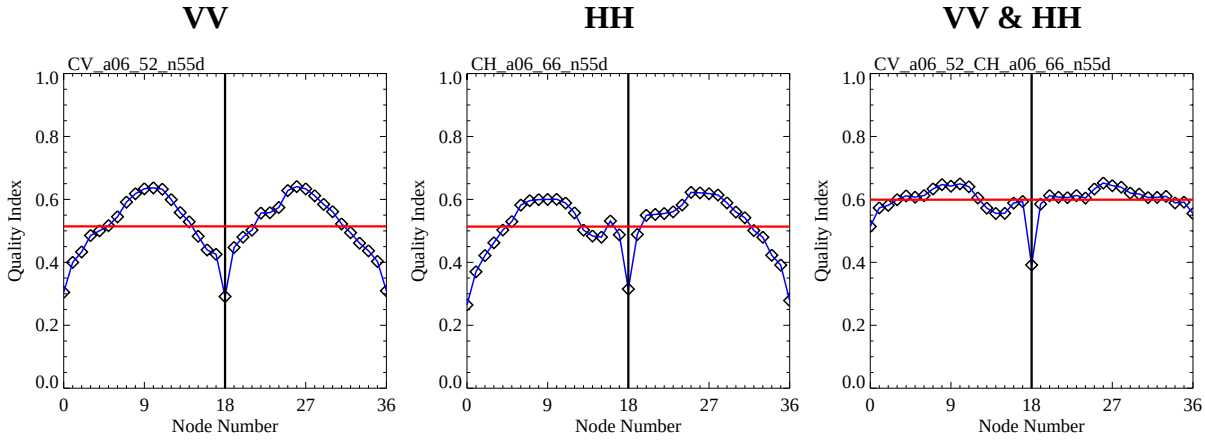


*Figure 27: Quality index curves for a high orbit (1075 km) and wide swath (1800 km) system with 5 KW pulse peak power. Further graphs are shown in Annex I.*

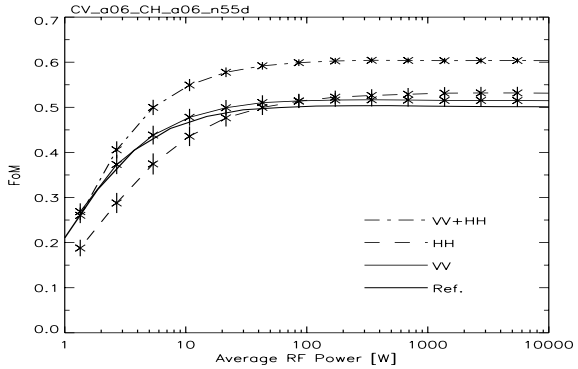


*Figure 28: FoM as a function of average RF power for a high orbit (1075 km), wide swath (1800 km) system.*

The summary of the simulation results in Figure 28 shows that all polarization modes have the same performance with respect to average RF power as the corresponding low orbit, but narrow swath instruments. Consequently, the gain for the higher orbit is the additional coverage due to the wider swath.

### *4.2. C-Band Polarimetric Systems*

In the Task-1 report, theoretical work by Tai et al. (2000) has been used for developing a polarimetric GMF for C-band. The important feature within the polarimetric measurement is an odd azimuthal behavior of the polarimetric correlation coefficient. In combination with an even azimuthal dependence of the NRCS at VV- and HH-polarization, respectively, there is great potential to solve the problem of ambiguous wind directions. A first experimental evidence for an odd polarimetric azimuthal signal and thus a confirmation of theoretical idea was recently published by Yueh et al. (2002) for a Ku-band airborne system. Presently, no experimental data are available at C-band. Thus, the used GMF is still of purely theoretical nature. The GMF given by Tsai et al. (2000) relates the correlation of the complex co- and cross-polarized radar returns to wind speed, wind direction, incidence angle and azimuth angle. This correlation has been in the analysis and is denote as the polarimetric channel in this document.

A polarimetric mode is technically a challenging issue since the signal level to be detected at cross-polarization is approximately 15 dB lower than that of co-polarization. Furthermore, it will be necessary to achieve a high isolation between the V- and H-channel even through a common rotary joint. However, it is not the purpose of this study to judge on these technical aspects, but these constraints have to be taken into consideration when comparing polarimetric systems to the others.

In the polarimetric option, two scenarios are possible. First, a semi polarimetric mode in which only one transmitter sends a vertically polarized signal which is detected simultaneously by two separate receivers having vertically and horizontally polarized antennae. Second, a fully polarimetric mode in which the transmitter also alternately uses both polarizations. With respect to RF power constraints, the first option seems to be favorable. However the question is “how much can the HH-polarization mode contribute in cases with low SNR for the polarimetric mode”.

### 4.2.1. Low Orbit and 1500 km Swath

For this simulation, polarimetric capability was added to the baseline system. From Figure 29, the following attributes of polarimetric measurements can been seen. The performance in wind retrieval is significantly better than for a VV-polarization system for both, the level of the FoM and the variability of performance across the swath. The price for this improvement compared to the baseline system is a significantly higher RF power consumption as can be seen from Figure 32.

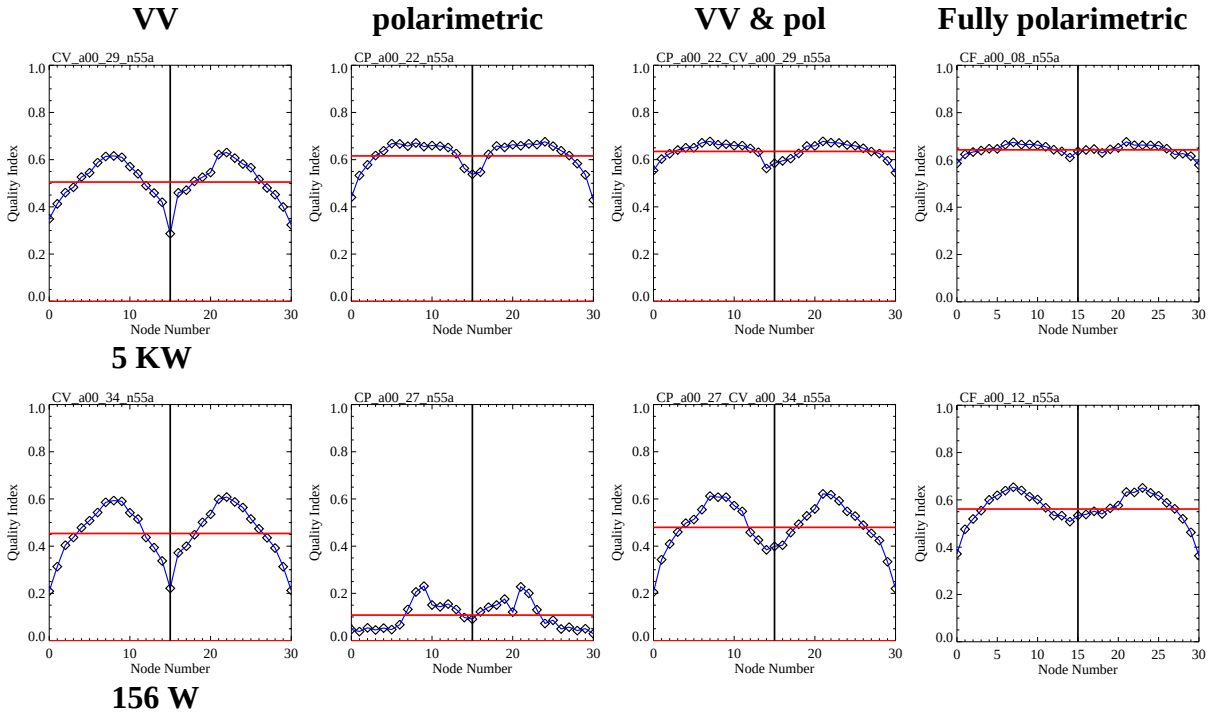


*Figure 29: Quality index curves for two different transmitter peak powers for the VV- and the polarimetric channel as well as for a combination of both (VV&pol) and a fully polarimetric system. The full set of graphs for all power settings is shown in Annex-K.*

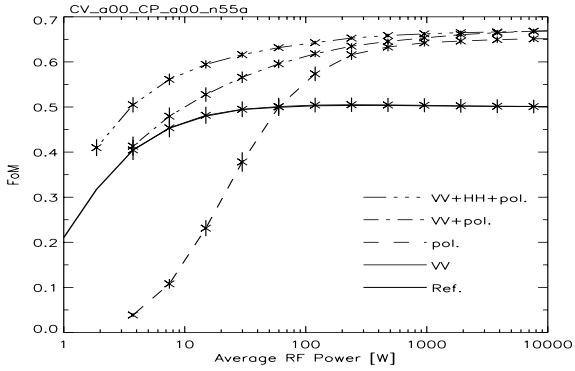


*Figure 30: FoM as a function of average RF power for a polarimetric system. VV+pol indicates a semi-polarimetric and VV+HH+pol a fully-polarimetric system.*

Figure 30 shows the impact of a polarimetric channel on the wind retrieval. Due to the low signal level at cross polarization more RF energy is required for the measurements, but then the performance increases significantly when including polarimetric information. For low average RF power, the fully polarimetric mode provides further gain in performance due to the contribution from the HH-polarization channel.

### 4.2.2. Low Orbit and 25 km Spatial Resolution

This system is the polarimetric extension of the instrument already described in Section 4.0.1. Similar improvements in wind retrieval are found at the cost of slightly higher RF power as can be seen from Figure 31 and Figure 32, respectively.

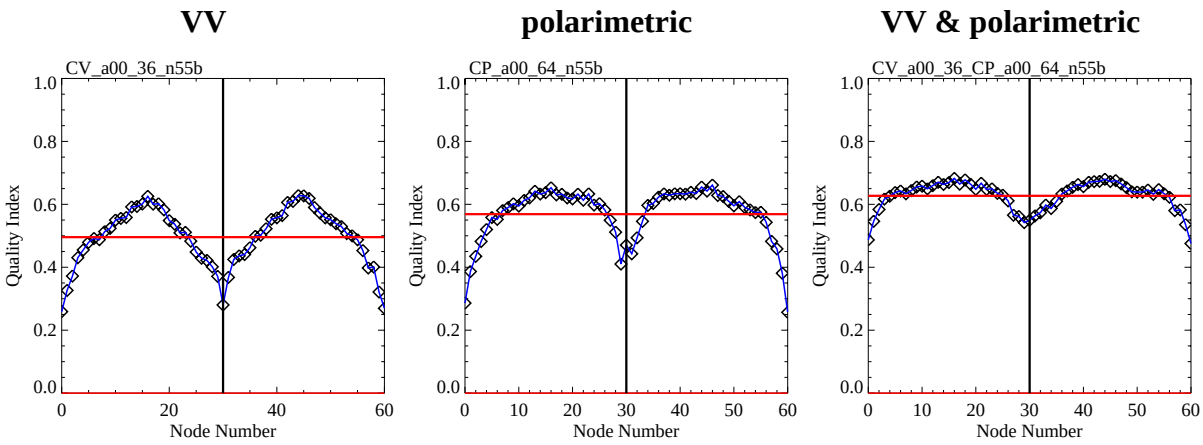


*Figure 31: Quality index curves for a high-resolution (25 km) semi-polarimetric system with a pulse peak power of 5 KW. Further graphs are shown in Annex E.*

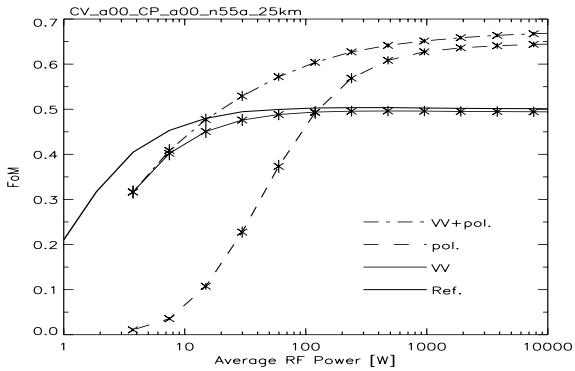


*Figure 32: FoM as a function of average RF power for a high resolution semi-polarimetric system.*

### 4.2.3. Low Orbit and 1800 km Swath

Being one of the favorable systems in this comparison, also the fully polarimetric capability has been added to this wide swath instrument. As expected, this system combines the better performance already achieved for the VV-polarization mode with an additional gain in retrieval quality due to a semi polarimetric mode and even more due to a fully polarimetric mode. The respective graphs are shown in Figure 33 and Figure 34.

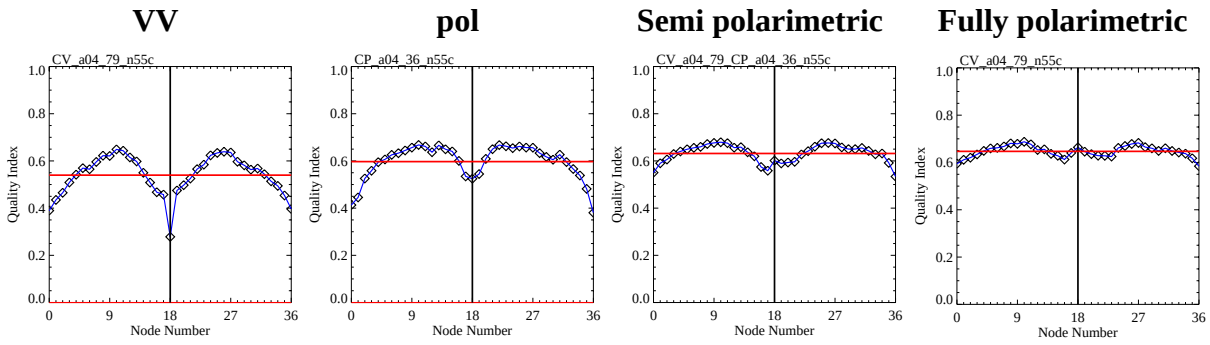


*Figure 33: Quality index curves for a fully-polarimetric wide swath system with 5 KW pulse peak power. Further graphs are shown in Annex L.*

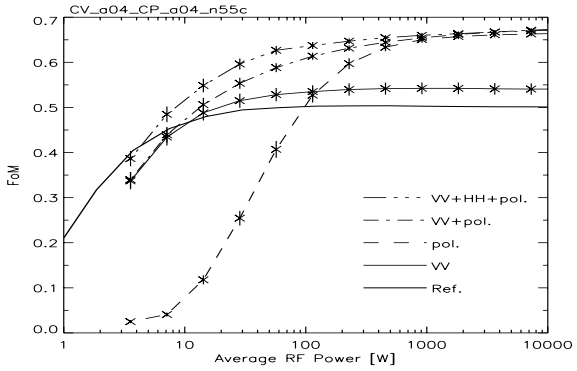


*Figure 34: FoM as a function of average RF power for a low-orbit, wide-swath, fully-polarimetric system.*

### 4.2.4. Low Orbit, 1800 km Swath and 25 km Resolution

This system is an upgrade of the previous 50 km resolution instrument. It requires more RF power for achieving the same performance as the lower-resolution system as can be seen when comparing Figure 34 and Figure 36.

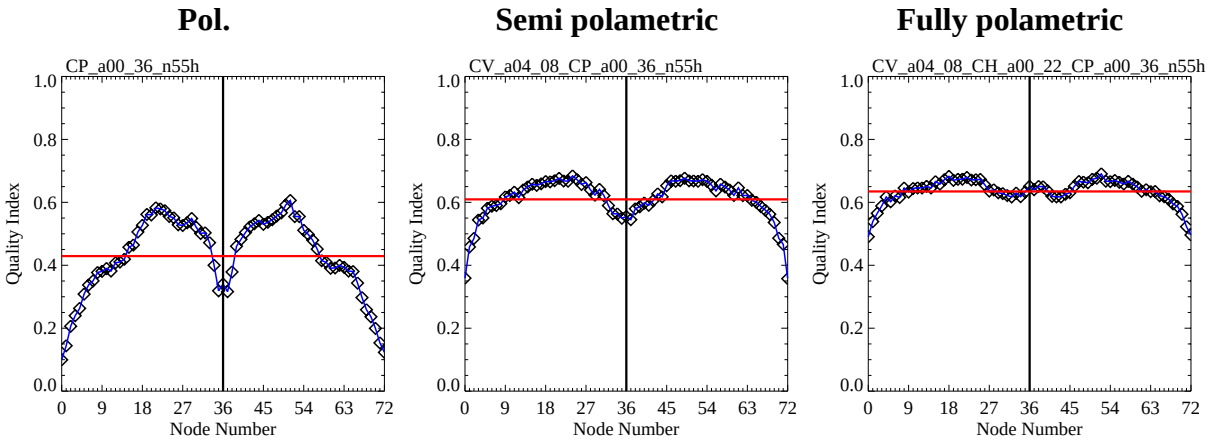


*Figure 35: Quality index curves for a wide-swath, high-resolution, and fully-polarimetric system for a pulse peak power of 5 KW. The full set of graphs is provided in Annex M.*

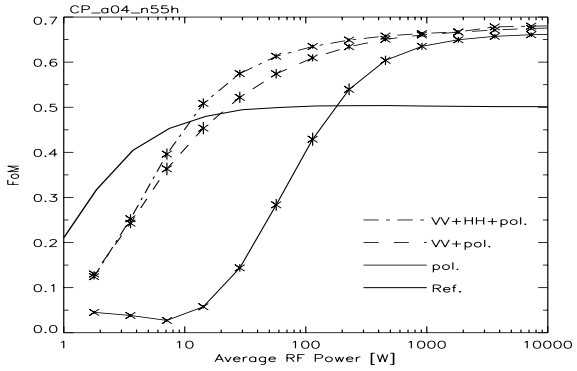


*Figure 36: FoM as a function of average RF power for a low-orbit, wide-swath, high-resolution, and fully-polarimetric system.*

### 4.2.5. Split-Beam Antenna

The concept of the split beam antenna did not show convincing results in a dual polarization system. The reason is in its measurement geometry. Therefore, it is not expected that a polarimetric version is performing better or comparable as the respective fan beam systems. However for completeness, the results are depicted in Figure 37 and Figure 38.

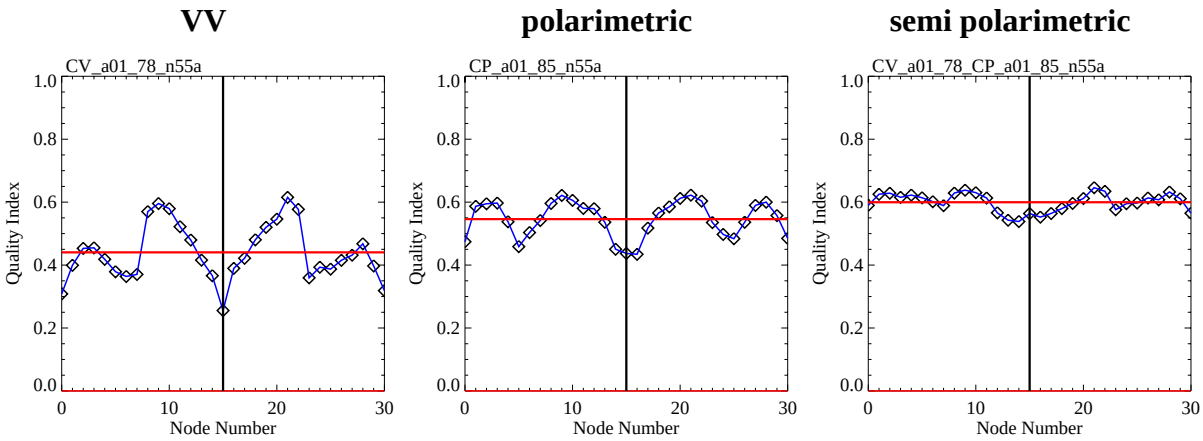


*Figure 37: Quality index curves for the split-beam polarimetric system for a pulse peak power of 5 KW. The full set of graphs is provided in Annex N.*

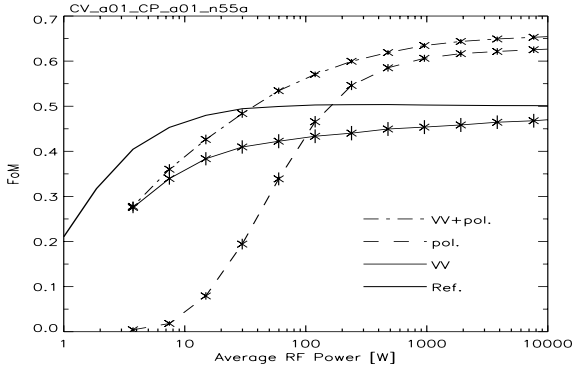


*Figure 38: FoM as a function of average RF power for a semi-polarimetric split beam system.*

### 4.2.6. High Orbit and 1800 km Swath

The reasons for choosing a higher orbit are discussed in chapter 4.1.5. As for the other systems, a polarimetric channel increases the performance at the cost of RF power. The respective graphs are shown in Figure 39 and Figure 40.

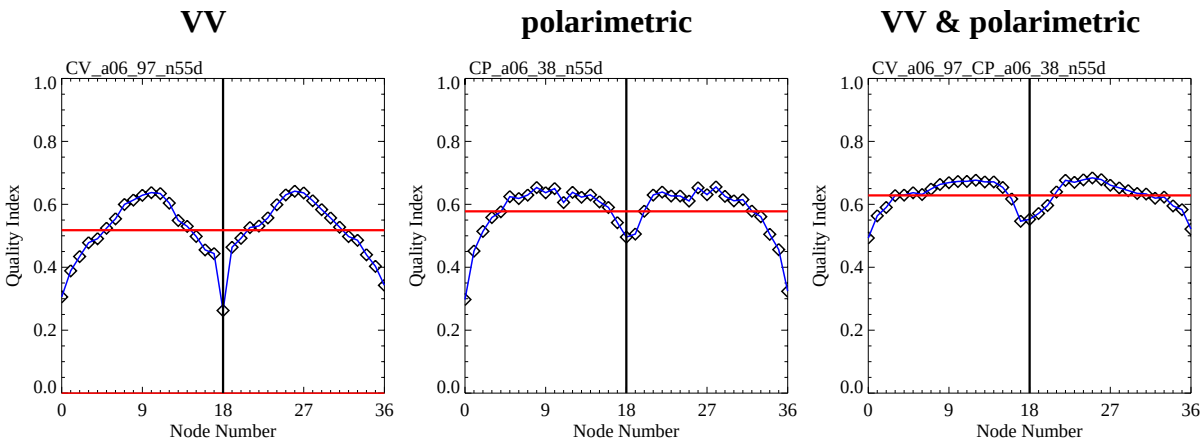


*Figure 39: Quality index curves for a high orbit (1075 km) polarimetric system for 5 KW pulse peak power. Further graphs are shown in Annex O.*

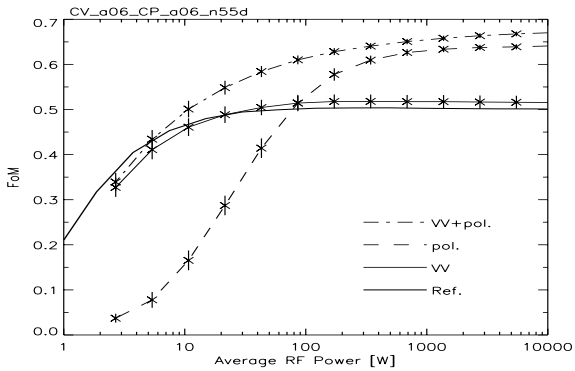


*Figure 40: FoM as a function of average RF power for a high orbit (1075 km) wide swath (1800 km) semi-polarimetric system.*

### 4.3. Additional Ku-Band Channel

Windscatterometers have been operated also at Ku-band, e.g. SASS on SEASAT, NSCAT on ADEOS, and SeaWinds on QuikSCAT. While SASS and NSCAT were fixed antenna fan-beam instruments like the AMI aboard ERS-1/-2 and ASCAT on MetOp, SeaWinds is a rotating pencil beam system and is thus comparable to the system under investigation. In Chapter 3, SeaWinds is being described and the results of a simulation of this system is shown there as well. Therefore, it is reasonable to study a Ku-band fan-beam system as well. This will be only for a basic configuration since it can be expected that further extensions in measurement geometry and polarimetric capability will have the same impact as for C-band. The reason for this is in the similarity of the GMF which are the limiting constraints in the system development.

This similarity is obvious from the graphs depicting the dependence of the quality index across the instrument swath. Examples are shown in Figure 41, while further graphs are given in Annex P.

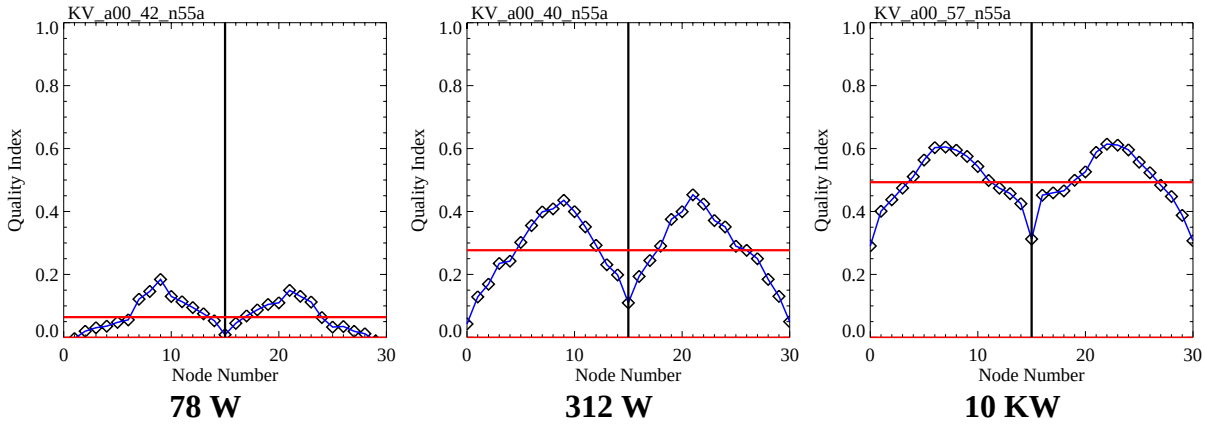


*Figure 41: Quality index curves for a VV-pol Ku-band system for different settings of pulse peak power. Further graphs are shown in Annex P.*

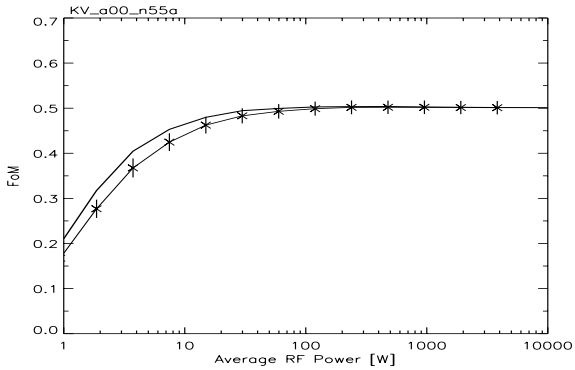


*Figure 42: FoM as a function of average RF power for a VV-polarization Ku-band system (thin curve). The thick solid line denotes the C-band reference system.*

Figure 42 depicts the dependence of the FoM on average RF power. There is very good agreement between the Ku-band and C-band system. Even the "final" FoM of the saturation level is identical, indicating that there is no

preference in choosing the radar frequency from this point of view. However, there are other arguments like antenna size on one side and atmospheric disturbances on the other side which are not subject of this study.

The required higher power at Ku-band reflects the fact that the gain of an equivalent ASCAT Mid-Beam antenna at Ku-band, i.e., with the dimension scaled by the frequency, is not sufficient to ensure a good SNR. A slightly larger antenna (in electrical sense) would be required to achieve a sufficient SNR.

### 4.3.1. Dual Polarization

So far, all spaceborne Ku-band wind scatterometers operated both at VV- and HH-polarization in order to reduce the number of ambiguous wind solutions. The results for such a system are depicted in Figure 43 and Figure 44. The performance of this Ku-band system is very similar to the comparable C-band instrument. However, Figure 44 indicates a slightly better performance of the C-band system for lower RF power.

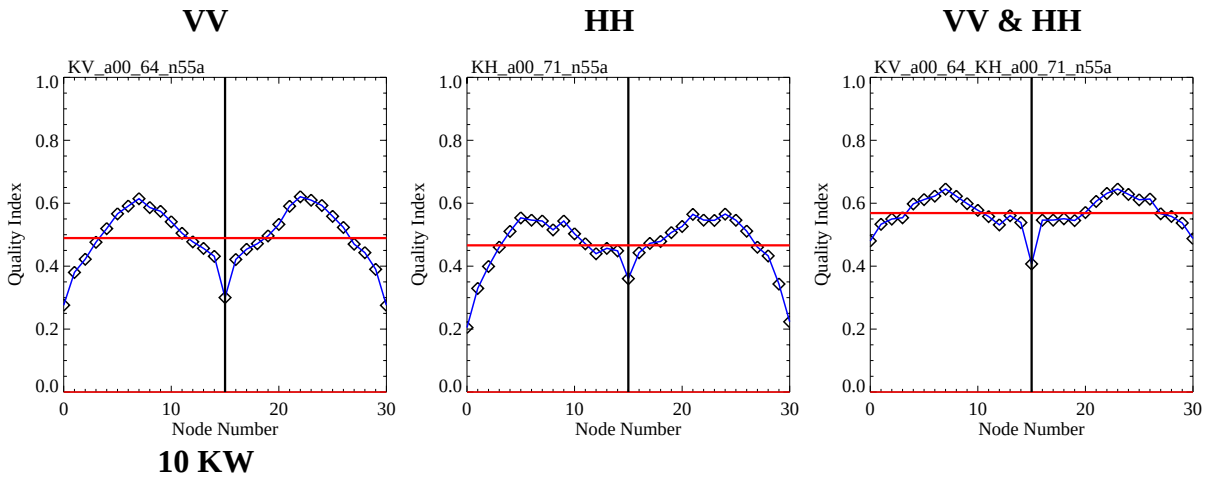


*Figure 43: Quality index curves for a dual polarization Ku-band system for comparison with the respective C-band system. Further graphs are shown in Annex Q.*

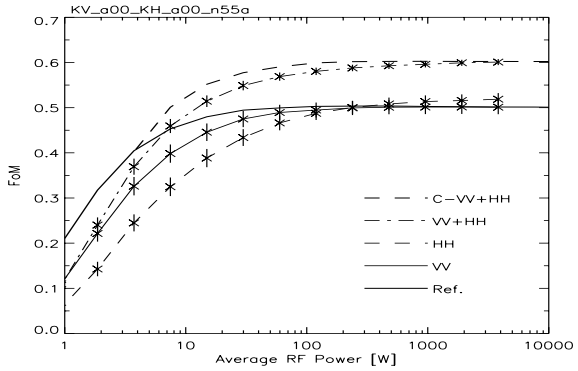


*Figure 44: FoM as a function of average RF power for a dual polarized Ku-Band system. The thick solid line denotes the reference system while the dashed thick indicates the dual polarized C-band version of this instrument.*

### 4.3.2. Combination of C-Band and Ku-Band

Another possibility to improve the wind retrieval performance of the reference system is to add a Ku-band channel. In order not to increase the complexity further only a two antennae system is being considered, thus further extensions like dual polarization or polarimetric instruments which would require 4 antennae will not be evaluated. However, since the GMF for C-band and Ku-band are very similar it is not expected that this combination will perform much better than a dual polarized system operating at one frequency only. The results are depicted in Figure 45 and Figure 46.

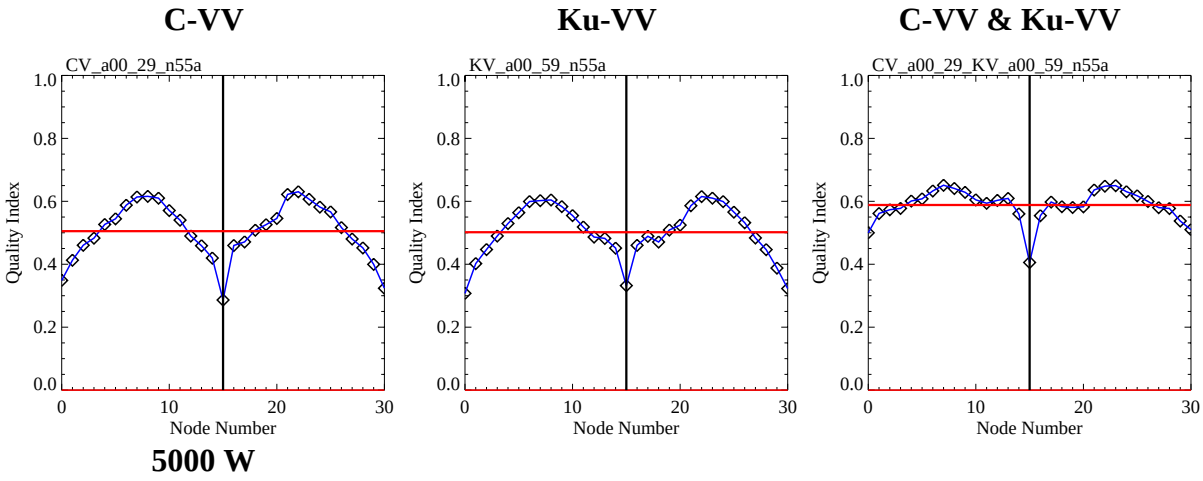


*Figure 45: Quality index curves for C-band and Ku-band VV-polarization systems and their combination for a pulse peak power of 5 KW. Further graphs are shown in Annex R.*

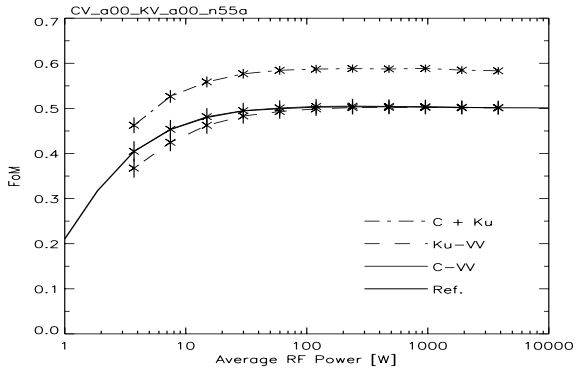


*Figure 46: FoM as a function of average RF power for a system combining C-band VV-polarization and Ku-band VV-polarization.*

## 5. System Comparisons

Within this study, various systems have been analyzed. On the radar side simulations were done for C- and Ku-band for vertical (VV) and horizontal (HH) polarizations as well as for polarimetric configuration. The measurement geometry includes low (725 km) and high (1075) orbits, narrow (1500 km) and wide (1800 km) swaths as well as low (50 km) and high (25 km) spatial resolutions. Special emphasis was put on the analysis of combinations of polarizations for the wind retrieval. Three typical examples are depicted in Figure 47 which shows the simulation results for a C-band dual polarization instrument (a), a C-band polarimetric system (b) and a combination of a C- and Ku-band vertically polarized scatterometer (c), all for a low orbit (725 km) and a narrow swath (1500 km).

*Dual-polarization C-band* *Polarimetric C-band* *C- & Ku-band*

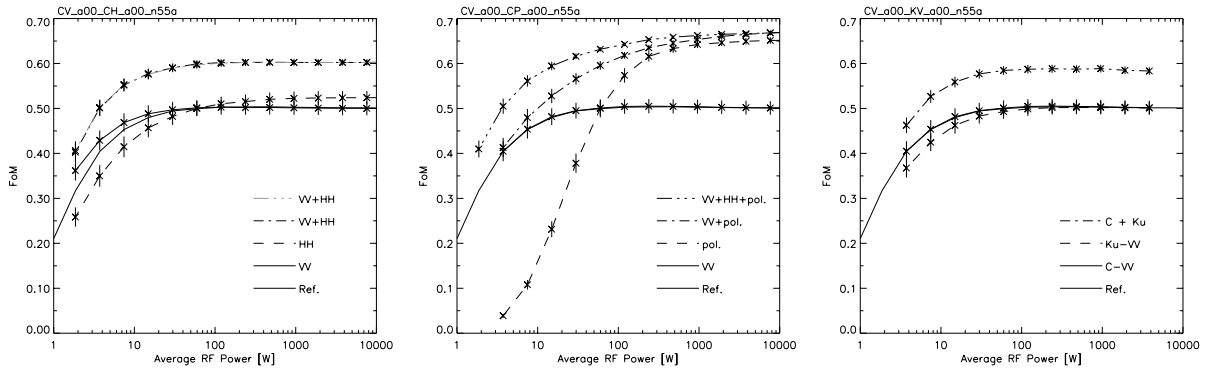


**(a)** **(b)** **(c)**

*Figure 47: FoM as a function of average RF power for a dual polarization C-band instrument (a), a polarimetric C-band system (b) and a combination of vertically polarized C- and Ku-band scatterometers (c). The error bars indicate the RMS variation of the FoM across the respective instrument swath.*

Considerable differences between the systems are obvious from these graphs. They also well reflect differences between the radar channels, e. g., the signal level at cross-polarization, which is important for the polarimetric mode, is approximately 15 dB lower than the VV-polarization measurements. In general, a considerable improvement in wind retrieval can be achieved when combining channels. Especially, the polarimetric mode has strong impact herein due to its capability of resolving wind direction ambiguities.

In order to compare the simulated systems, a reference performance point is being computed from the respective curve of FoM versus average RF power. Therefore, a fifth-order polynomial is fitted through the data and the point which is 10% below the saturation level is derived. This reference point allows to relate the system costs in terms of power consumption to the achieved performance in wind retrieval. This criterion reflects that power consumption is a critical issue for spaceborne instruments. However, the technical complexity of the evaluated systems ranges from simple single polarization scatterometers to fully polarimetric systems which require some challenging technical solutions prior to their implementation. Thus, a detailed comparison will be done separately for the different instrument types.

Figure 48 summarizes the performance parameters for the simulated instruments. The performance parameters for ERS and ASCAT were derived in the same way as for the RFSCAT systems and they are included in the graph. However, care must be taken when directly comparing the values for ERS and ASCAT with RFSCAT systems because the FoM is a mean value for the entire swath of RFSCAT while both ERS and ASCAT cover only a portion of this swath as shown in Figure 49. The latter of course is the region with optimum viewing geometry for a wind scatterometer and thus with best performance. From Figure 49, it can be seen that there is only a small performance difference between ERS and the reference RFSCAT system for the portion of the swath equally covered by both instruments. Thus, the difference between both systems indicated in Figure 48 could mislead. The FoM used herein is optimized for comparing different RFSCAT system, but not for a comparison with other systems having a different viewing geometry.

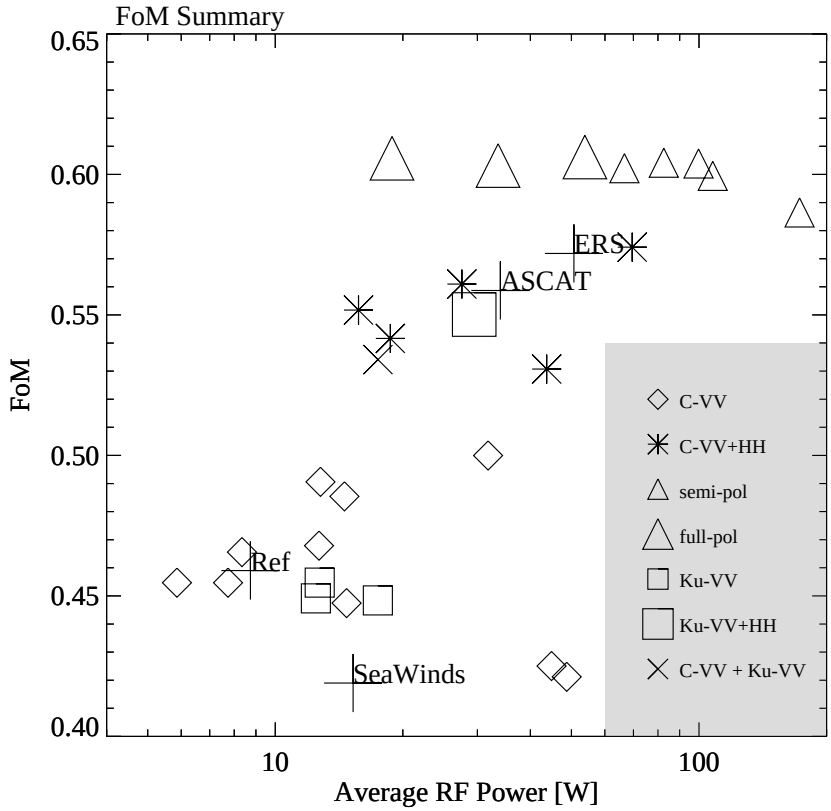


*Figure 48: Summary of the performance of the simulated systems. Labeled crosses indicate ERS, ASCAT and SeaWinds as well as the reference RFSCAT system (Ref), the diamonds and stars denote single polarization and dual-polarized C-band systems, respectively. Polarimetric systems are marked by triangles, whereby the larger triangles indicate fully polarimetric systems. Ku-band systems are represented by squares and the (x) marks a combination of C- and Ku-band.*

The main message of Figure 48 is that the performance increases with instrument complexity and average RF power, which is not a surprise. However, one can clearly discriminate three regions of complexity for which it is worthwhile to compare the systems therein, because they differ considerably in FoM and power consumption. These regions can be separated by two thresholds for the FoM at 0.51 and 0.58 and they are related to single channel systems (either in polarization or frequency and FoM<0.51), dual channel systems (0.51<FoM<0.58), and polarimetric systems (FoM>0.58). It is worth noting that the two systems indicated by the diamonds with FoM of about 0.42 and average RF power above 40 W are split-beam instruments.

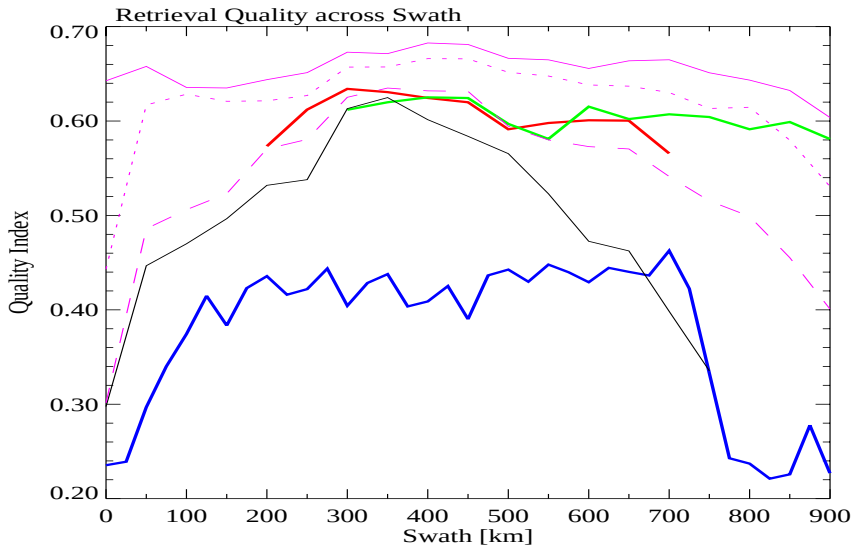


*Figure 49: Summary of the performance across swath for representative systems ERS, ASCAT, SeaWinds, and the reference RFSCAT are shown in red, green, blue and black, respectively. From top to bottom the pink curves indicate a fully polarimetric, dual-polarized, and wide swath single polarization system.*

### *5.1. Single Channel Instruments*

Only vertically polarized systems are considered herein although corresponding horizontally polarized systems have also been simulated for the analysis of systems carrying both. In general, HH-polarization systems perform slightly better than the VV-polarization instruments but at considerably higher average RF power. Thus, it is not advisable to employ HH polarization on a "simple" wind scatterometer.

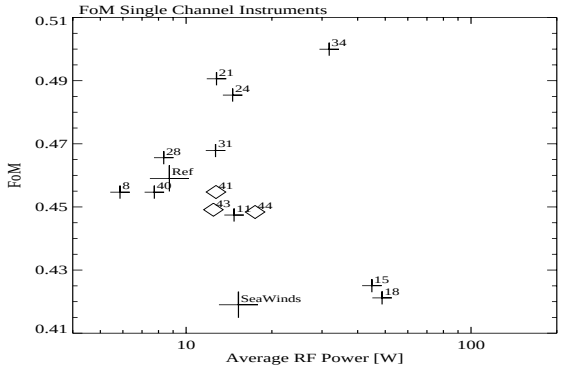


*Figure 50: FoM of single channel instruments as function of average RF power. Crosses and diamonds denote C- and Ku-band respectively. The simulation numbers refer to details given in Table 9.*

In Figure 50, several systems are conspicuous for different reasons. Number 15 and 18 denote simulations of split-beam instruments. It was already noticed that this concept is not suitable for RFSCAT. A remarkably higher FoM is found for simulation numbers 21 and 24 which are related to wide swath (1800 km) low orbit systems. Here the increase in incidence angle provides better performance at a moderate increase in average RF power as compared to the reference RFSCAT. Within the central "cloud" of instruments, minor but noticeable differences are the higher power consumption of Ku-band (41,43, and 44) and of the high resolution C-band (11) systems as well as a slightly higher FoM of the other two wide swath instruments (28 and 31).

| Number | Name | Orbit [km] | Swath [km] | Resolution [km] | PRF [Hz] | FoM | Average RF Power [W] |
|---|---|---|---|---|---|---|---|
| Ref. | | 725 | 1500 | 50 | 239 | 0.459031 | 8.73438 |
| 8 | pcvch1-CV | 725 | 1500 | 50 | 119 | 0.454677 | 5.85938 |
| 11 | pcv3-CV | 725 | 1500 | 25 | 239 | 0.447442 | 14.7344 |
| 15 | pcvch2-CV | 725 | 1500 | 50 | 119 | 0.425041 | 44.8594 |
| 18 | pcvcp2-CV | 725 | 1500 | 50 | 239 | 0.421187 | 48.7344 |
| 21 | pcvch4-CV | 725 | 1800 | 50 | 114 | 0.490590 | 12.7813 |
| 24 | pcvcp4-CV | 725 | 1800 | 50 | 228 | 0.485432 | 14.5625 |
| 28 | pcvch5-CV | 1075 | 1800 | 50 | 86 | 0.465587 | 8.34375 |
| 31 | pcvcp5-CV | 1075 | 1800 | 50 | 172 | 0.467851 | 12.6875 |
| 34 | .pcvch6-CV | 725 | 1800 | 25 | 228 | 0.499969 | 31.7813 |
| 40 | pcvkv1-CV | 725 | 1500 | 50 | 239 | 0.454673 | 7.73437 |
| 41 | pcvkv1-KV | 725 | 1500 | 50 | 239 | 0.454727 | 12.7344 |
| 43 | pkv1-KV | 725 | 1500 | 50 | 239 | 0.449124 | 12.4668 |
| 44 | pkvkh1-KV | 725 | 1500 | 50 | 119 | 0.448398 | 17.4668 |

*Table 9: Details of the simulations of the single channel instruments shown in Figure 50.*

### *5.2. Dual Polarization/Frequency Instruments*

These instruments are derived from combinations of single channels systems already shown in the previous section. Figure 51 summarizes their performances. The picture is very similar to single-channel instruments. The following system can clearly be differentiated: again the split-beam system (17) performs worst, the Ku-band (46) and the high-resolution C-band (36) instruments requires the most RF power. Both wide-swath instruments (23 & 36) again have the highest FoM. The other systems including the combination of C- and Ku-band (42) are close together, thus is not possible from these simulation to judge on these small differences.

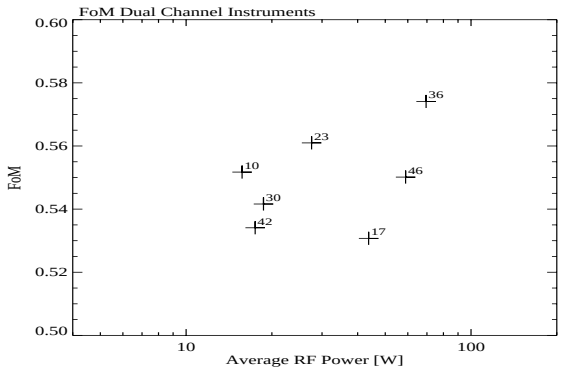


*Figure 51: FoM of dual channel instruments as function of average RF power. The simulation numbers refer to details given in Table 10.*

| Number | Name | Orbit [km] | Swath [km] | Resolution [km] | PRF [Hz] | FoM | Average RF Power [W] |
|---|---|---|---|---|---|---|---|
| 10 | pcvch1-CV&CH | 725 | 1500 | 50 | 119 | 0.551733 | 15.7187 |
| 17 | pcvch2-CV&CH | 725 | 1500 | 50 | 119 | 0.530732 | 43.7188 |
| 23 | pcvch4-CV&CH | 725 | 1800 | 50 | 114 | 0.560985 | 27.5624 |
| 30 | pcvch5-CV&CH | 1075 | 1800 | 50 | 86 | 0.541615 | 18.6875 |
| 36 | pcvch6-CV&CH | 725 | 1800 | 25 | 114 | 0.574103 | 69.5624 |
| 42 | pcvkv1-CV&KV | 725 | 1500 | 50 | 239 | 0.534081 | 17.4688 |
| 46 | pkvkh1-KV&KH | 725 | 1500 | 50 | 114 | 0.550143 | 58.9336 |

*Table 10: Details of the simulations of the dual channel instruments shown in Figure 51.*

### *5.3. Polarimetric Instruments*

The systems with the best performance in this comparison are polarimetric instruments. Although their FoM are close together, Figure 52 reveals some differences between them. Again the split-beam (20) performs worst. The two fully polarimetric systems (14 and 27) require less RF power as the semi-polarimetric systems (13,26, and 33) for the same performance which is due to the significant gain in performance at lower RF power from the HH-polarization channel. For these instruments larger incidence angles are not that important, therefore the wide swath instrument (27) does not perform better than the standard system (14), but require more RF power due to the lower signal level at higher incidence angles with the gain of a wider coverage.

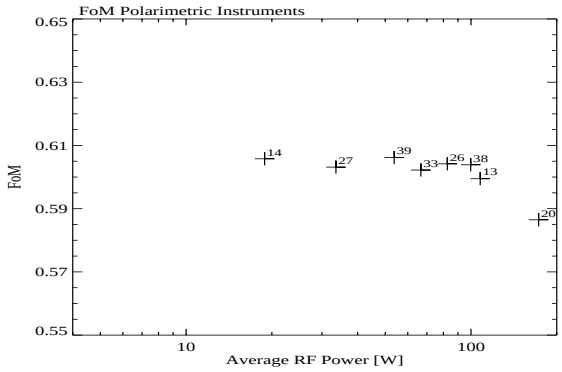


*Figure 52: FoM of polarimetric instruments as a function of average RF power. The simulation numbers refer to details given in Table 11.*

| Number | Name | Orbit [km] | Swath [km] | Resolution [km] | PRF [Hz] | FoM | Average RF Power [W] |
|---|---|---|---|---|---|---|---|
| 13 | pcv3-CV&CP | 725 | 1500 | 25 | 239 | 0.599477 | 107.734 |
| 14 | pcfp-CF | 725 | 1500 | 50 | 119 | 0.605762 | 18.8594 |
| 20 | pcvcp2-CV&CP | 725 | 1500 | 50 | 239 | 0.586467 | 172.734 |
| 26 | pcvcp4-CV&CP | 725 | 1800 | 50 | 228 | 0.604185 | 82.5625 |
| 27 | pcvcp4-CF | 725 | 1800 | 50 | 114 | 0.603142 | 33.5625 |
| 33 | pcvcp5-CV&CP | 1075 | 1800 | 50 | 172 | 0.602215 | 66.6875 |
| 38 | pcfp6-CV&CP | 725 | 1800 | 25 | 228 | 0.603883 | 99.7812 |
| 39 | pcfp6-CFP | 725 | 1800 | 25 | 114 | 0.606188 | 53.7812 |

*Table 11: Details of the simulations of the polarimetric instruments shown in Figure 52.*

# 6. Recommendations

Presently, we cannot present the ultimate rotating fan-beam scatterometer since the number of constraints in system design is fairly high and not all of them could be considered in this study. However from the analysis, the following recommendations can be given.

The systems are discussed in order of their technical complexity:

**A simple system** would be a C-band VV-polarization scatterometer based on known components. The simulations show clearly that large incidence angles are desired. Therefore, it is no alternative to increase the orbit height in order to save RF power by decreasing the maximum incidence angle. As shown by the system number 21 in Figure 50, a significant improvement in performance can be gained at moderate cost in RF power by increasing the incidence angle by 4 degrees. Furthermore, the swath width is increased by 20% as well. From Figure 49, it can be seen that this instrument has a similar performance as ERS for the portion of the swath covered by ERS as well. However at the outer swath, this system will not achieve the performance of ASCAT.

**An intermediate system** will carry an additional HH-polarization channel. Here the same argument on measurement geometry apply as for the simple system. From Figure 49, it can be seen that such a system can compete in performance with ASCAT and provides more information around the satellite ground track.

**A complex system** will be a polarimetric fan-beam instrument. However, the simulations are based on a theoretical GMF which still requires further experimental evidence at C-band. There will be serious technical complexity to be solved. But even at moderate cost for RF power a significant gain in wind retrieval can be achieved.

It was shown that from a certain point of instrument performance (SNR), the wind retrieval limits the performance of the RFSCAT. This is partly due to the geophysical noise within the resolution cell, caused by the wind variability within this cell, and partly due to the method applied for wind retrieval.

Further investment for improving these techniques will be the cheapest way of gaining performance.

## 7. References

Lin, C.-C., B. Rommen, J.J.W.Wilson, F. Impagnatiello, and P.S.Park, An analysis of a rotating, range-gated, fanbeam spaceborne scatterometer concept, IEEE Transactions on Geoscience and Remote Sensing, Vol.38, No.5, 2114-2121.

Lungu, T., Editor., QuikSCAT science data product user's manual – Version 2.2, Jet Propulsion Laboratory, D18053, December 2001.

Spencer, M.W., C. Wu, and D. G. Long, Improved resolution backscatter measurements with the SeaWinds pencil beam scatterometer, IEEE Transactions on Geoscience and Remote Sensing, Vol.38, No.1, 89-104, 2000.

Tsai, W.-Y., S.V. Nghiem, J.N. Huddleston, M.W. Spencer, B.W. Stiles, and R.D. West, Polarimetric scatterometry: a promising technique for improving ocean surface wind measurements from space, IEEE Transactions on Geoscience and Remote Sensing, Vol.38, No.4, 1903-1921, 2000.

Yueh, S.H., W. J .Wilson, and S. Dinardo, Polarimetric radar remote sensing of ocean surface wind, IEEE Transactions on Geoscience and Remote Sensing, Vol.40, No.4, 793-800, 2002.

## 8. Annex A – FoM for Range and Pulse Skip Factors

The following table summarizes the graphs of the quality index versus node number for various settings of the Range and Pulse Skip factors in the simulation of the baseline instrument. The settings for Range Skip (first number) and Pulse Skip (second number) are indicated below the graphs.

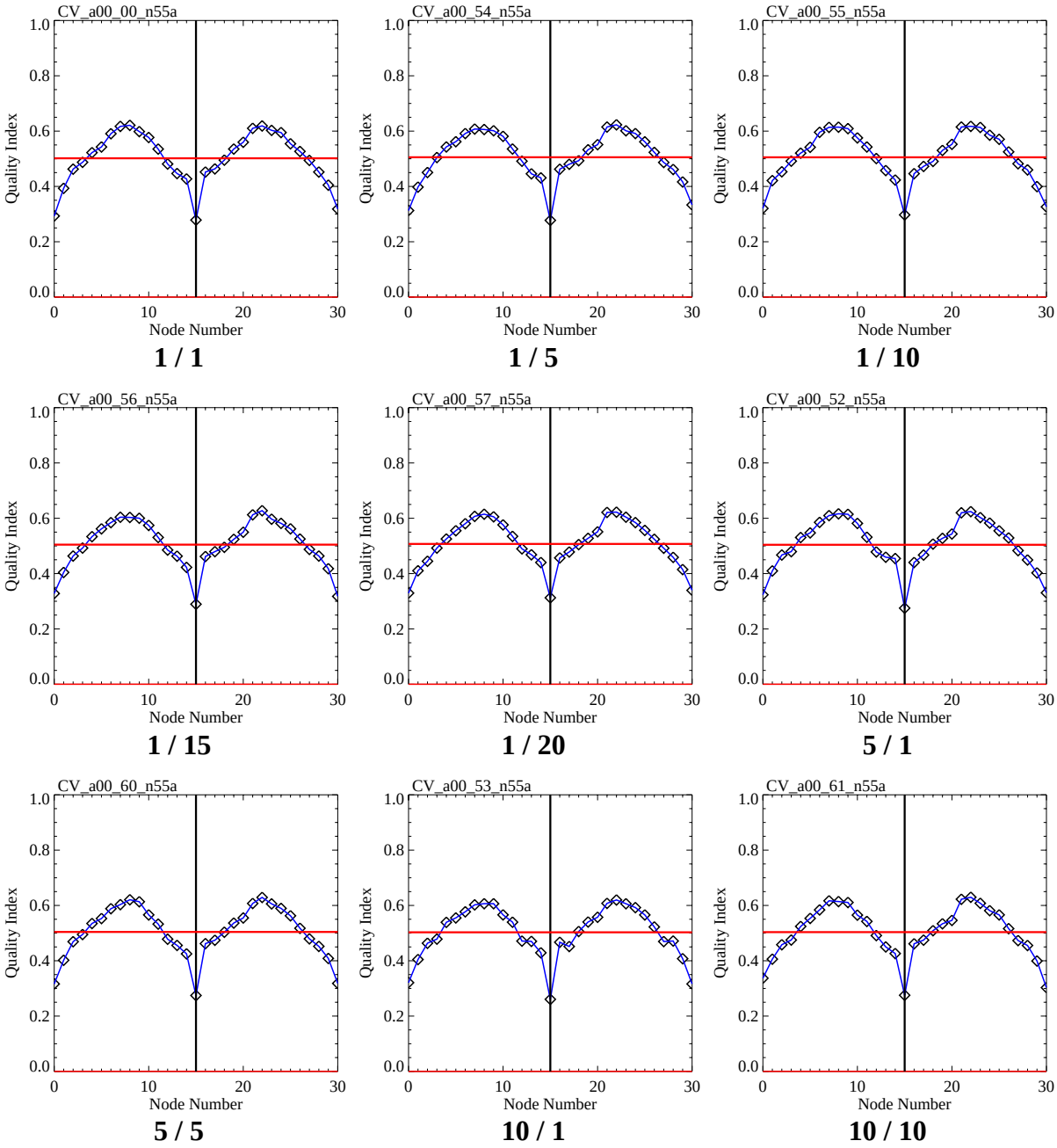


**1 / 1** **1 / 5** **1 / 10**

**1 / 15** **1 / 20** **5 / 1**

**5 / 5** **10 / 1** **10 / 10**

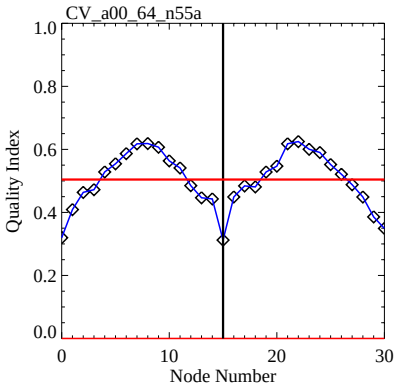


**10 / 20**

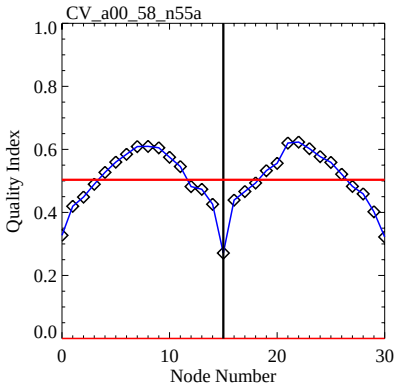


**15 / 1**

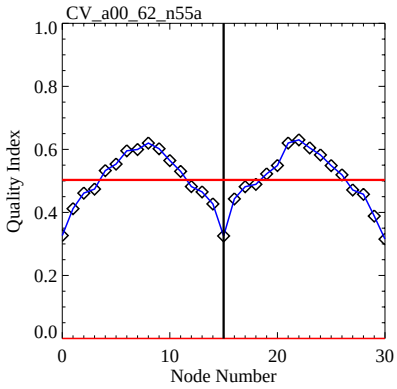


**15 / 15**

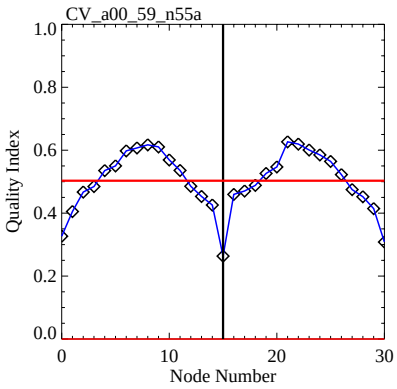


**20 / 1**

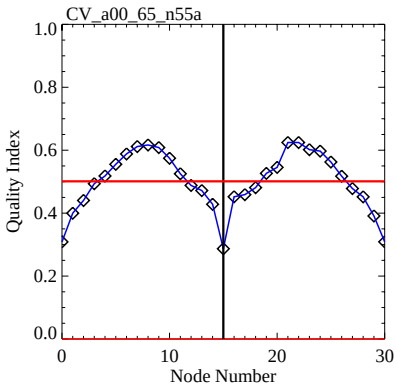


**20 / 10**

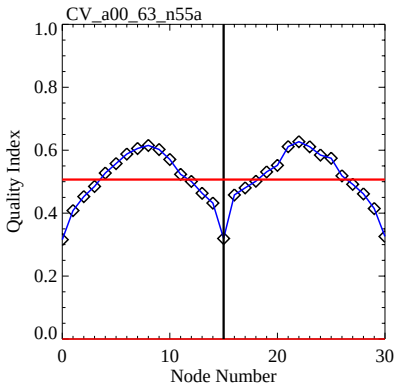


**20 /20**

## 9. Annex B – FoM versus Pulse Peak Power

The following table summarizes the graphs of the quality index versus node number for various settings of the pulse peak power for the baseline instrument. The power setting is indicated below the graphs.

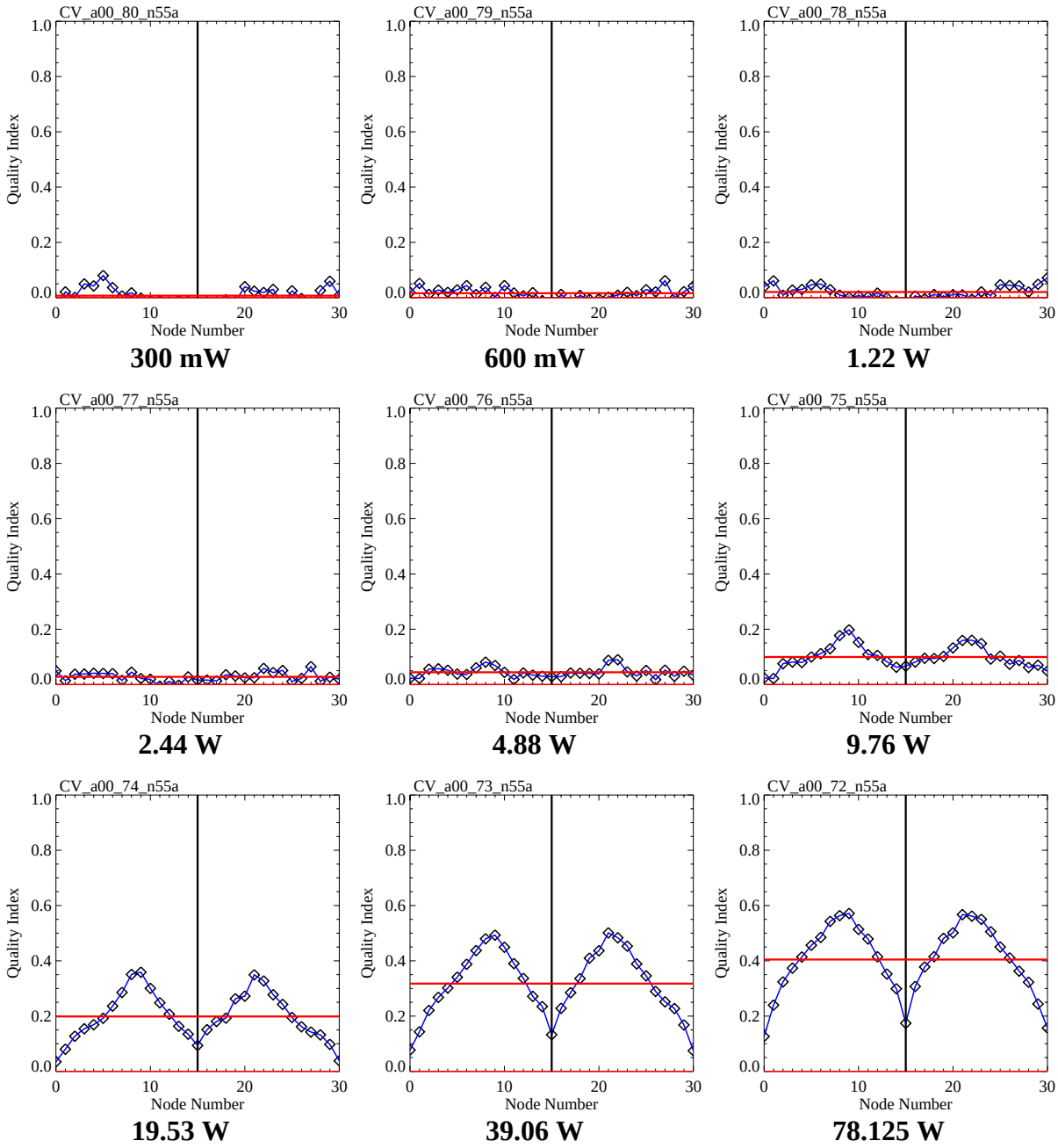


**300 mW** **600 mW** **1.22 W**

**2.44 W** **4.88 W** **9.76 W**

**19.53 W** **39.06 W** **78.125 W**

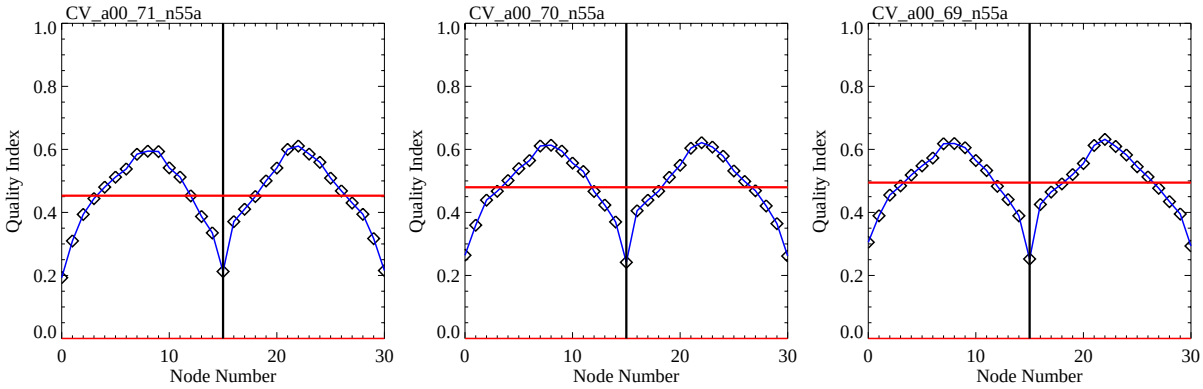


**156.25 W** **312.5 W** **625 W**

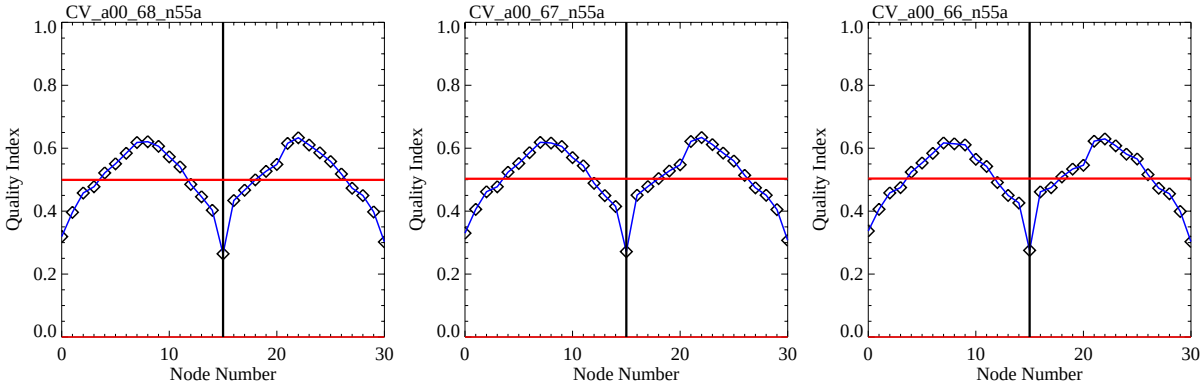


**1250 W** **2500 W** **5000 W**

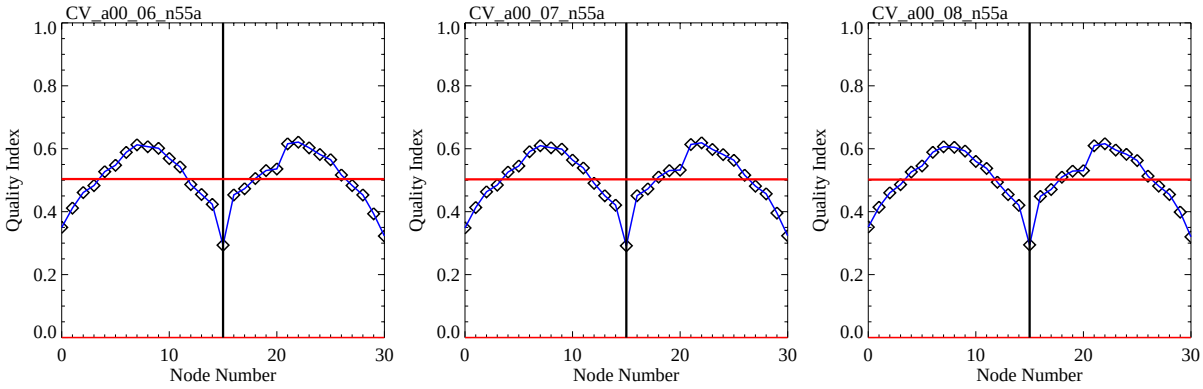


**10 KW** **20 KW** **40 KW**

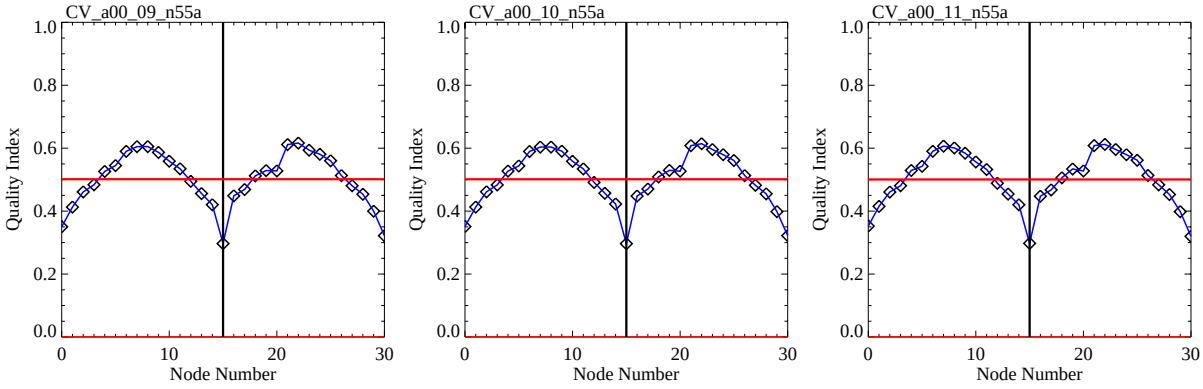


**80 KW** **160 KW** **320 KW**

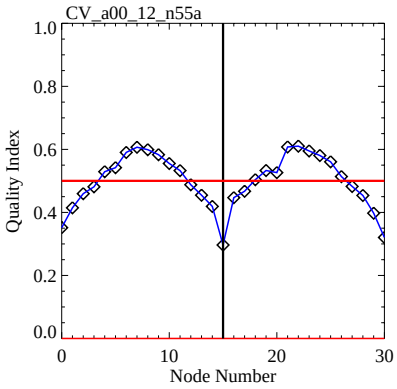


**640 KW**

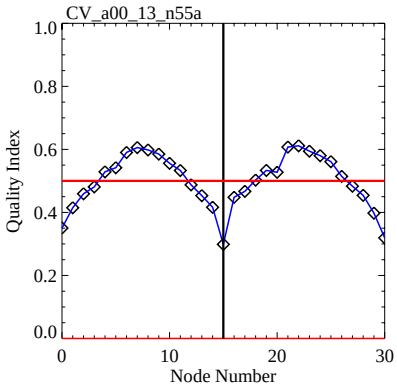


**1.28 MW**

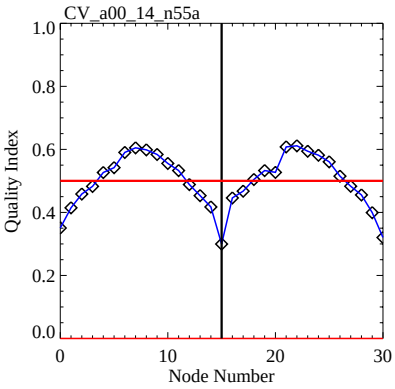


**2.56 MW**

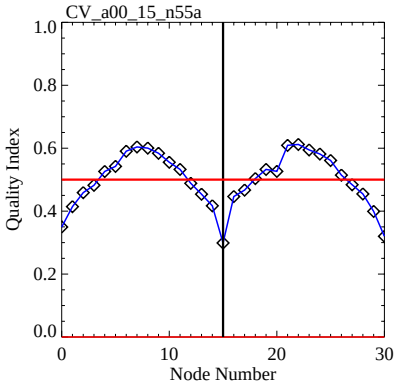


**5.12 MW**

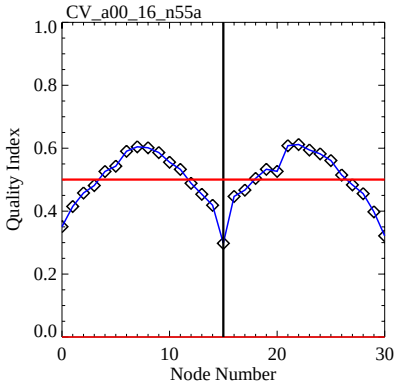


**10.24 MW**

## 10. Annex C – FoM versus Antenna Scan Rate

The following table summarizes the graphs of the quality index versus node number for various settings of the antenna scan rate and pulse peak power in the simulation of the baseline instrument. The setting for antenna scan rate is indicated below the graphs varies with line while the pulse peak power constant for each column. The spatial resolution is 50 km.

| Pulse Peak Power | 39 W | 78 W | 156 W |
|---|---|---|---|
| 0.3 rpm | 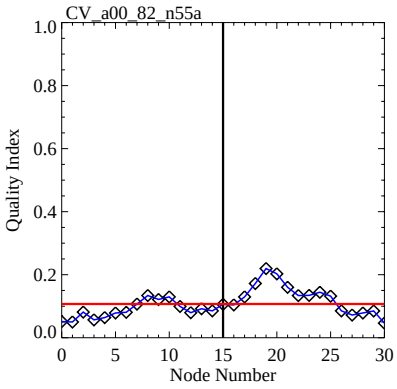 | 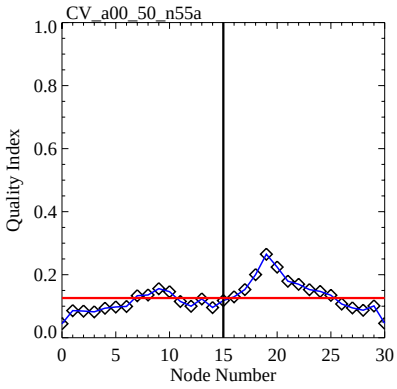 | 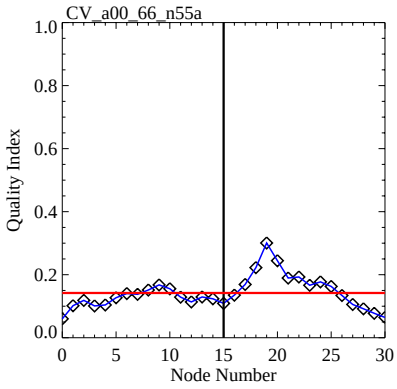 |
| 0.6 rpm | 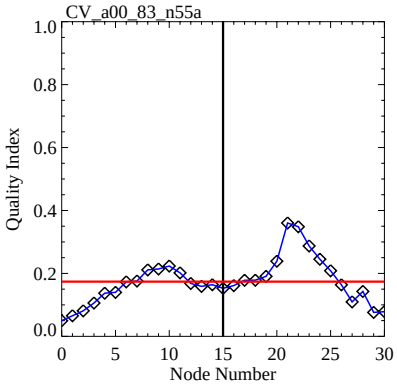 | 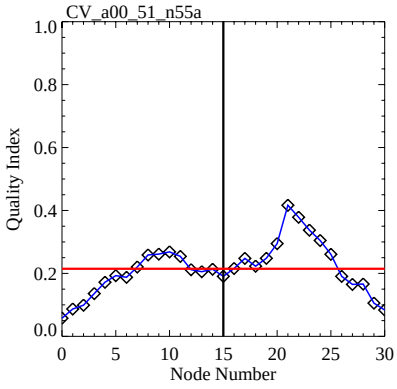 | 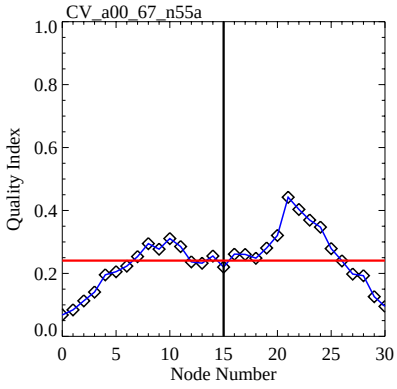 |
| 0.9 rpm | 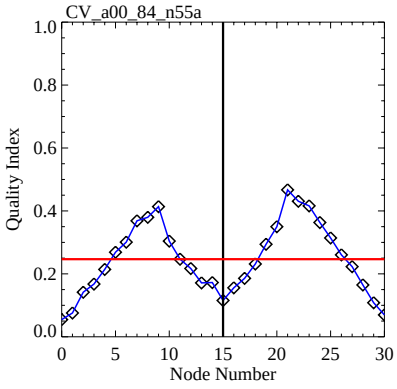 | 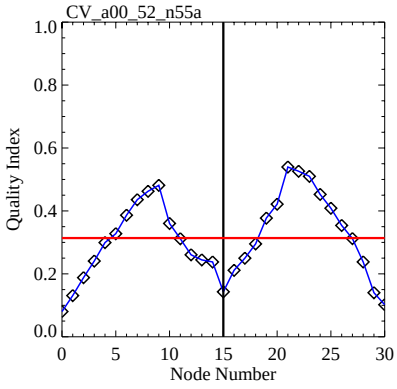 | 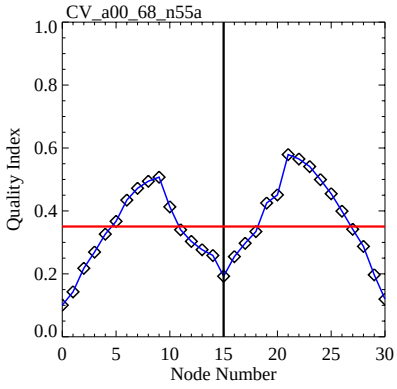 |

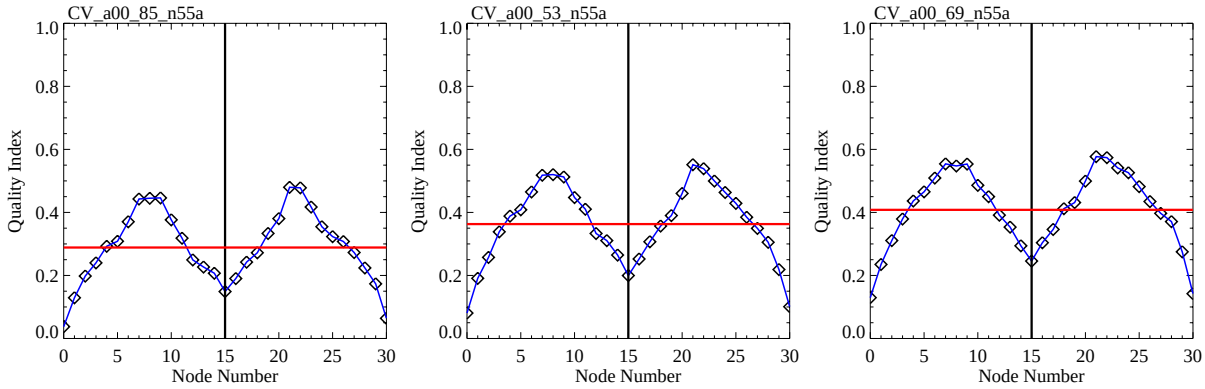


**1.2 rpm**

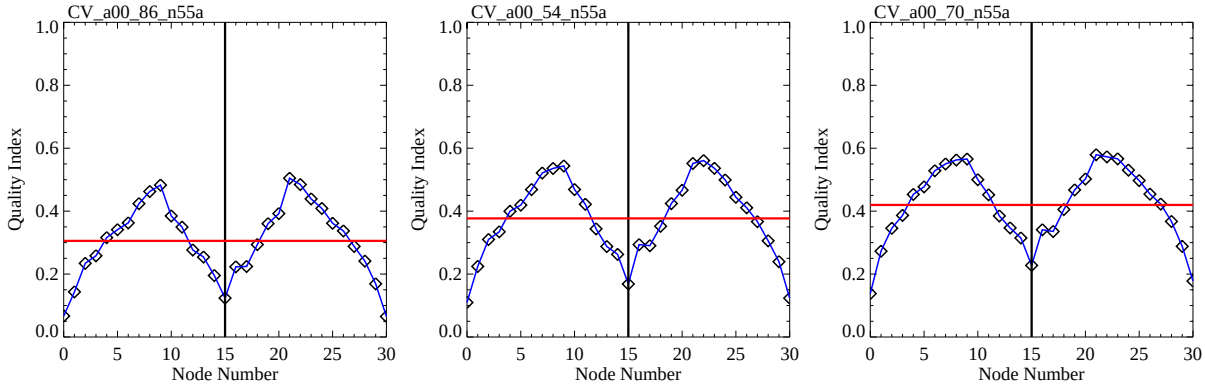


**1.5 rpm**

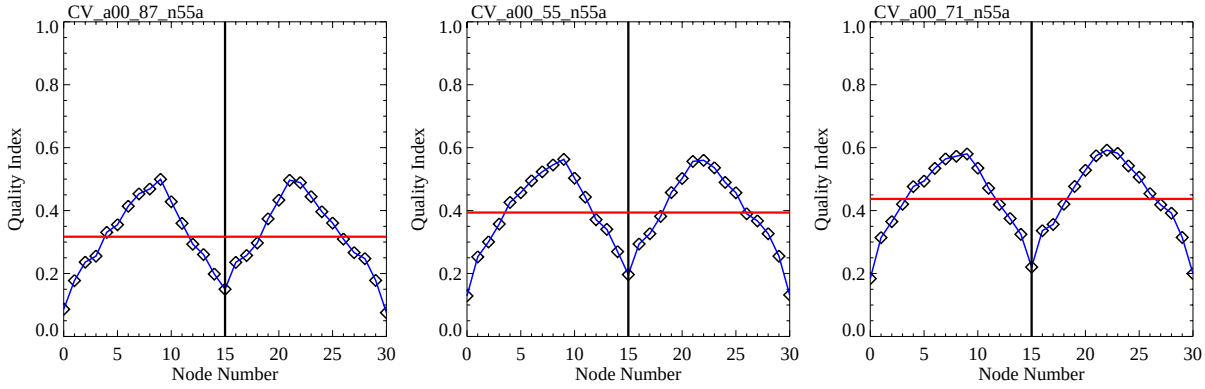


**2.0 rpm**

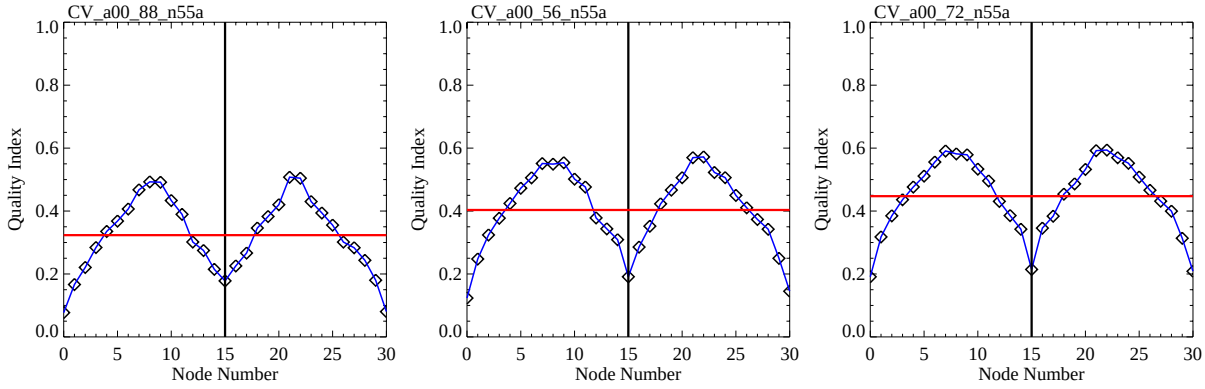


**2.5 rpm**

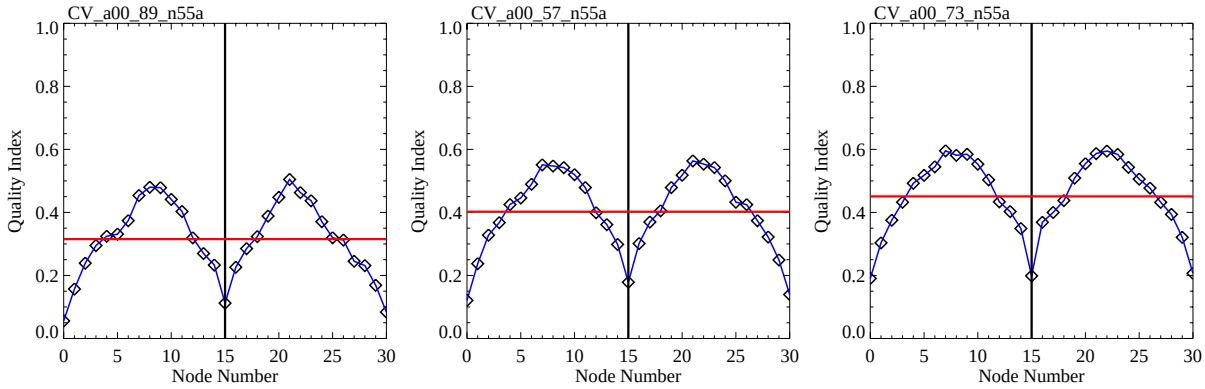


**3.0 rpm**

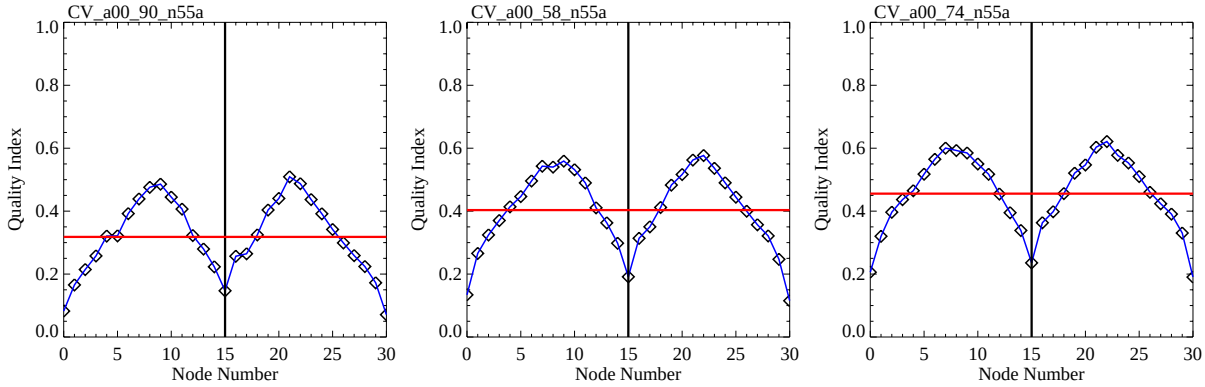


**3.5 rpm**

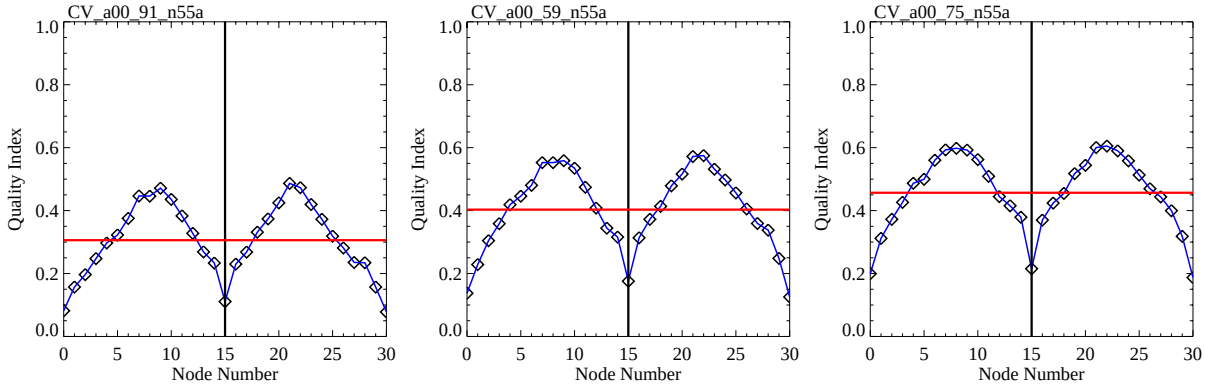


**4.0 rpm**

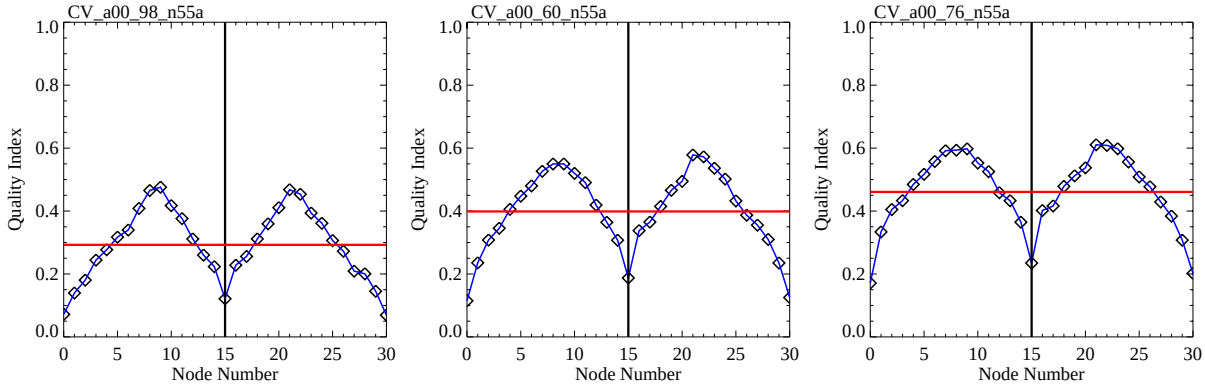


**5.0 rpm**

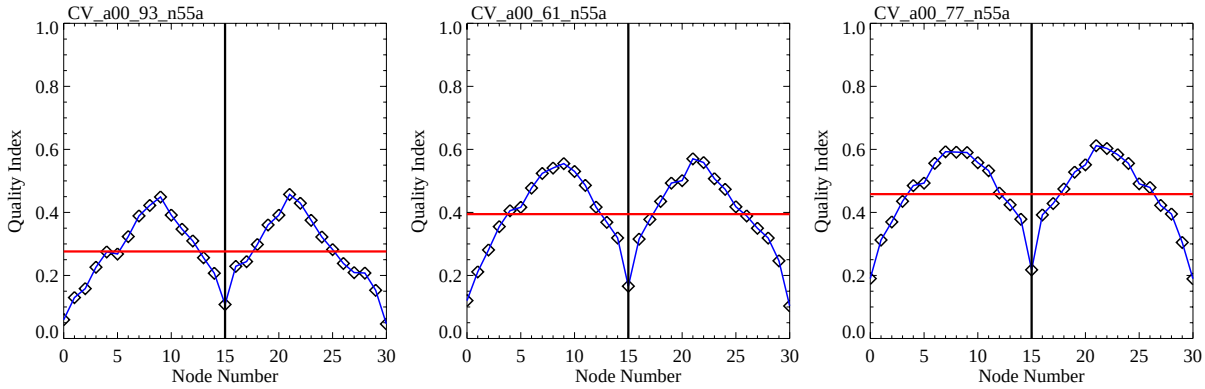


**6.0 rpm**

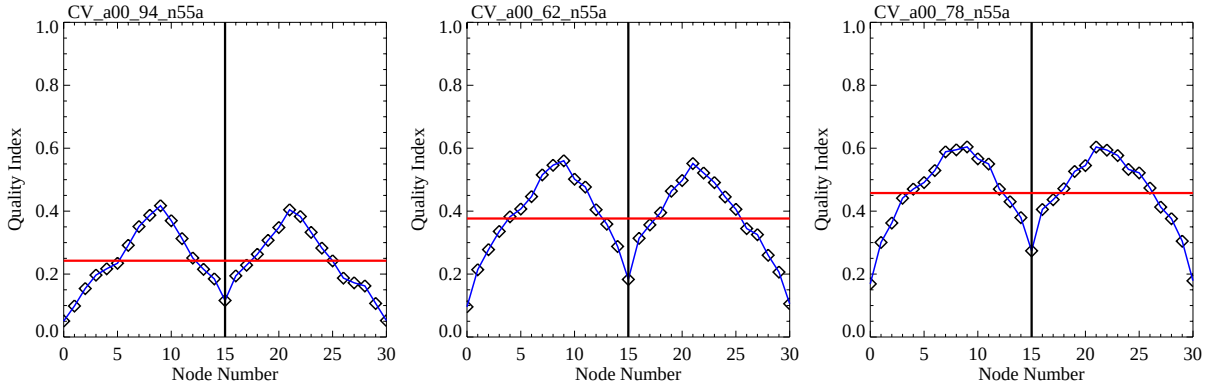


**8.0 rpm**

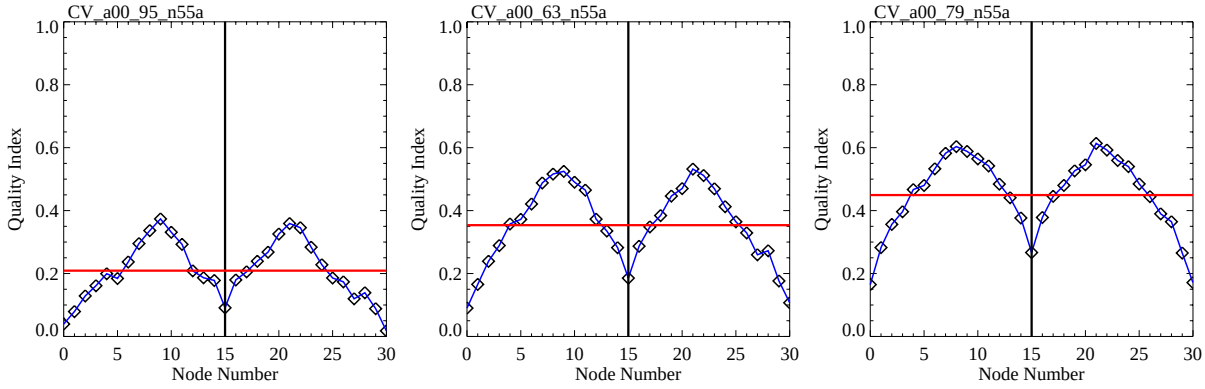


**10 rpm**

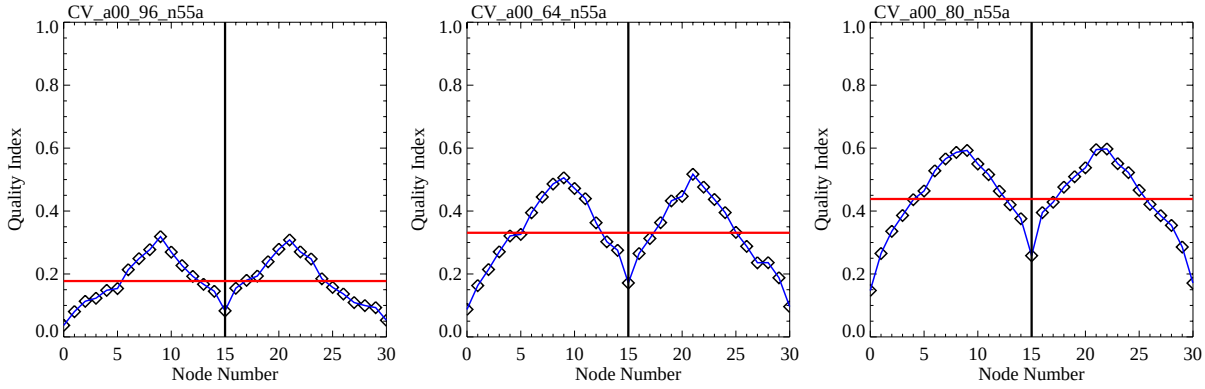


**12 rpm**

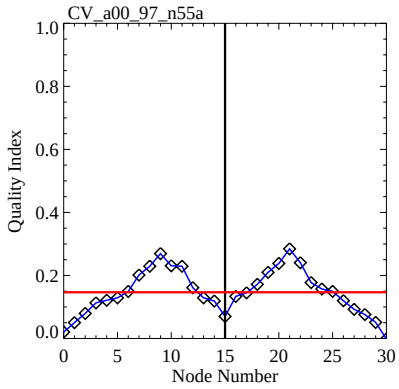


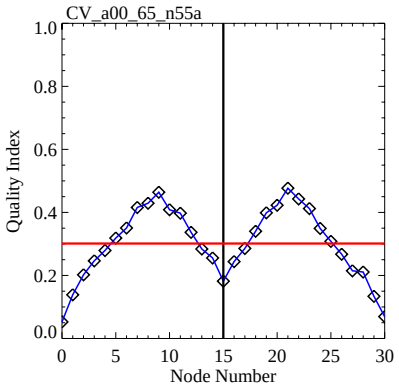


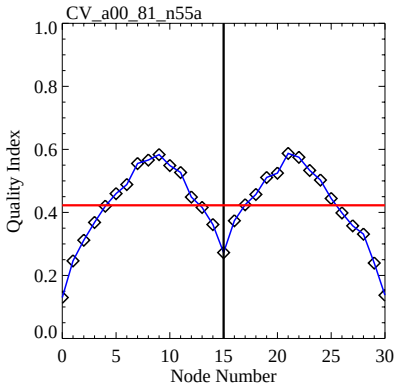


**14 rpm**

**Pulse Peak Power 312 W** **625 W** **2500 W**

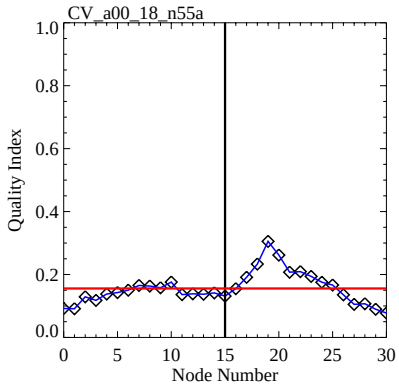


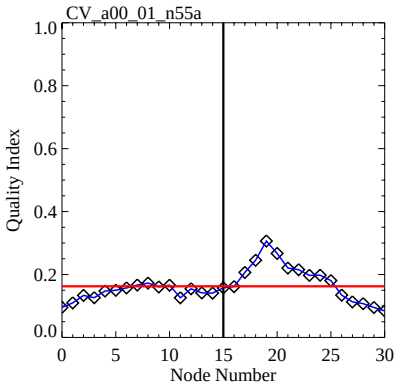


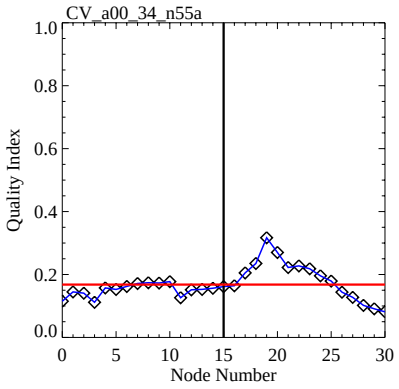


**0.3 rpm**

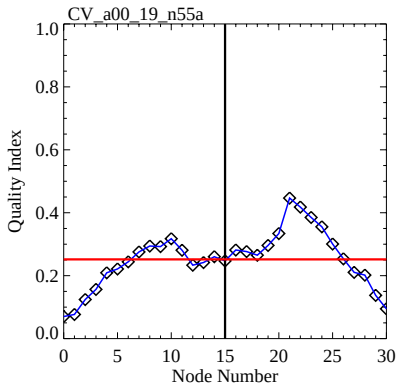


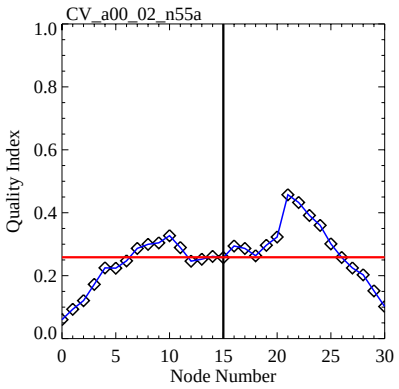


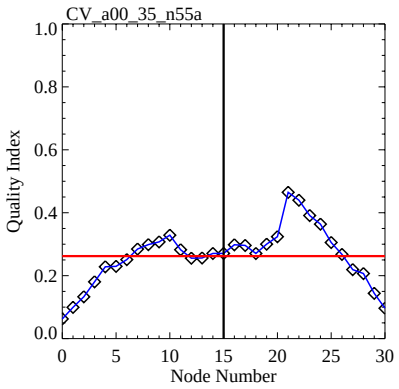


**0.6 rpm**

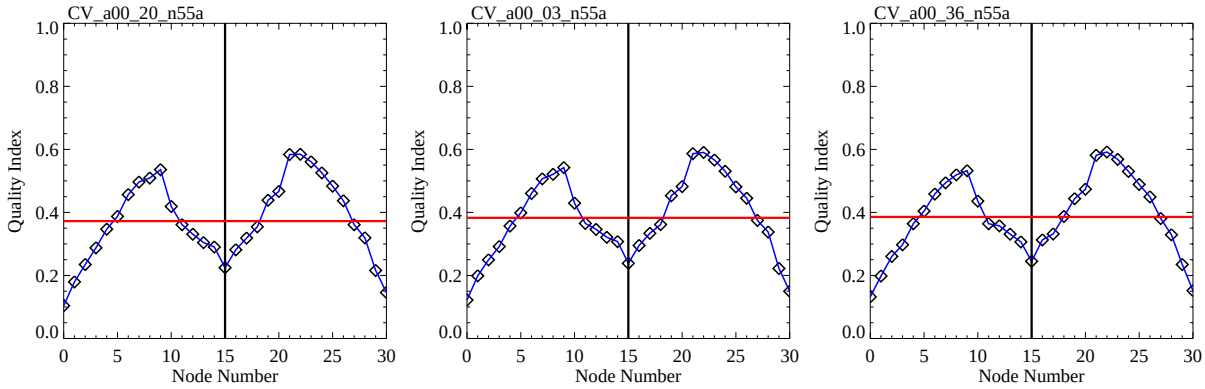


**0.9 rpm**

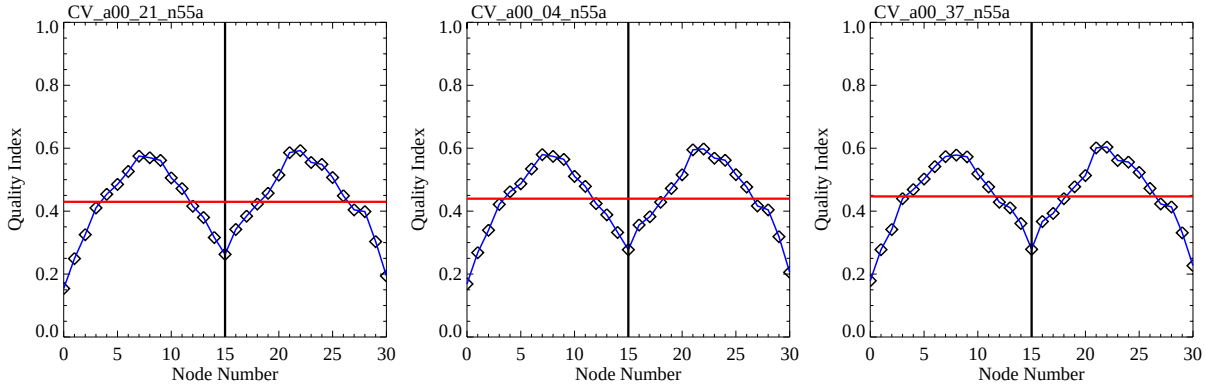


**1.2 rpm**

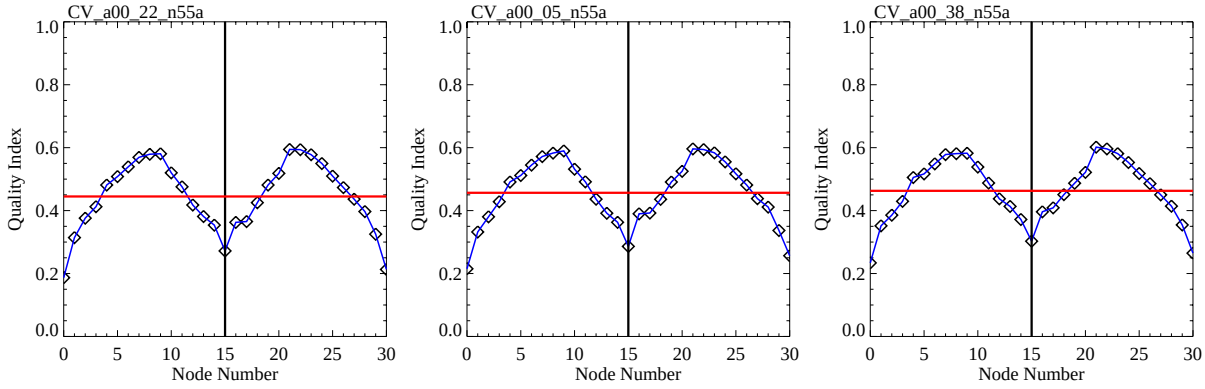


**1.5 rpm**

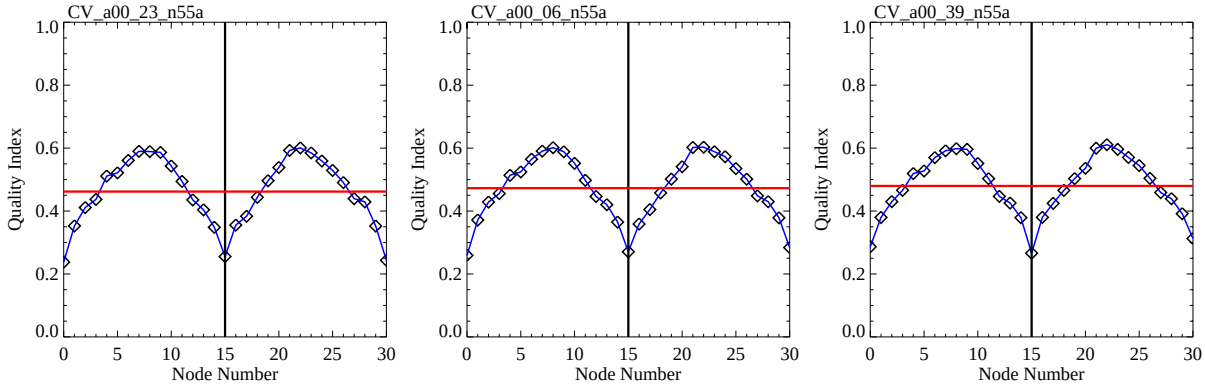


**2.0 rpm**

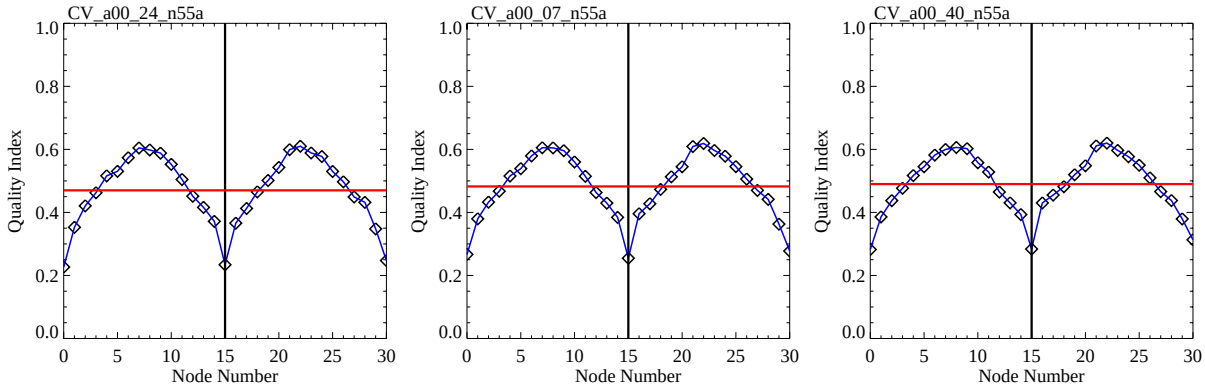


**2.5 rpm**

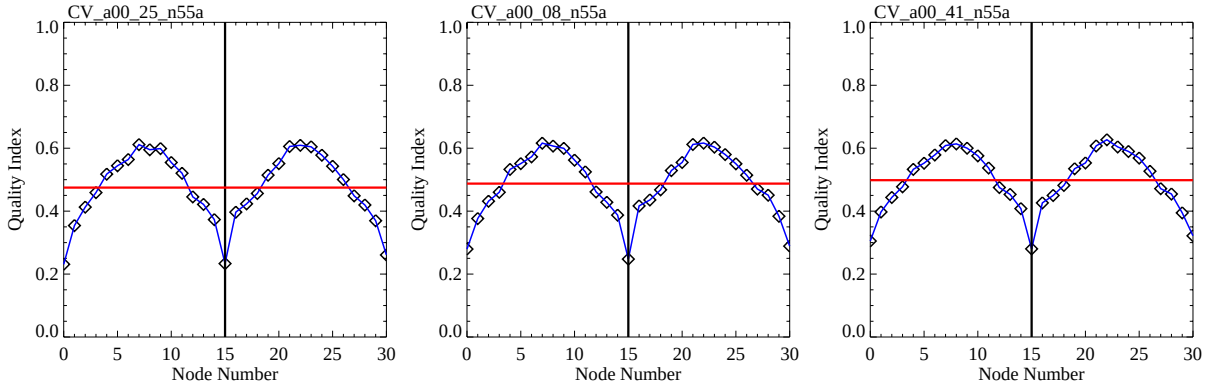


**3.0 rpm**

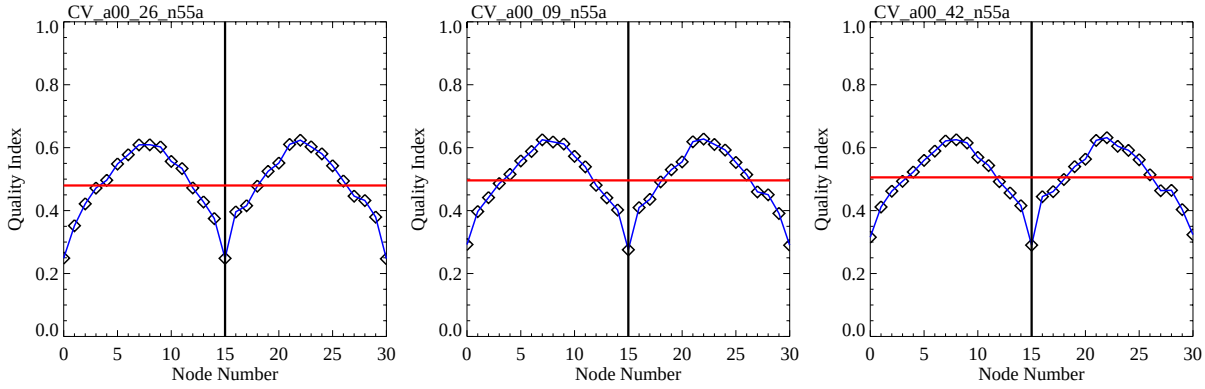


**3.5 rpm**

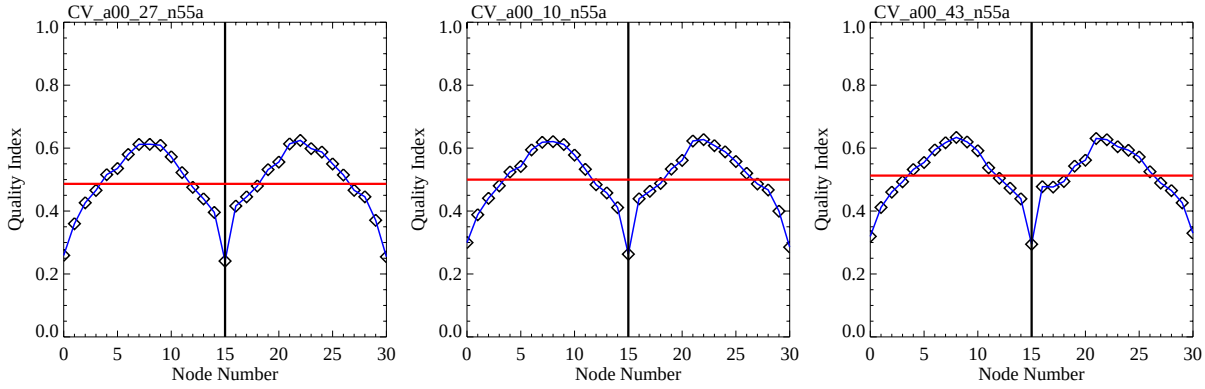


**4.0 rpm**

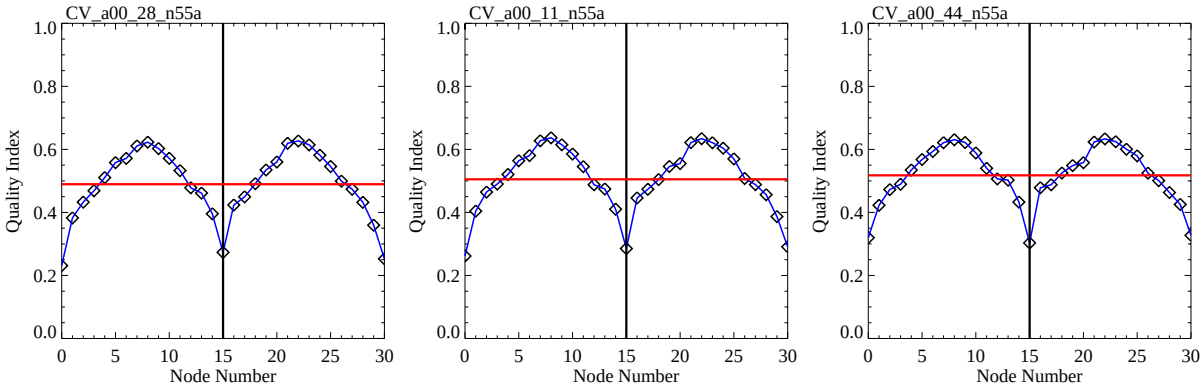


**5.0 rpm**

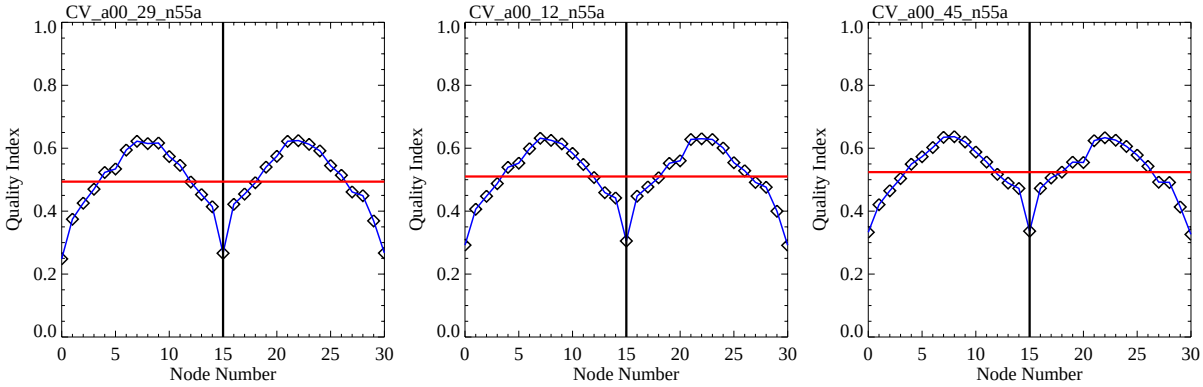


**6.0 rpm**

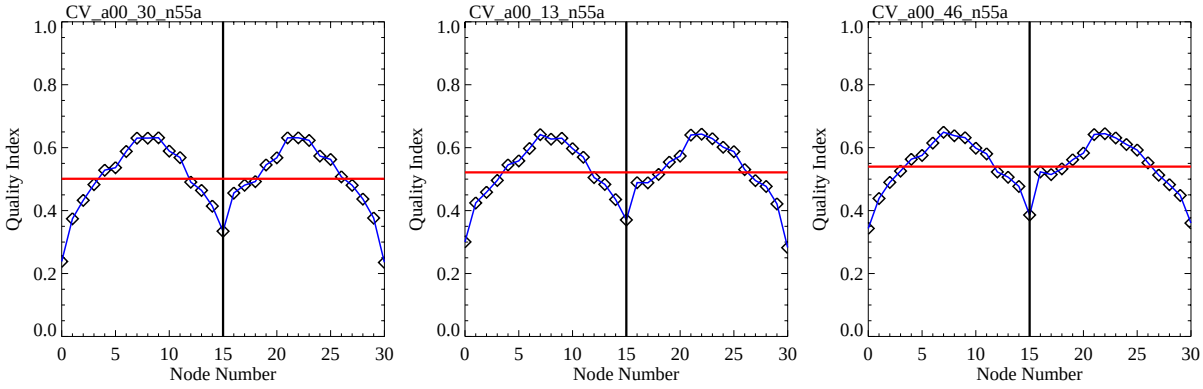


**8.0 rpm**

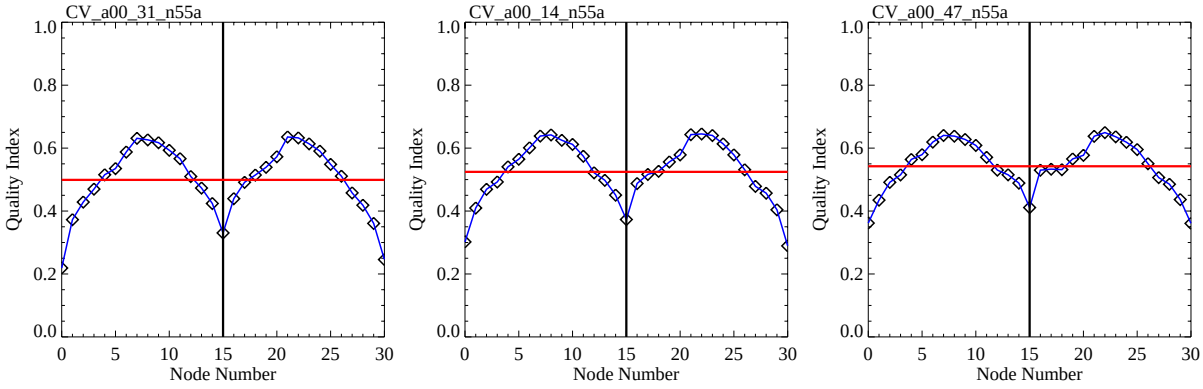


**10 rpm**

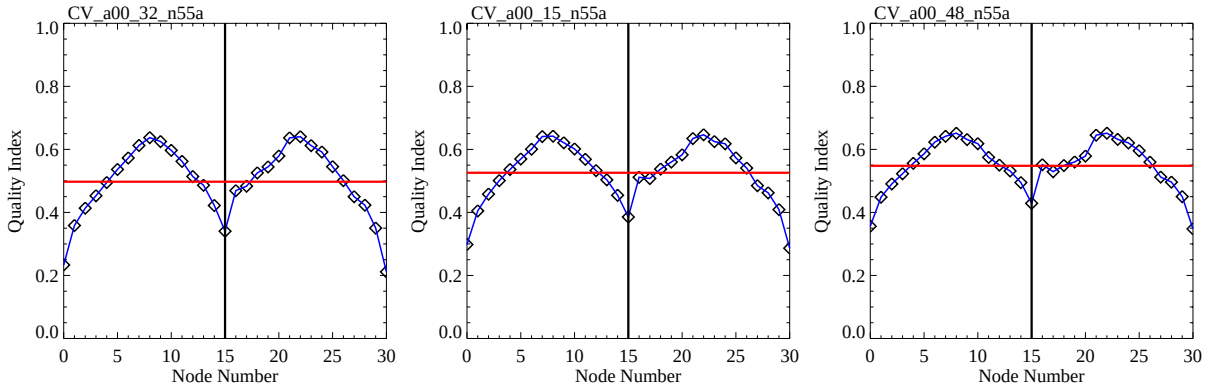
CV_a00_32_n55a
CV_a00_15_n55a
CV_a00_48_n55a
Quality Index
Node Number

**12 rpm**

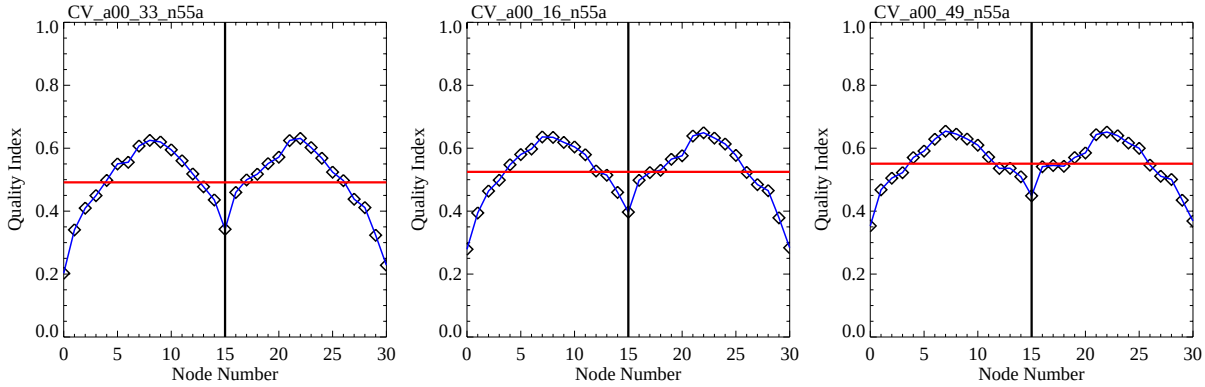
CV_a00_33_n55a
CV_a00_16_n55a
CV_a00_49_n55a
Quality Index
Node Number

**14 rpm**

## Spatial Resolution 25 km

**Pulse Peak Power 39 W** **78 W** **156 W**

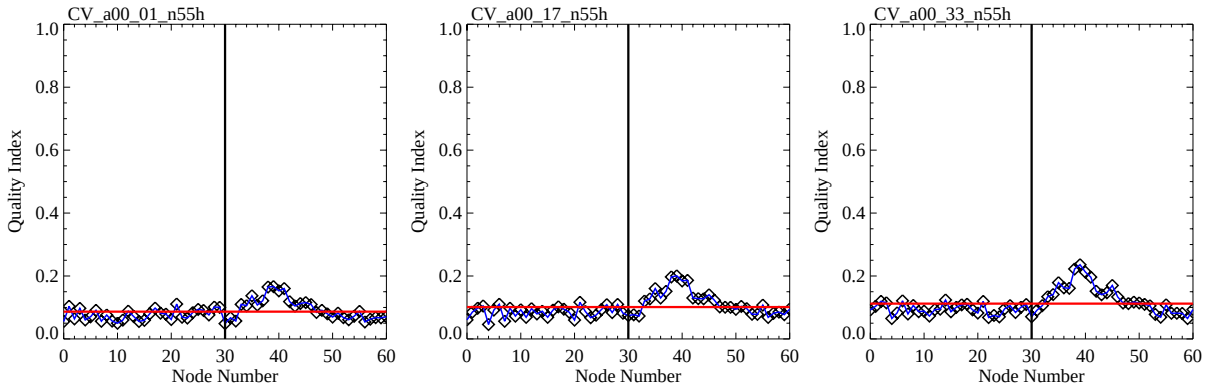


**0.3 rpm**

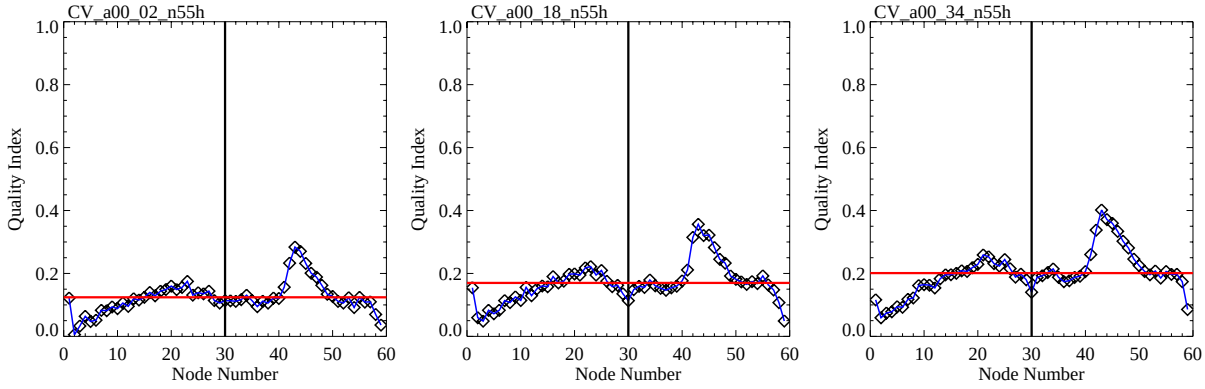


**0.6 rpm**

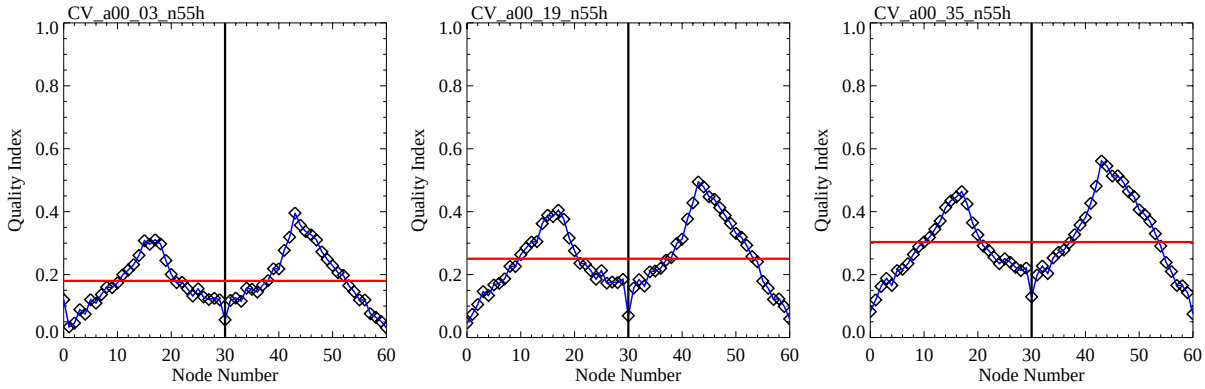


**0.9 rpm**

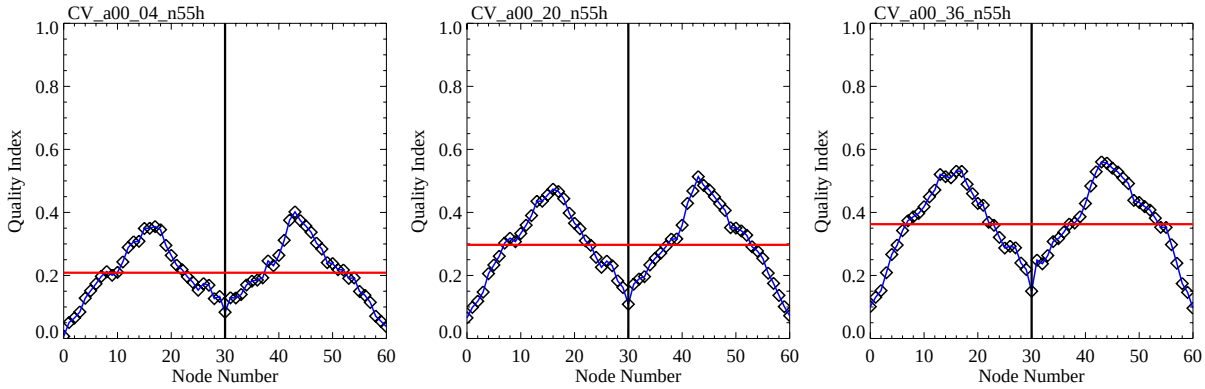


**1.2 rpm**

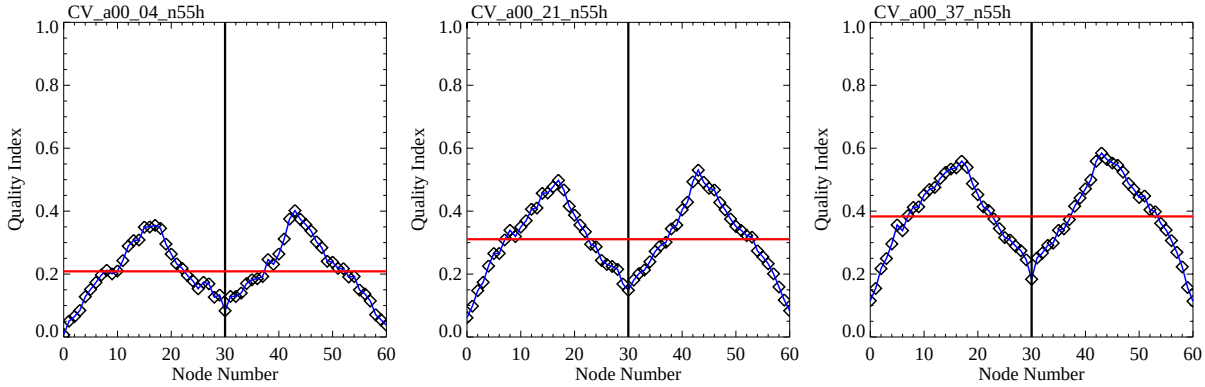


**1.5 rpm**

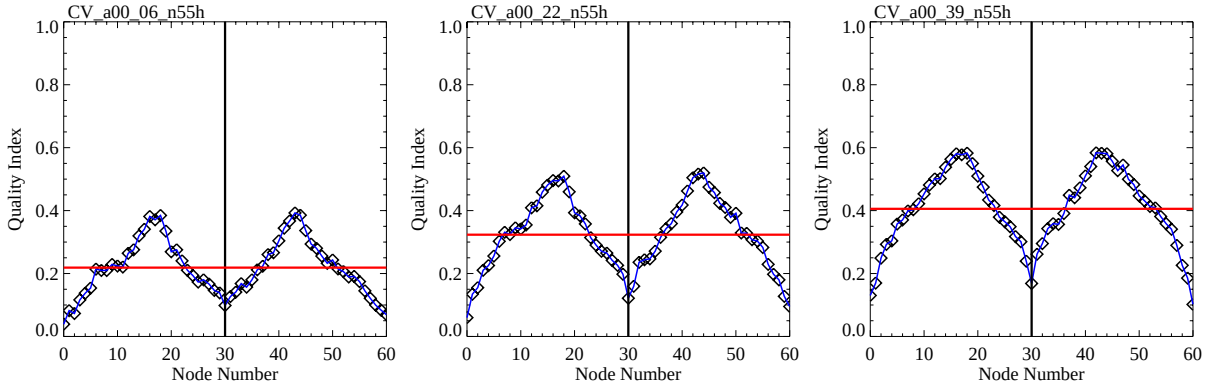


**2.0 rpm**

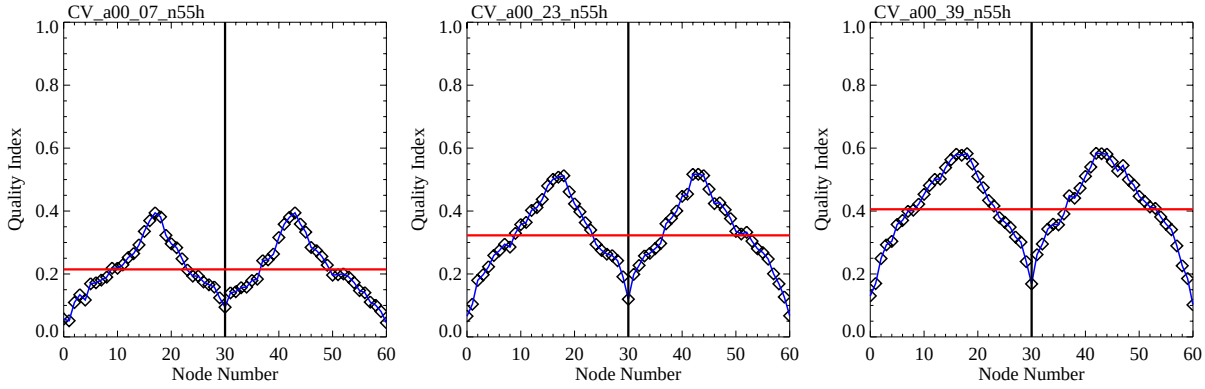


**2.5 rpm**

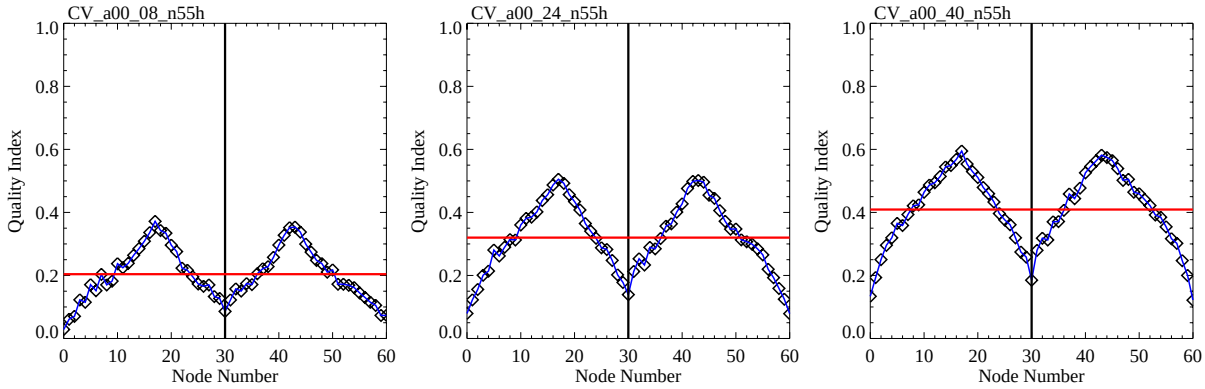


**3.0 rpm**

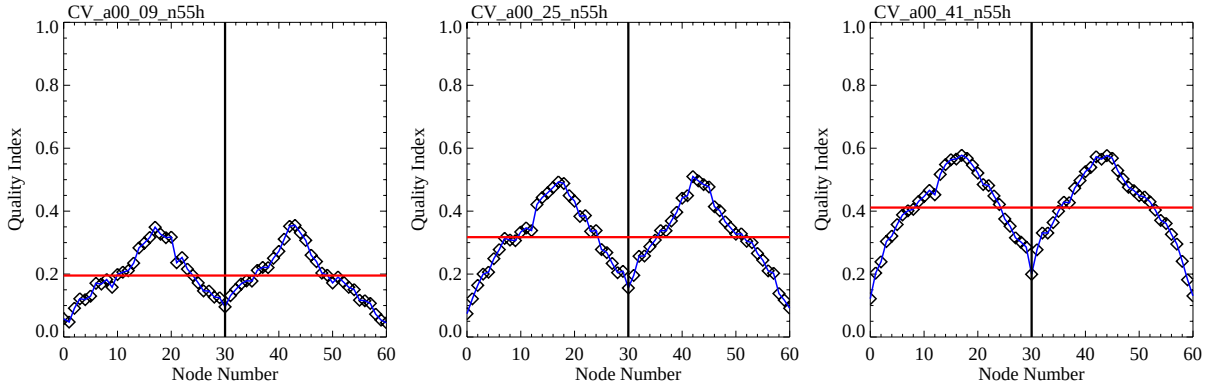


**3.5 rpm**

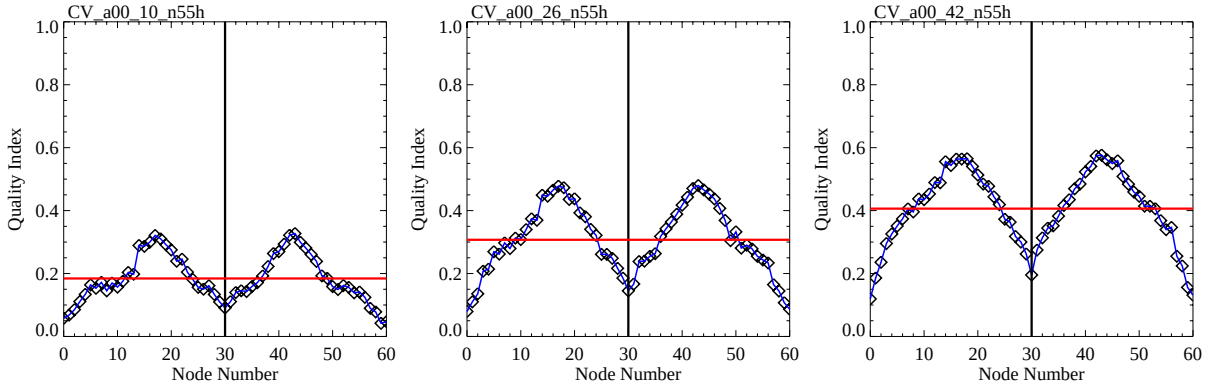


**4.0 rpm**

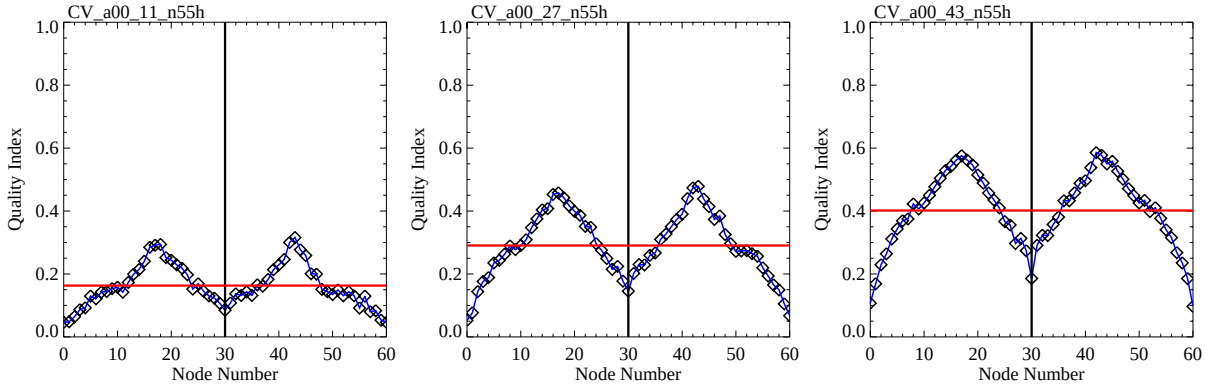


**5.0 rpm**

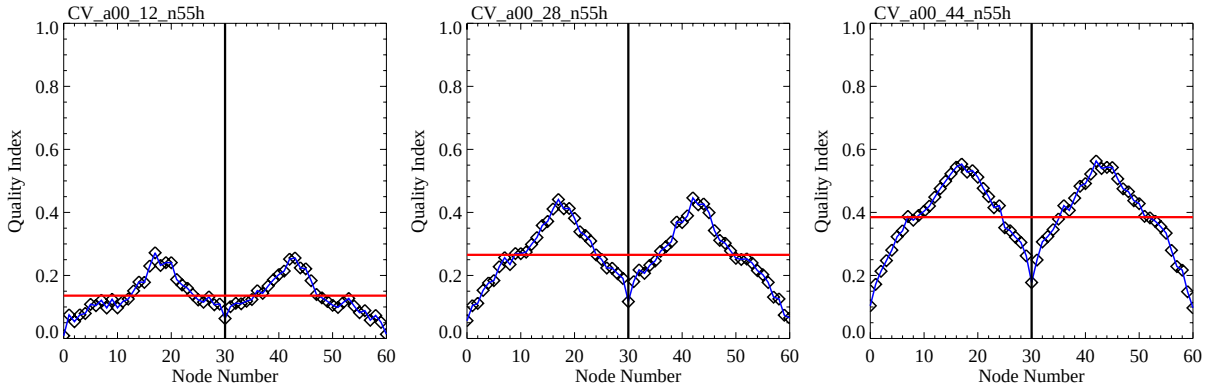


**6.0 rpm**

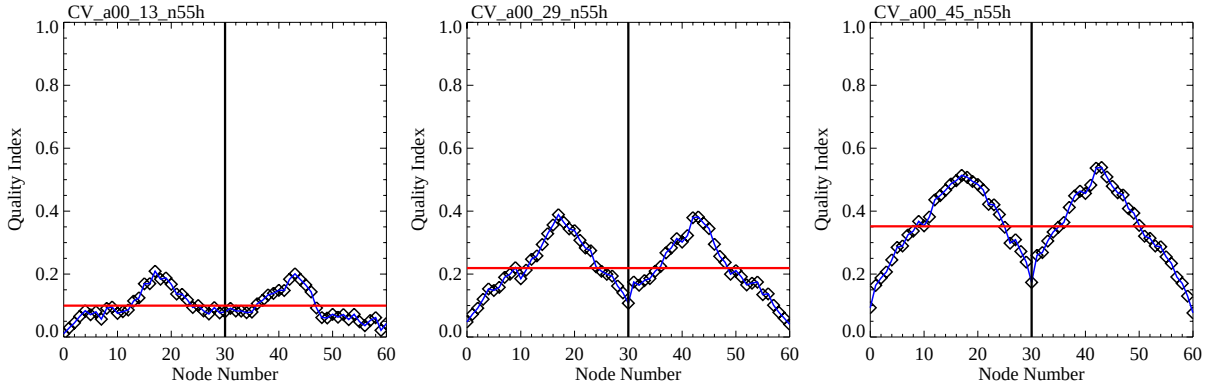


**8.0 rpm**

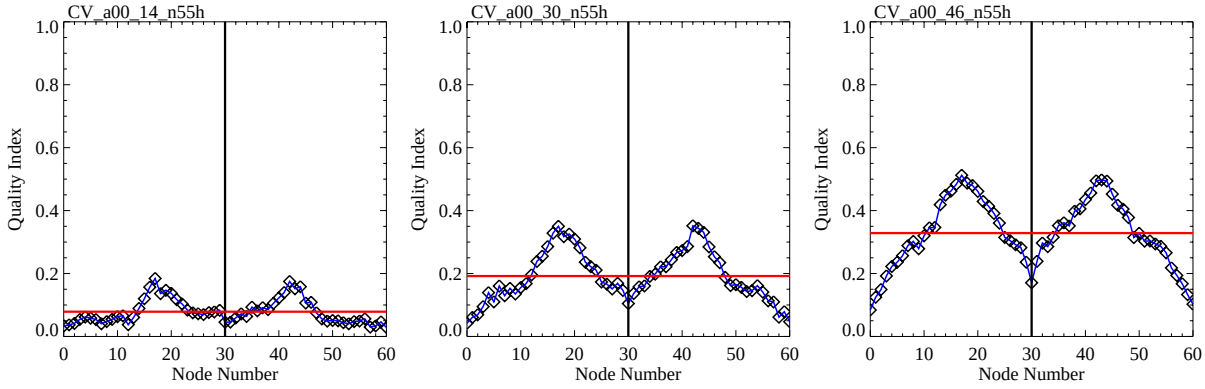


**10 rpm**

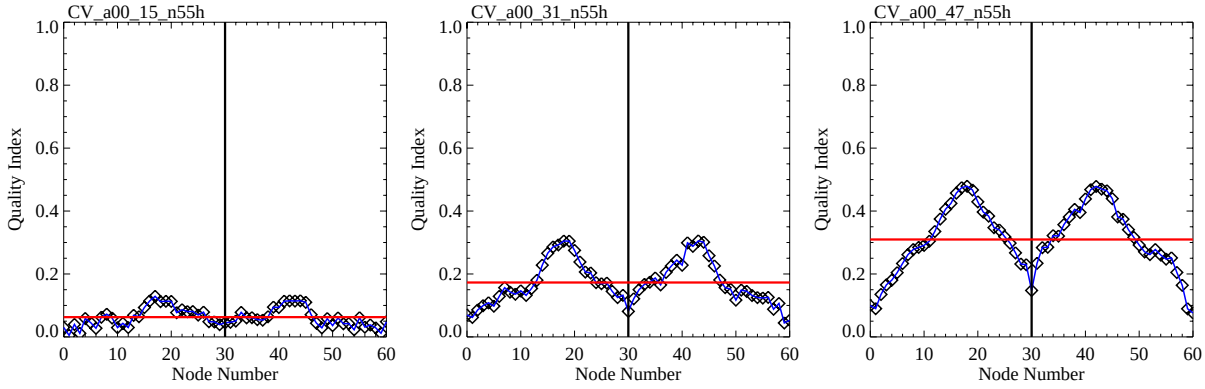


**12 rpm**

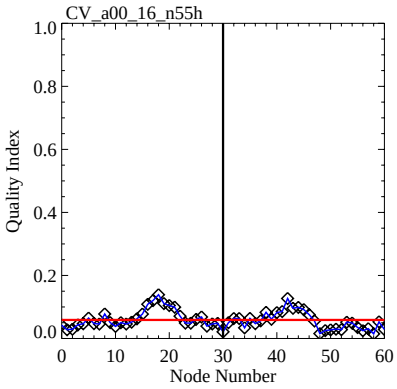


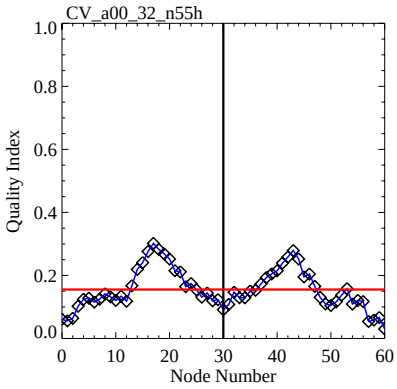


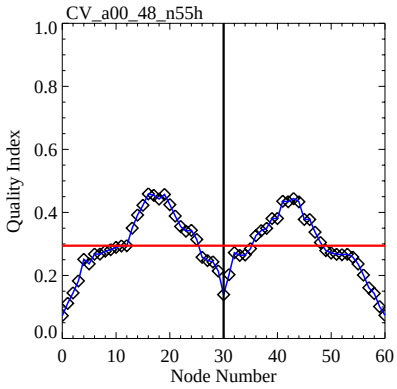


**14 rpm**

**Pulse Peak Power 312 W** **625 W** **2500 W**

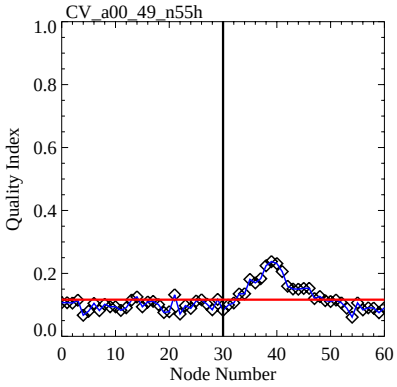


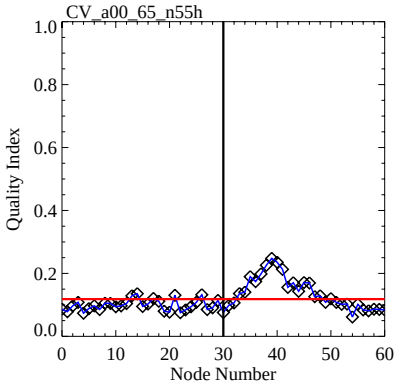


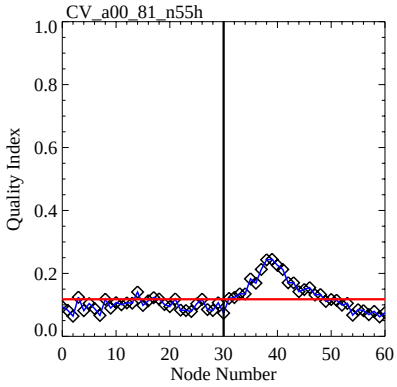


**0.3 rpm**

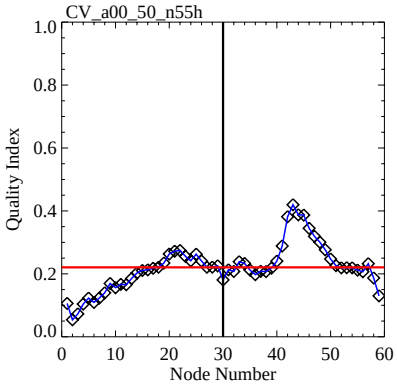


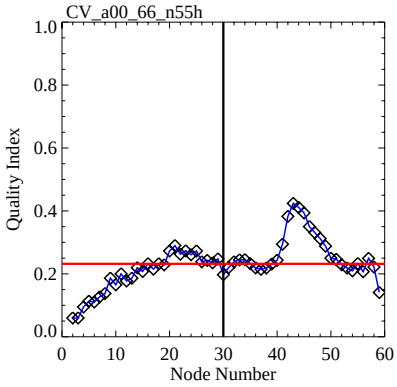


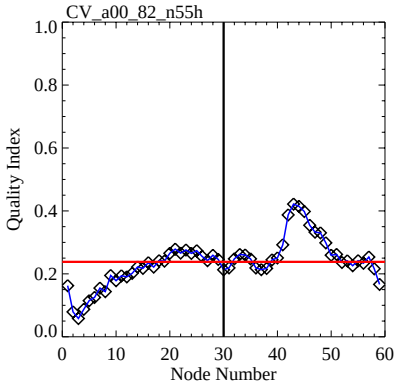


**0.6 rpm**

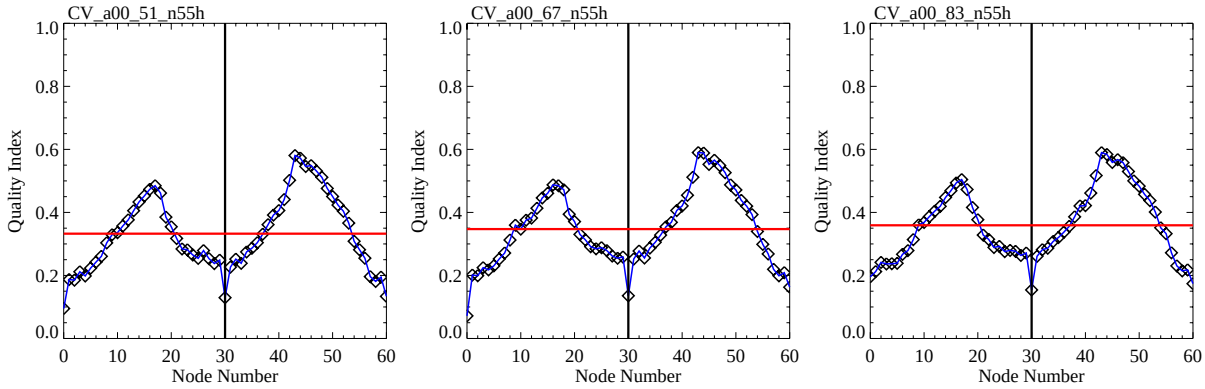


**0.9 rpm**

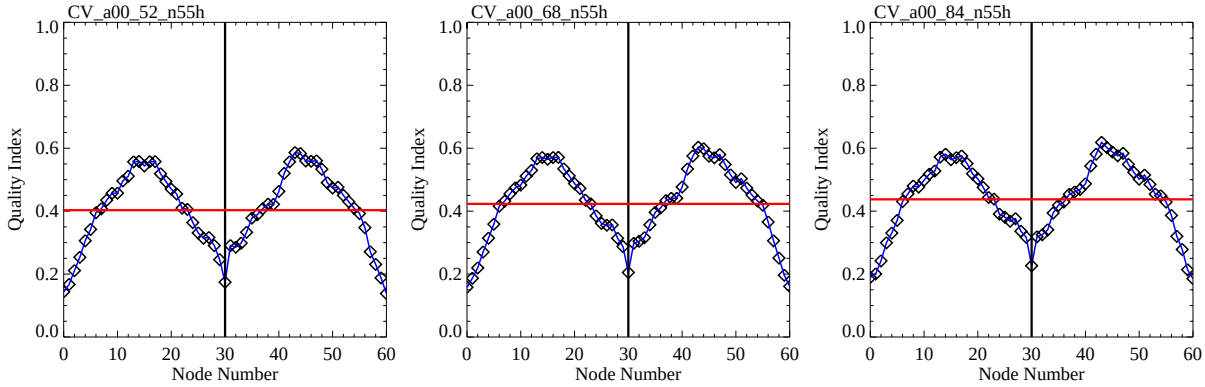


**1.2 rpm**

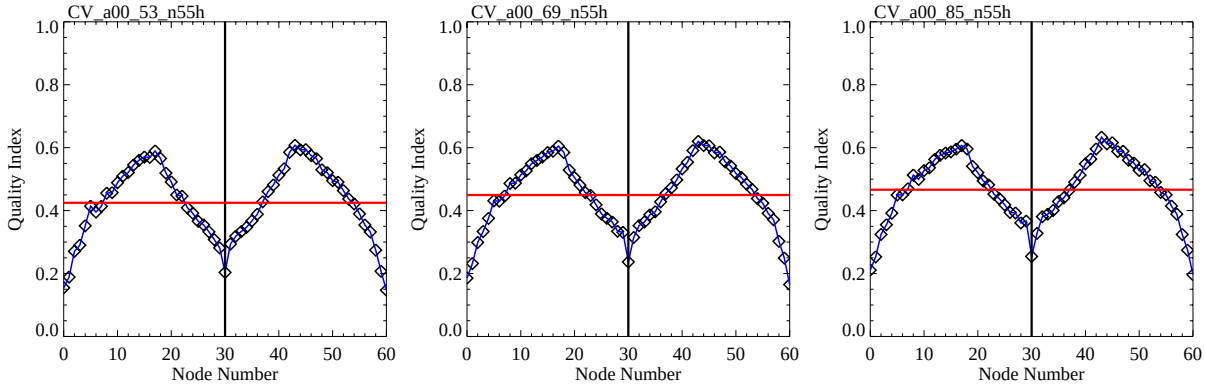


**1.5 rpm**

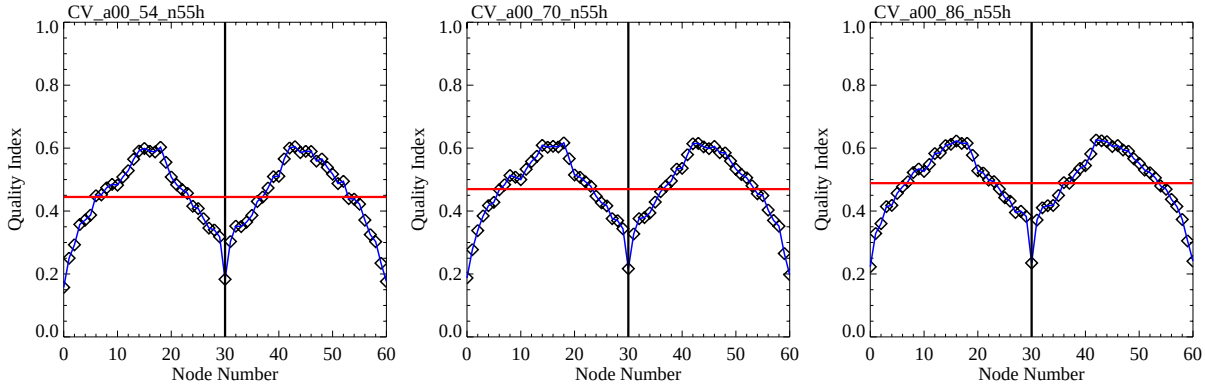


**2.0 rpm**

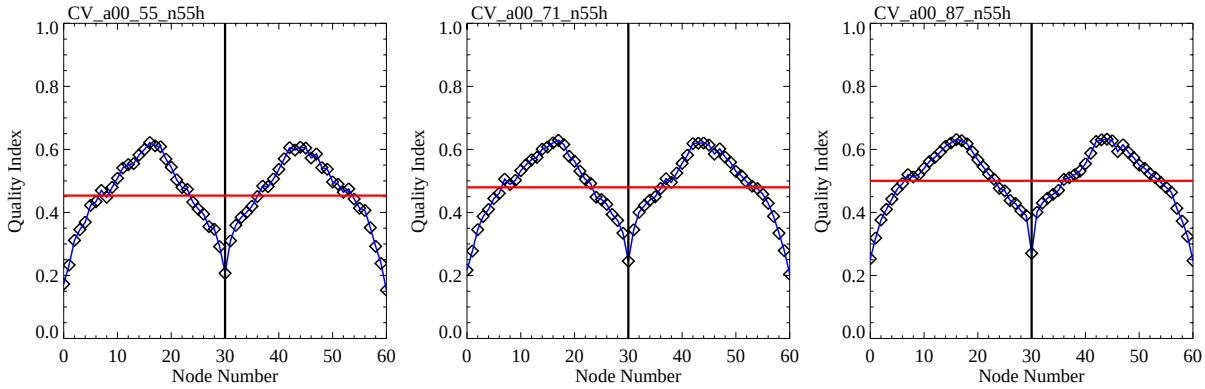


**2.5 rpm**

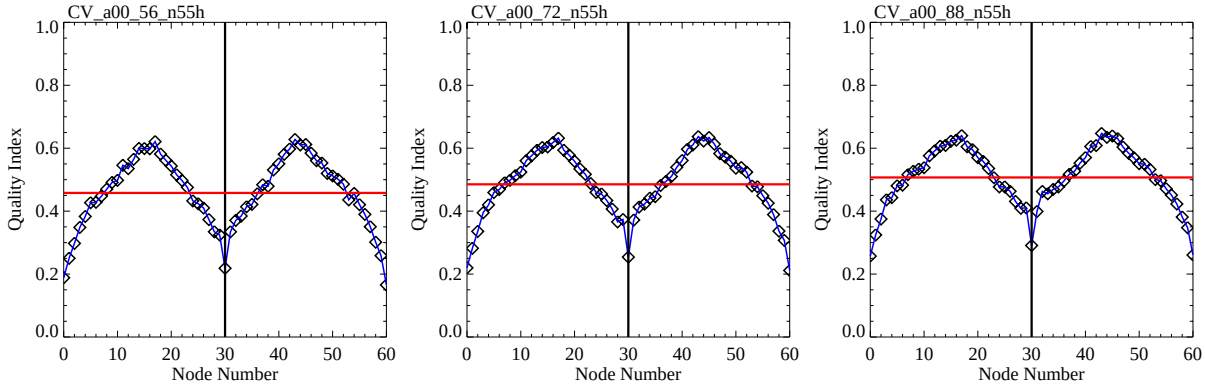


**3.0 rpm**

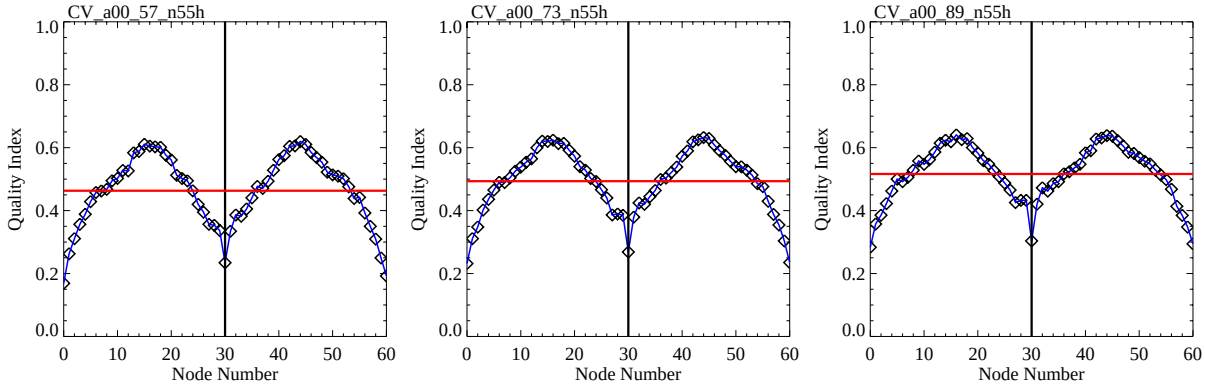


**3.5 rpm**

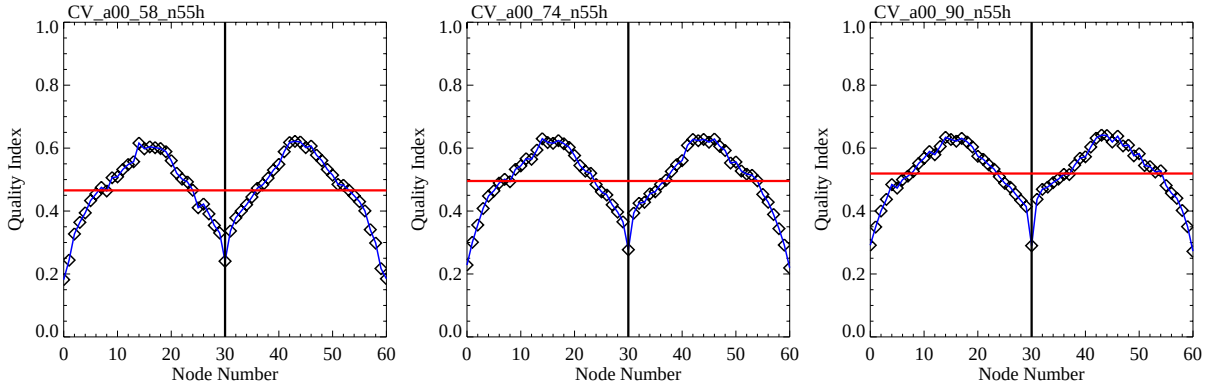


**4.0 rpm**

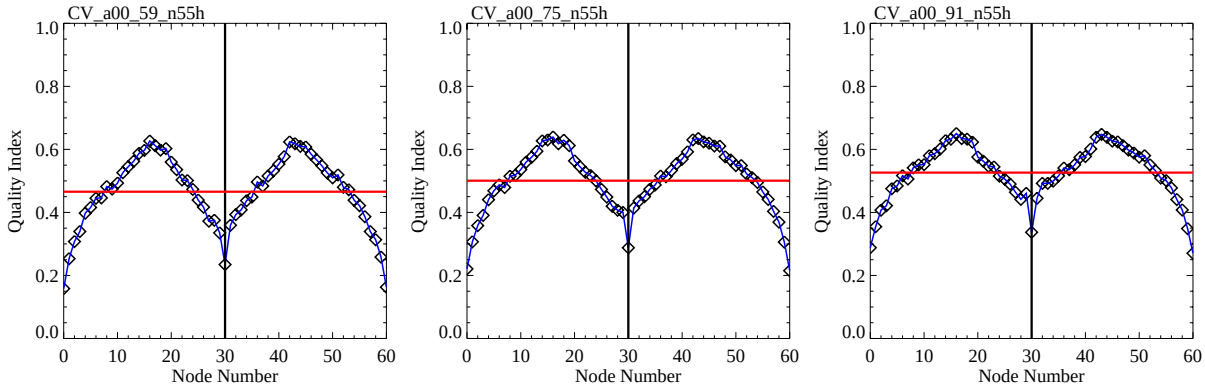


**5.0 rpm**

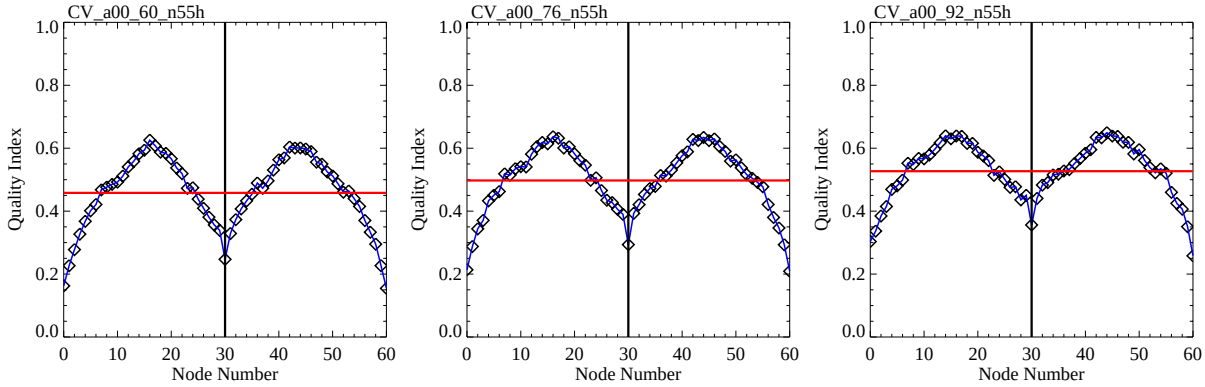


**6.0 rpm**

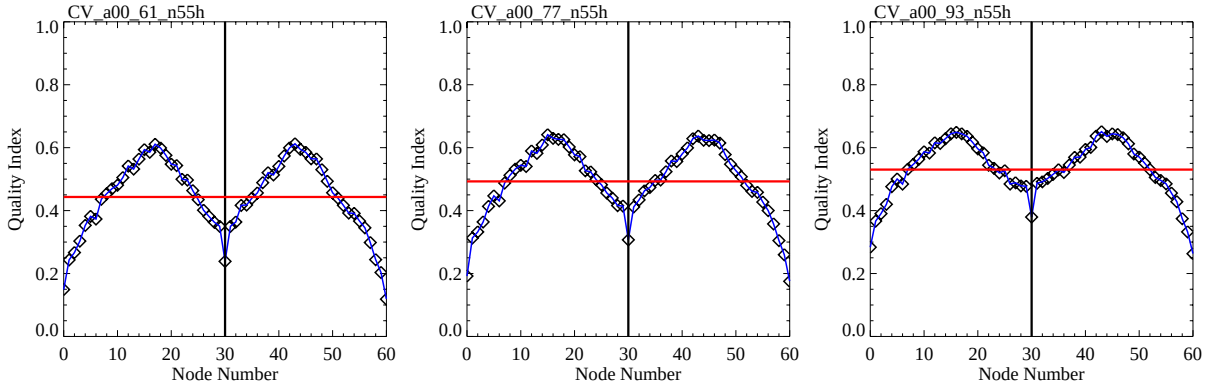


**8.0 rpm**

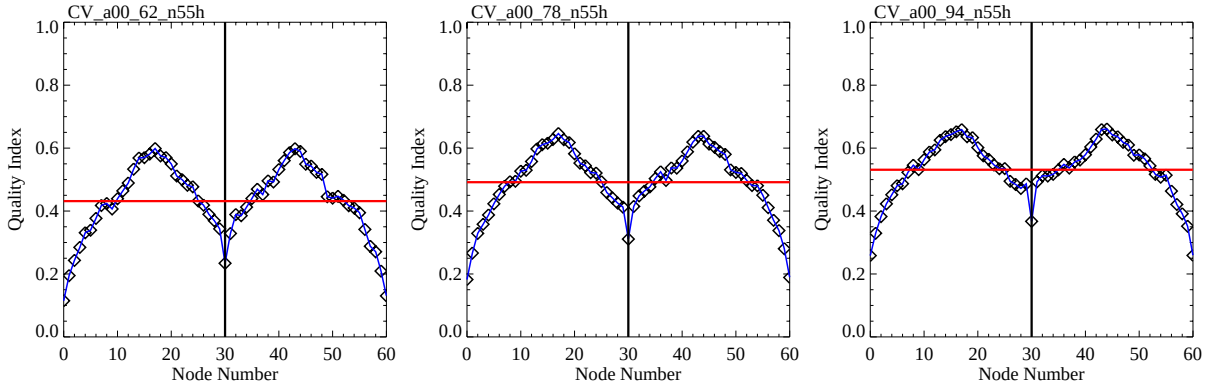


**10 rpm**

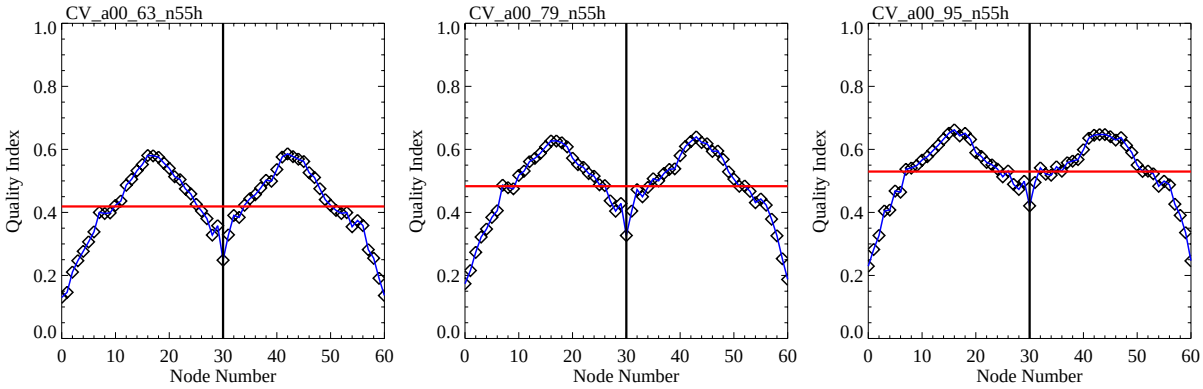
CV_a00_63_n55h
CV_a00_79_n55h
CV_a00_95_n55h
Quality Index
Node Number

**12 rpm**

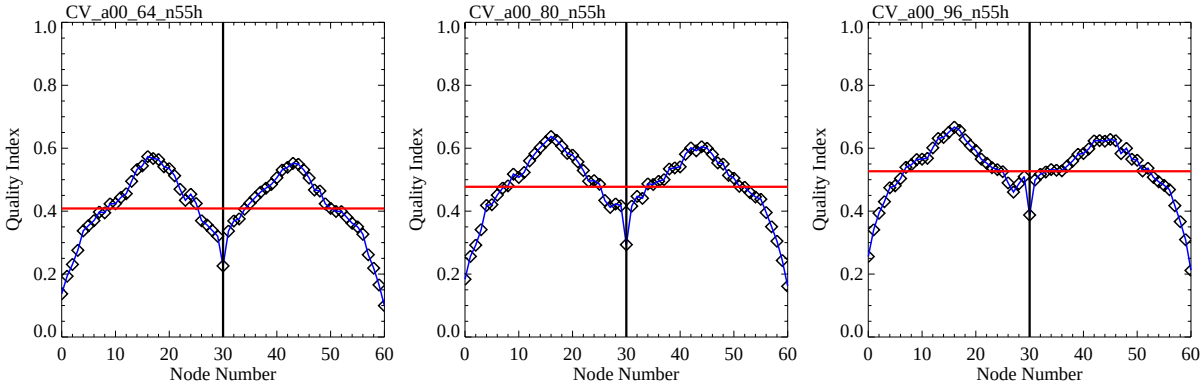
CV_a00_64_n55h
CV_a00_80_n55h
CV_a00_96_n55h
Quality Index
Node Number

**14 rpm**

## Number of views at different scan rates

The following table summarizes the graphs of the number of measurements (views) versus node number for various settings of the antenna scan rate in the simulation of the baseline instrument. The setting for antenna scan rate is indicated below the graphs.

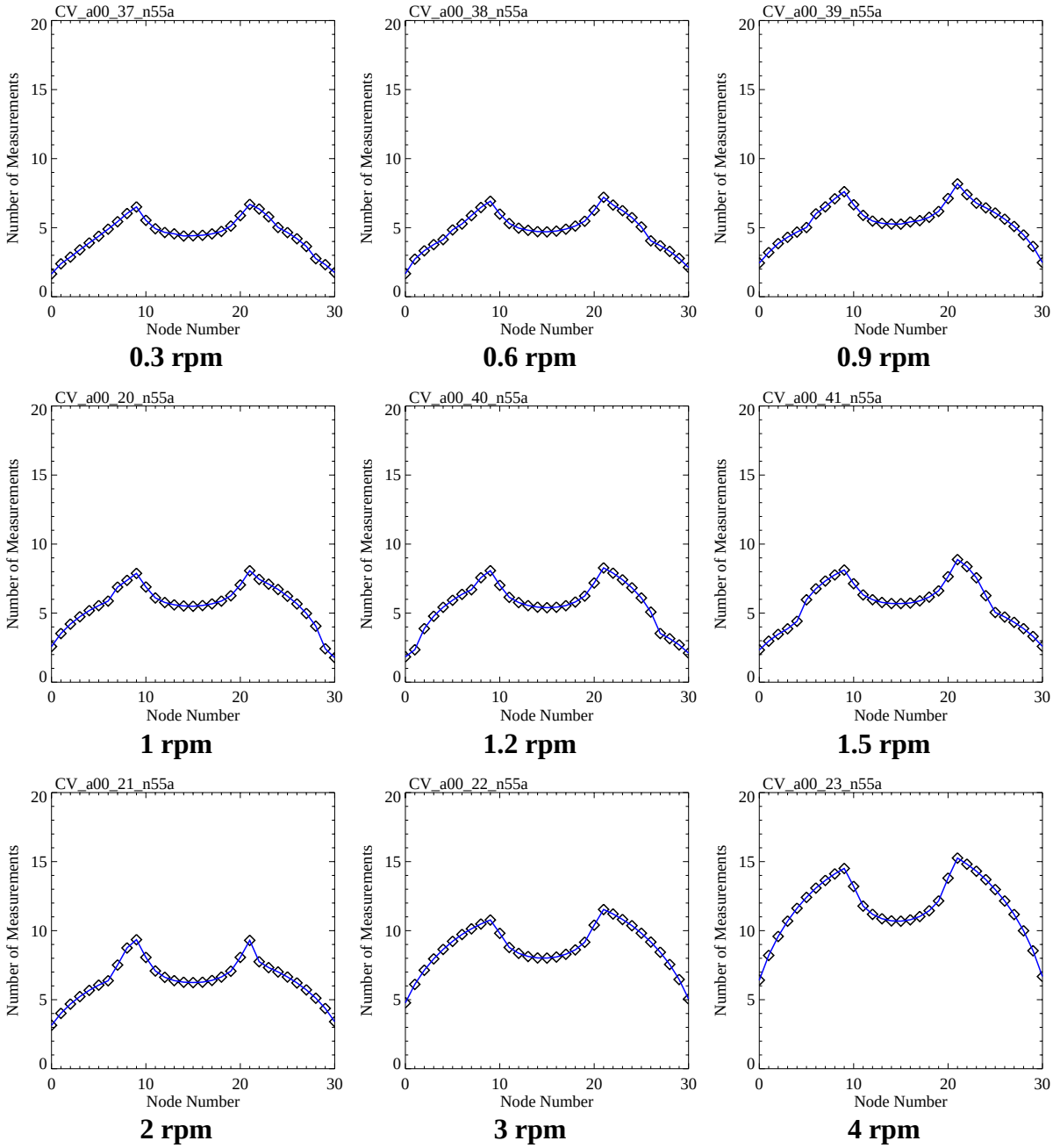

## 11. Annex D – C-Band with Alternating VV & HH Polarization

The following table summarizes the graphs of the quality index versus node number for a single antenna dual-polarized C-band system. The pulse peak power decrease from 640 KW to 78 W in steps of 3 dB. For the wind retrieval only VV-polarization and only HH-polarization data as well as both data together was used in the wind retrieval.

Orbit height - 725 km
Swath width - 1500 km
Resolution - 50 km

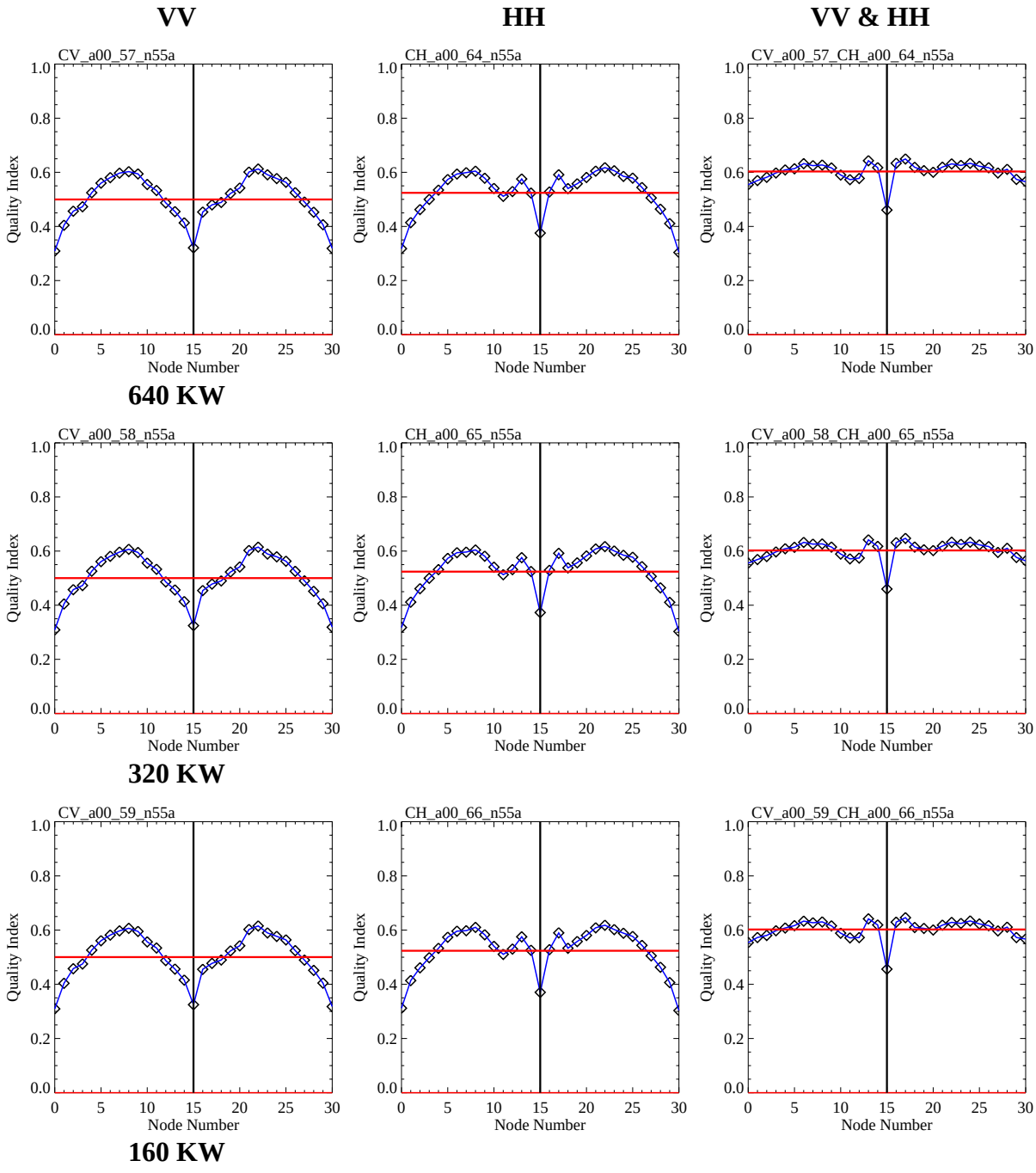

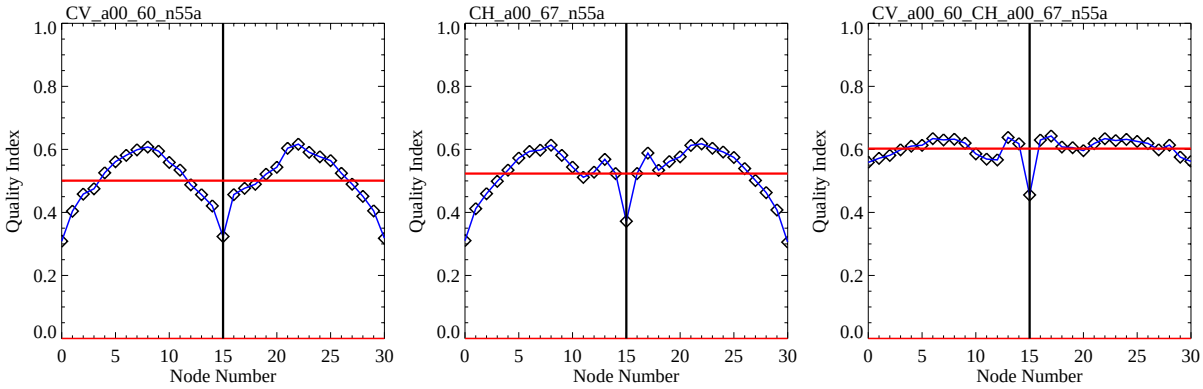


**80 KW**

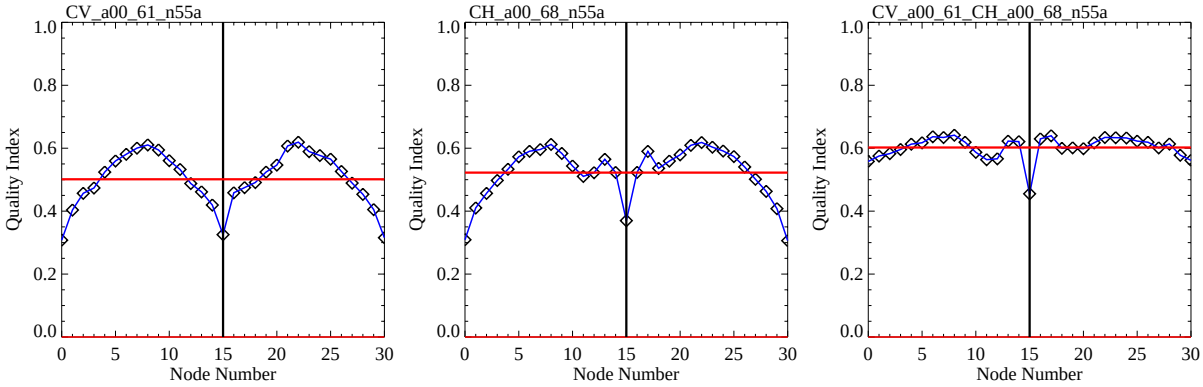


**40 KW**

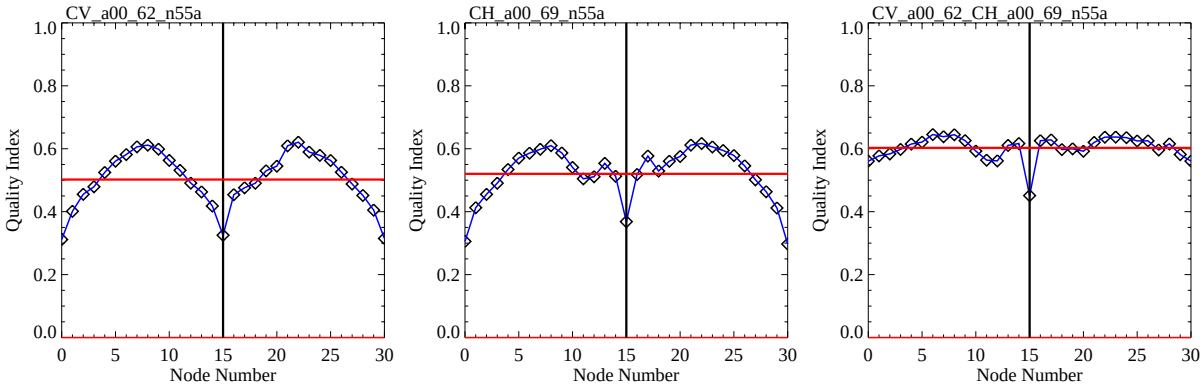


**20 KW**

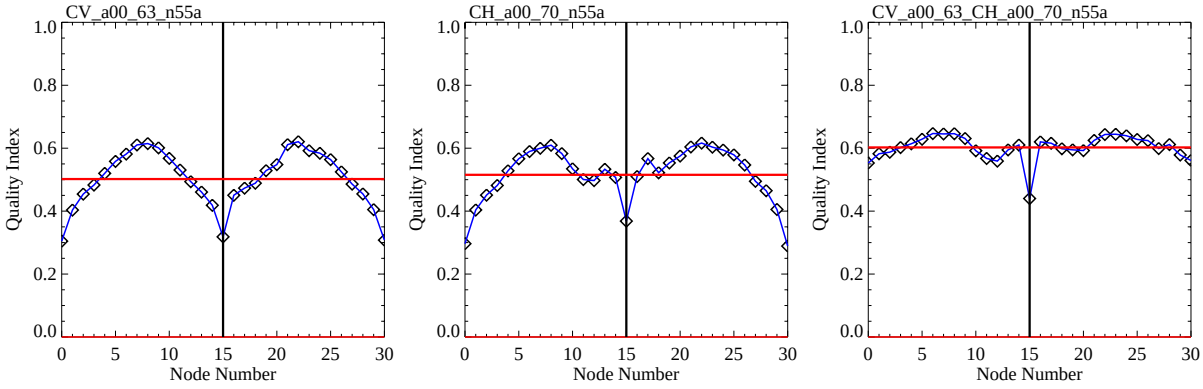


**10 KW**

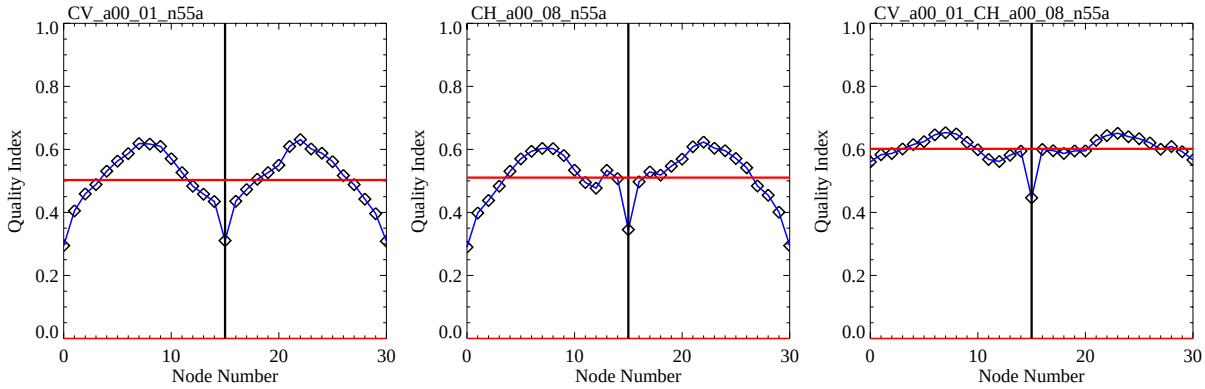


**5000 W**

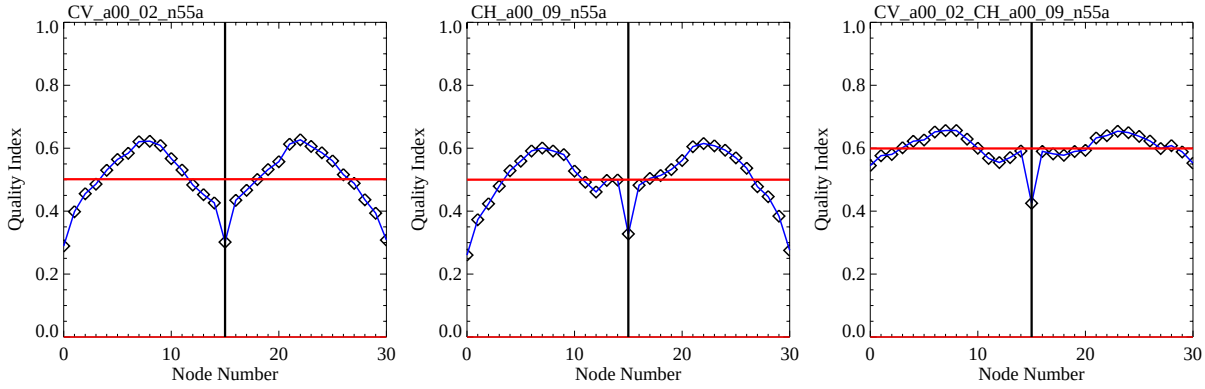


**2500 W**

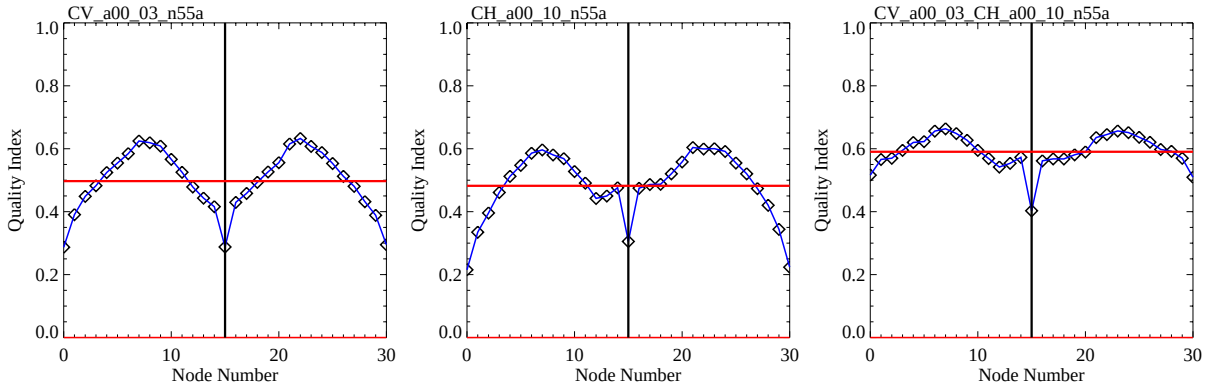


**1250 W**

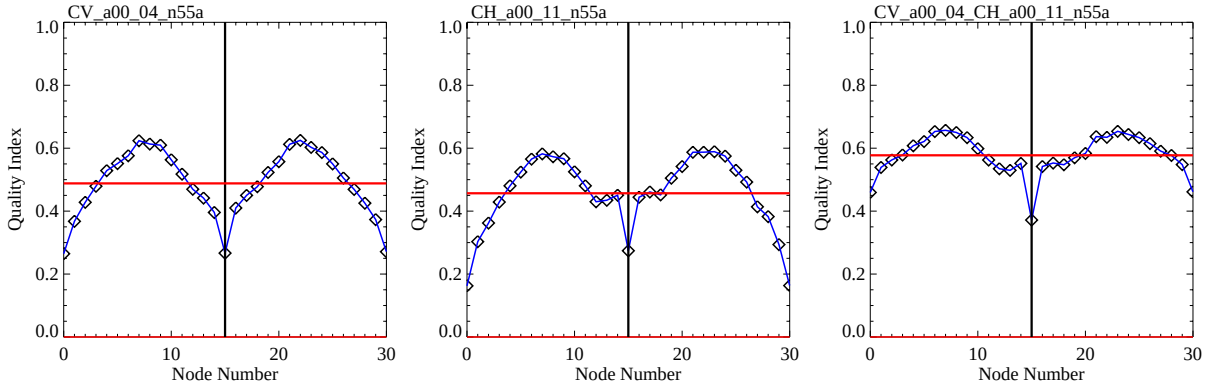


**625 W**

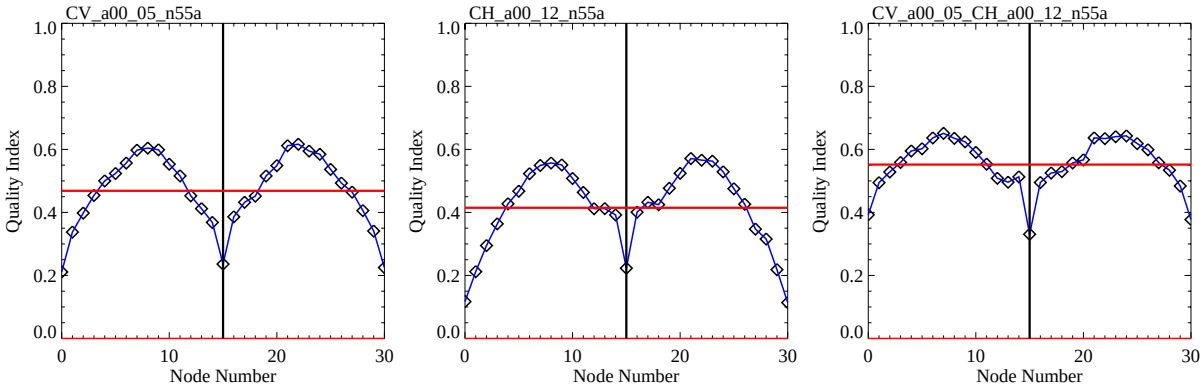


**312 W**

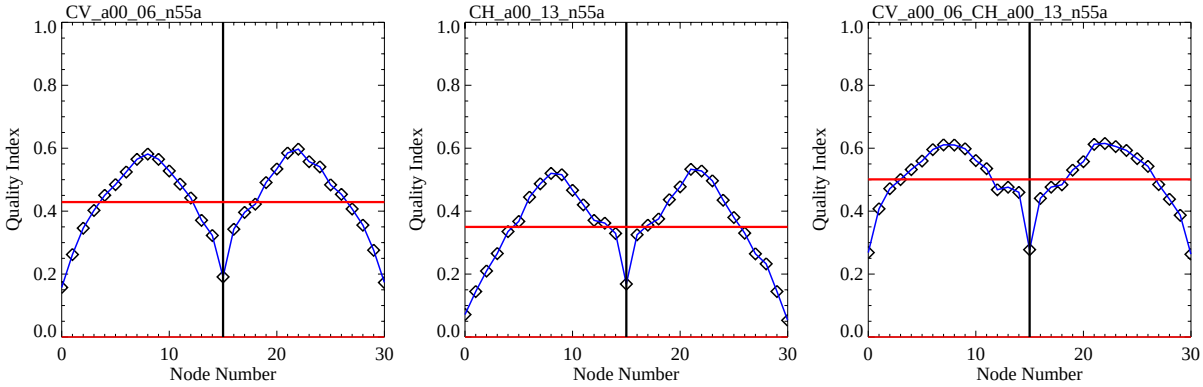


**156 W**

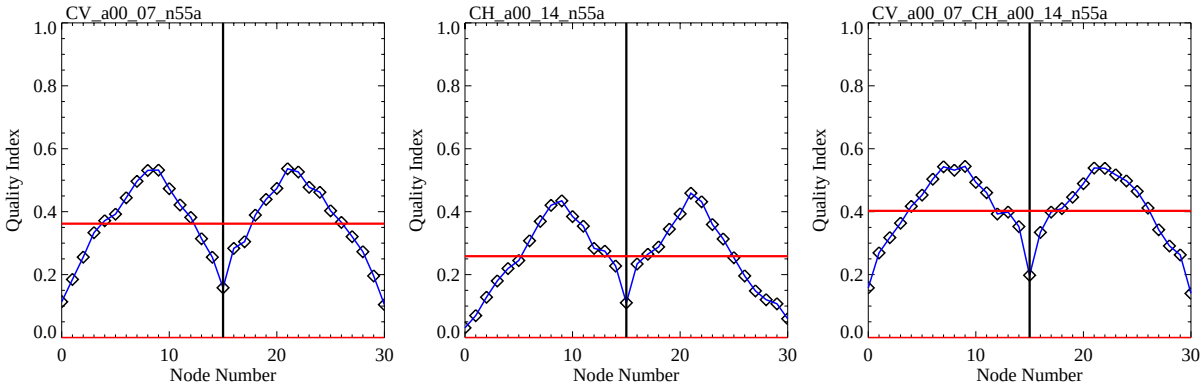


**78 W**

Combination of VV and HH polarization data for a system with two separate antennae of Option C.

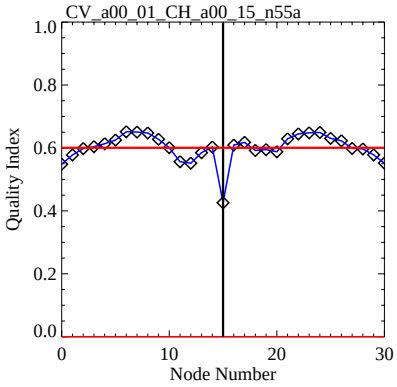


**5000 W**

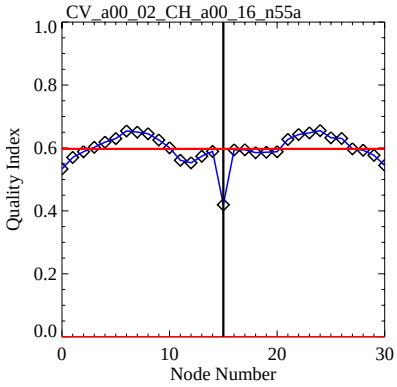


**2500 W**

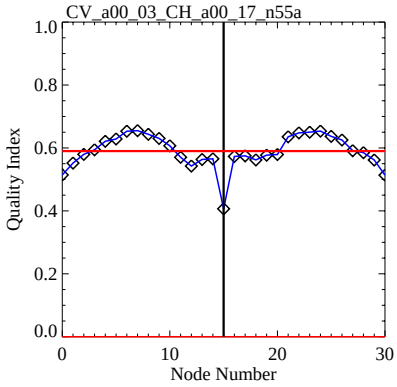


**1250 W**

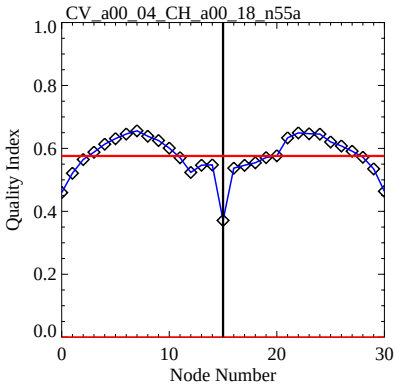


**625 W**

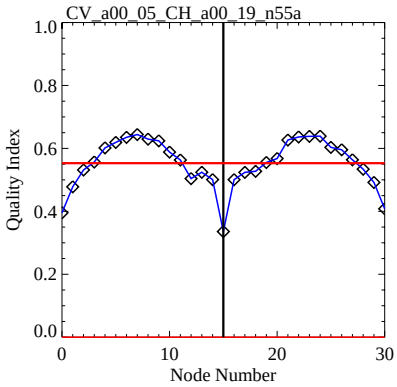


**312 W**

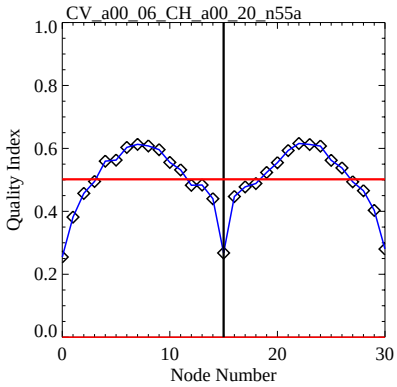


**156 W**

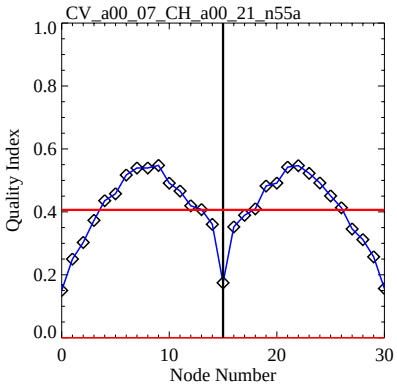


**78 W**

## 12. Annex E – 25 Km Resolution Mode

The following table summarizes the graphs of the quality index versus node number for a polarimetric C-band system. The pulse peak power decrease from 640 KW to 78 W in steps of 3 dB. For the wind retrieval only VV-polarization and only polarimetric data as well as both data together was used.

Orbit height - 725 km
Swath width - 1500 km
Resolution - 25 km

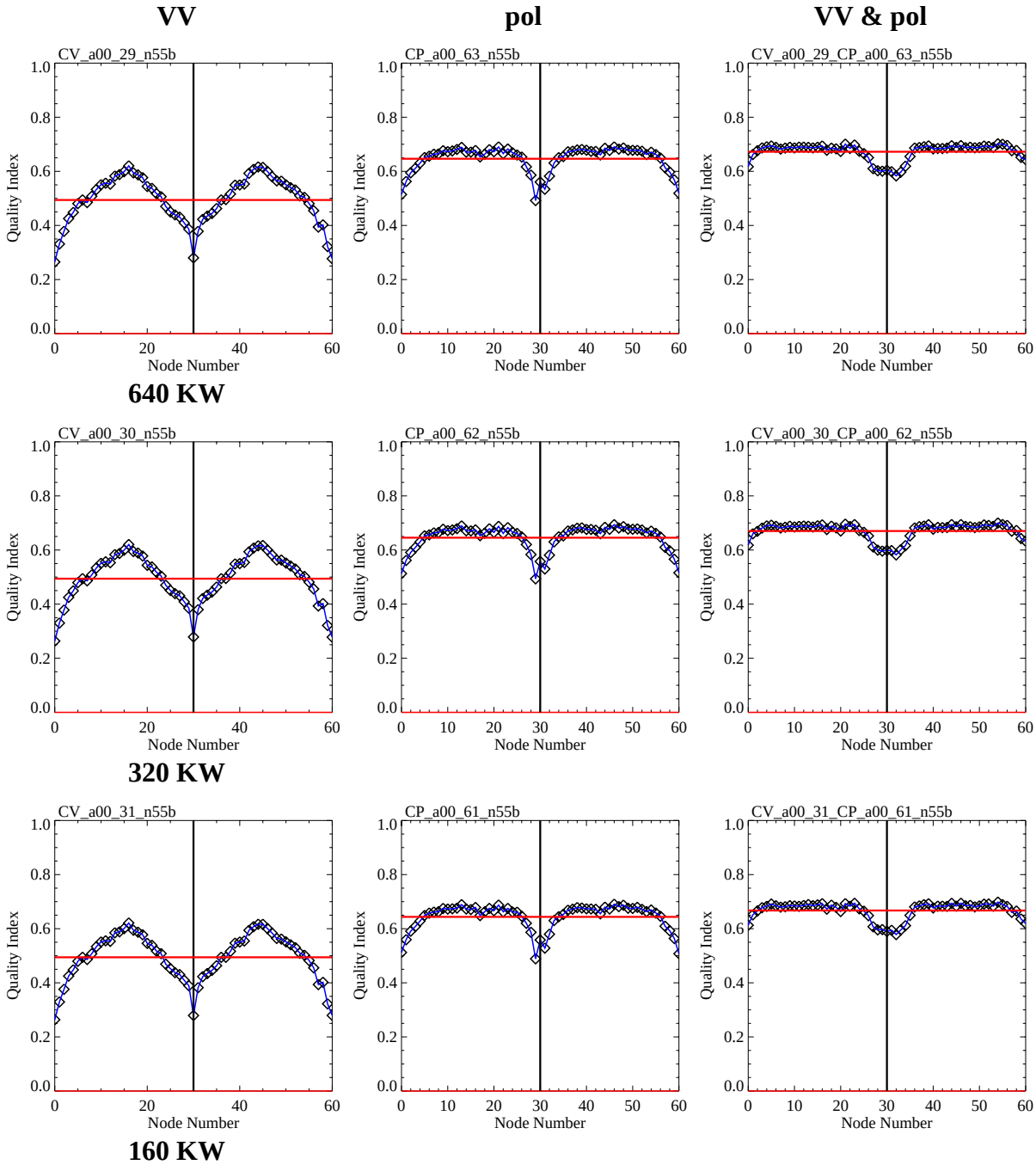

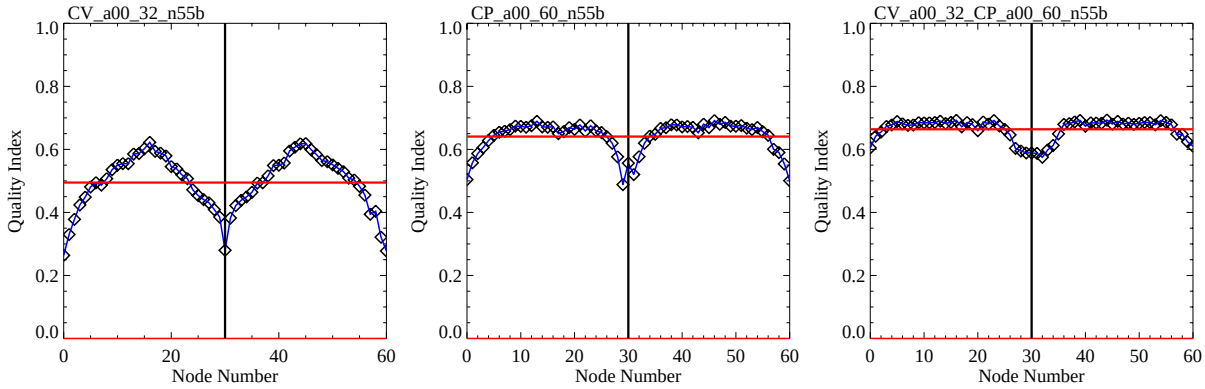


**80 KW**

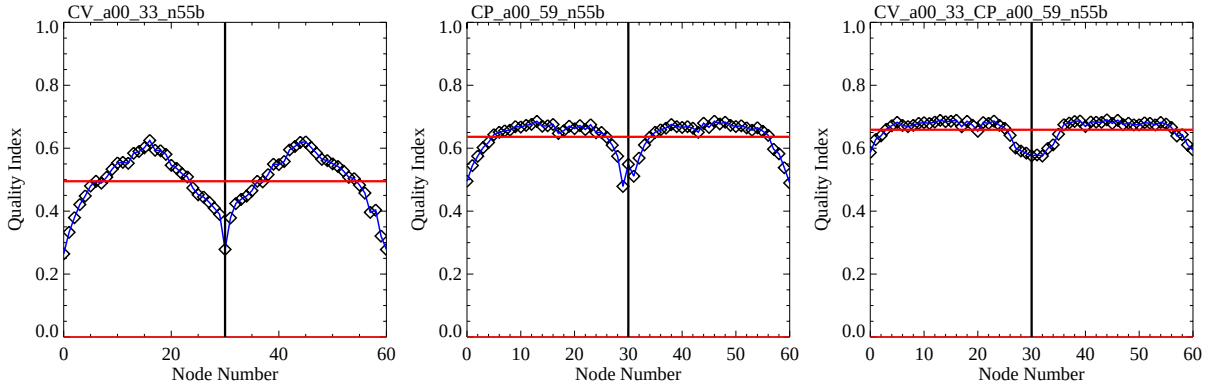


**40 KW**

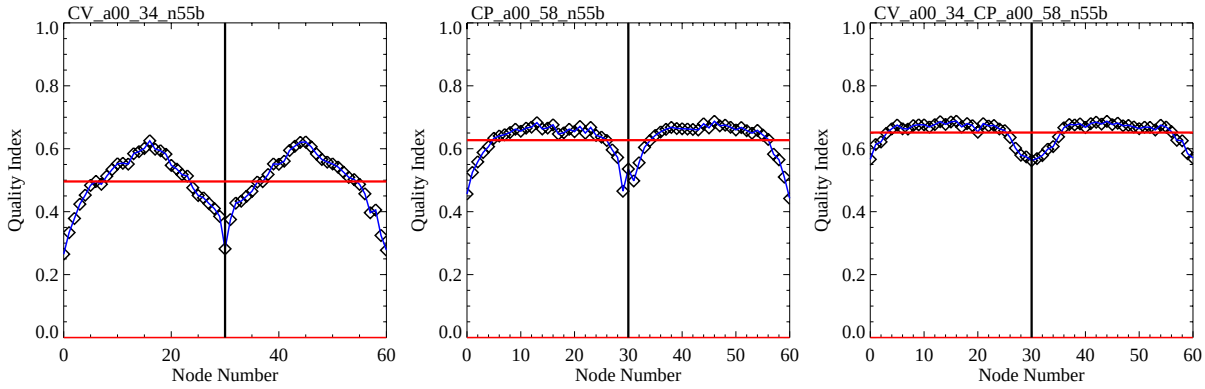


**20 KW**

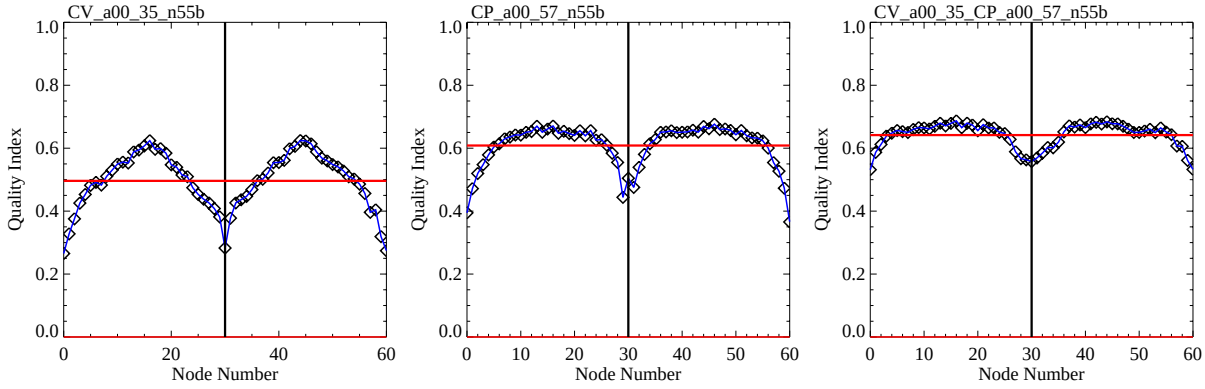


**10 KW**

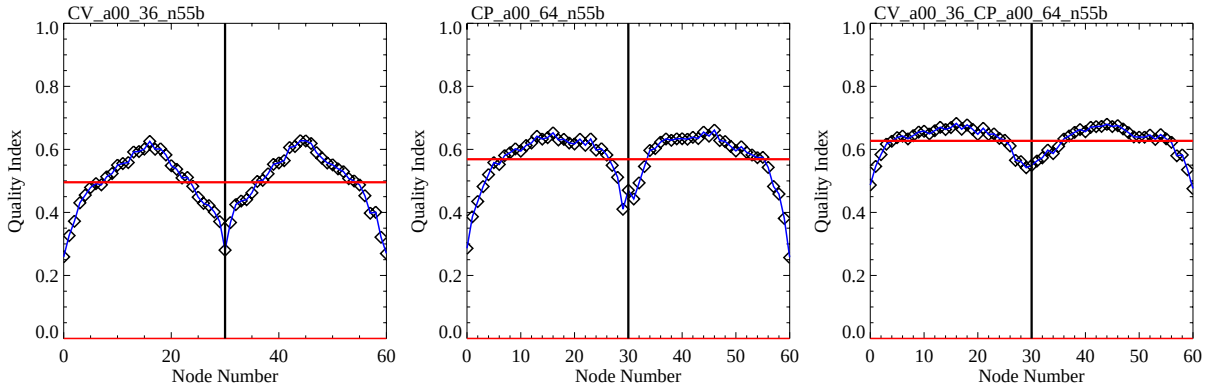


**5000 W**

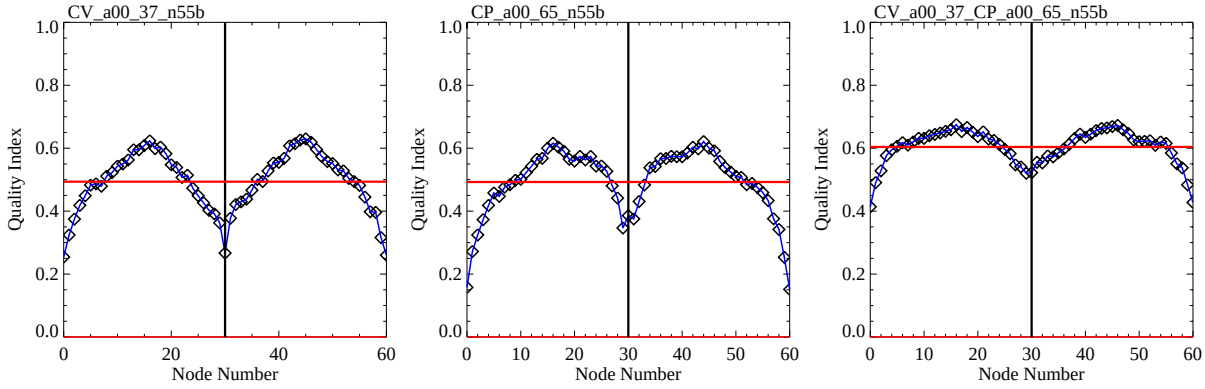


**2500 W**

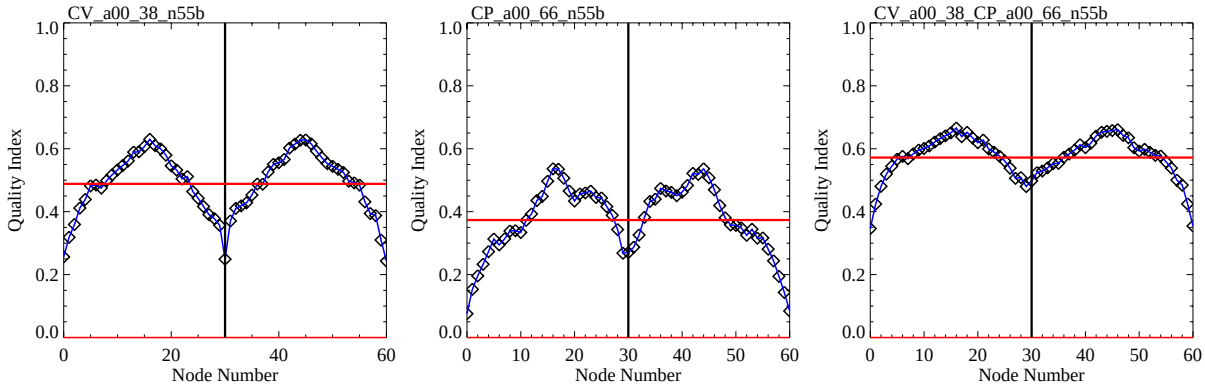


**1250 W**

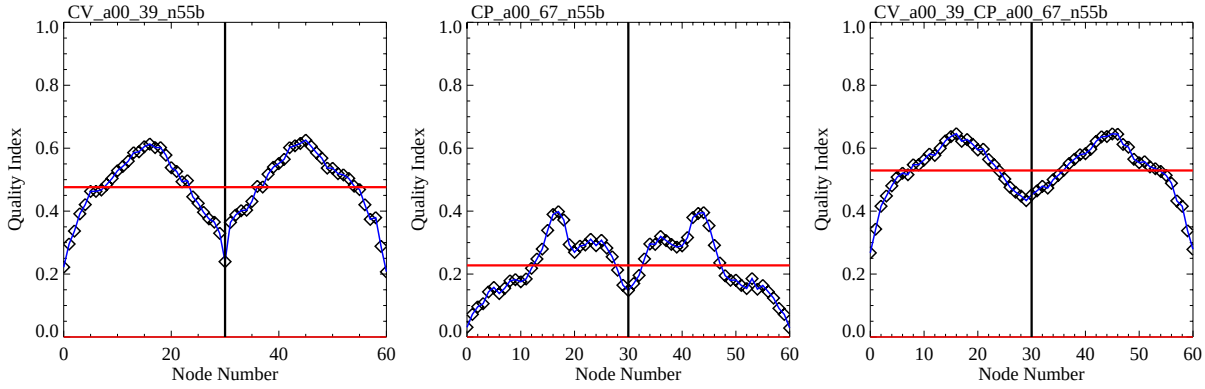


**625 W**

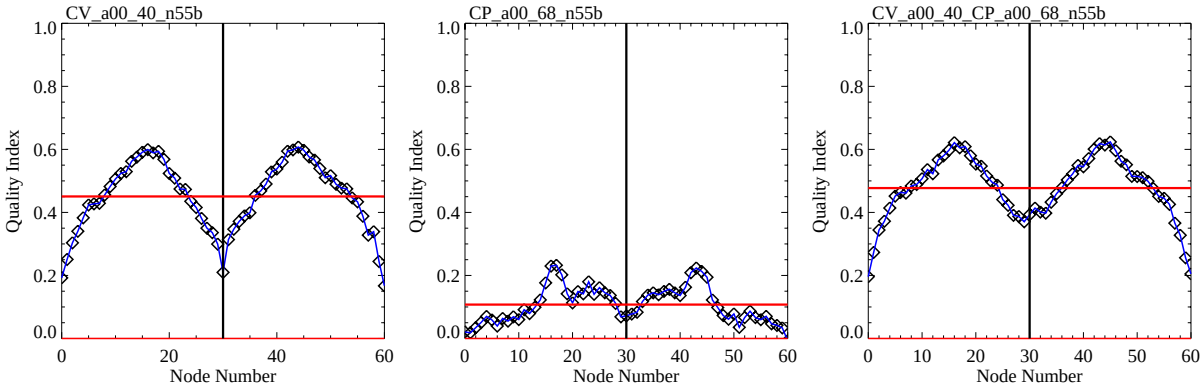


**312 W**

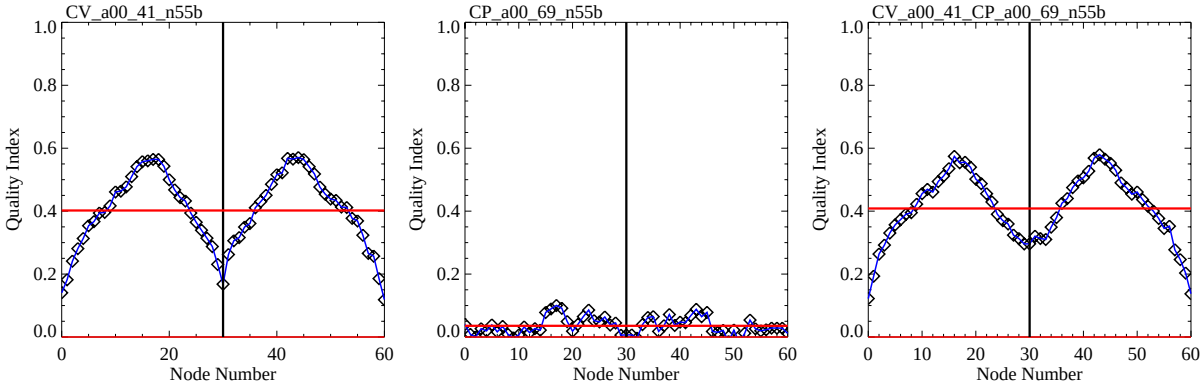


**156 W**

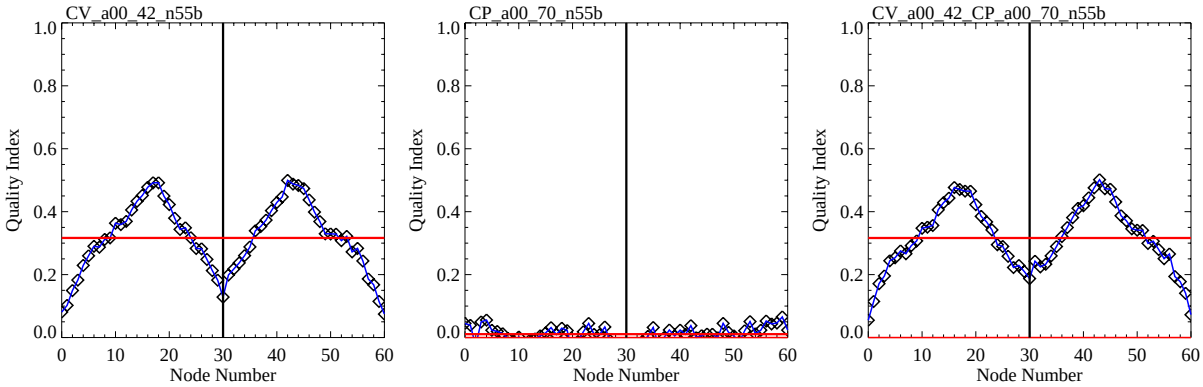


**78 W**

## 13. Annex F – Wide Swath (1800 km) Mode

The following table summarizes the graphs of the quality index versus node number for a dual-polarized C-band system. The pulse peak power decrease from 640 KW to 78 W in steps of 3 dB. For the wind retrieval only VV-polarization and only HH-polarization data as well as both data together was used.

Orbit height - 725 km
Swath width - 1800 km
Resolution - 50 km

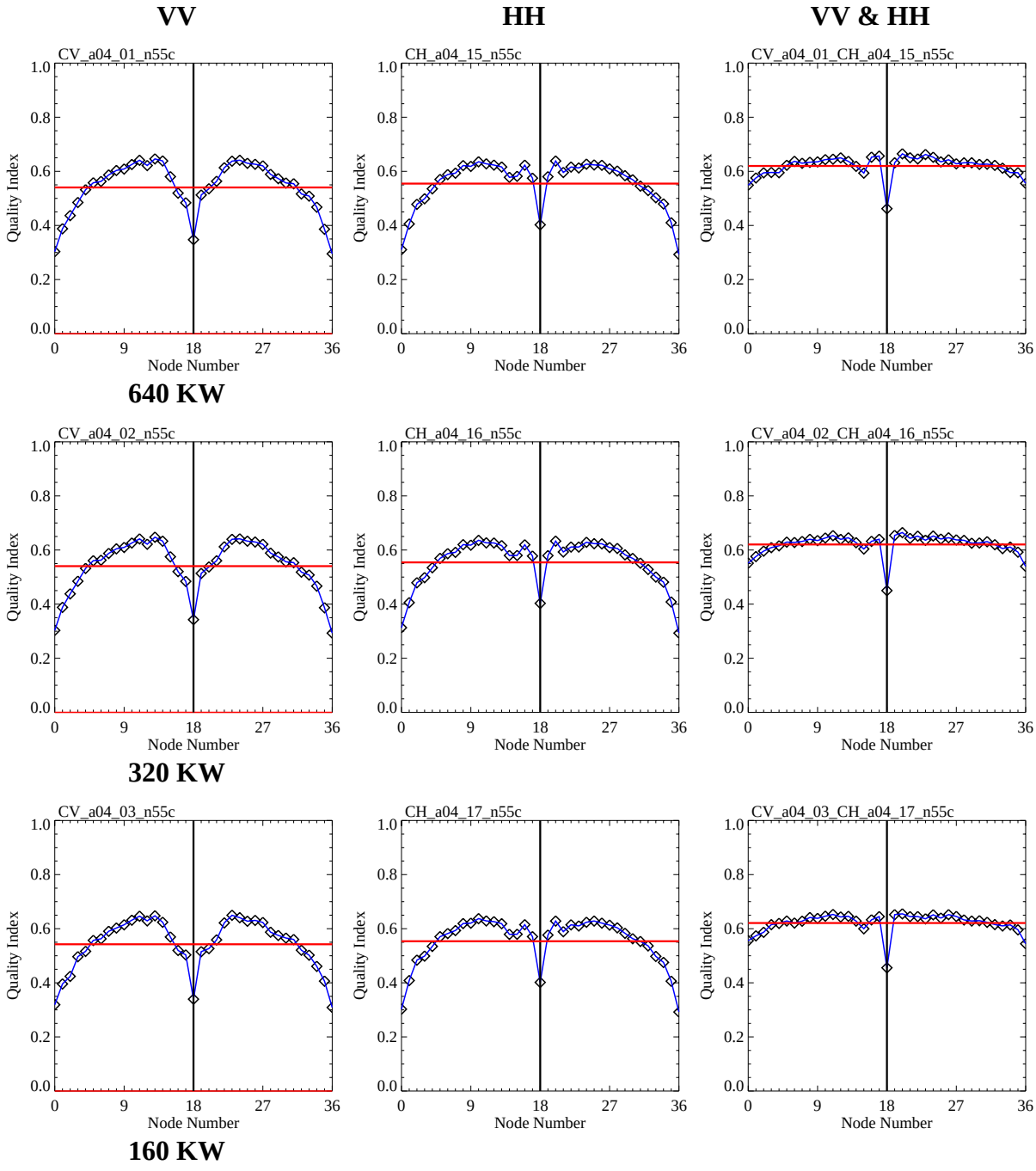

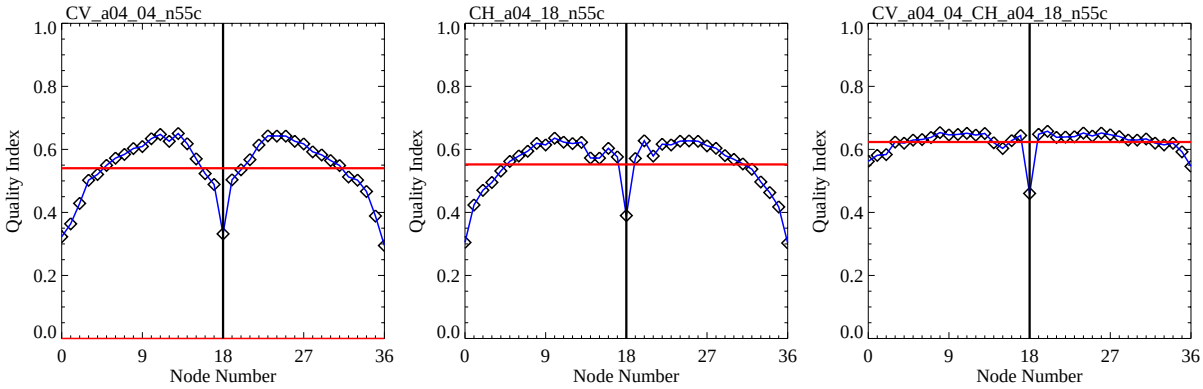


**80 KW**

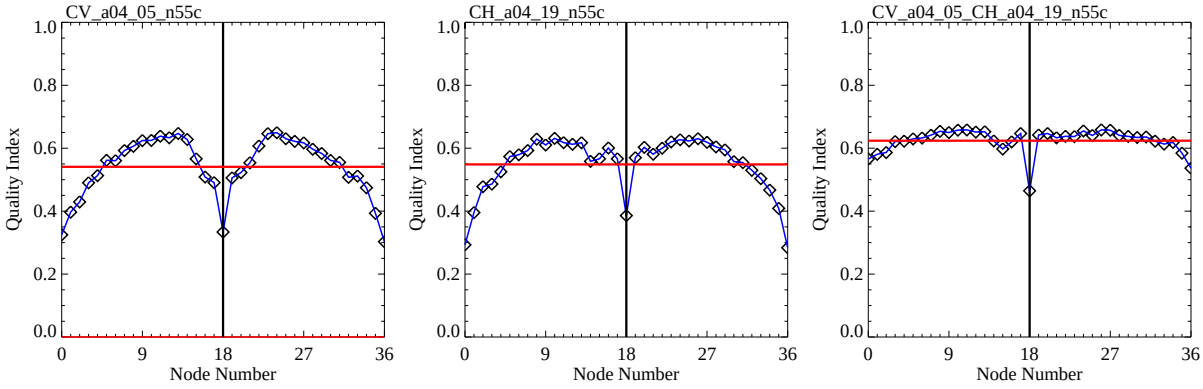


**40 KW**

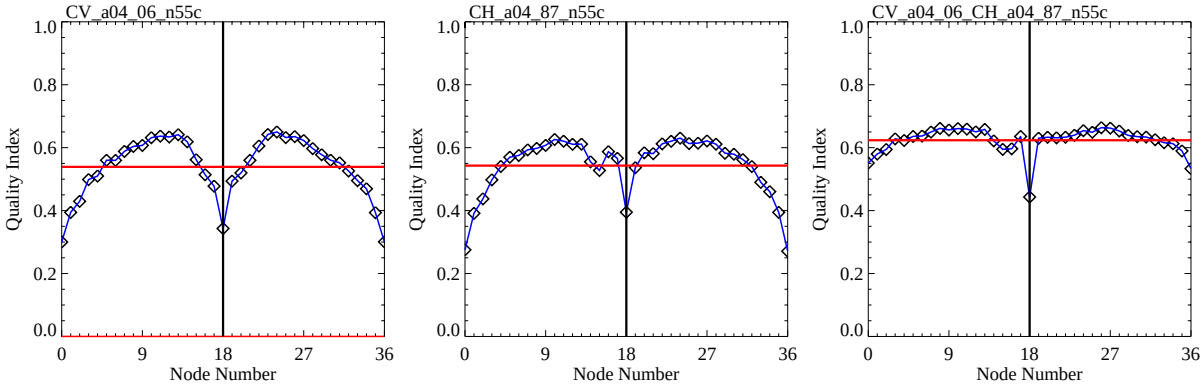


**20 KW**

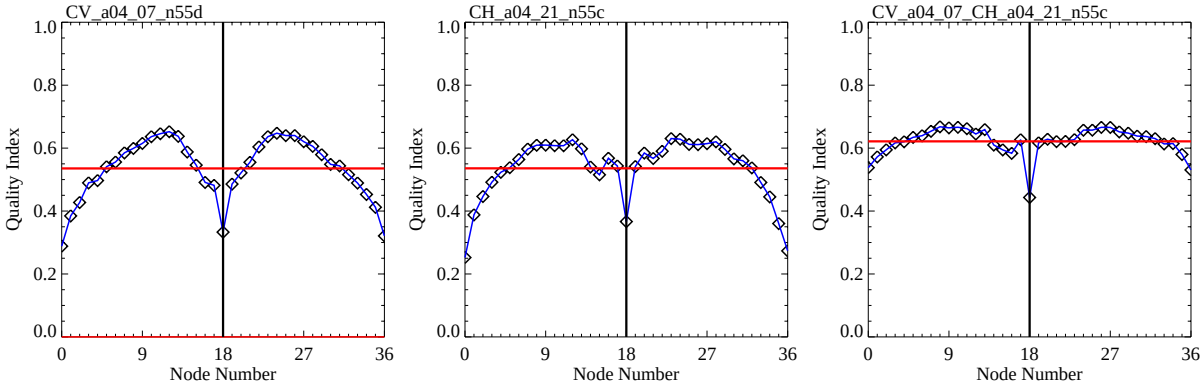


**10 KW**

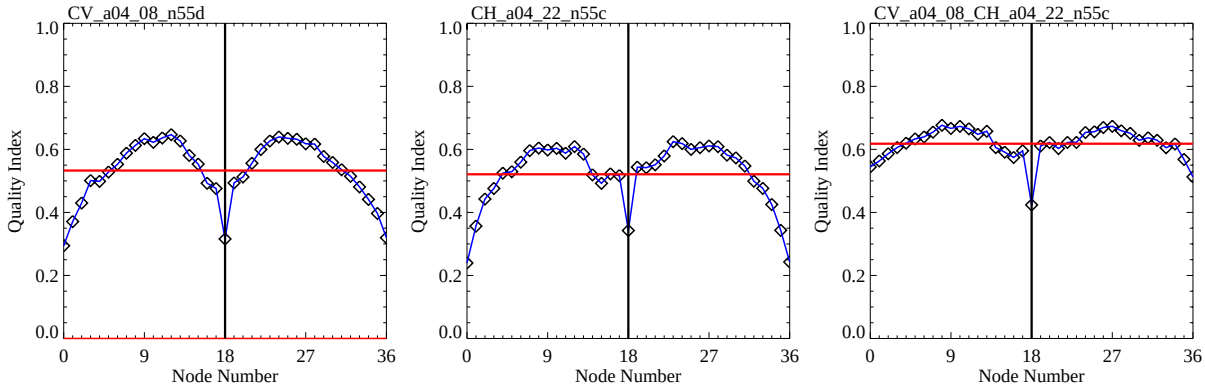


**5000 W**

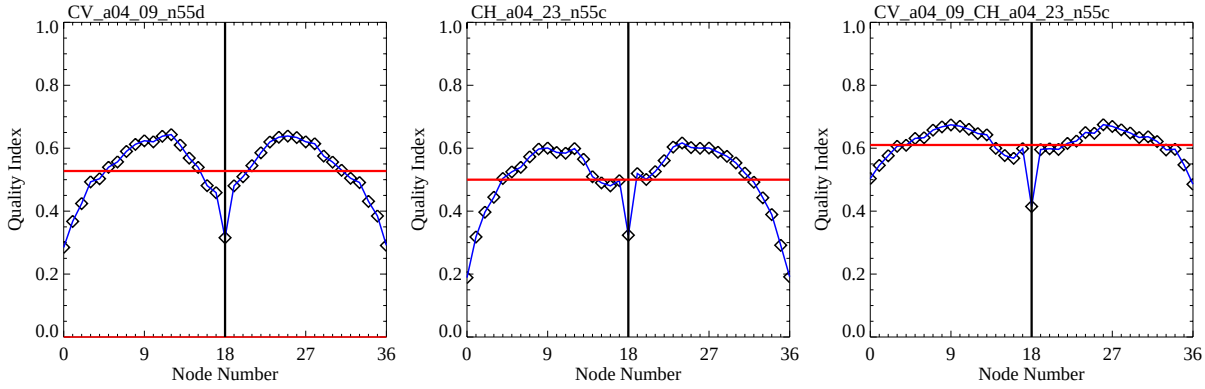


**2500 W**

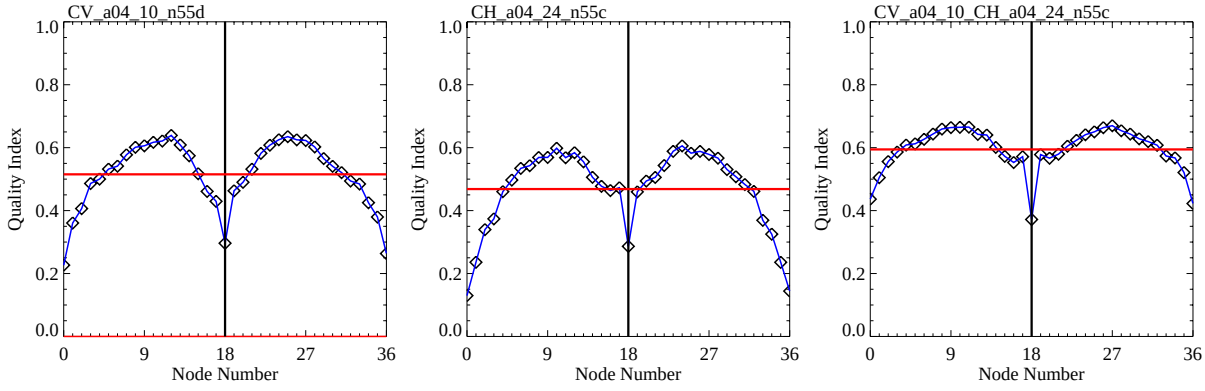


**1250 W**

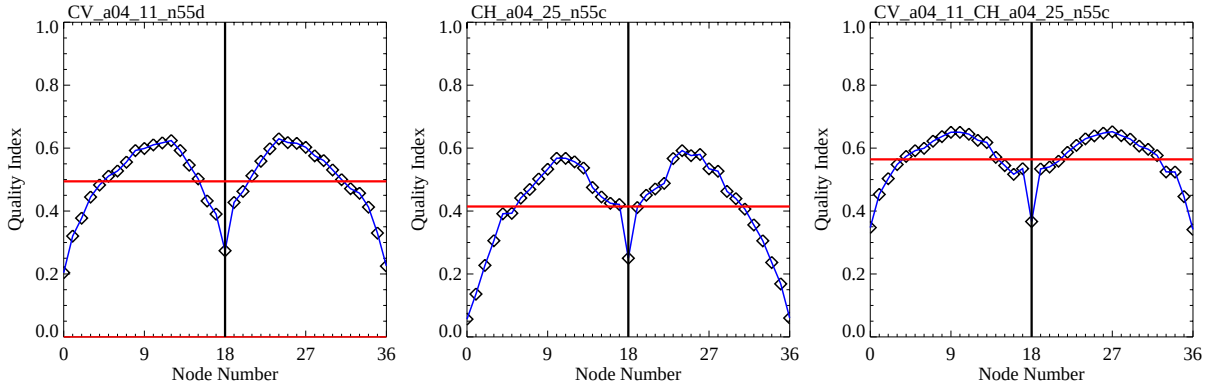


**625 W**

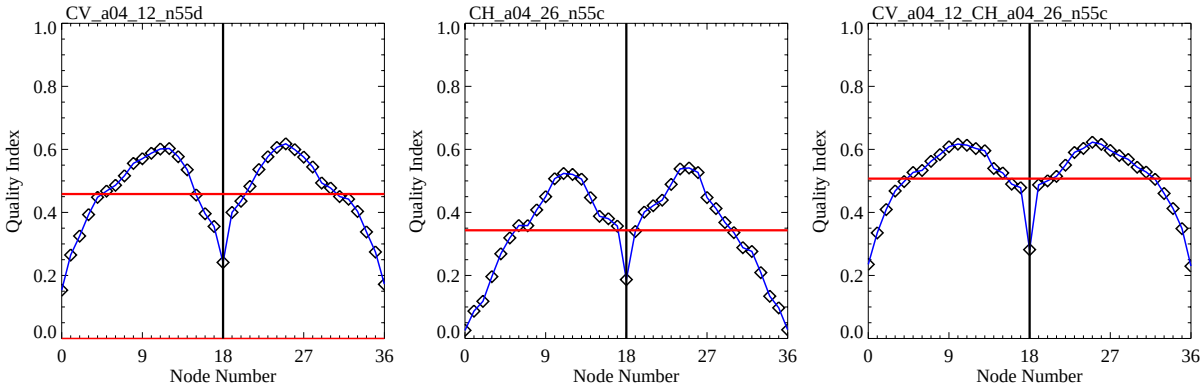


**312 W**

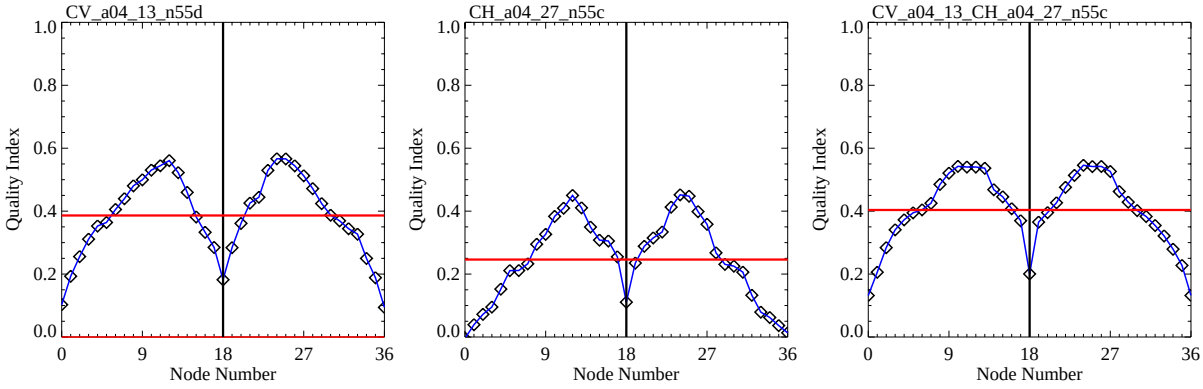


**156 W**

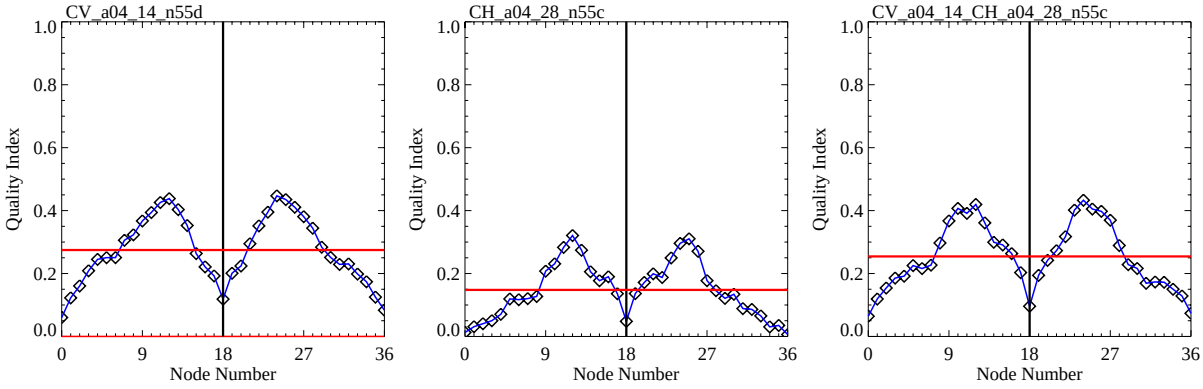


**78 W**

## 14. Annex G – Wide Swath and 25 km Resolution

The following table summarizes the graphs of the quality index versus node number for a wide swath (1800 km), high resolution (25 km) C-band system with VV and HH polarization. The pulse peak power decrease from 640 KW to 78 W in steps of 3 dB. For the wind retrieval only VV-polarization and only HH-polarization data as well as both data together was used.

Orbit height - 725 km
Swath width - 1800 km
Resolution - 25 km

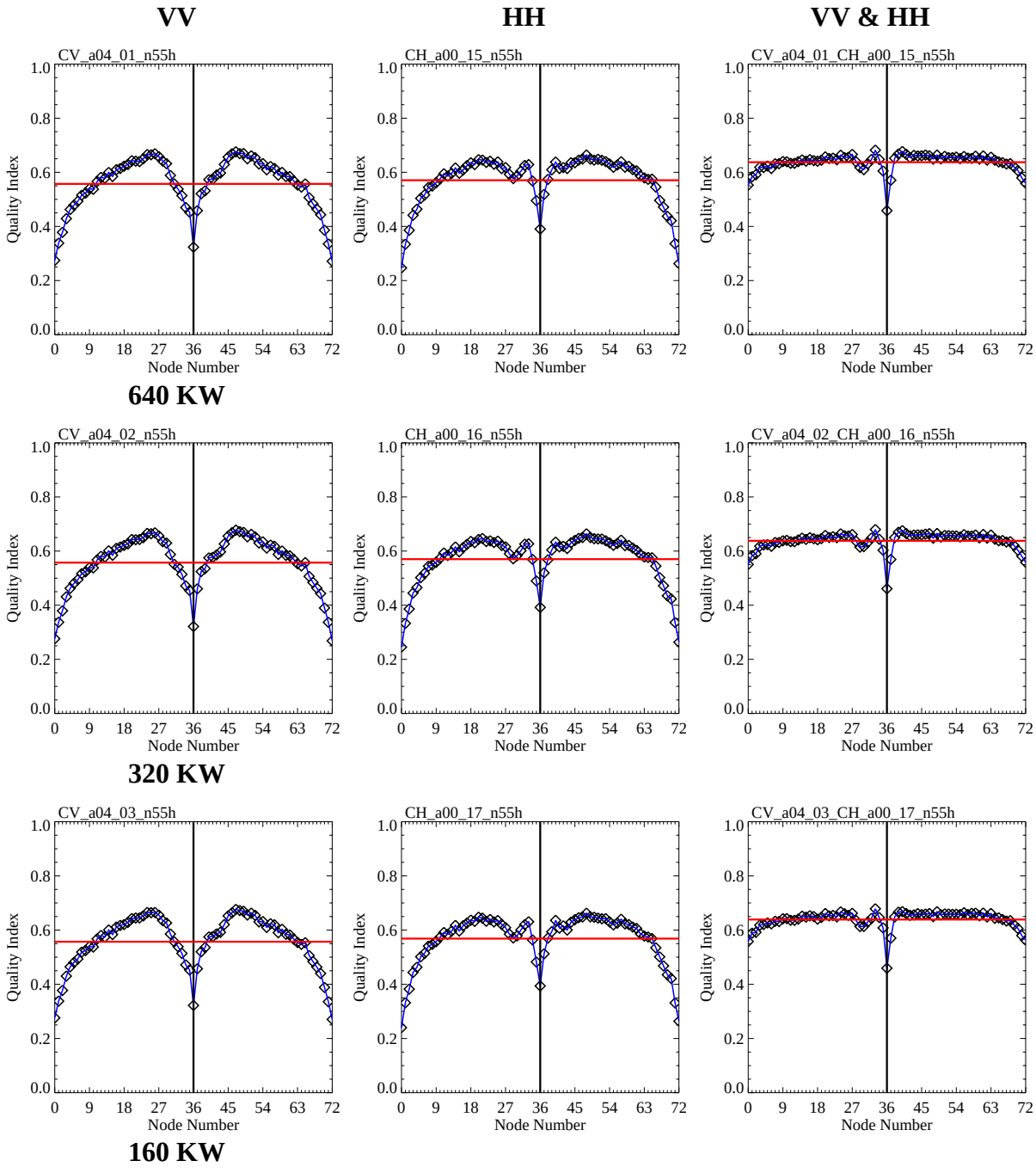

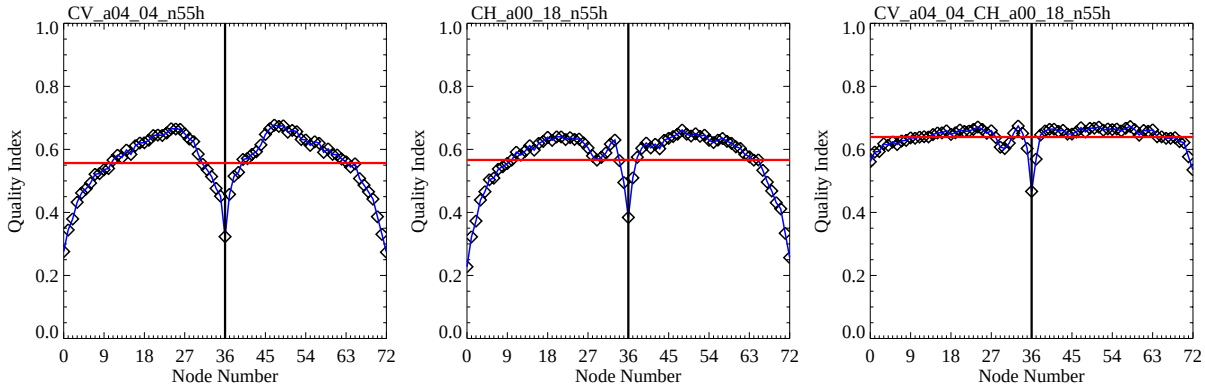


**80 KW**

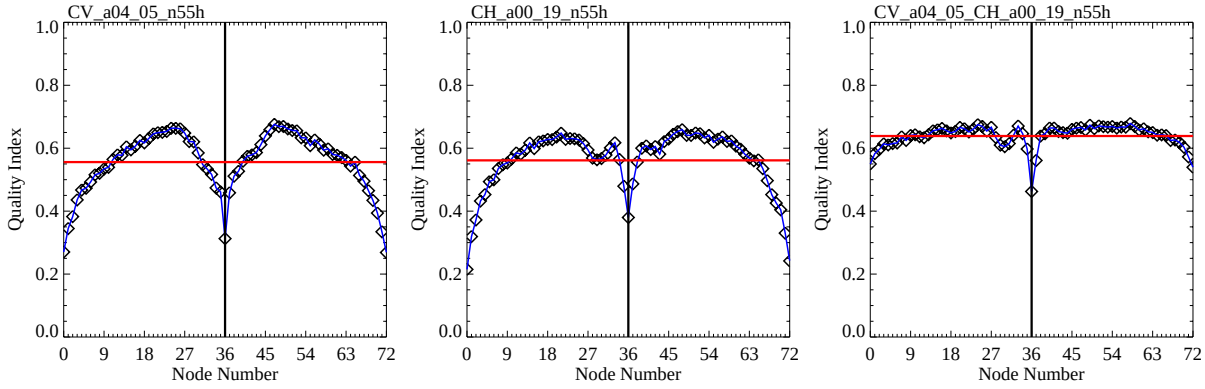


**40 KW**

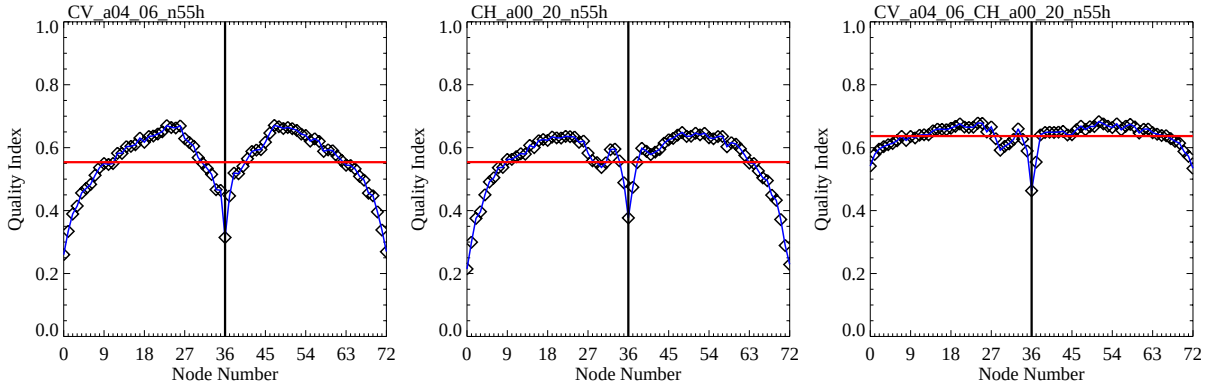


**20 KW**

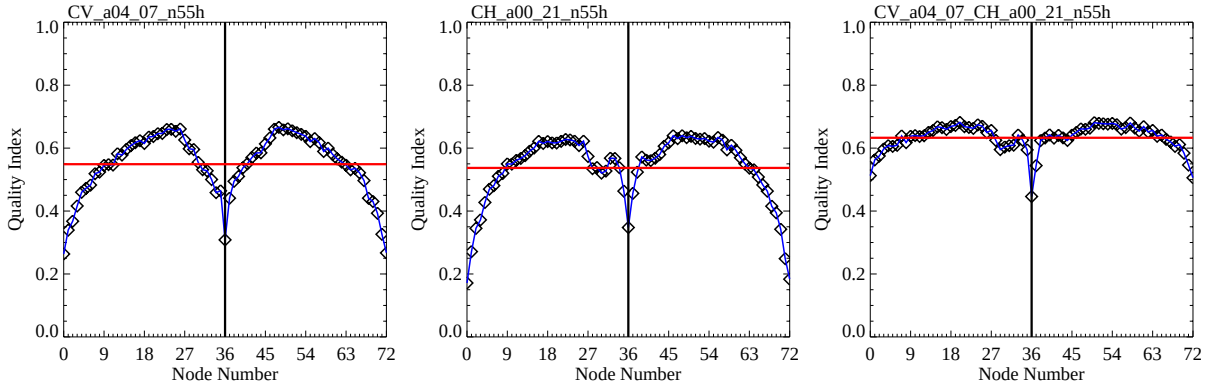


**10 KW**

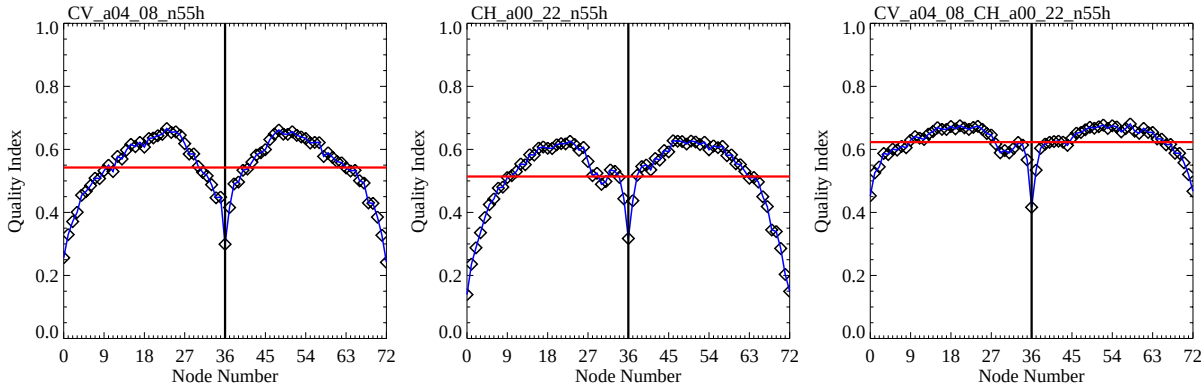


**5 KW**

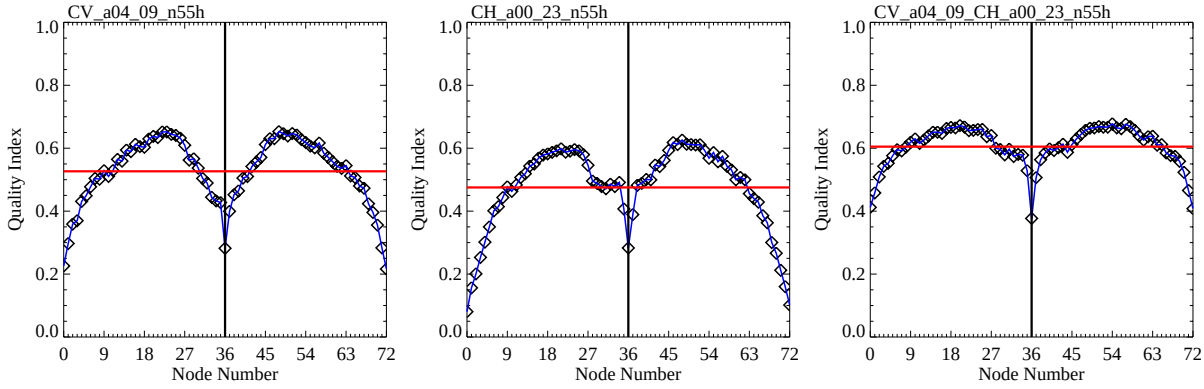


**2500 W**

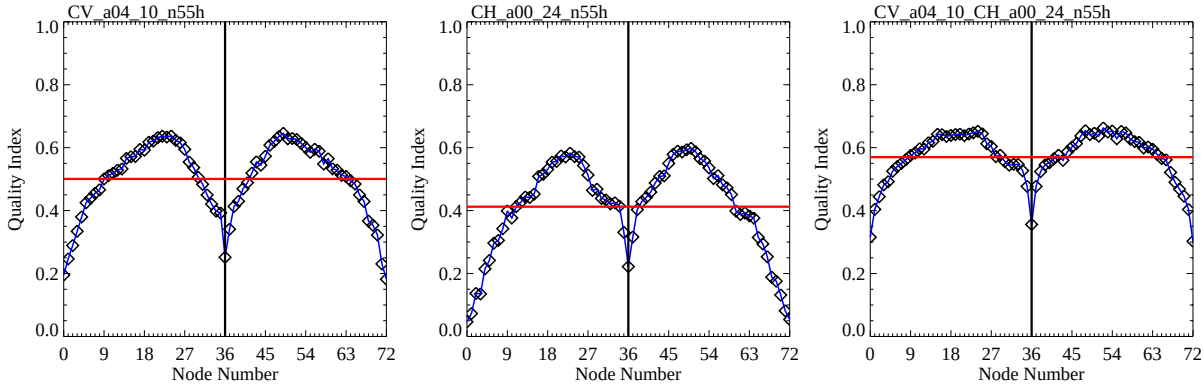


**1250 W**

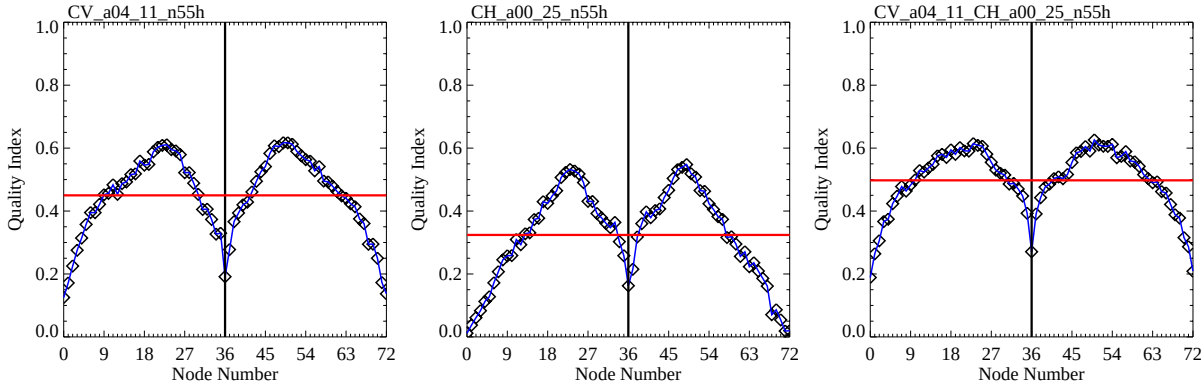


**625 W**

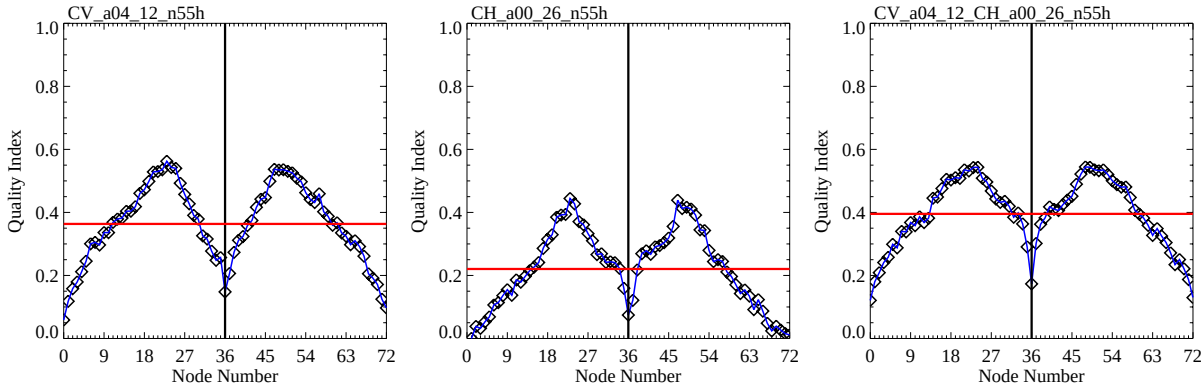


**312 W**

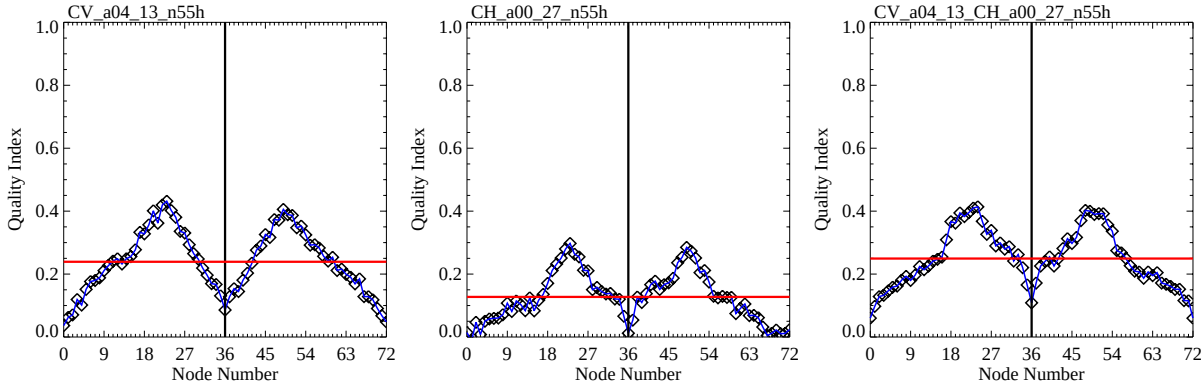


**156 W**

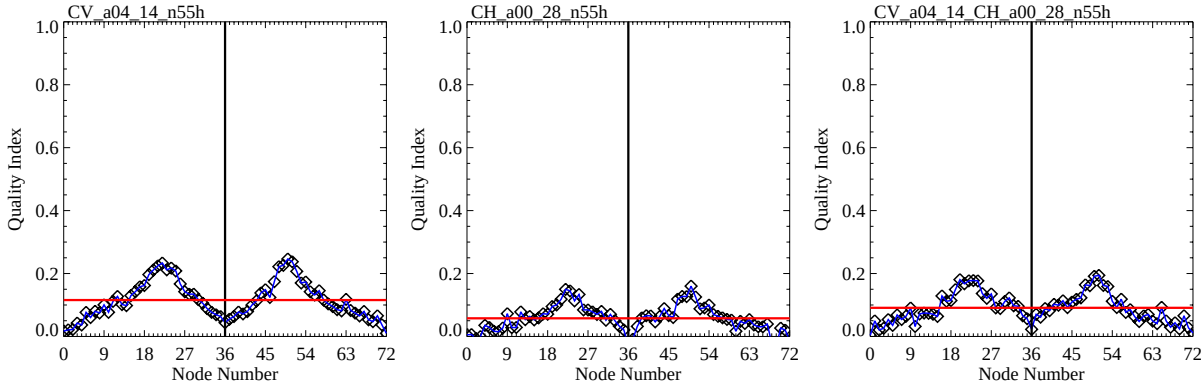


**78 W**

## 15. Annex H – Split-Beam Antenna VV & HH polarization

The following table summarizes the graphs of the quality index versus node number for a dual-beam single antenna C-band system with VV and HH polarization. The pulse peak power decrease from 640 KW to 78 W in steps of 3 dB. For the wind retrieval only VV-polarization and only HH-polarization data as well as both data together was used.

Orbit height - 725 km
Swath width - 1500 km
Resolution - 50 km

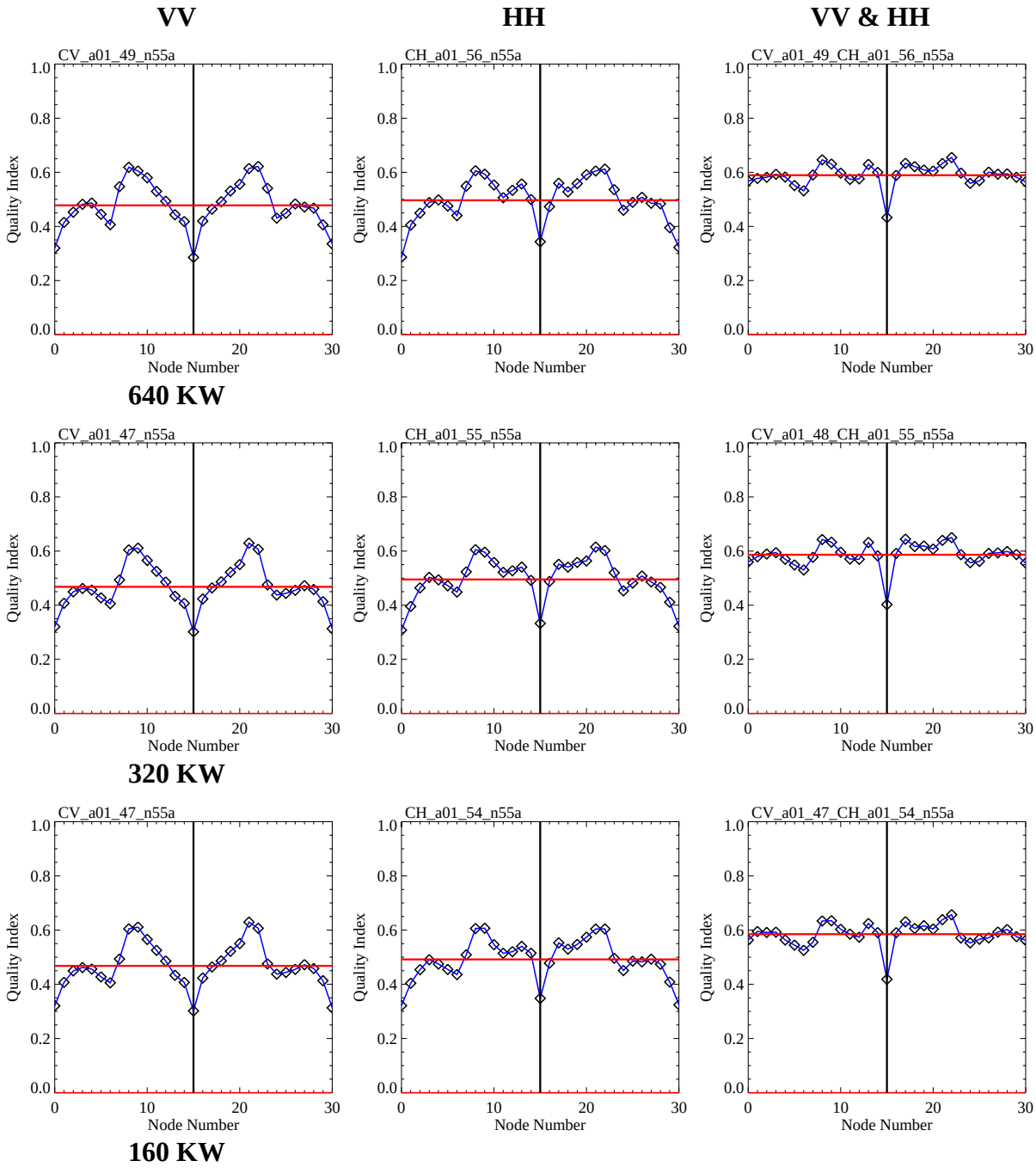

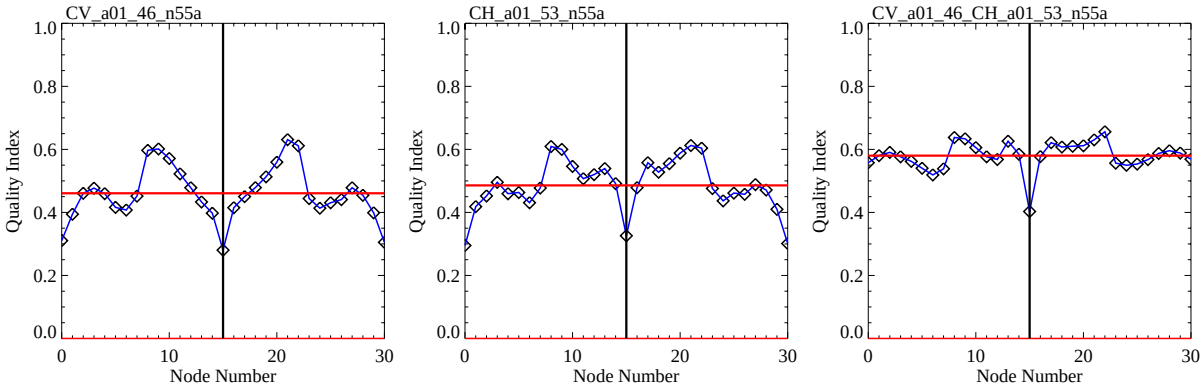


**80 KW**

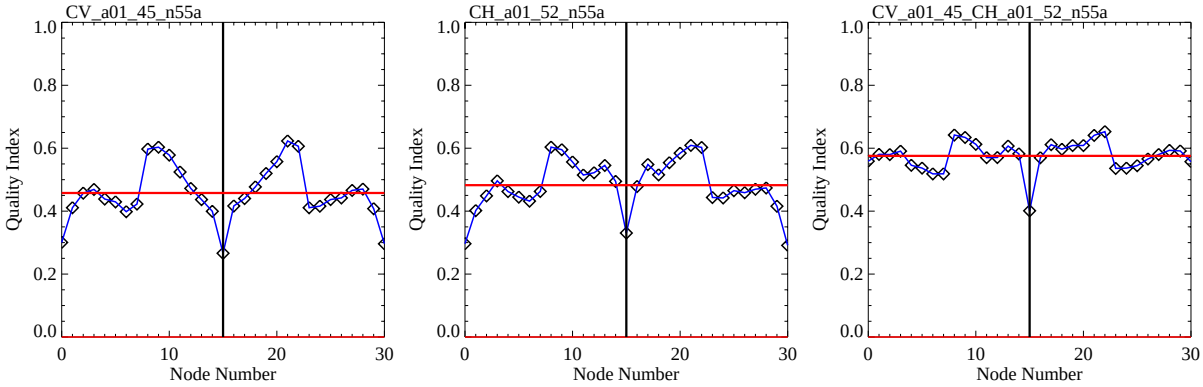


**40 KW**

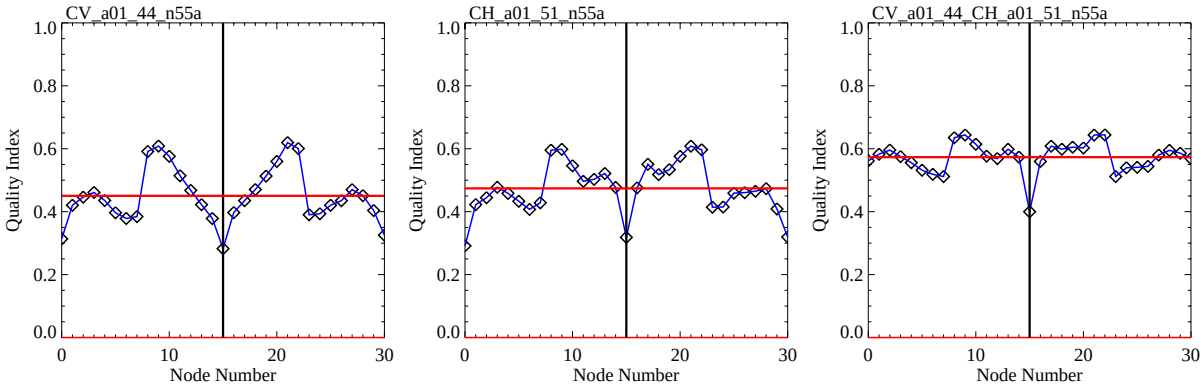


**20 KW**

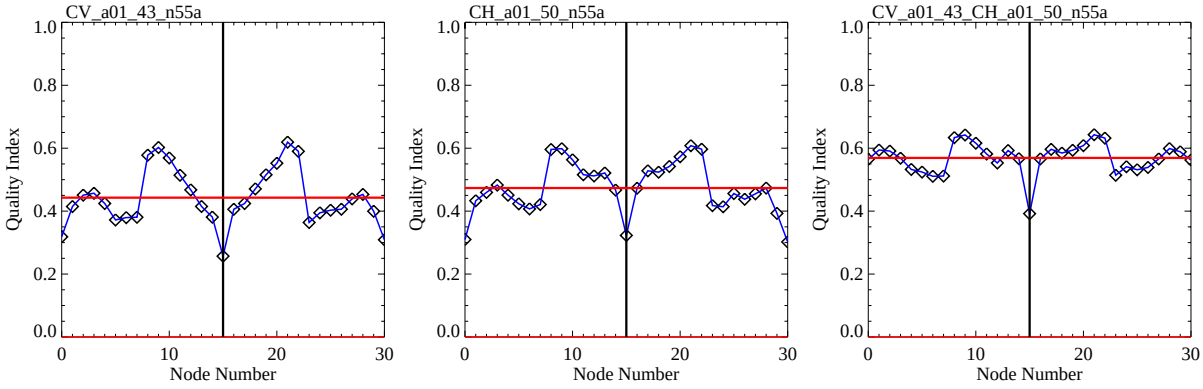


**10 KW**

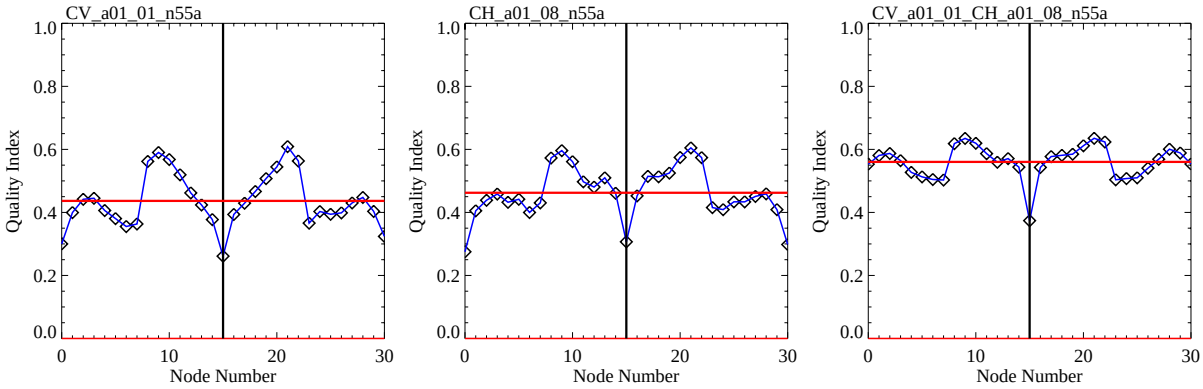


**5 KW**

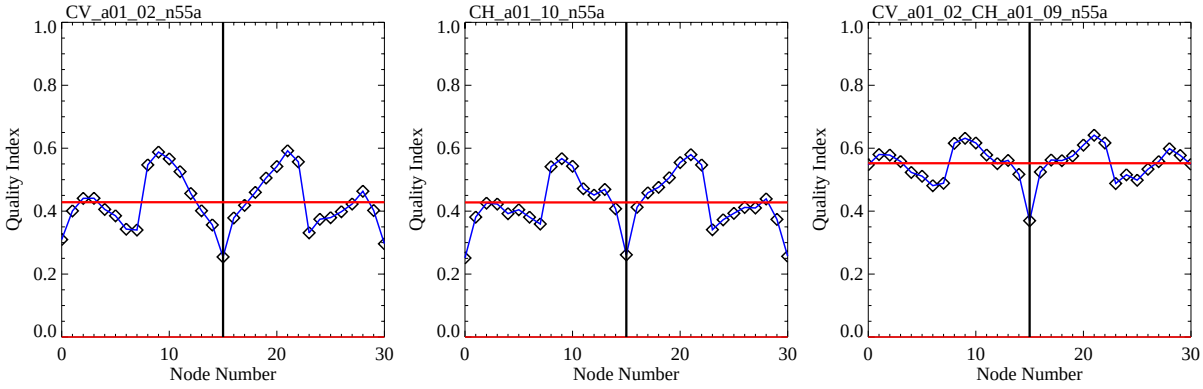


**2500 W**

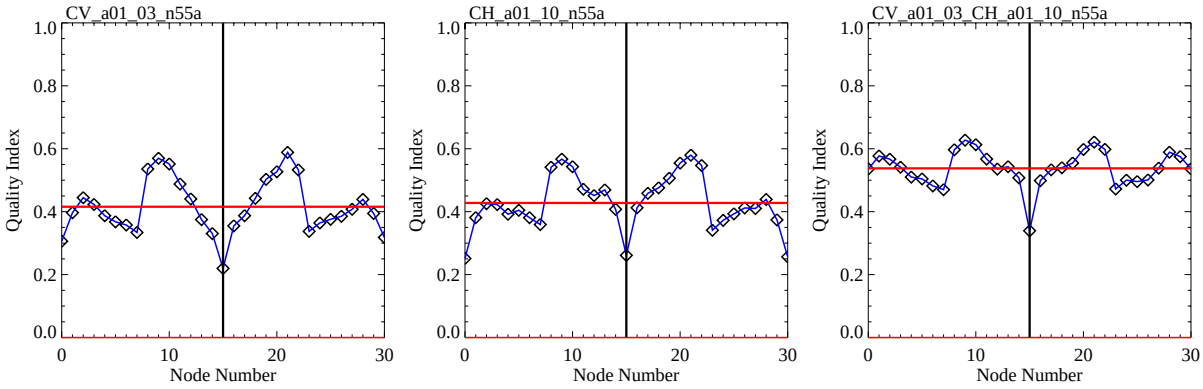


**1250 W**

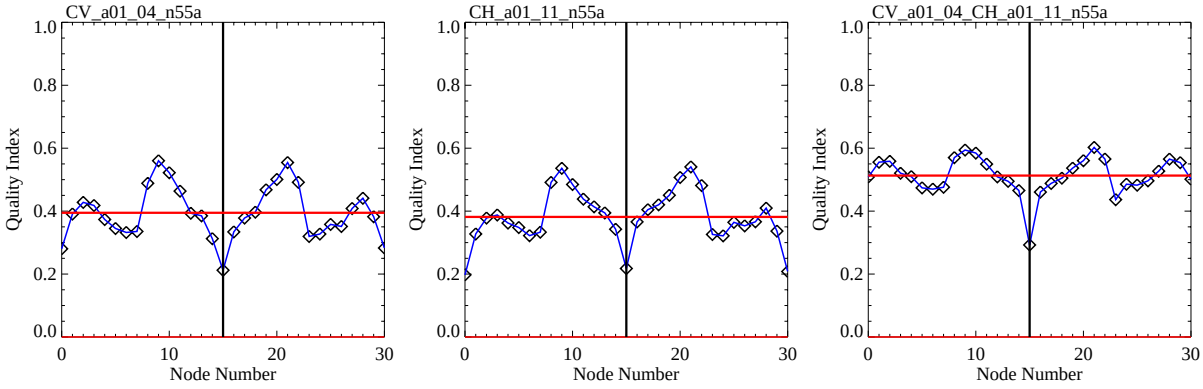


**625 W**

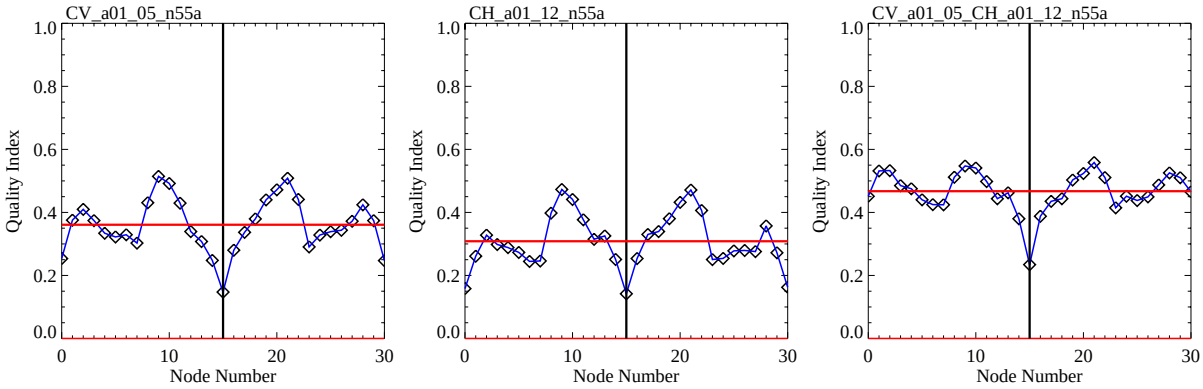


**312 W**

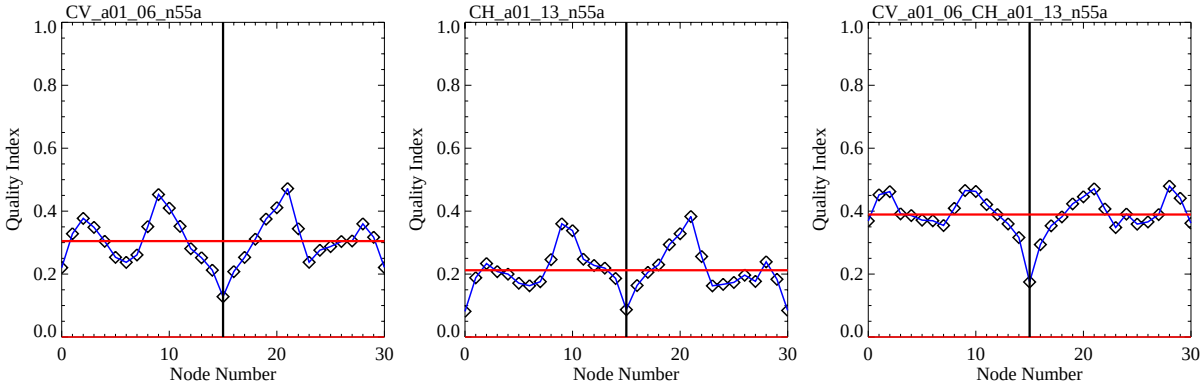


**156 W**

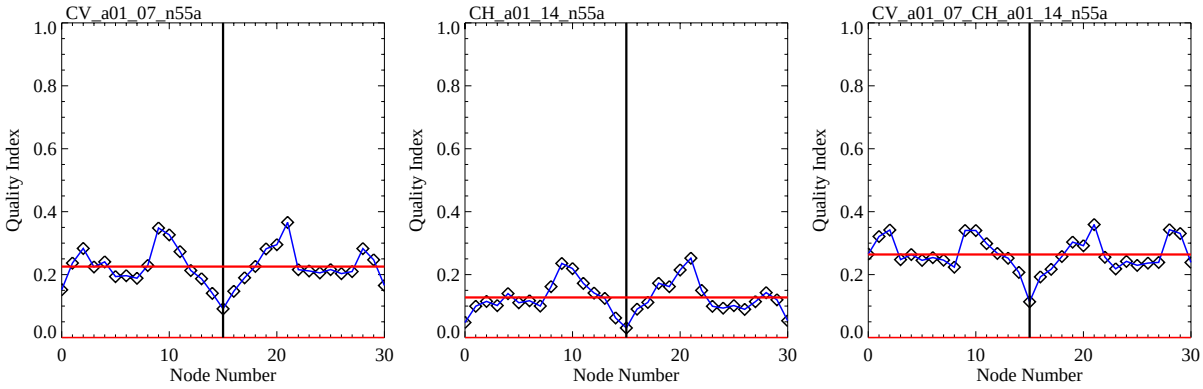


**78 W**

## 16. Annex I – High Orbit (1075 km) Dual-Polarized System

The following table summarizes the graphs of the quality index versus node number for a dual-polarized C-band system. The pulse peak power decrease from 640 KW to 78 W in steps of 3 dB. For the wind retrieval only VV-polarization and only HH-polarization data as well as both data together was used.

Orbit height - 1075 km
Swath width - 1800 km
Resolution - 50 km

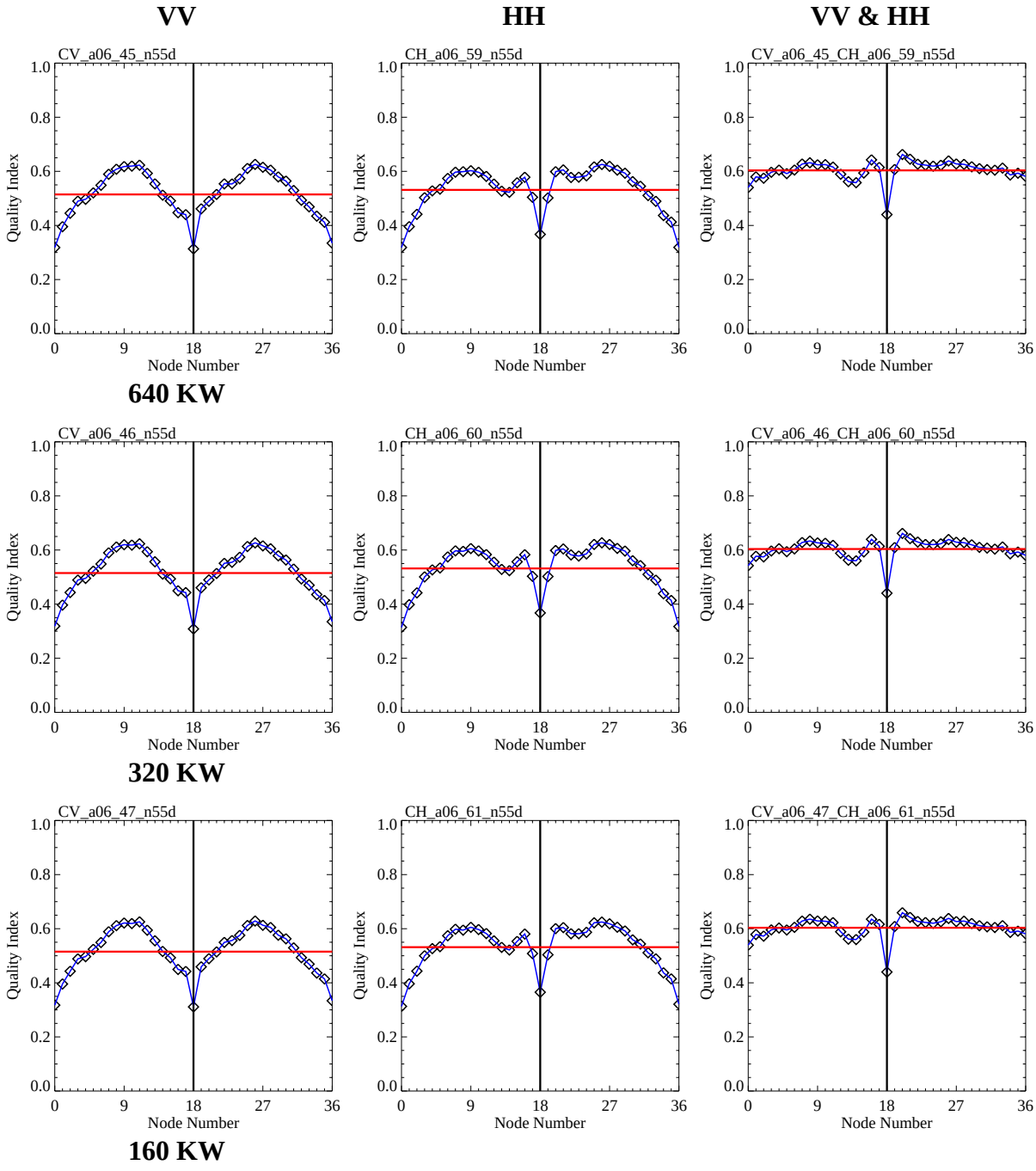

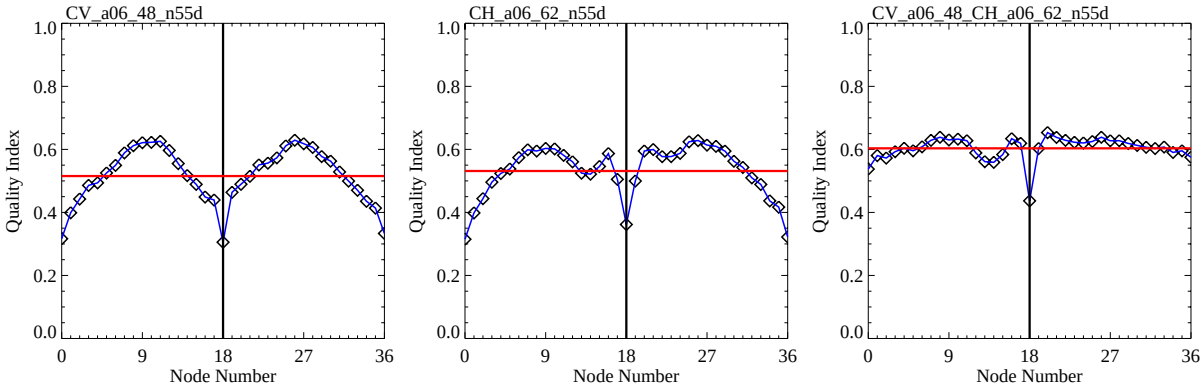


**80 KW**

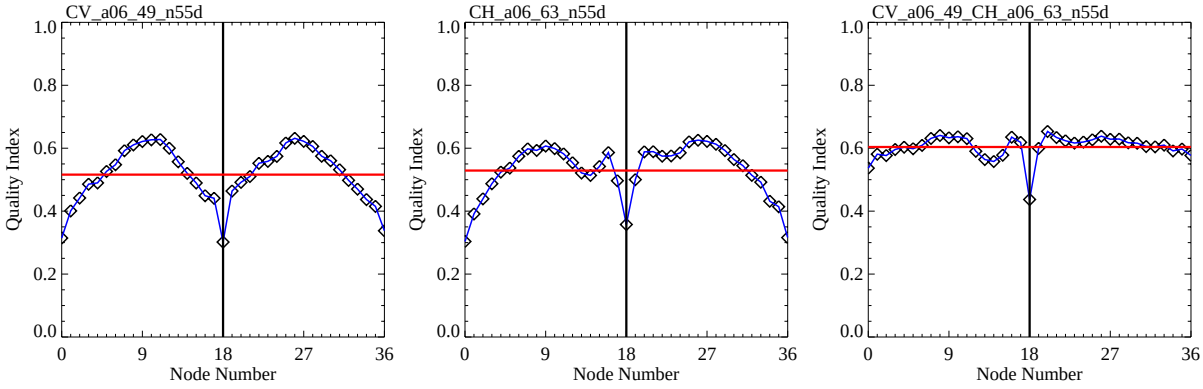


**40 KW**

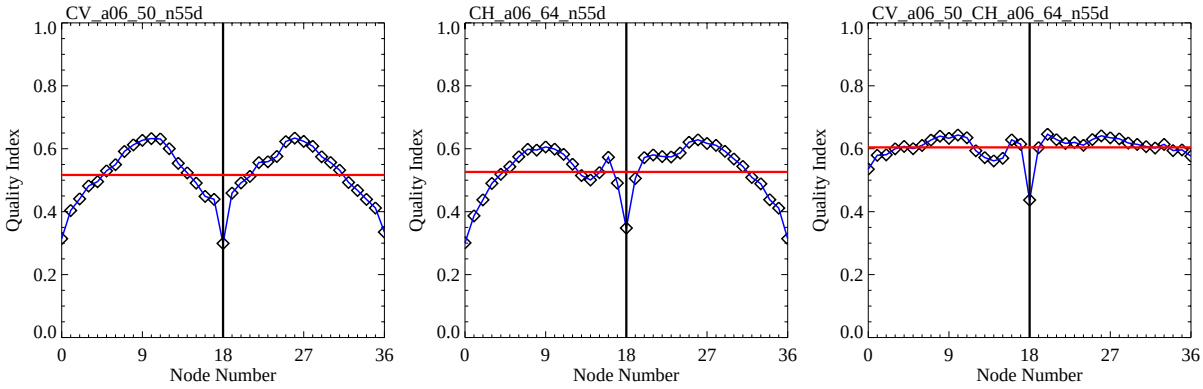


**20 KW**

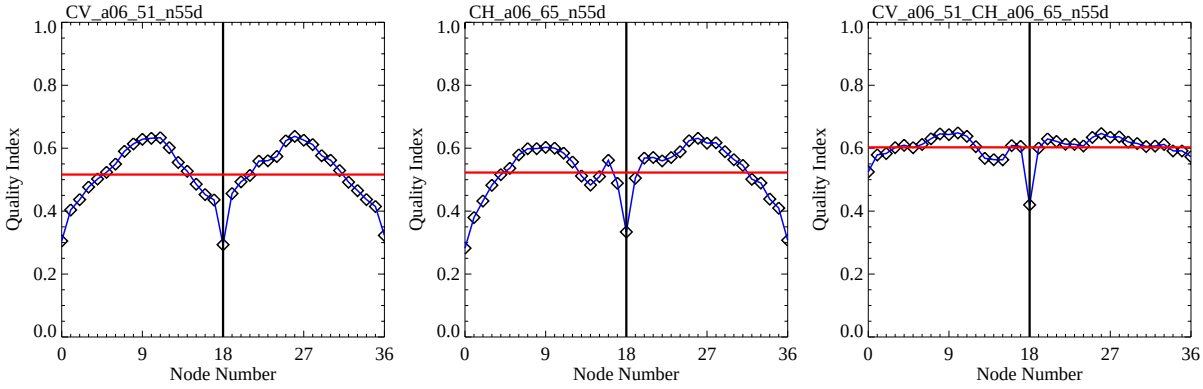


**10 KW**

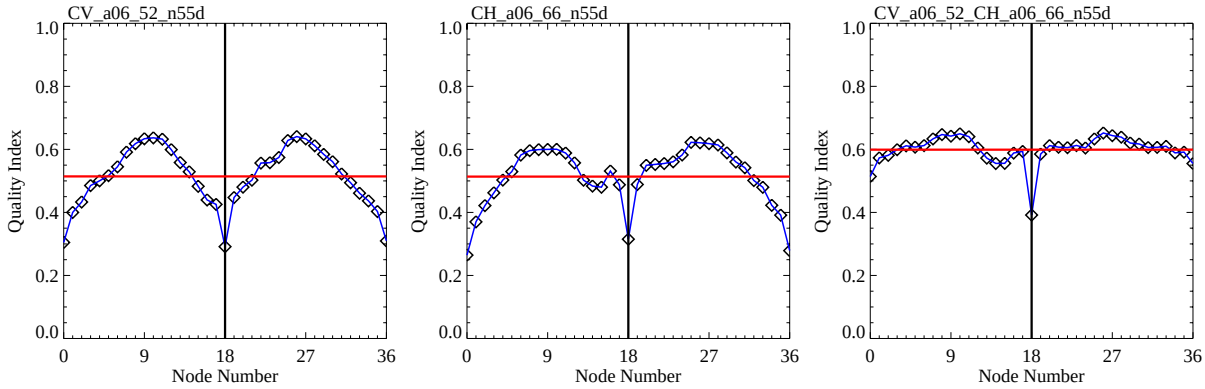


**5000 W**

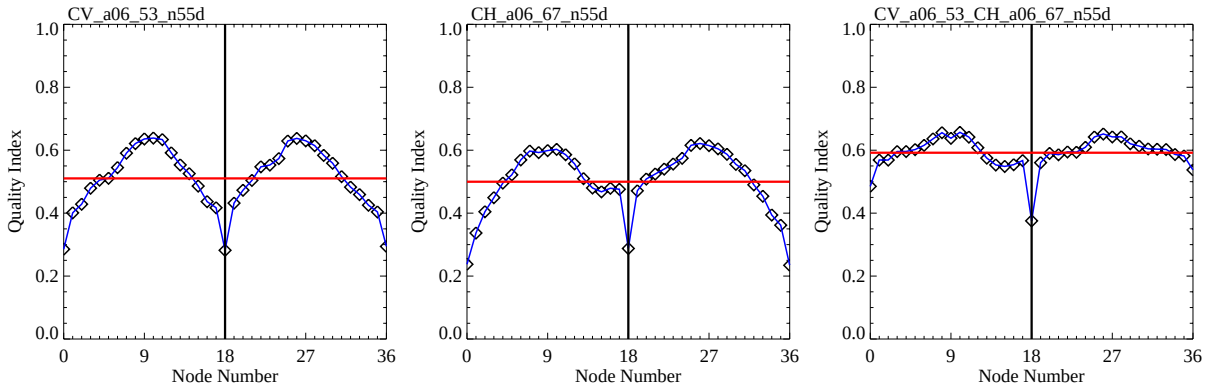


**2500 W**

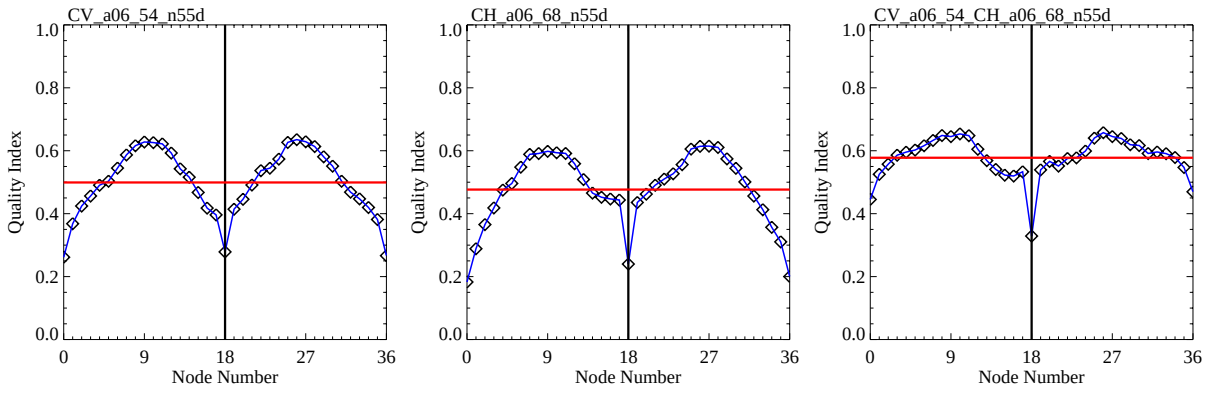


**1250 W**

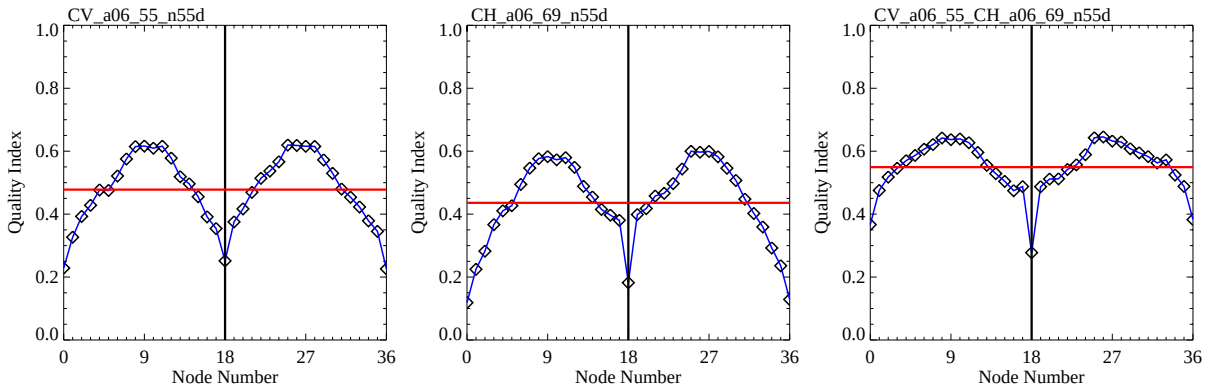


**625 W**

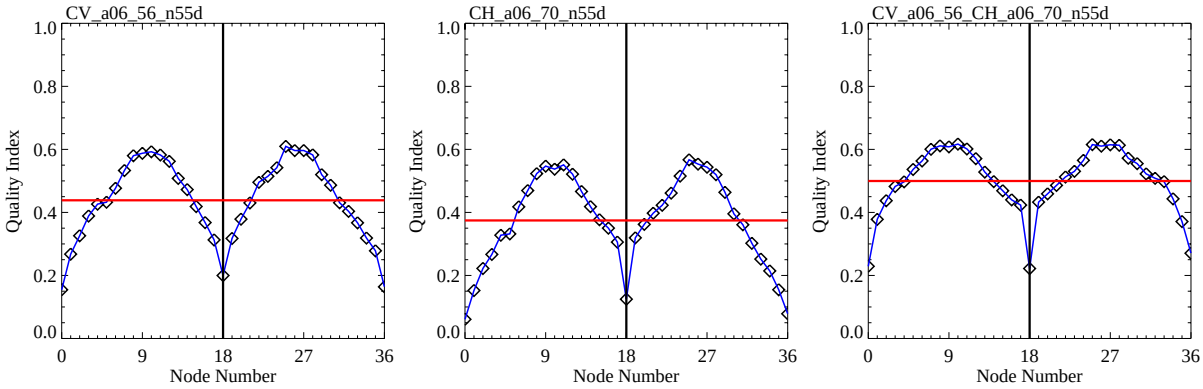


**312 W**

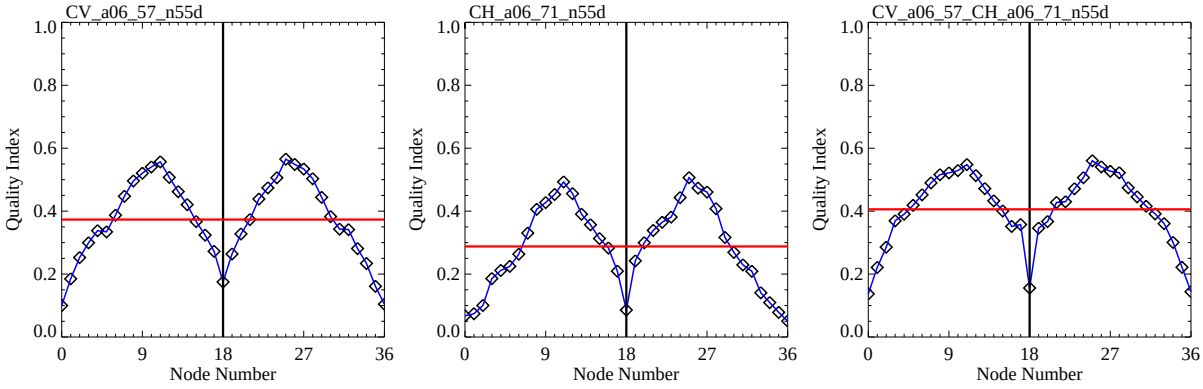


**156 W**

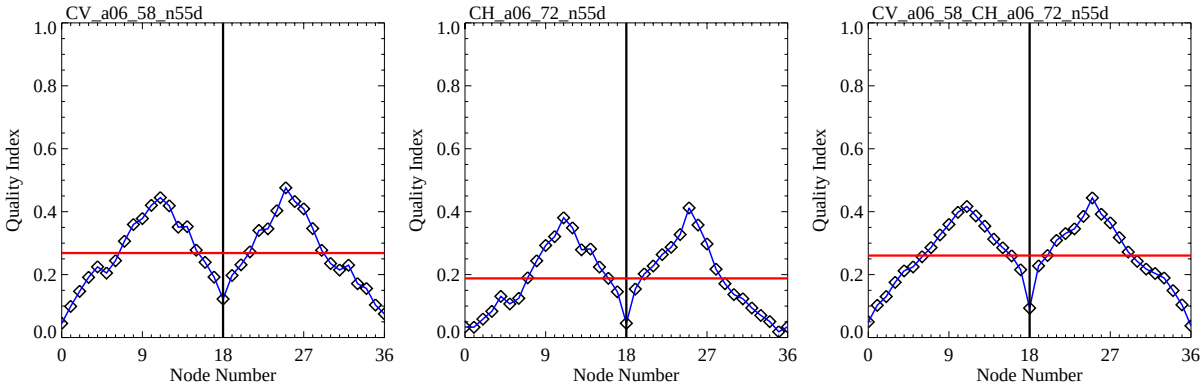


**78 W**

## 17. Annex K – Polarimetric C-band System

The following table summarizes the graphs of the quality index versus node number for a polarimetric C-band system. The pulse peak power decrease from 640 KW to 78 W in steps of 3 dB. For the wind retrieval only VV-polarization and only polarimetric data as well as both data together was used.

Orbit height - 725 km
Swath width - 1500 km
Resolution - 50 km

| VV | Pol. | VV & Pol. |
|---|---|---|
| 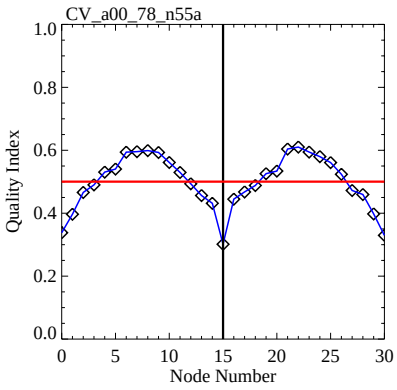 | 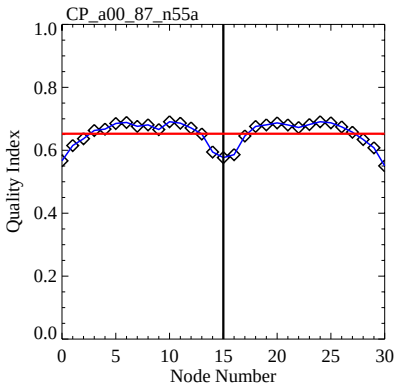 | 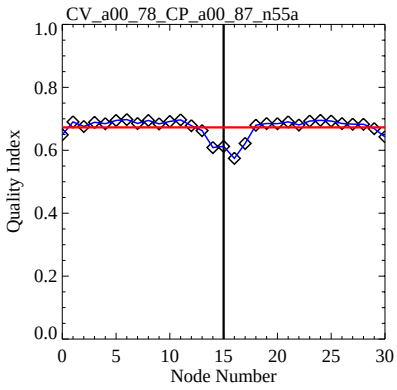 |
| **640 KW** | | |
| 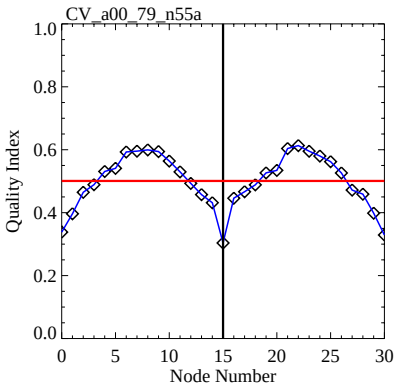 | 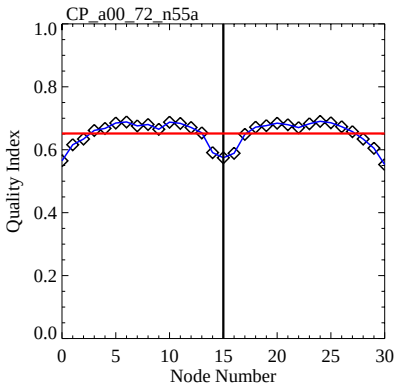 | 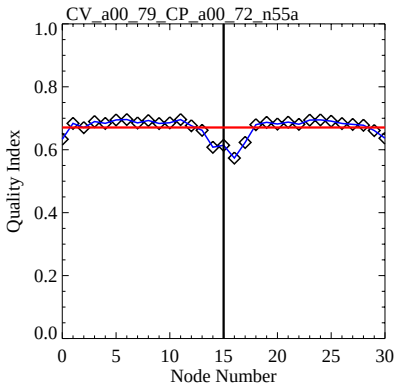 |
| **320 KW** | | |
| 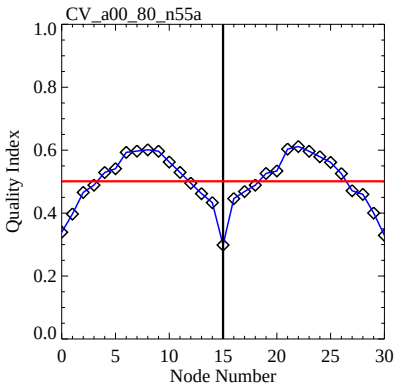 | 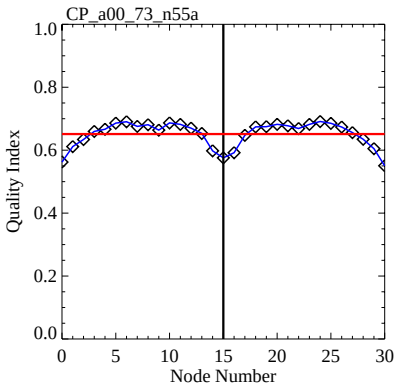 | 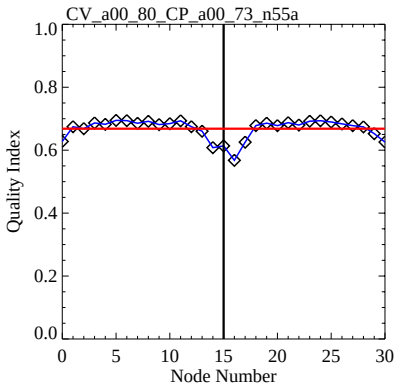 |
| **160 KW** | | |

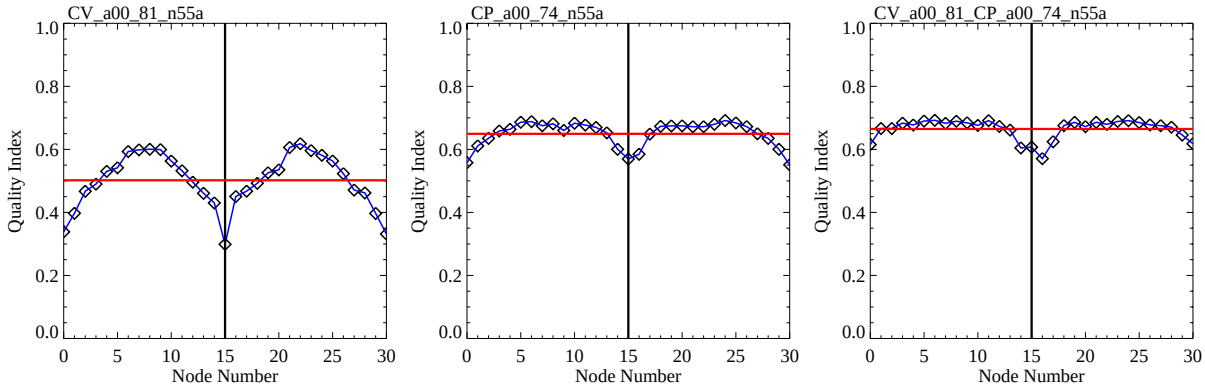


**80 KW**

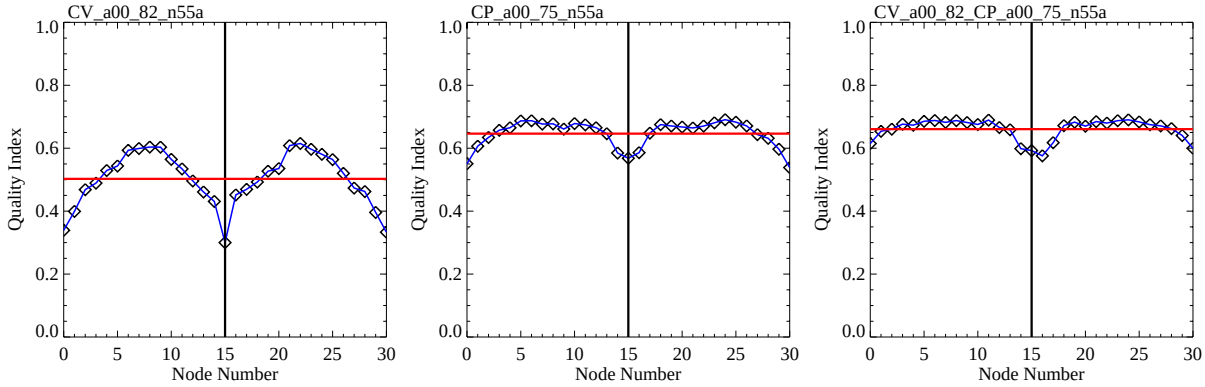


**40 KW**

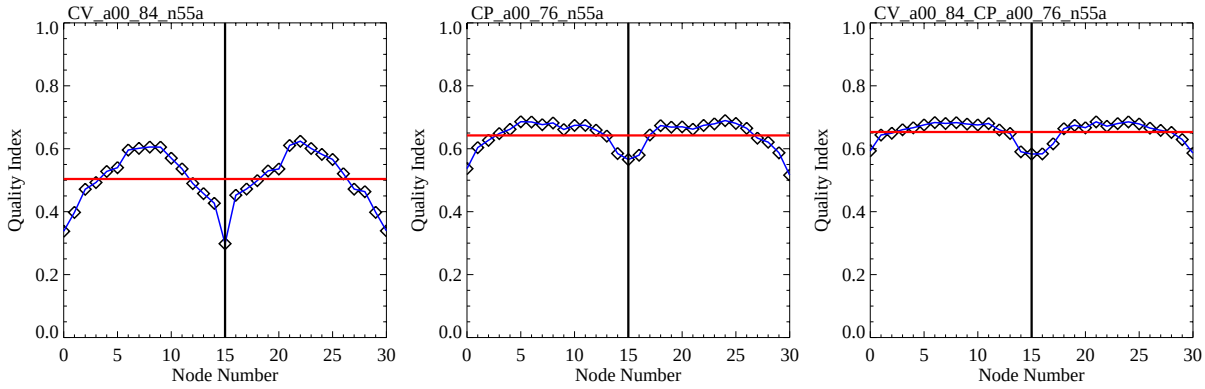


**20 KW**

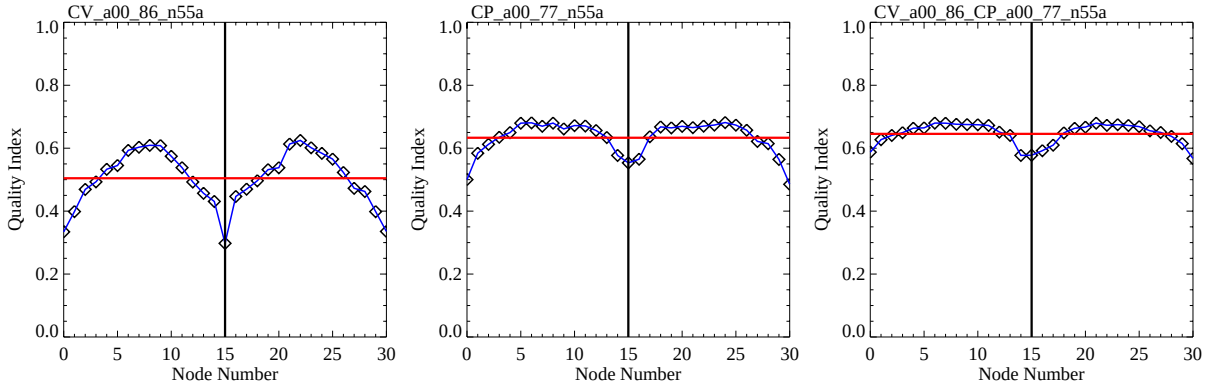


**10 KW**

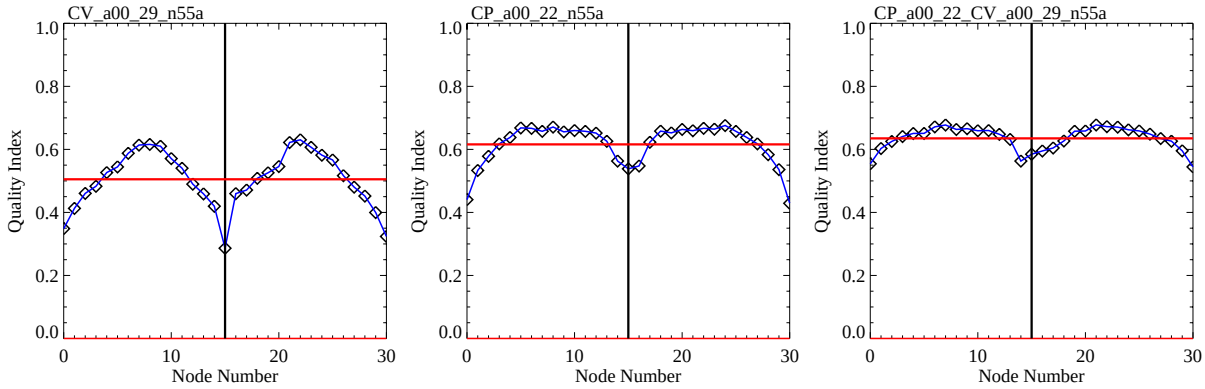


**5000 W**

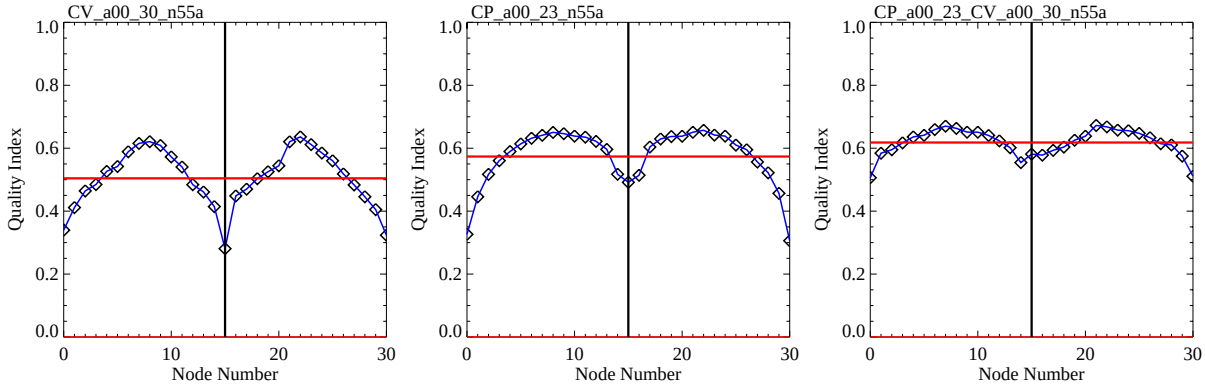


**2500 W**

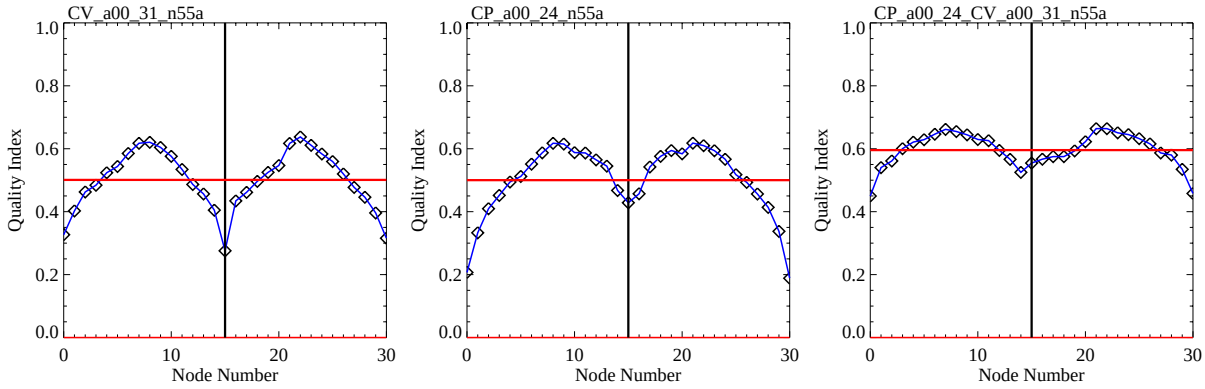


**1250 W**

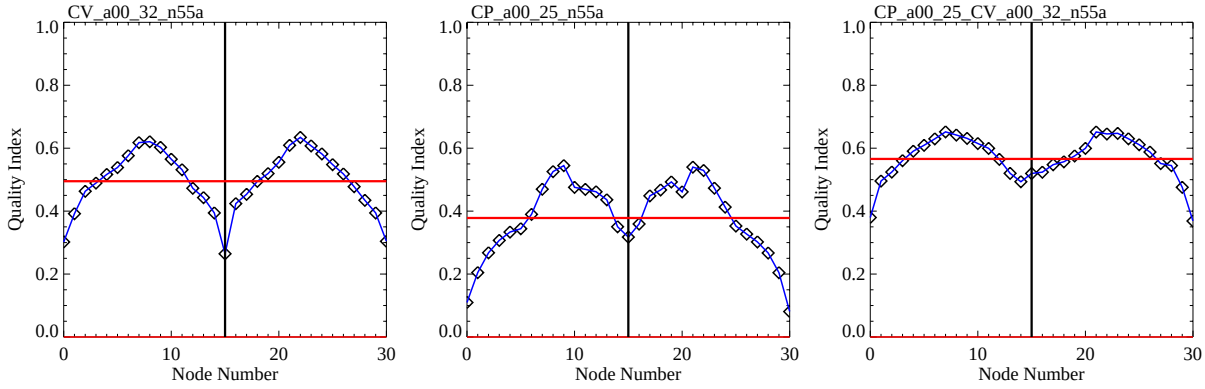


**625 W**

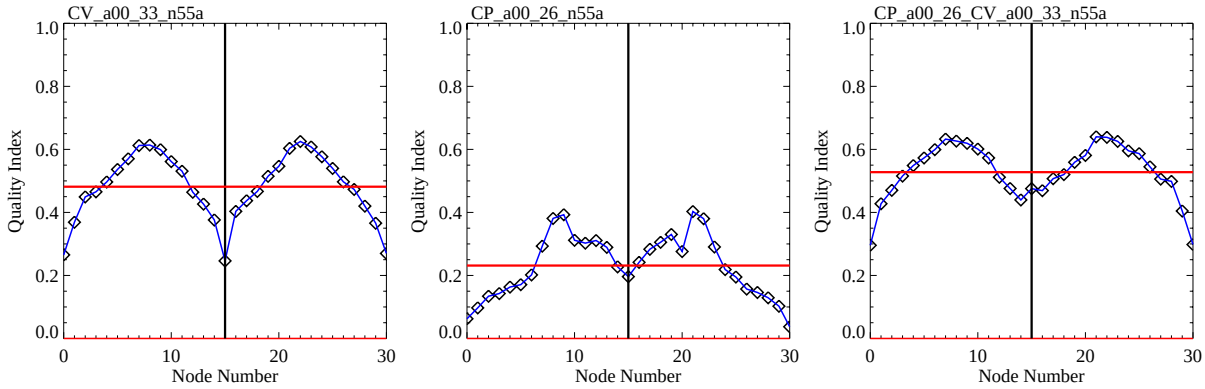


**312 W**

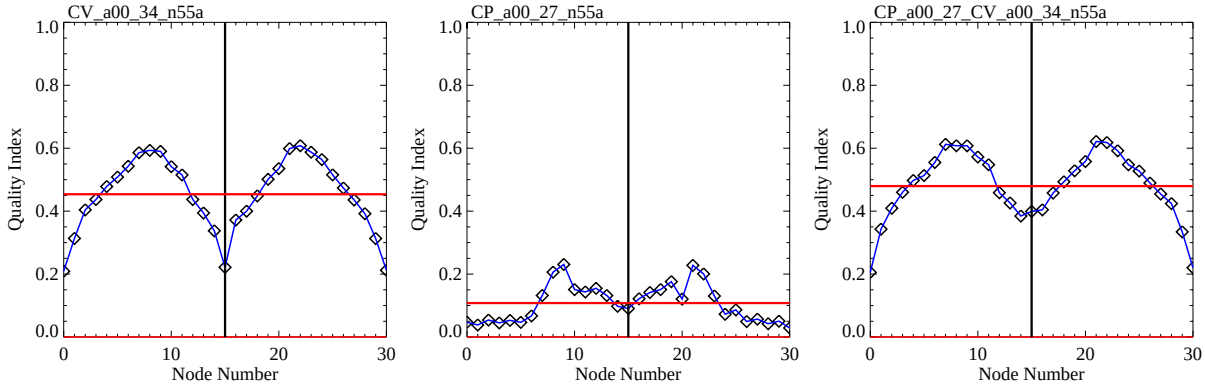


**156 W**

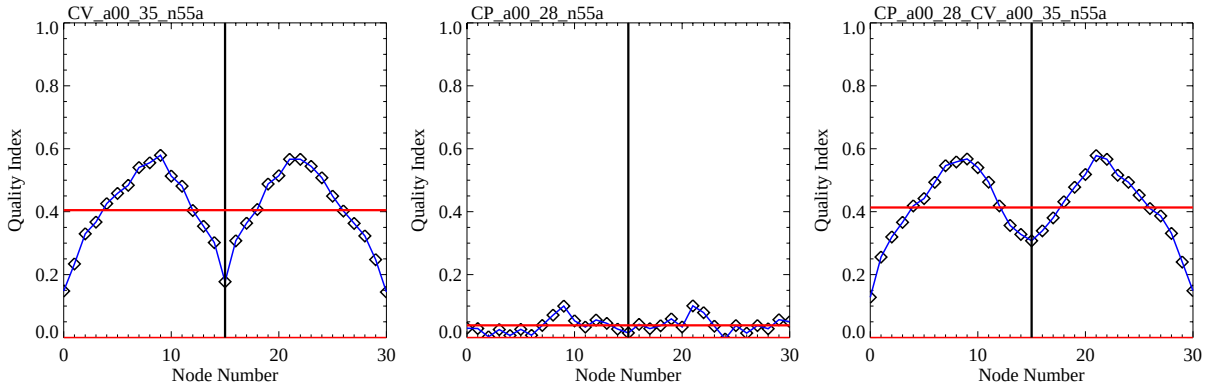


**78 W**

The following table depicts the FoM curves for the fully polarimetric system. The PRF had to be reduced to 119 Hz in order to transmit alternatingly with vertical and horizontal polarization. Therefore, these curves cannot be compared directly for the same pulse peak power.

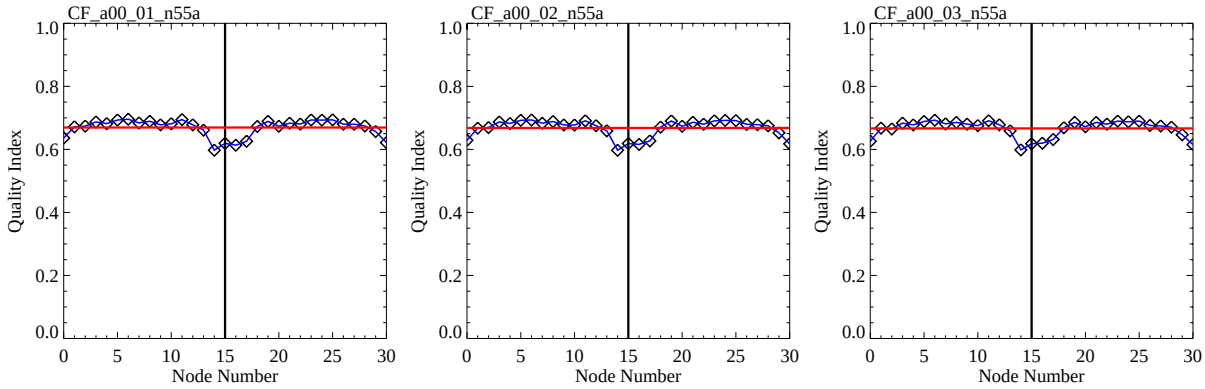


**640 KW** **320 KW** **160 KW**

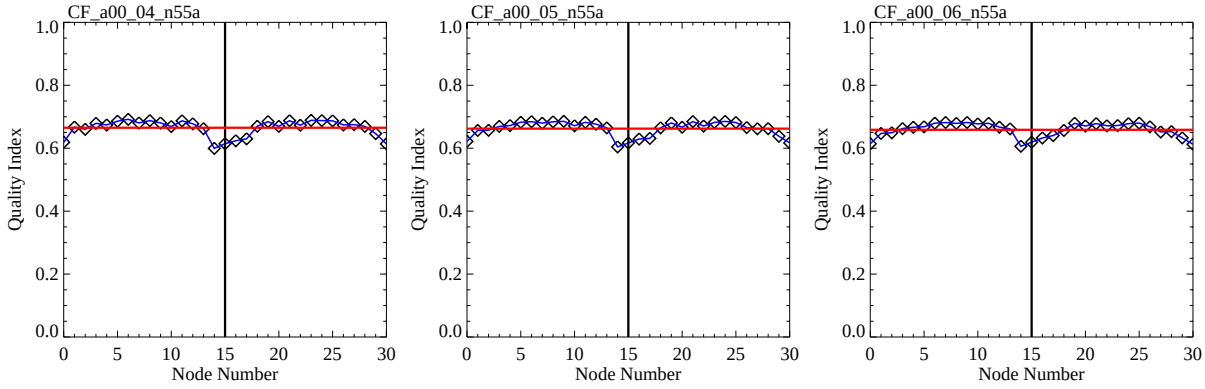


**80 KW** **40 KW** **20 KW**

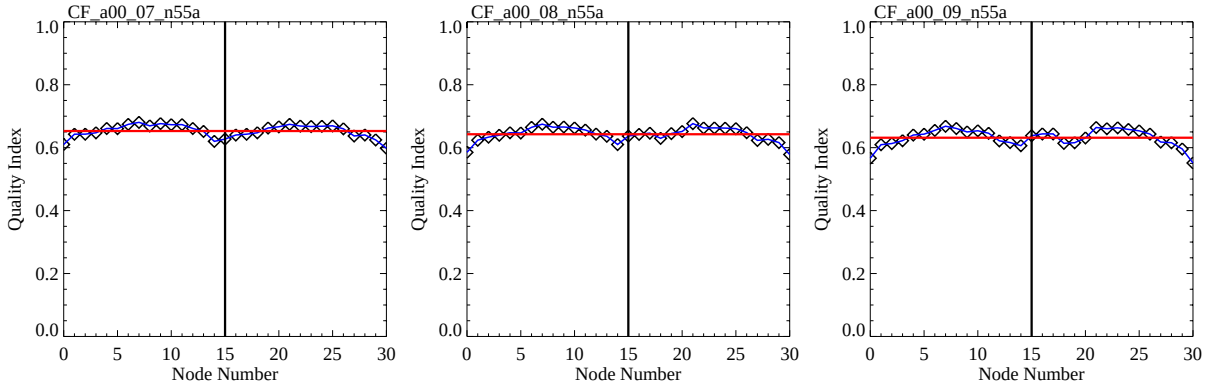


**10 KW** **5 KW** **2500 W**

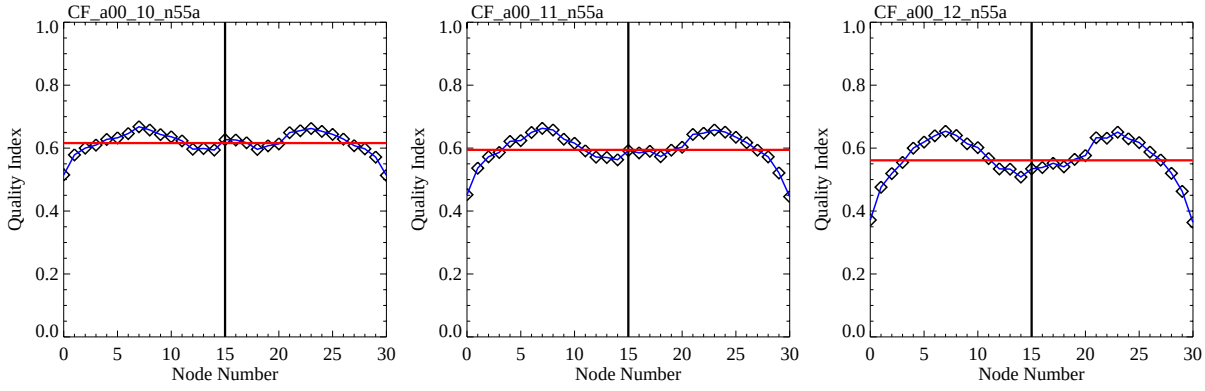


**1250 W** **625 W** **312 W**

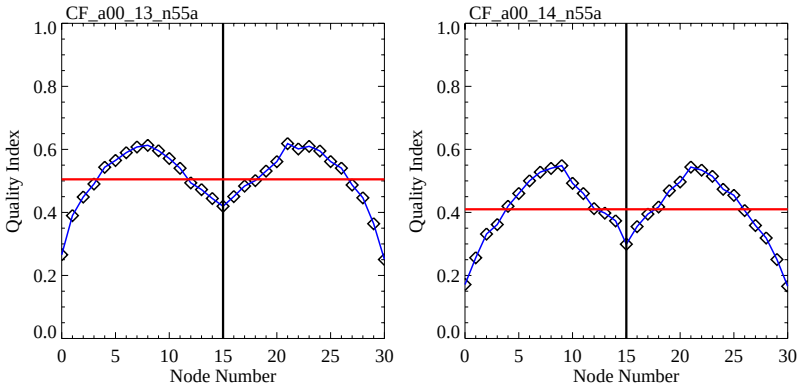
CF_a00_13_n55a
Quality Index
Node Number
CF_a00_14_n55a
Quality Index
Node Number

**156 W** **78 W**

## 18. Annex L – Wide Swath (1800 km) Polarimetric System

The following table summarizes the graphs of the quality index versus node number for a single antenna polarimetric C-band system. The pulse peak power decrease from 640 KW to 78 W in steps of 3 dB. For the wind retrieval only VV-polarization and only polarimetric data as well as both data together was used.

Orbit height - 725 km
Swath width - 1800 km
Resolution - 50 km

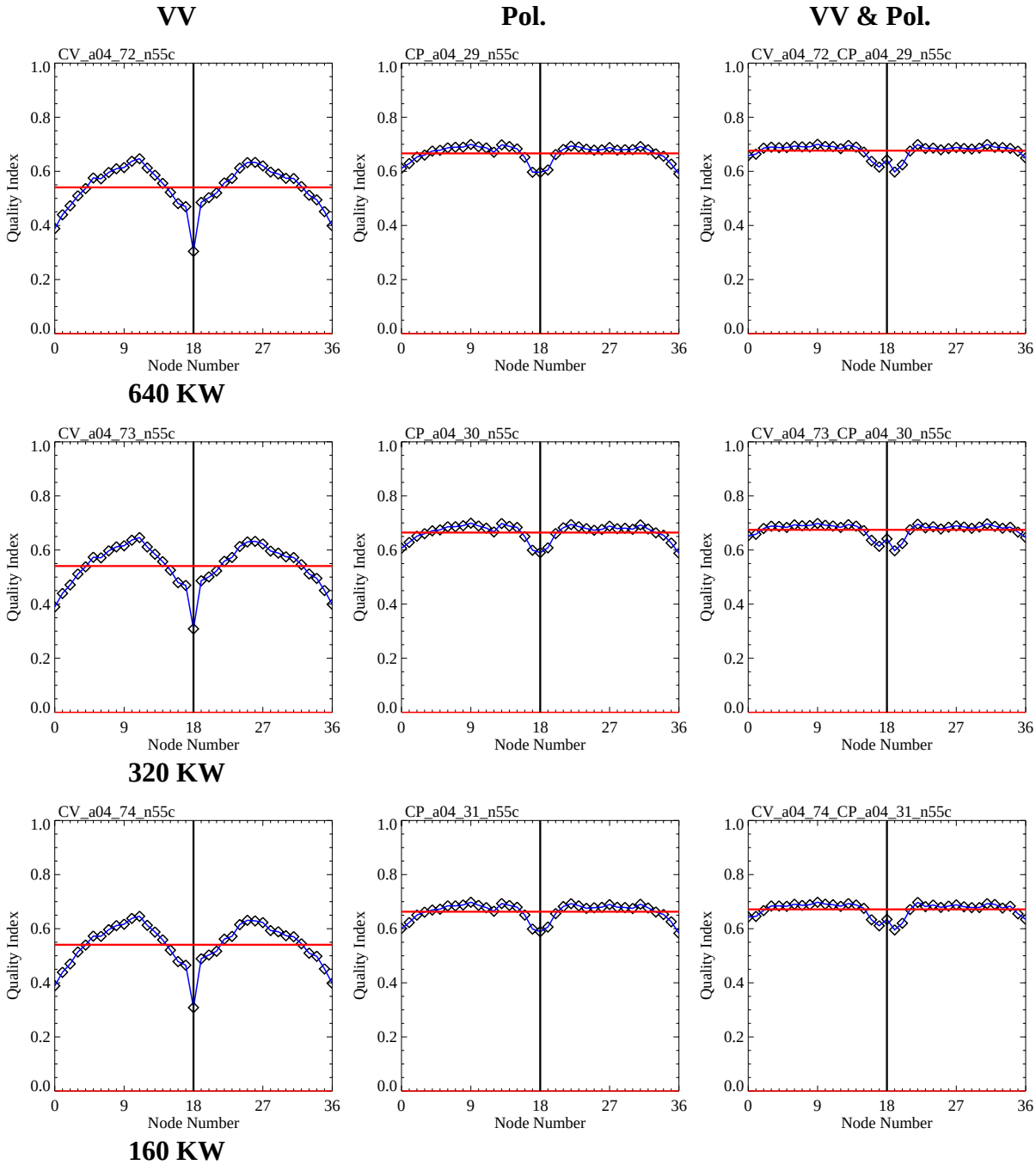

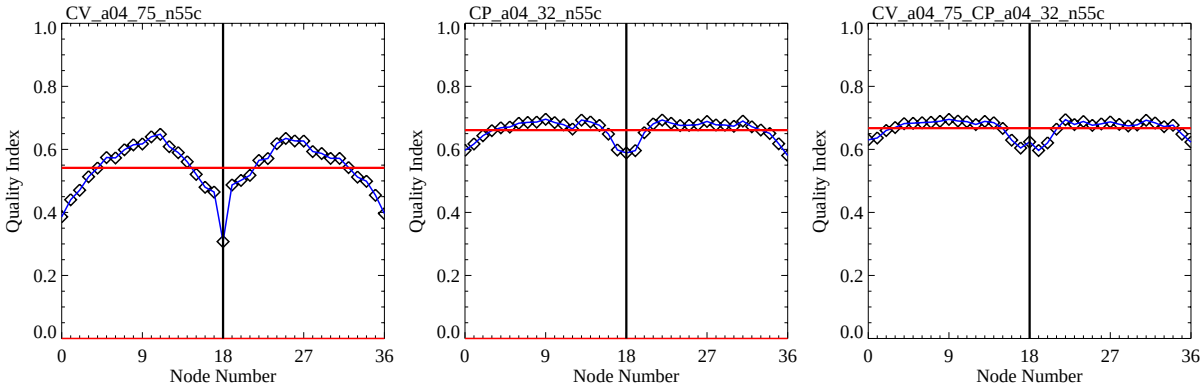


**80 KW**

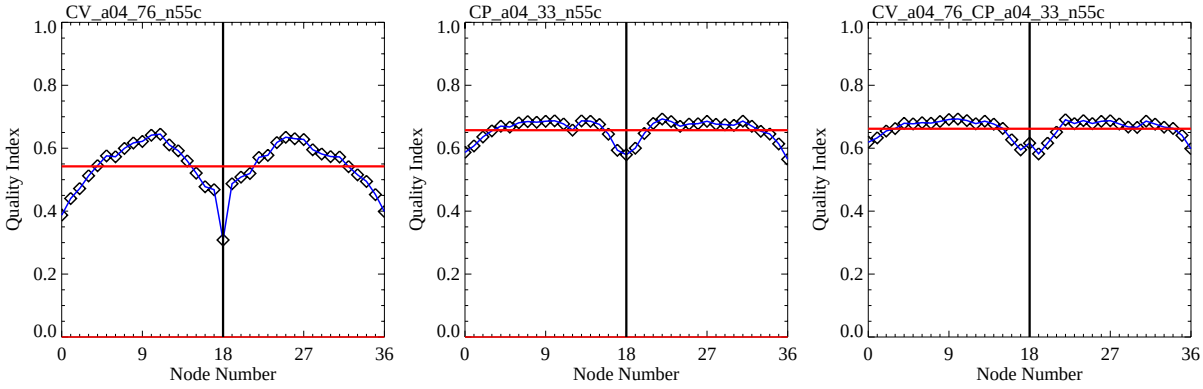


**40 KW**

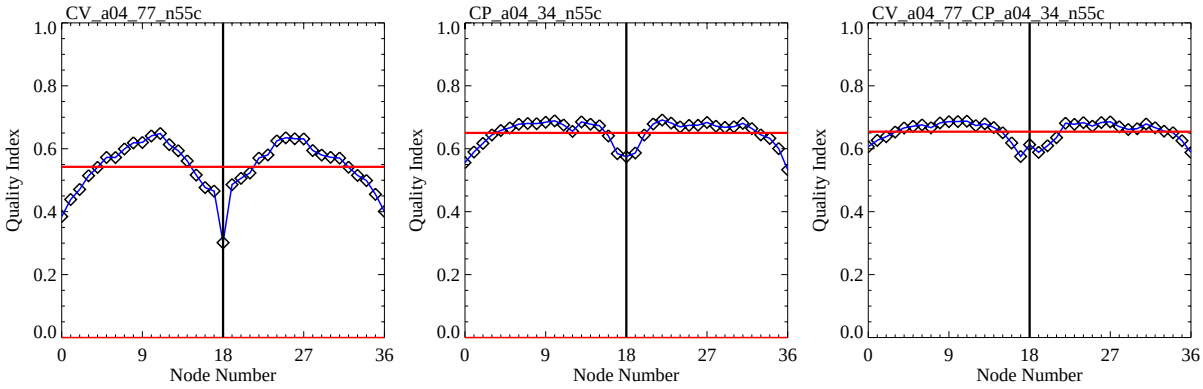


**20 KW**

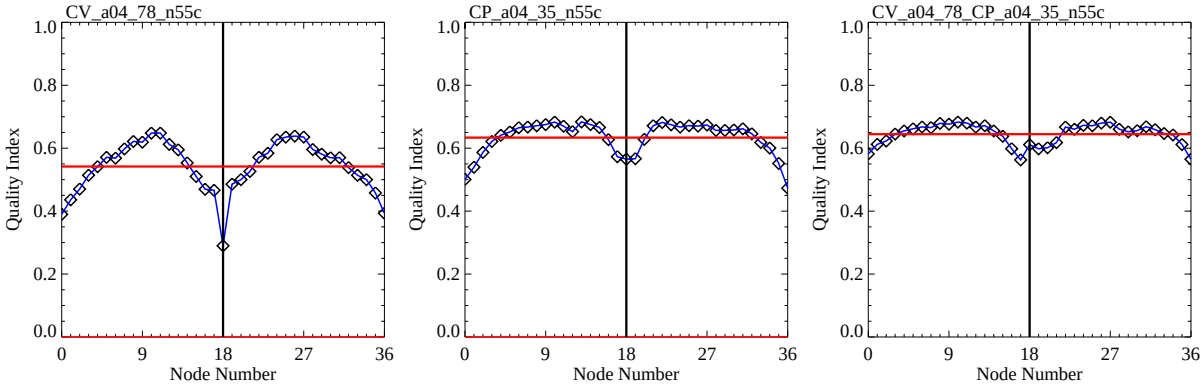


**10 KW**

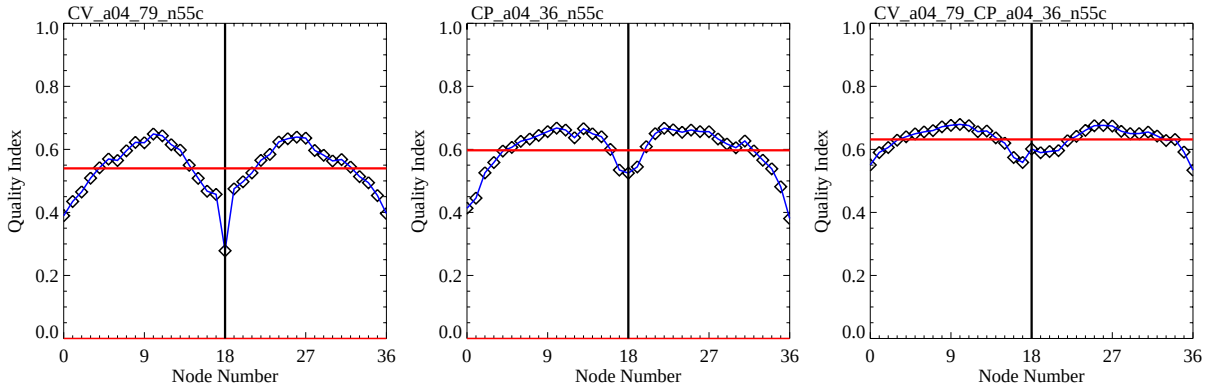


**5000 W**

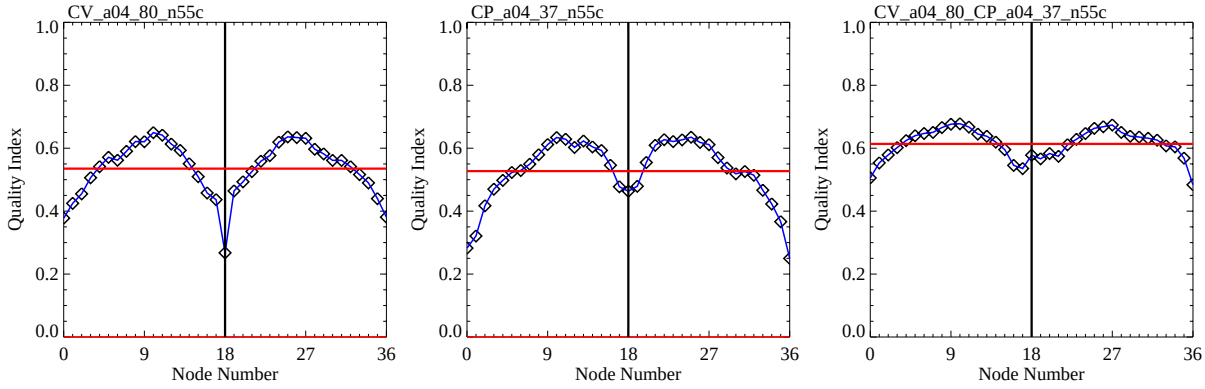


**2500 W**

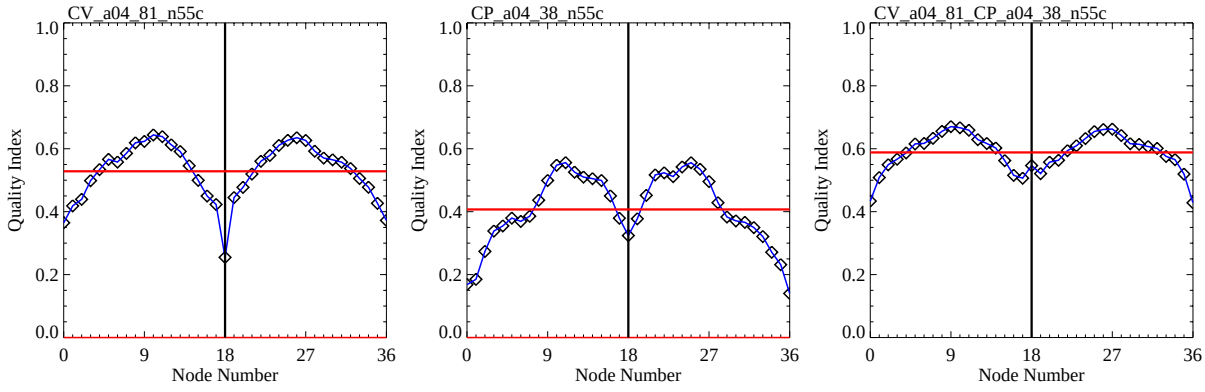


**1250 W**

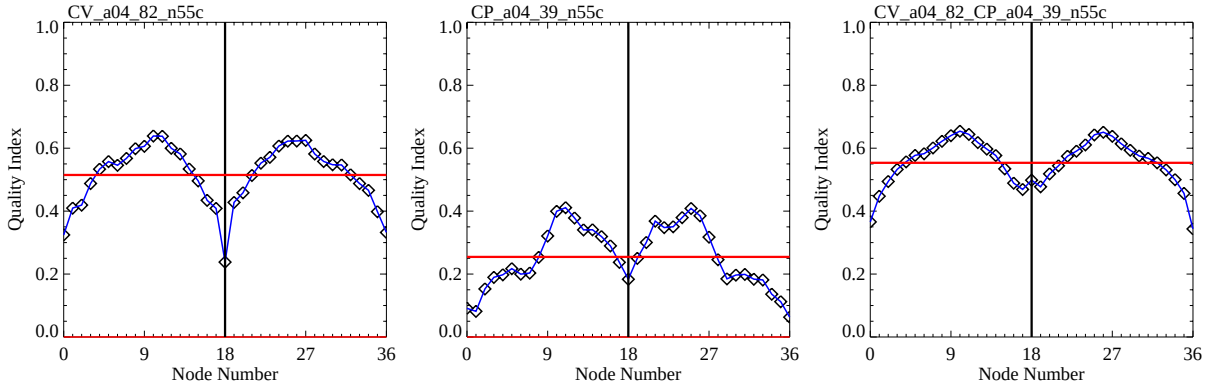


**625 W**

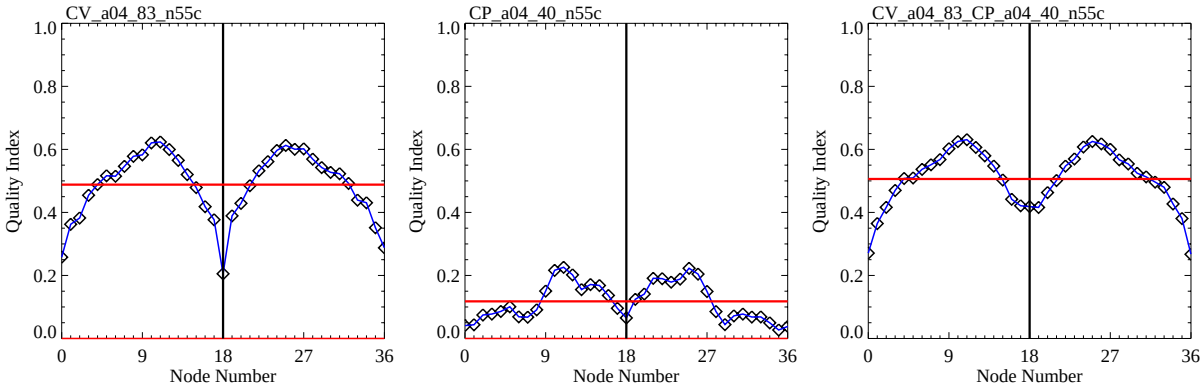


**312 W**

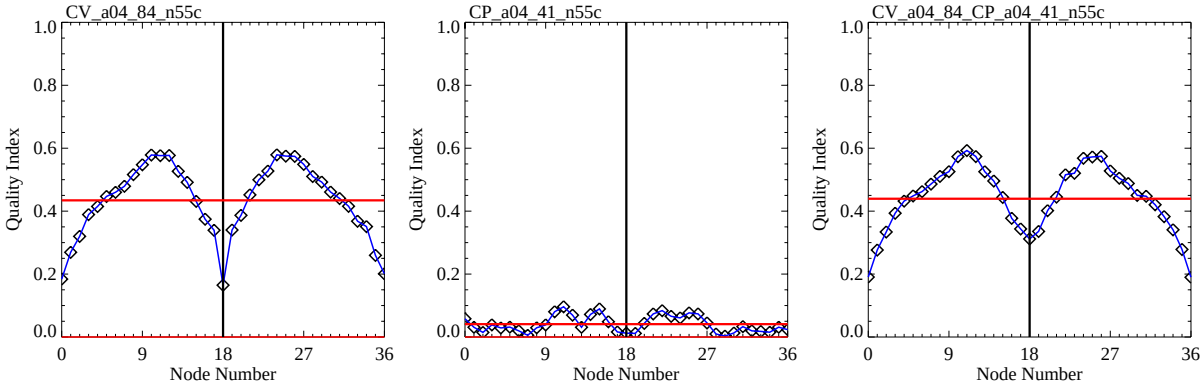


**156 W**

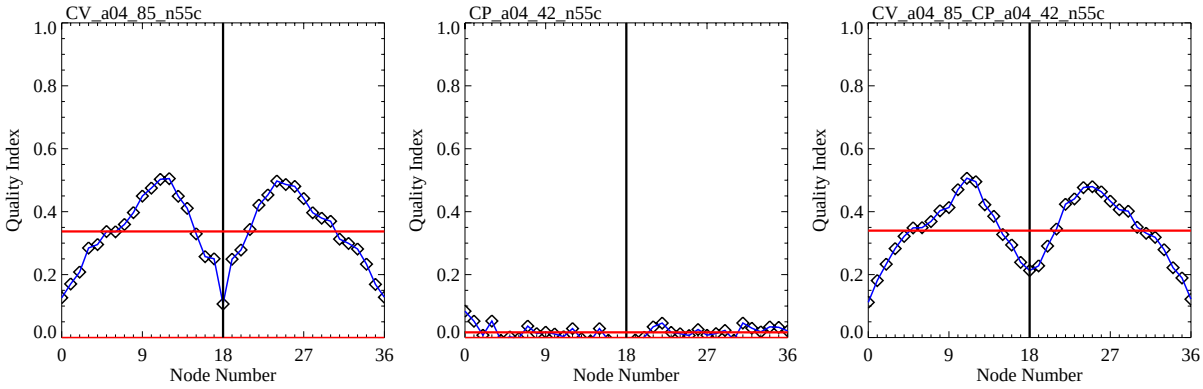


**78 W**

The following graphs are for the respective fully polarimetric system.

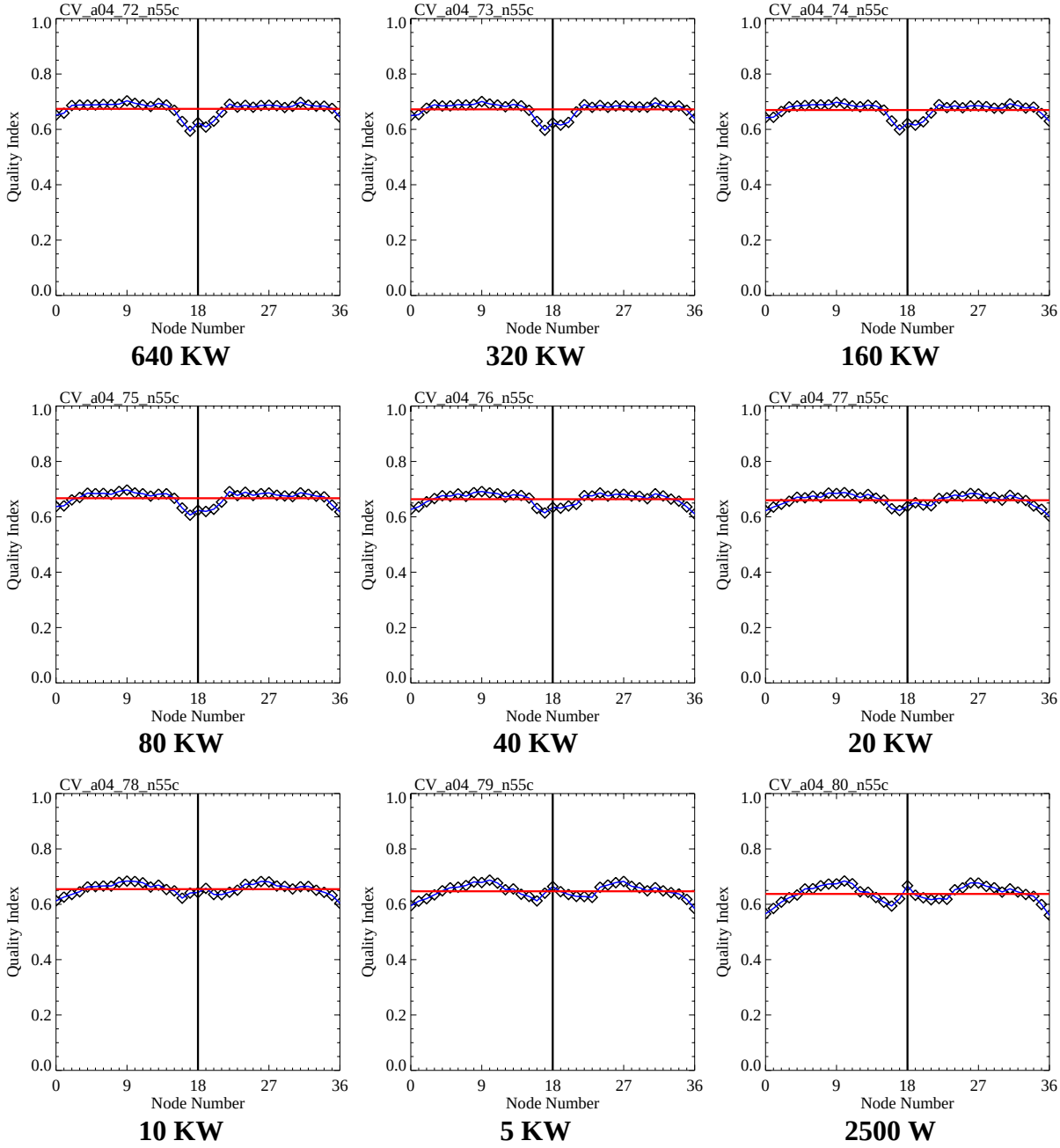

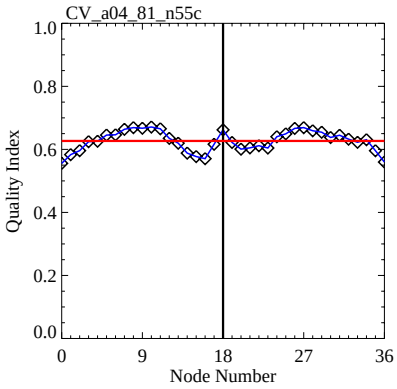


**1250 W**

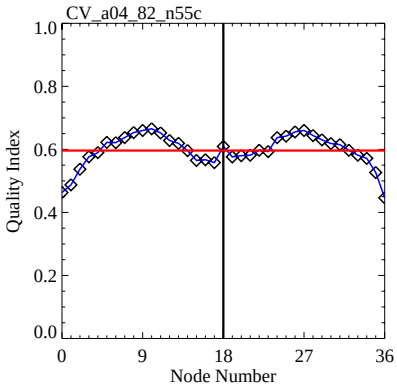


**625 W**

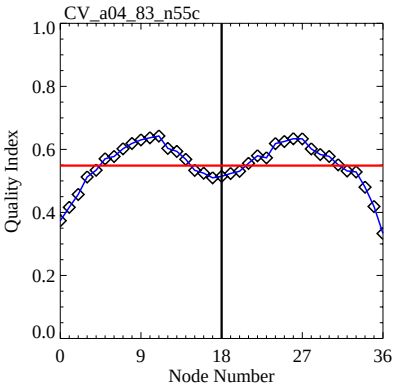


**312 W**

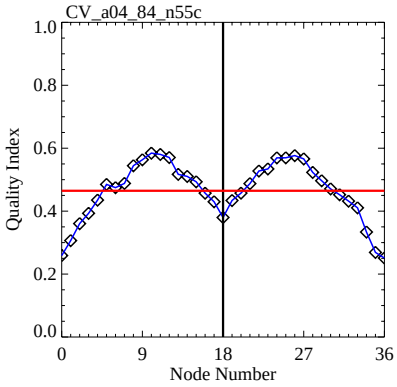


**156 W**

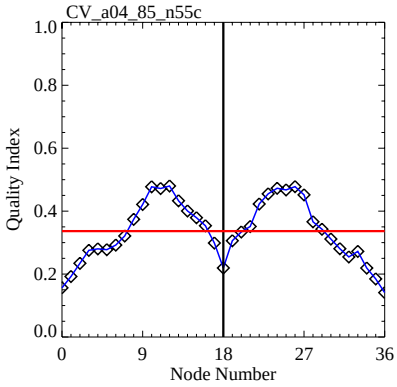


**78 W**

## 19. Annex M – Wide Swath and 25 km Resolution Polarimetric System

The following table summarizes the graphs of the quality index versus node number for a single antenna polarimetric C-band system. The pulse peak power decrease from 640 KW to 78 W in steps of 3 dB. For the wind retrieval polarimetric data (CP), VV-polarization plus polarimetric data (CV & CP) as well as fully polarimetric data (CV & CH & CP) was used.

Orbit height - 725 km
Swath width - 1800 km
Resolution - 25 km

| CP | CV & CP | CV & CH & CP |
|---|---|---|
| 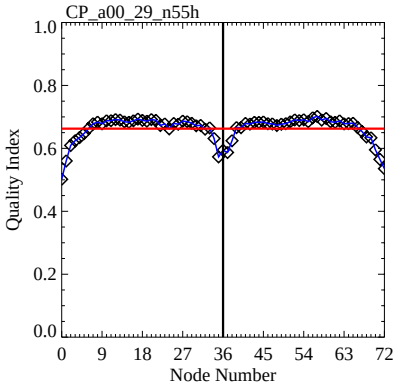 | 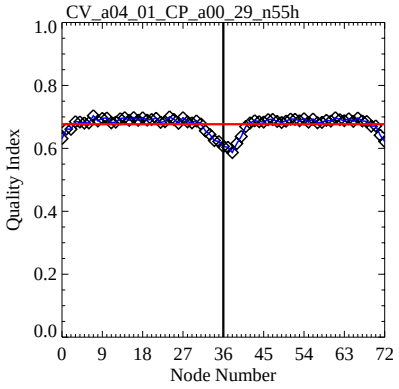 | 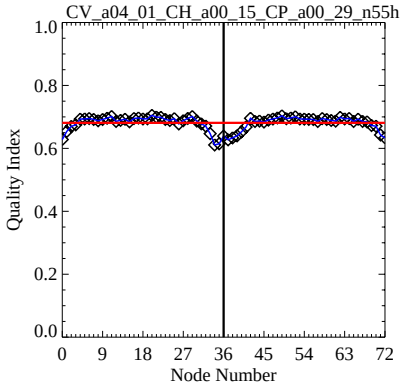 |
| **640 KW** | | |
| 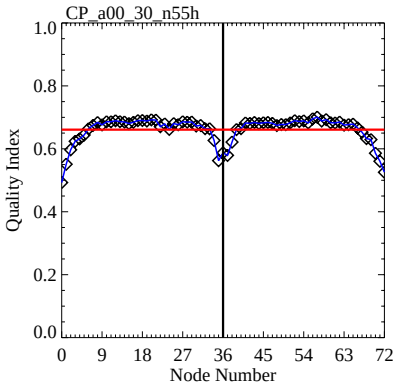 | 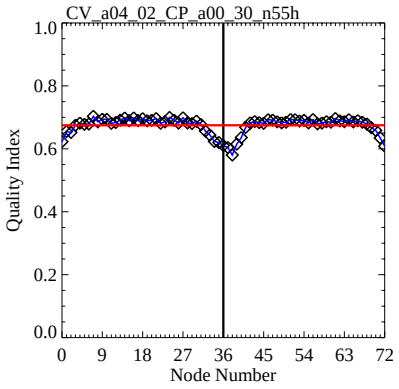 | 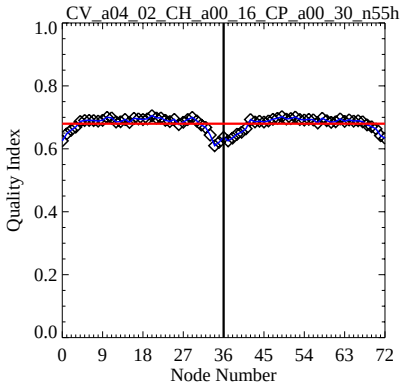 |
| **320 KW** | | |
| 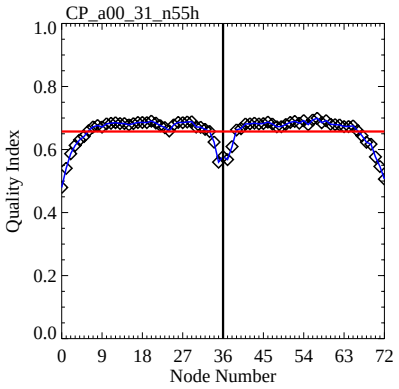 | 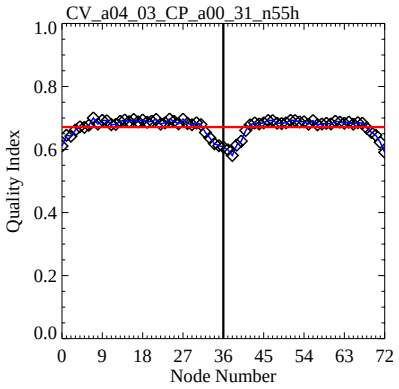 | 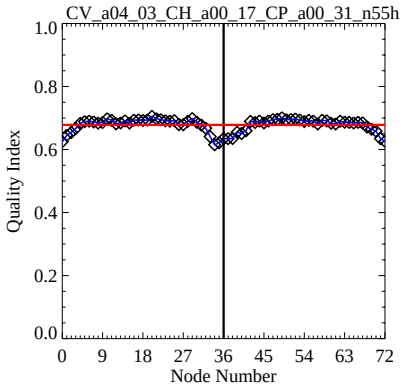 |
| **160 KW** | | |

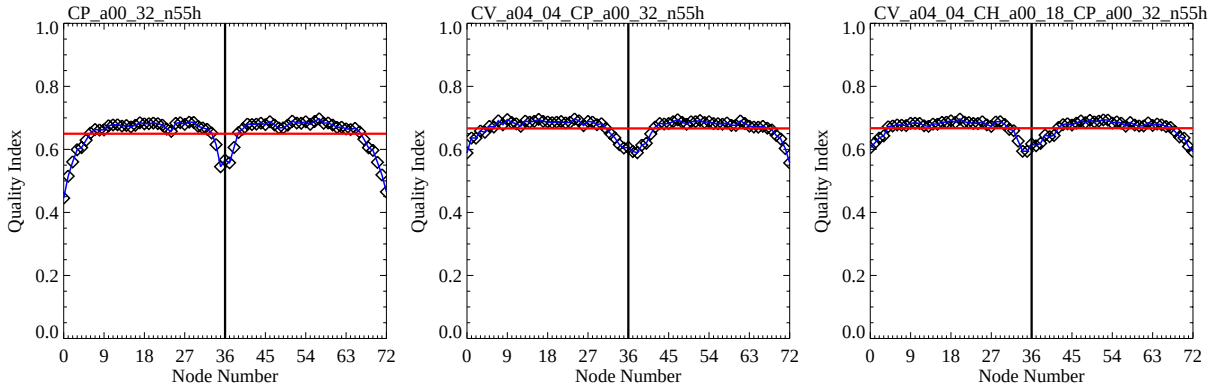


**80 KW**

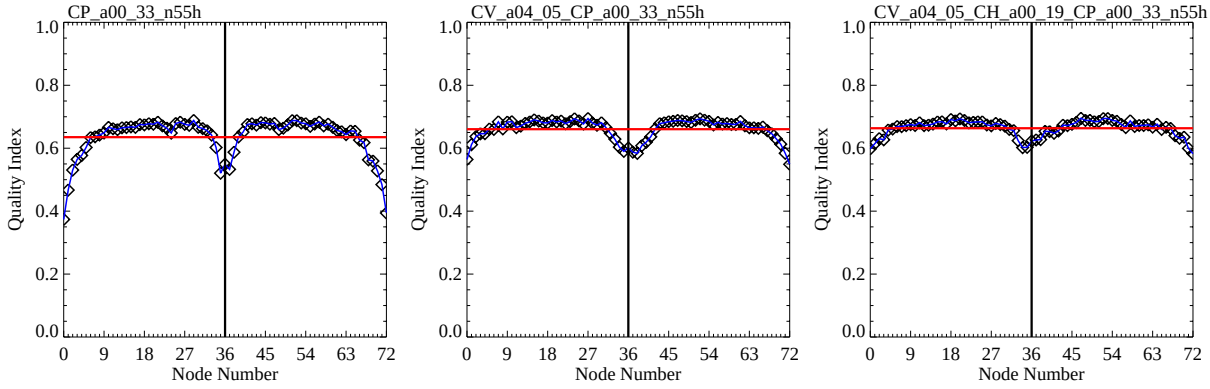


**40 KW**

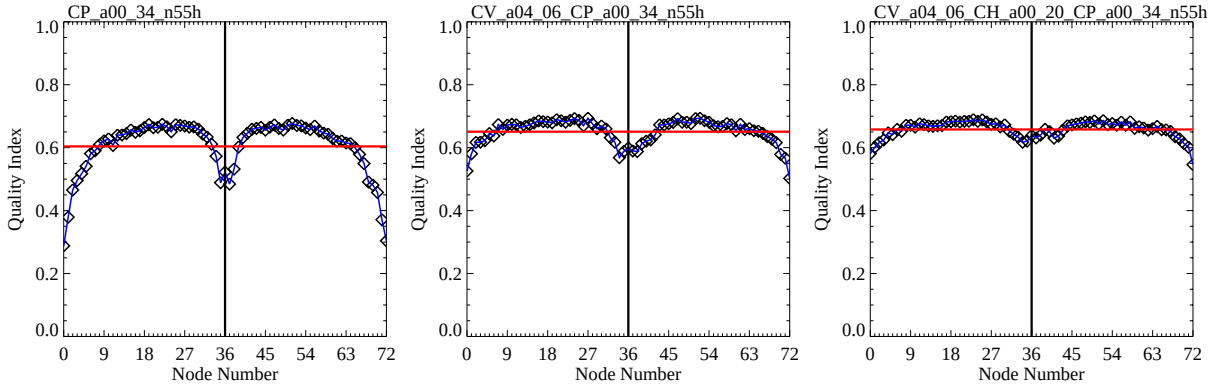


**20 KW**

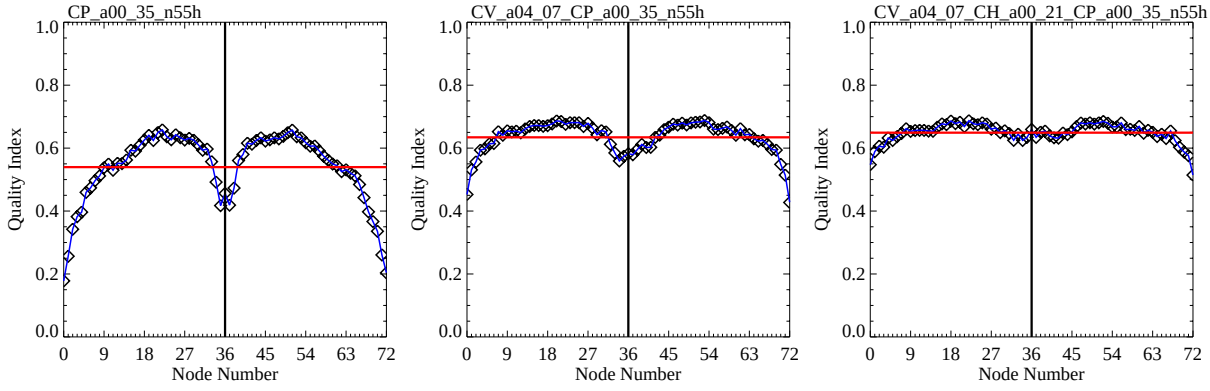


**10 KW**

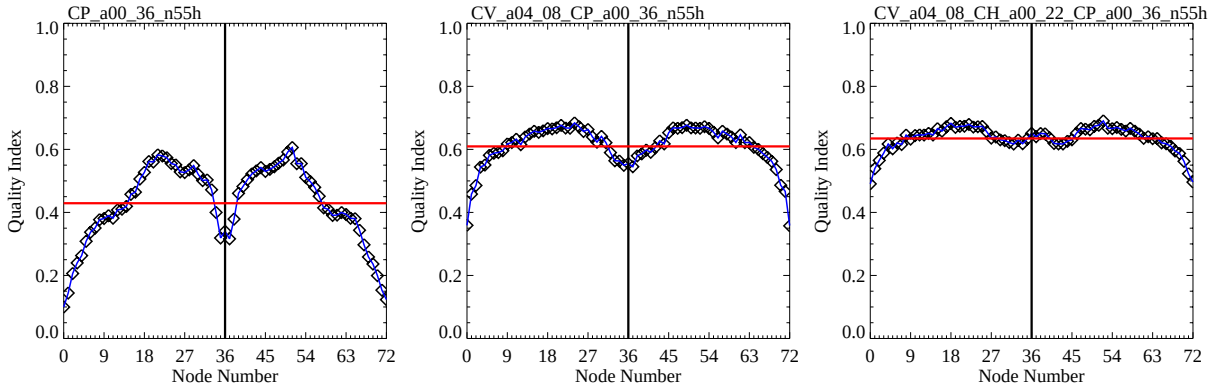


**5 KW**

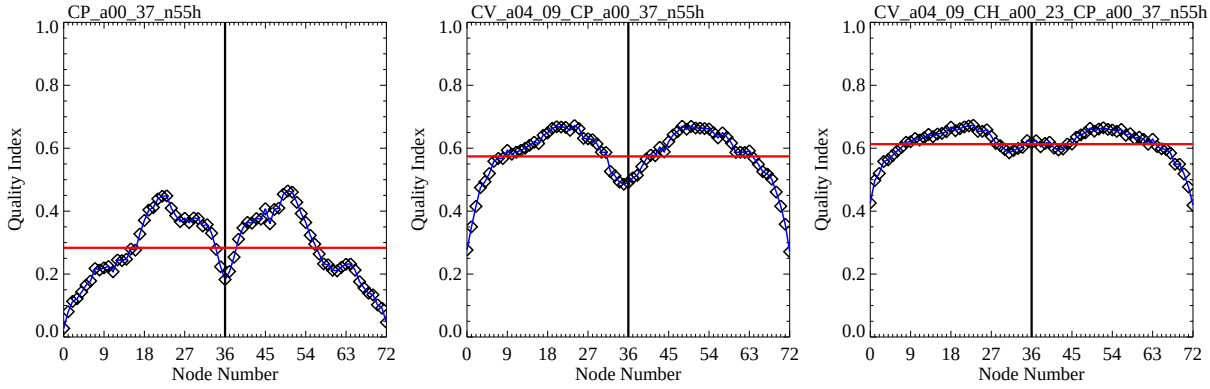


**2500 W**

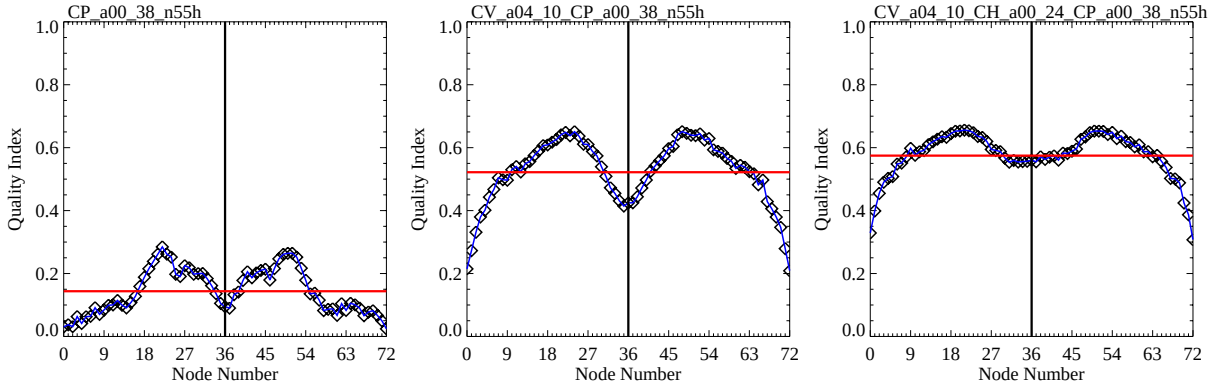


**1250 W**

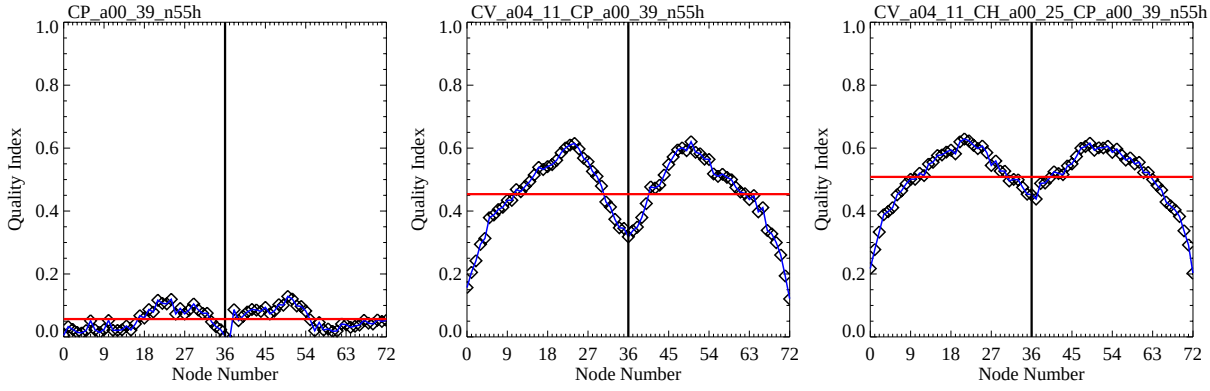


**625 W**

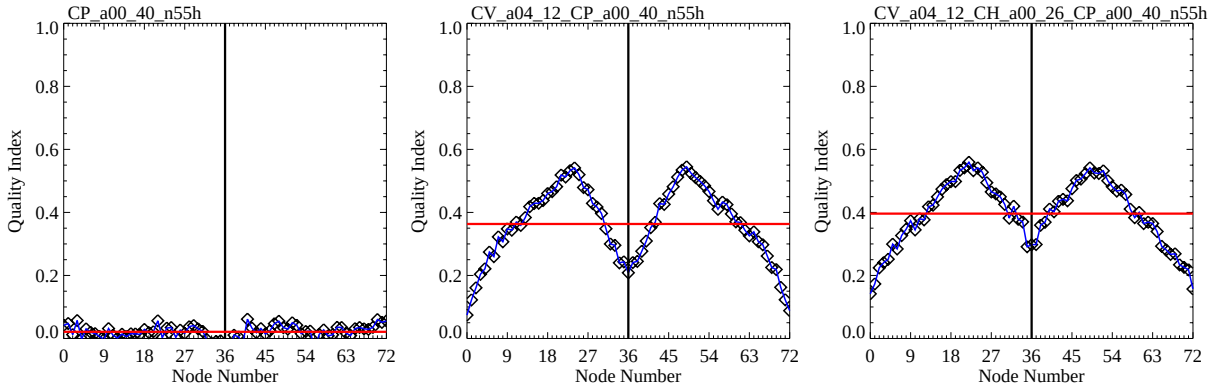


**312 W**

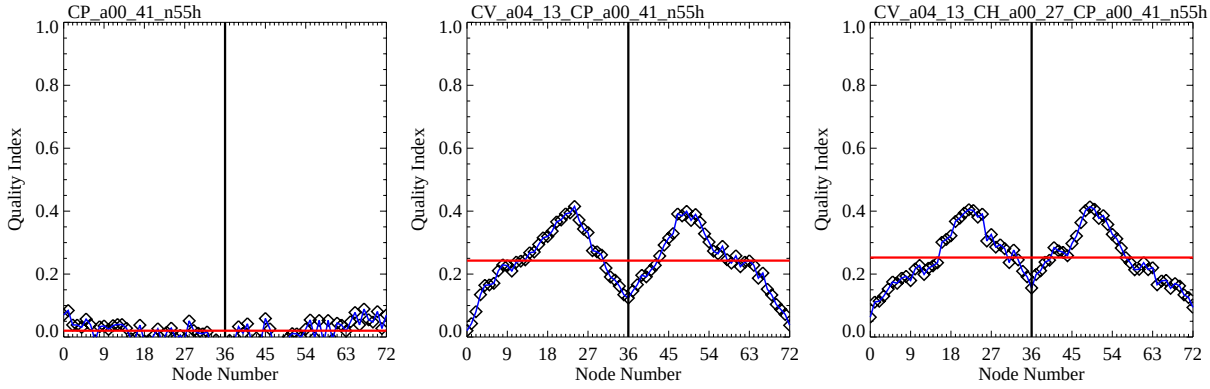


**156 W**

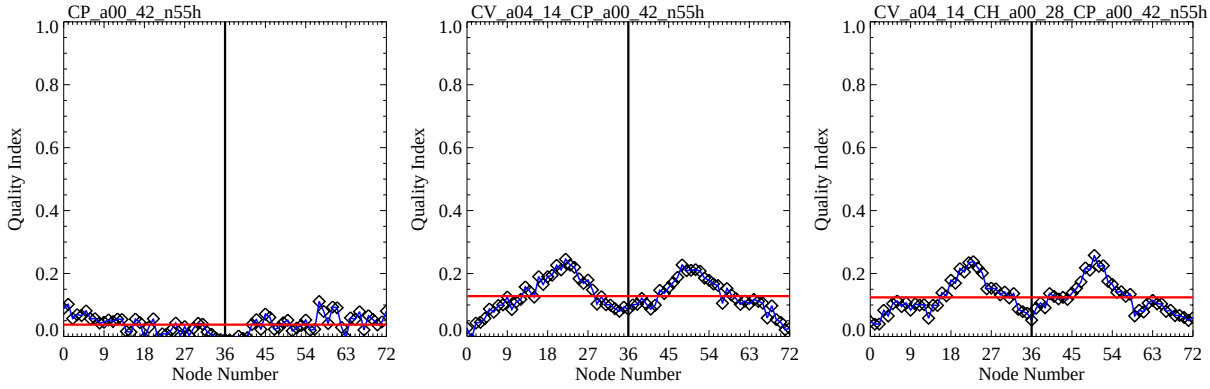


**78 W**

## 20. Annex N – Split-Beam Polarimetric System

The following table summarizes the graphs of the quality index versus node number for a single antenna dual-beam polarimetric C-band system. The pulse peak power decrease from 640 KW to 78 W in steps of 3 dB. For the wind retrieval only VV-polarization and only polarimetric data as well as both data together was used.

Orbit height - 725 km
Swath width - 1500 km
Resolution - 50 km

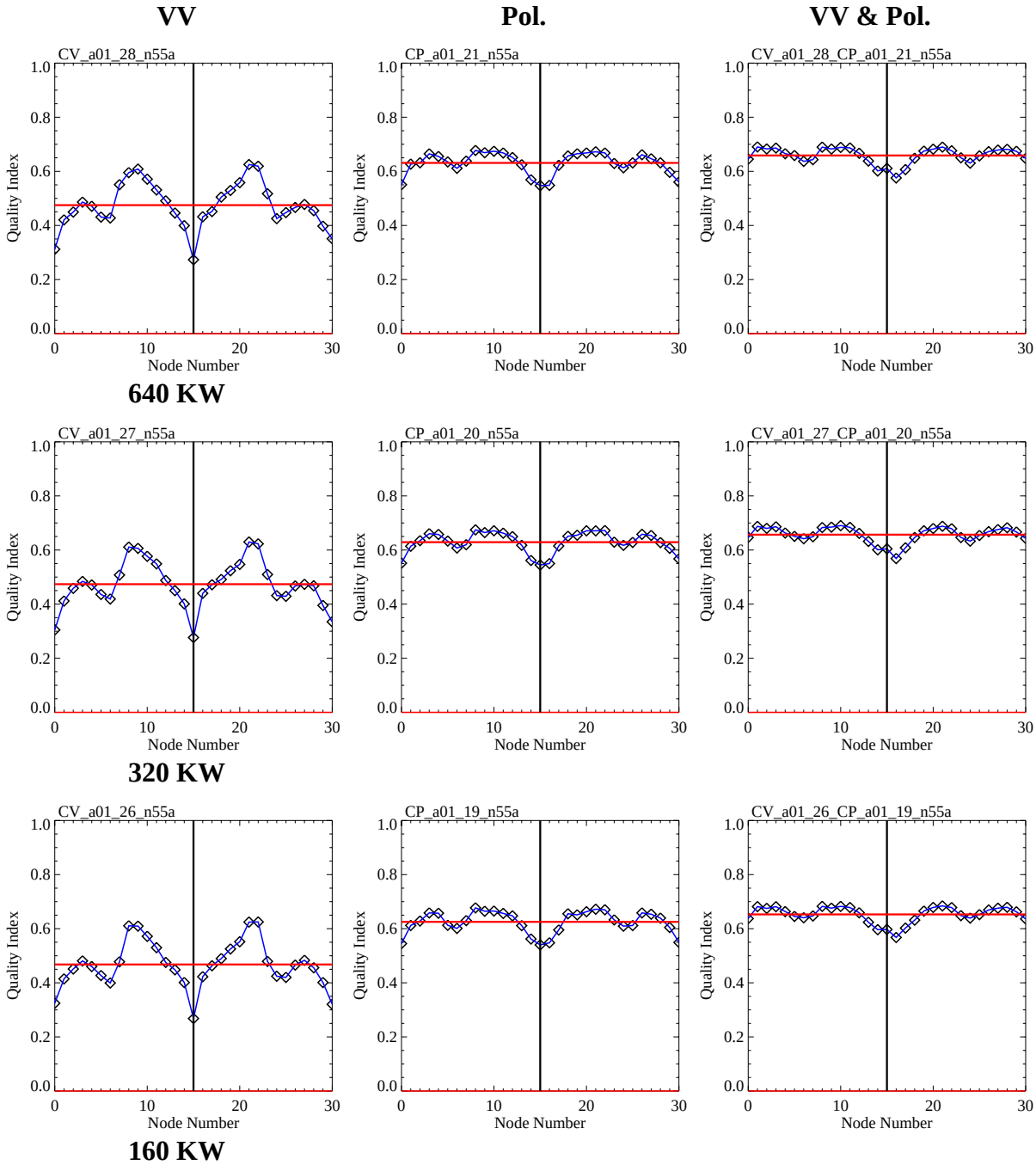

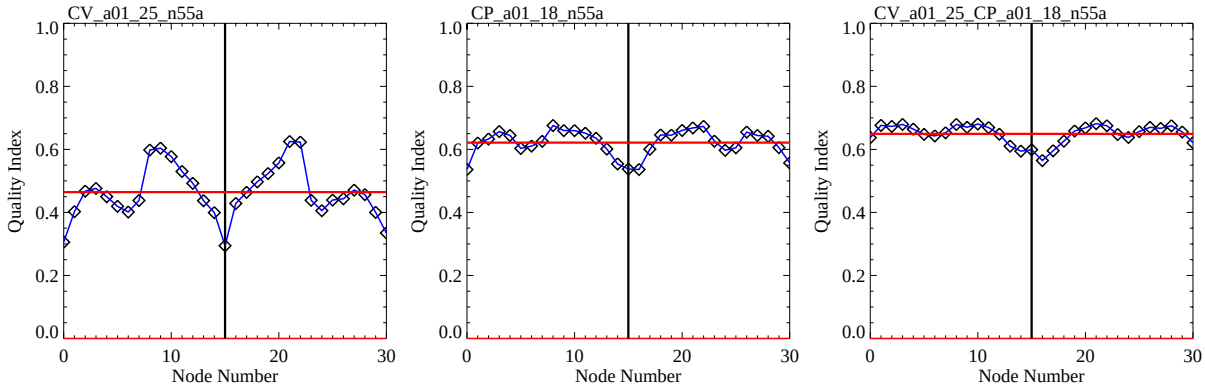


**80 KW**

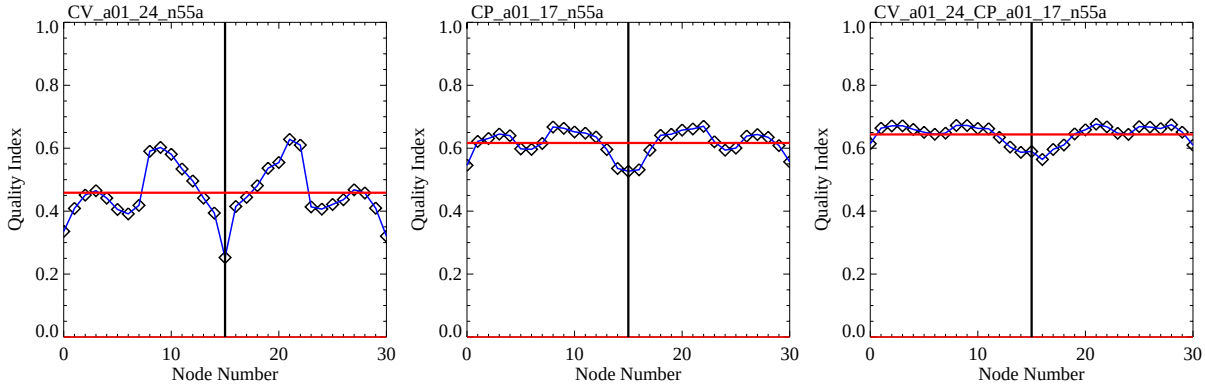


**40 KW**

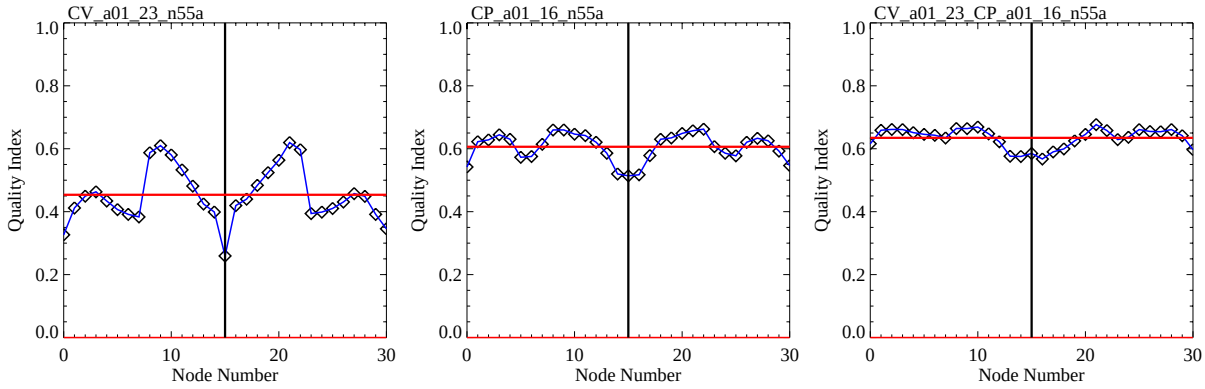


**20 KW**

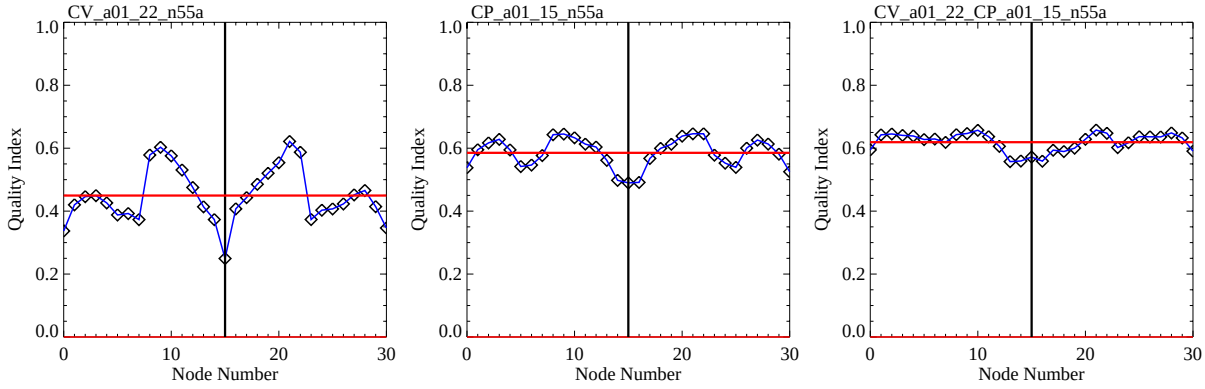


**10 KW**

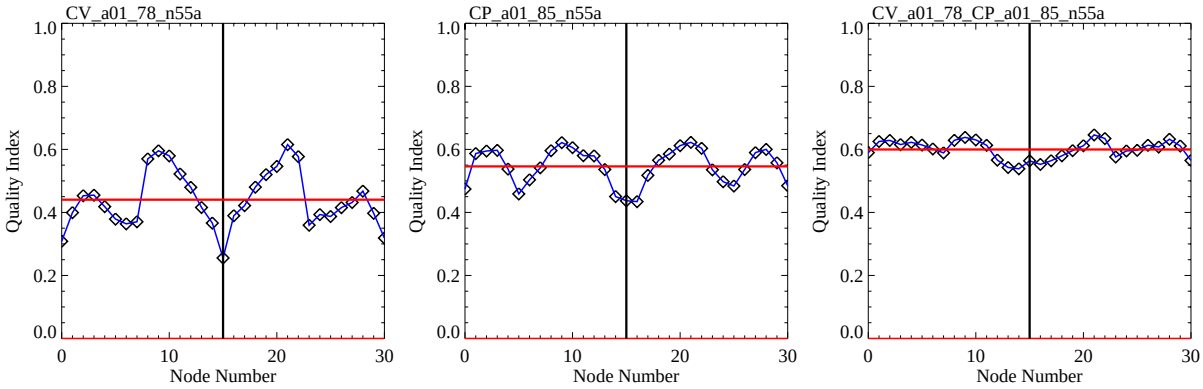


**5 KW**

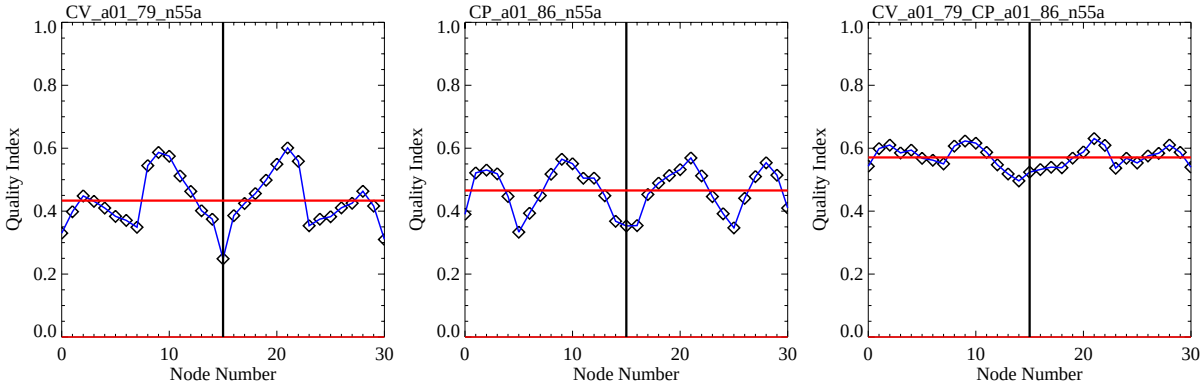


**2500 W**

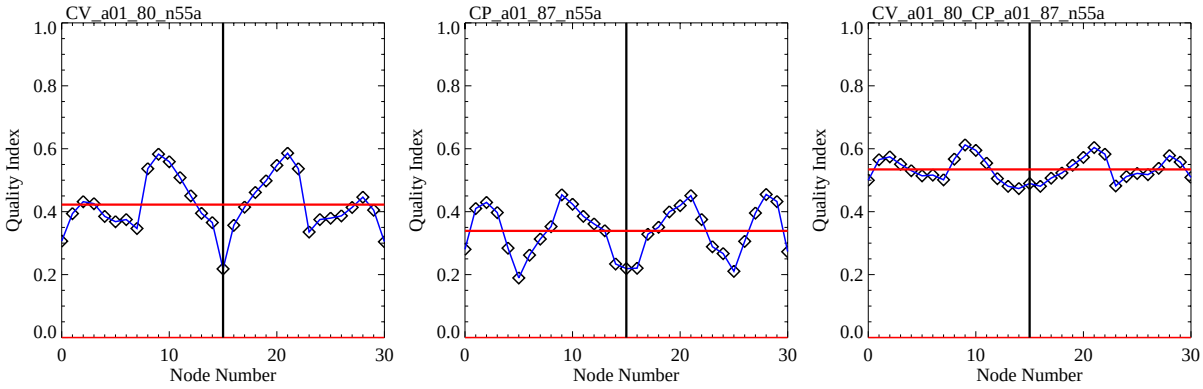


**1250 W**

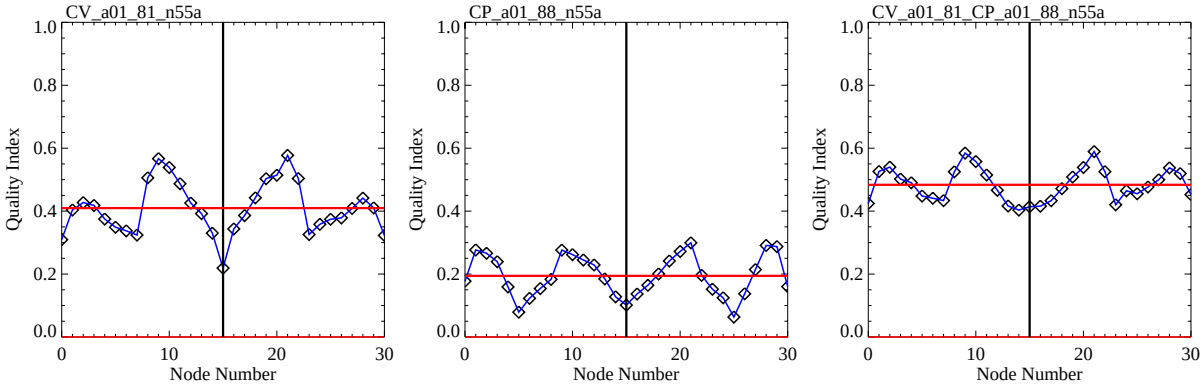


**625 W**

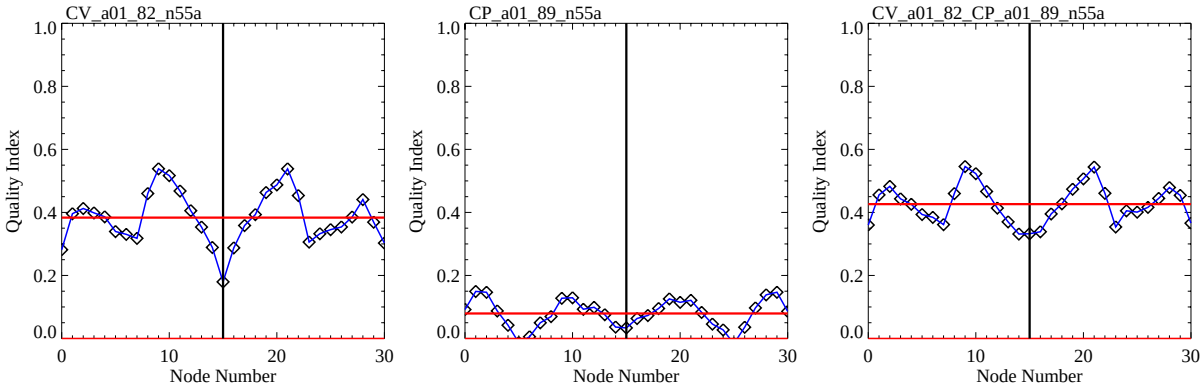


**312 W**

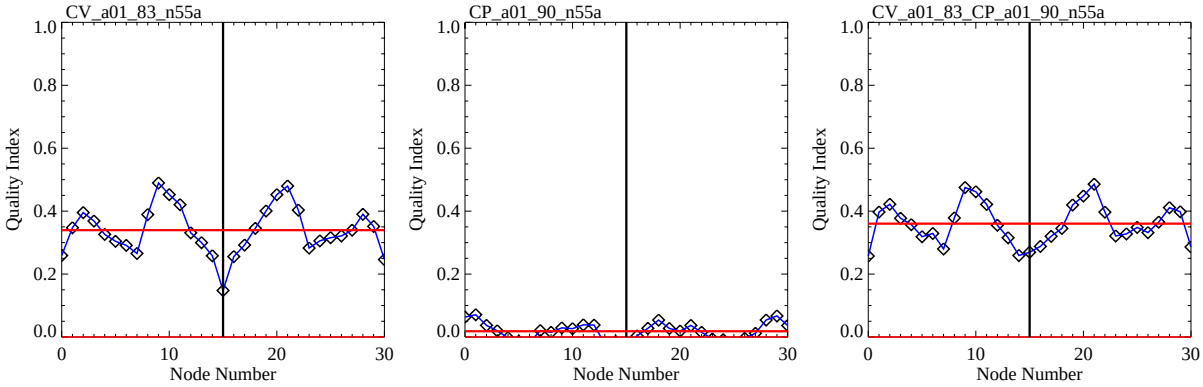


**156 W**

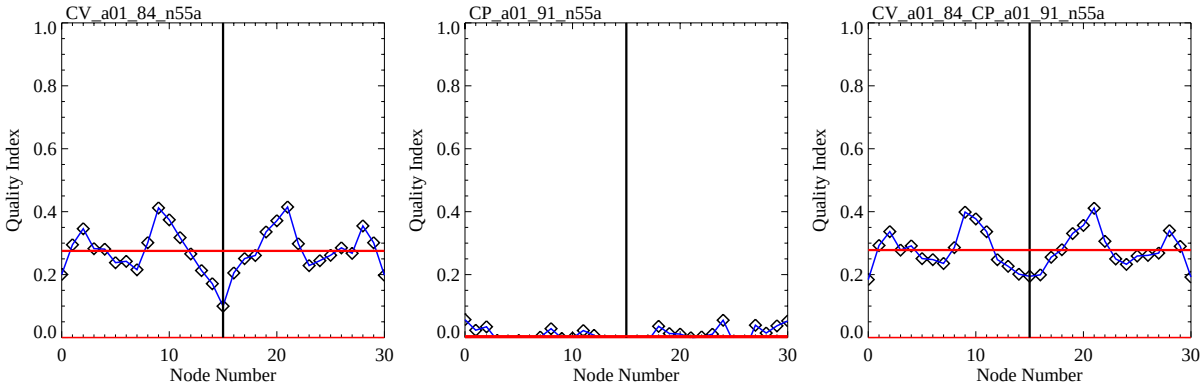


**78 W**

## 21. Annex O – High Orbit (1075 km) Polarimetric System

The following table summarizes the graphs of the quality index versus node number for a polarimetric C-band system. The pulse peak power decrease from 640 KW to 78 W in steps of 3 dB. For the wind retrieval only VV-polarization and only polarimetric data as well as both data together was used.

Orbit height - 1075 km
Swath width - 1800 km
Resolution - 50 km

Pcvcp5

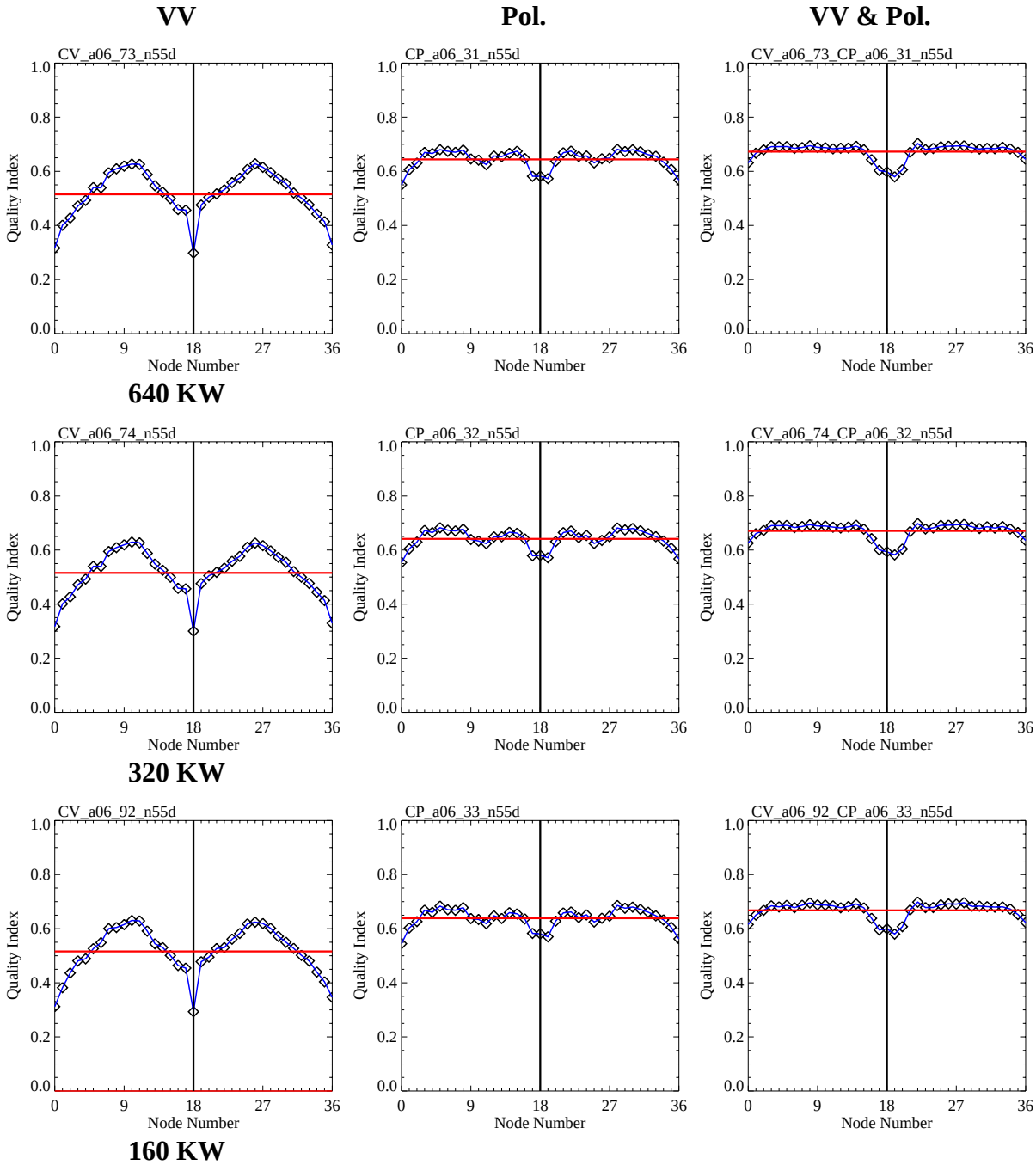

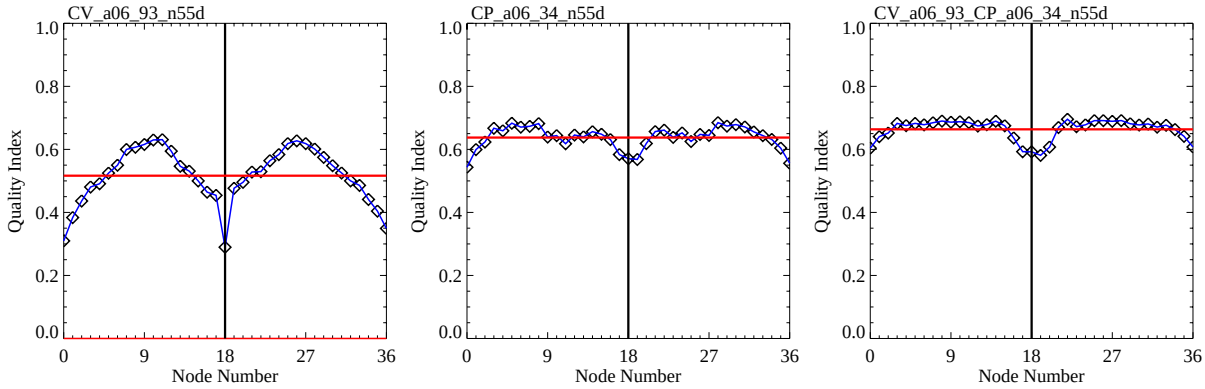


**80 KW**

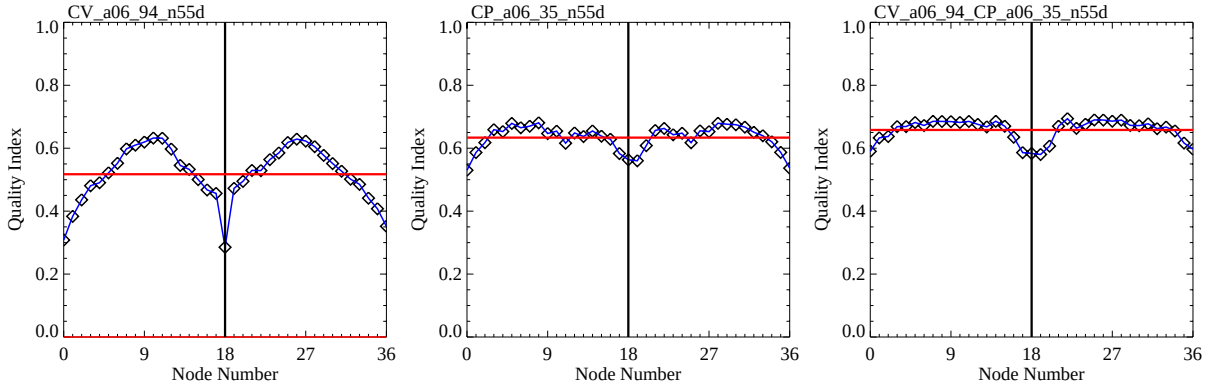


**40 KW**

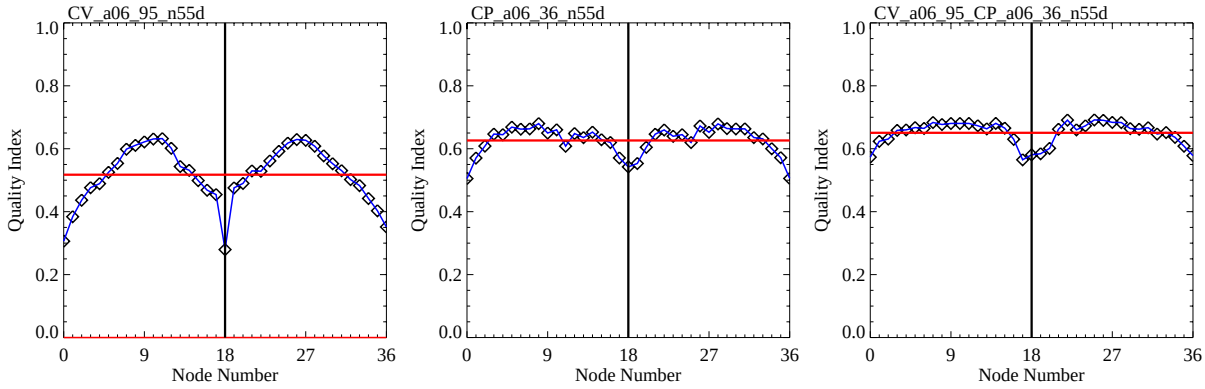


**20 KW**

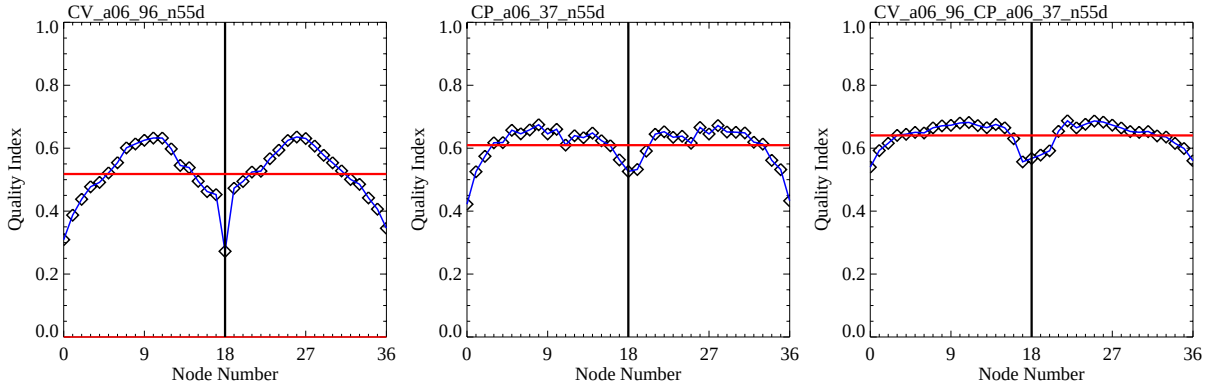


**10 KW**

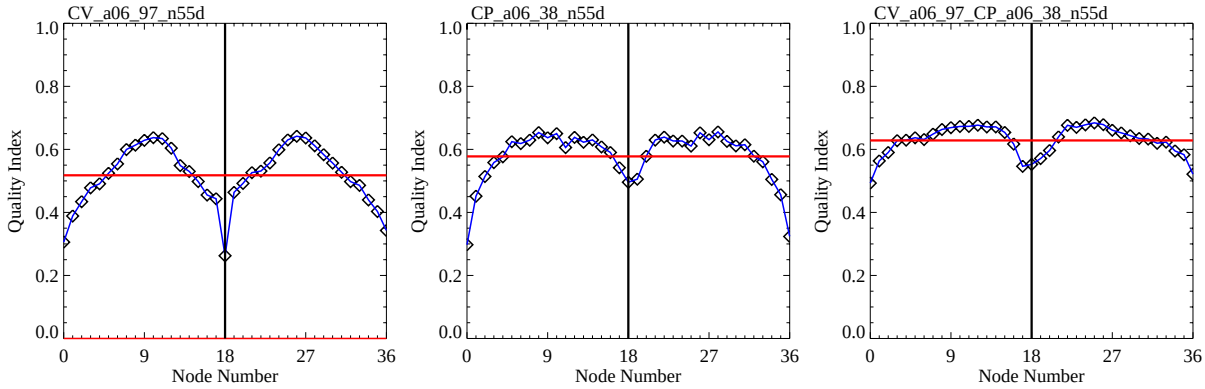


**5000 W**

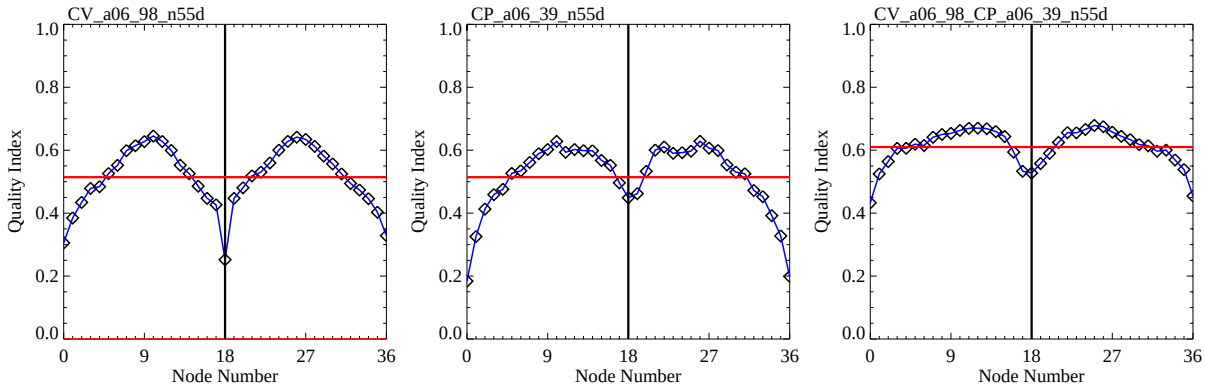


**2500 W**

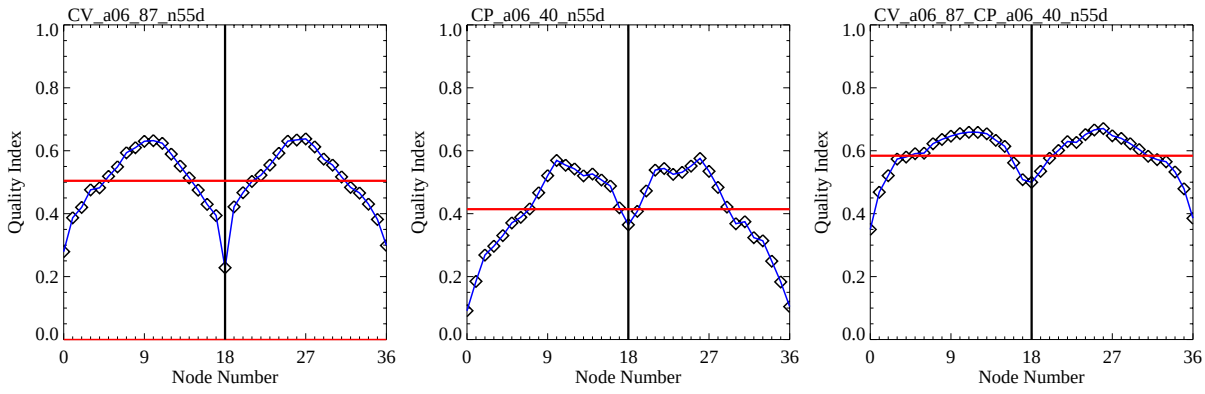


**1250 W**

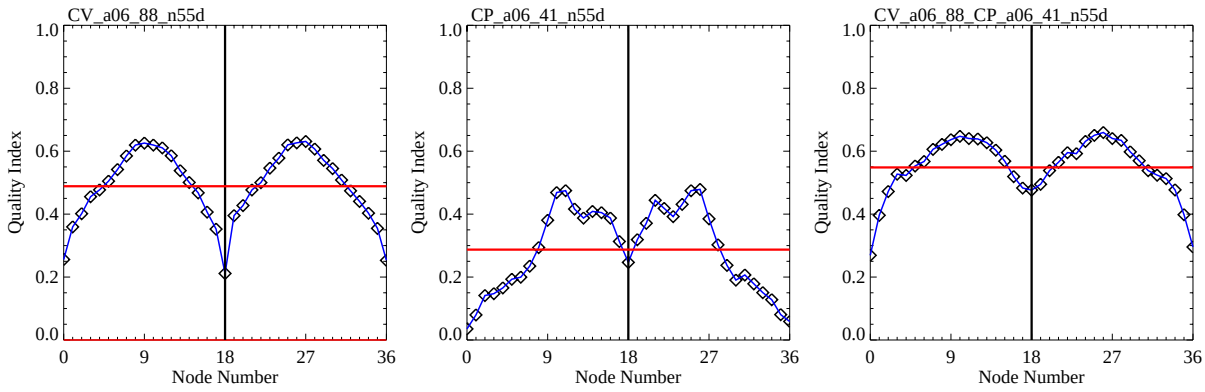


**625 W**

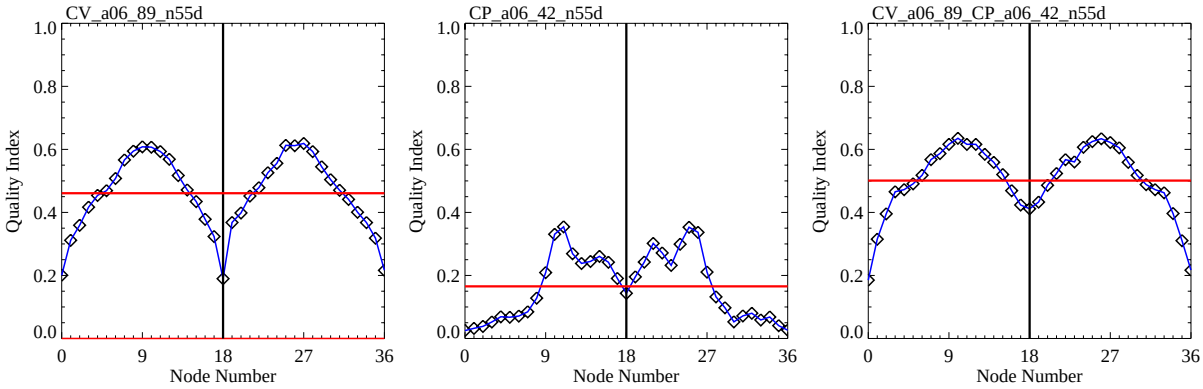


**312 W**

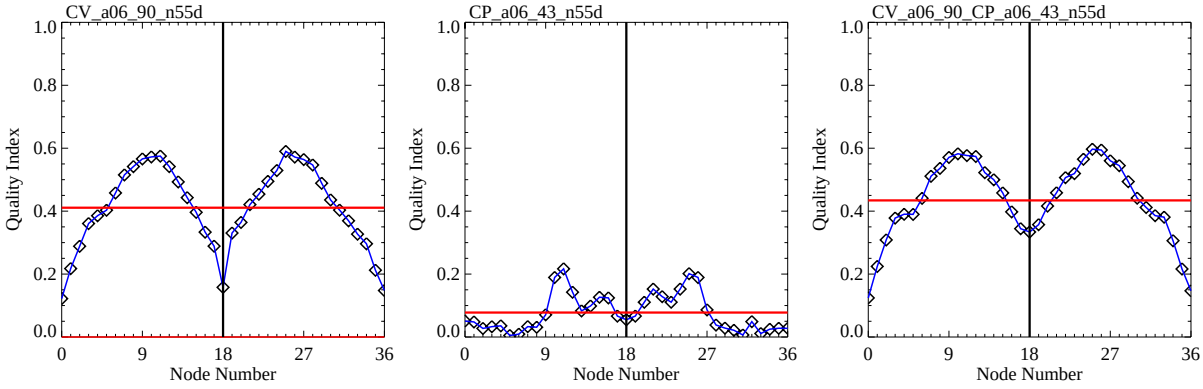


**156 W**

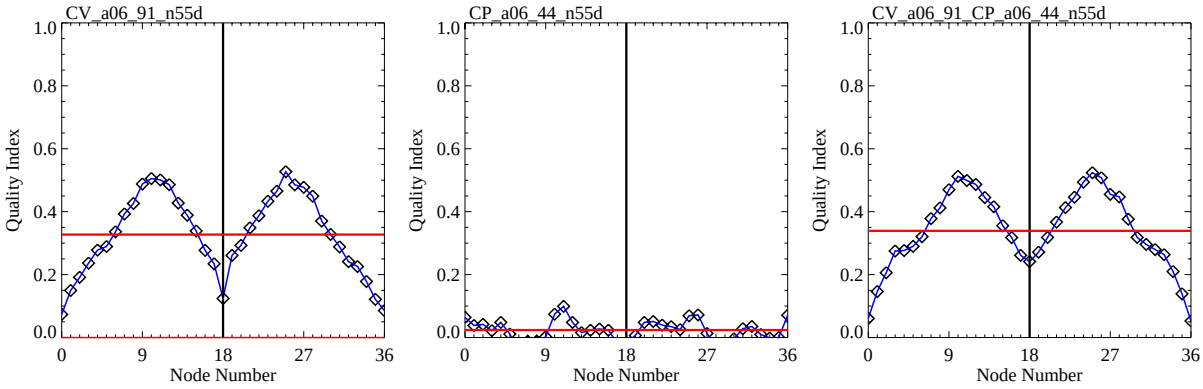


**78 W**

## 22. Annex P – FoM versus Pulse Peak Power for Ku-Band

The following table summarizes the graphs of the quality index versus node number for a VV-polarized Ku-band system. The pulse peak power decrease from 640 KW to 78 W in steps of 3 dB.

Orbit height - 725 km
Swath width - 1500 km
Resolution - 50 km

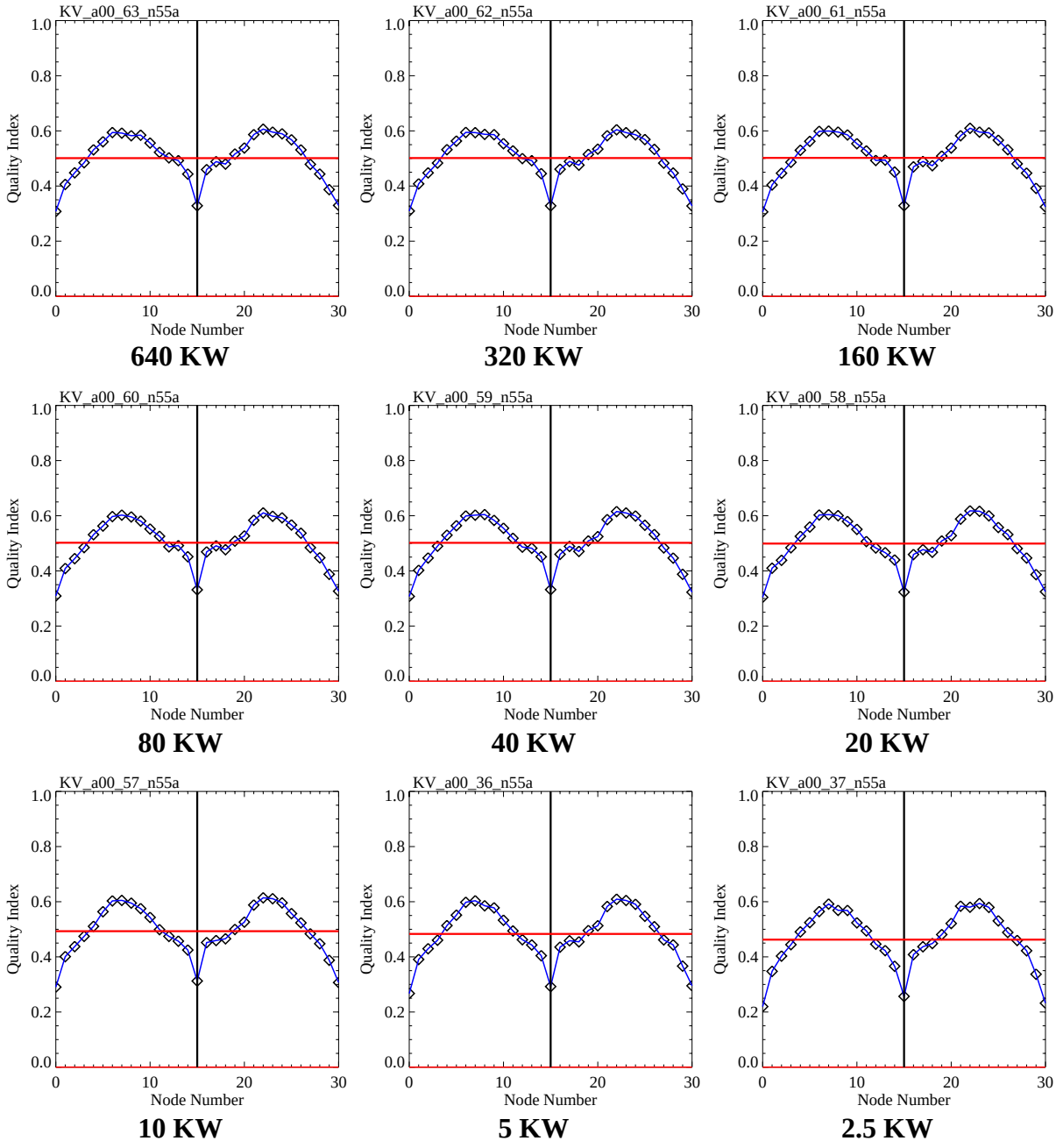

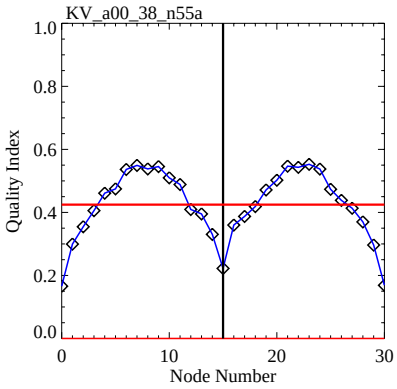


**1250 W**

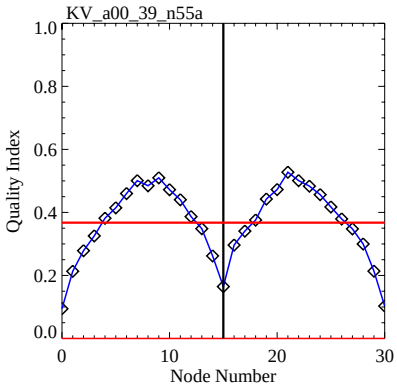


**625 W**

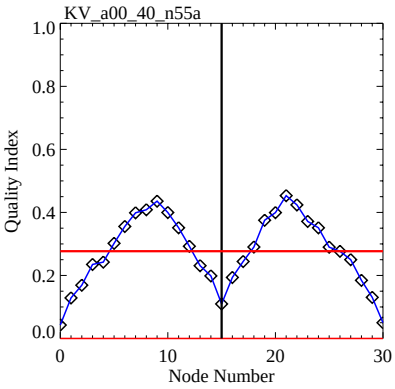


**312 W**

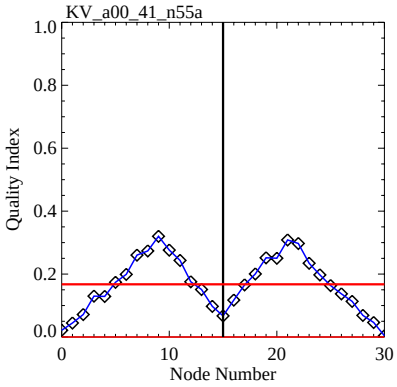


**156 W**

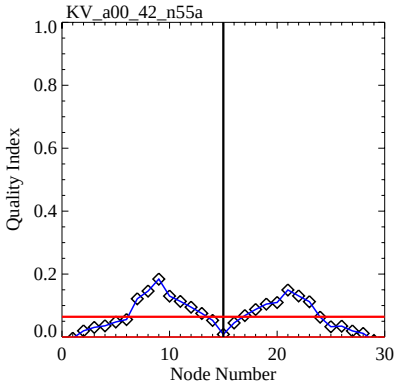


**78 W**

## 23. Annex Q – Dual Polarization Ku-Band System

The following table summarizes the graphs of the quality index versus node number for a single antenna dual-polarized Ku-band system. The pulse peak power decrease from 640 KW to 78 W in steps of 3 dB. For the wind retrieval only VV-polarization and only HH-polarization data as well as both data together was used.

Orbit height - 725 km
Swath width - 1500 km
Resolution - 50 km

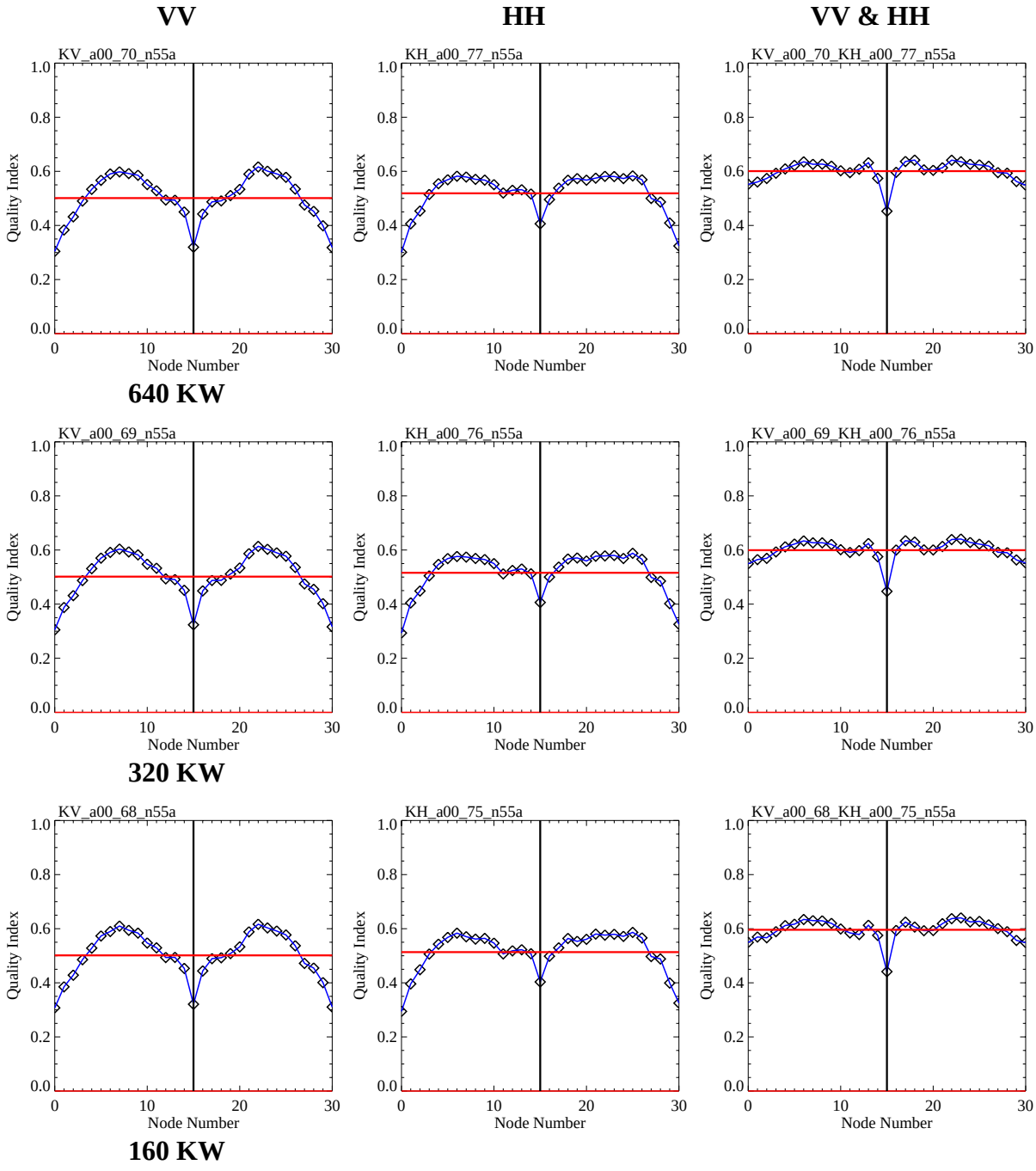

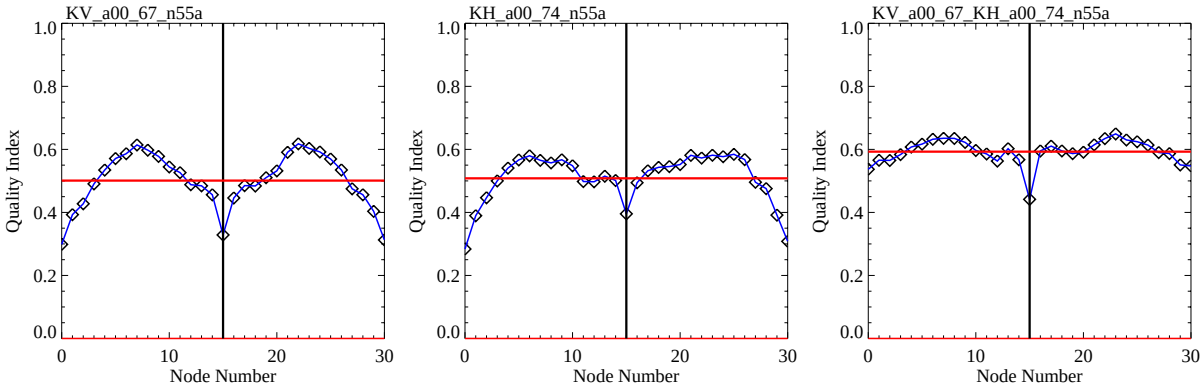


**80 KW**

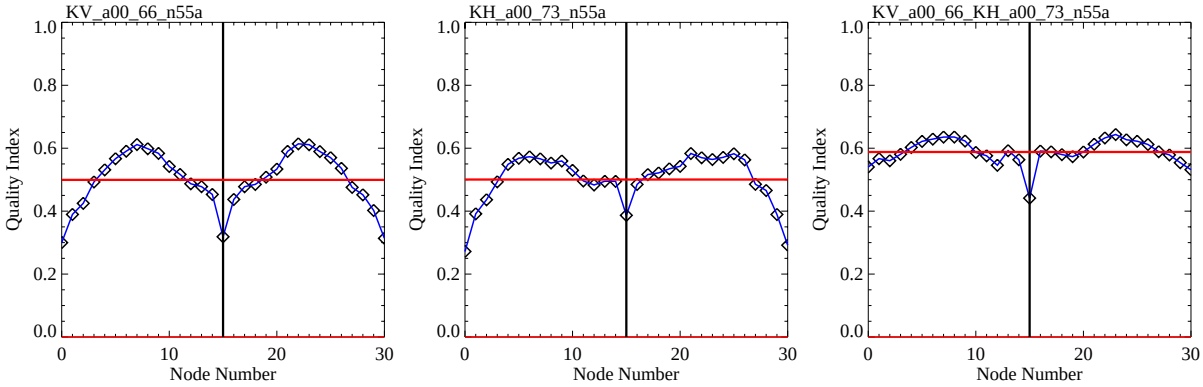


**40 KW**

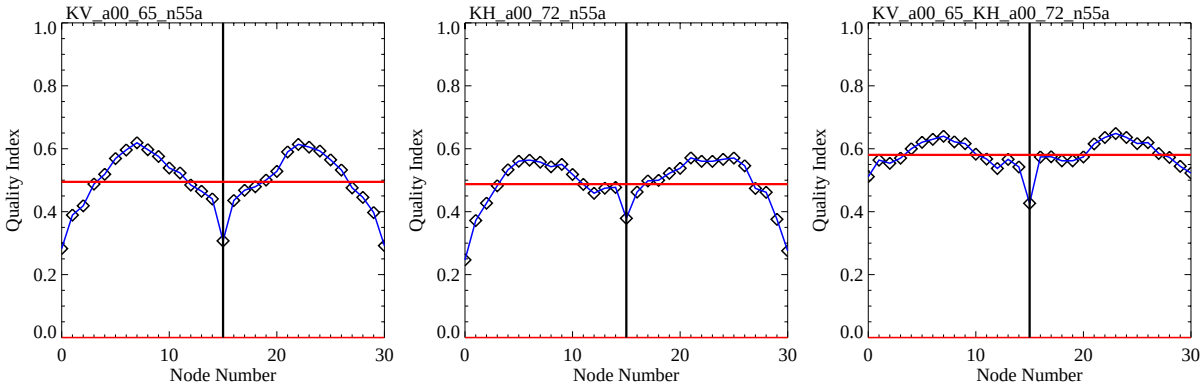


**20 KW**

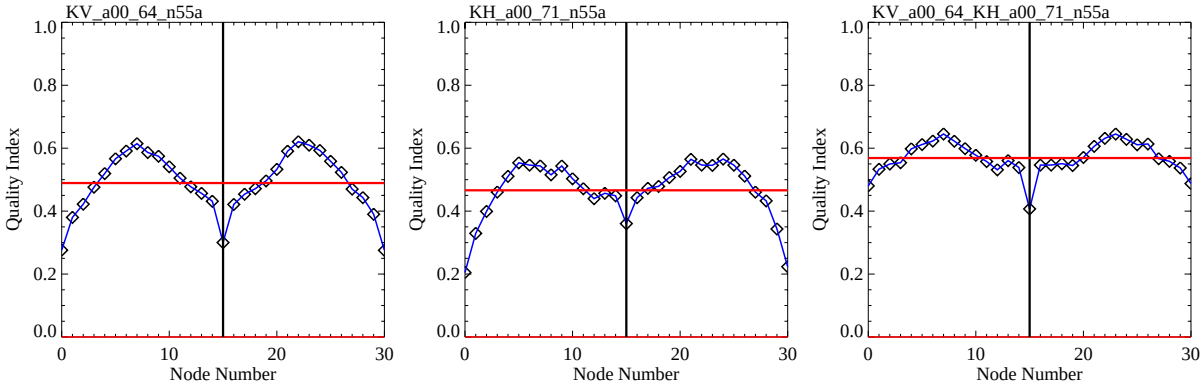


**10 KW**

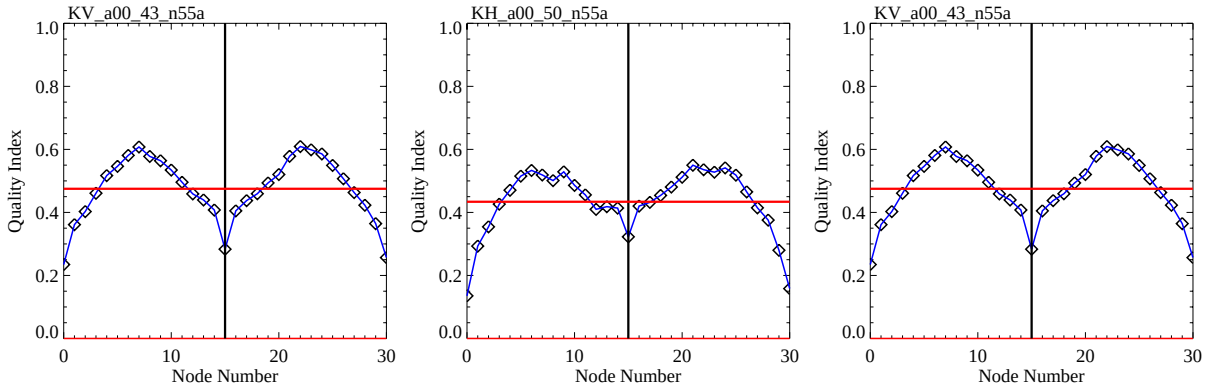


**5 KW**

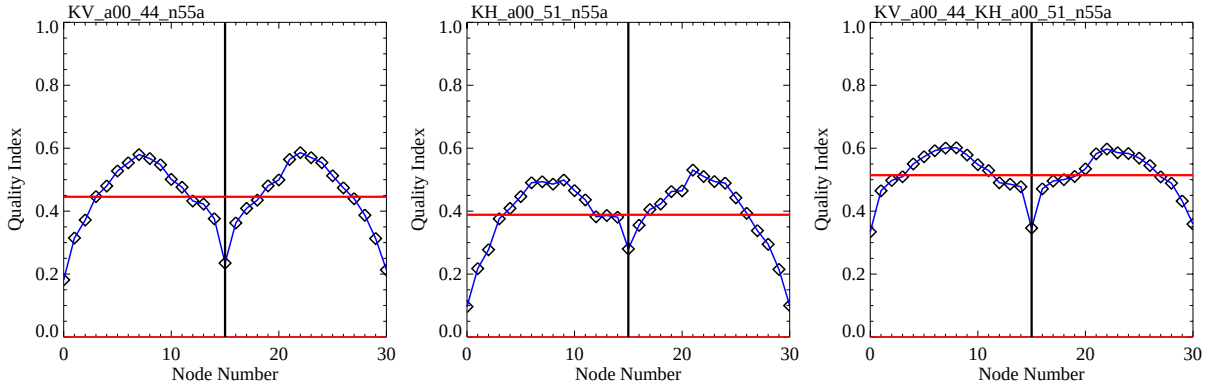


**2500 W**

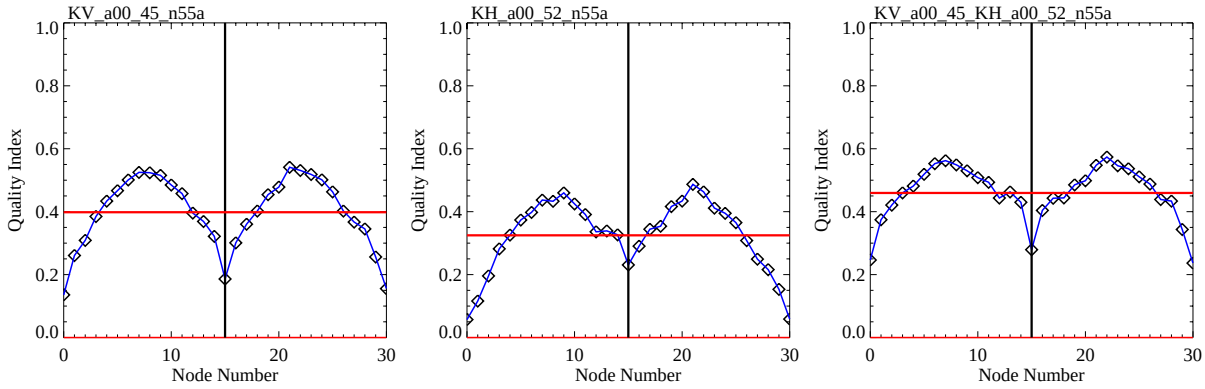


**1250 W**

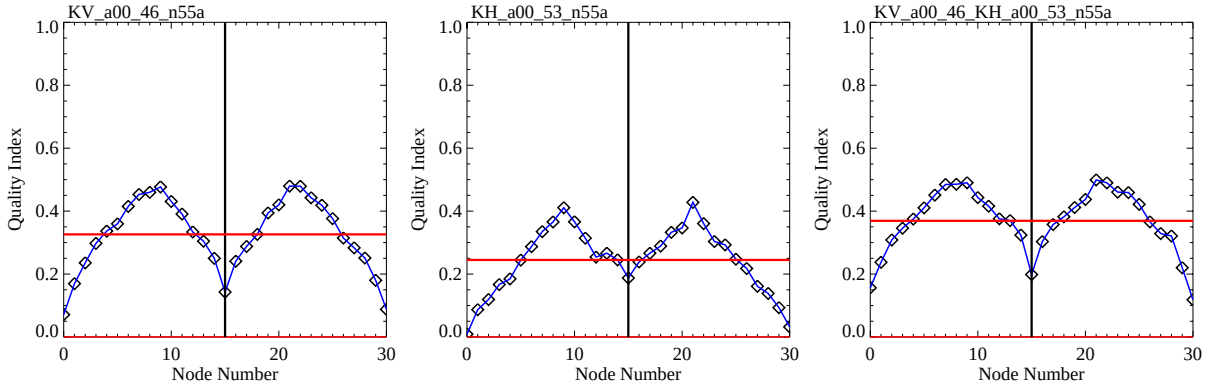


**625 W**

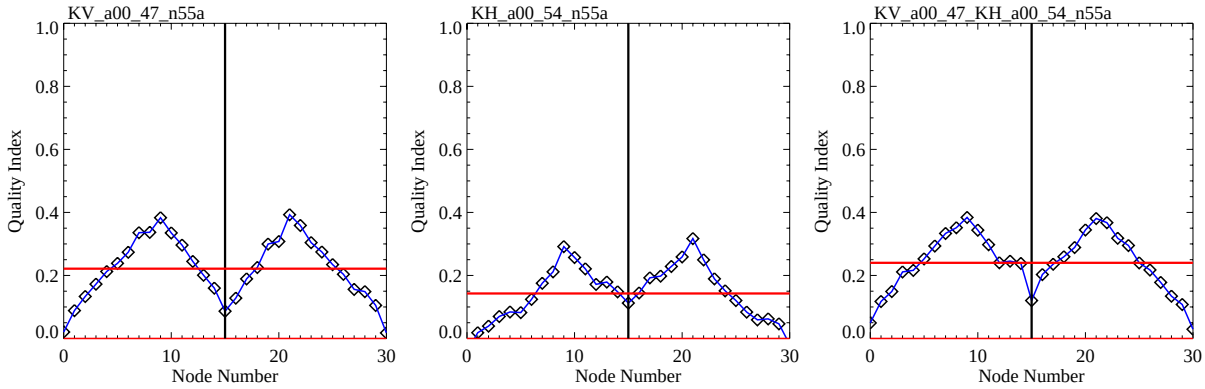


**312 W**

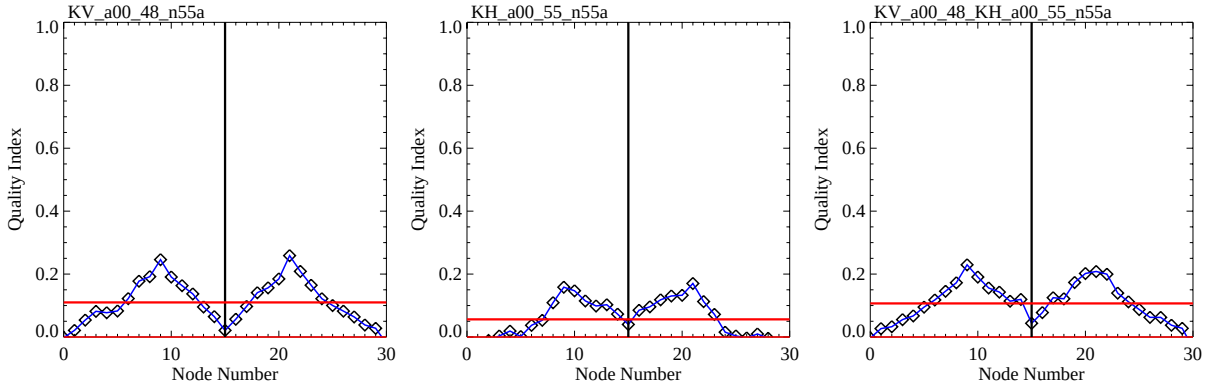


**156 W**

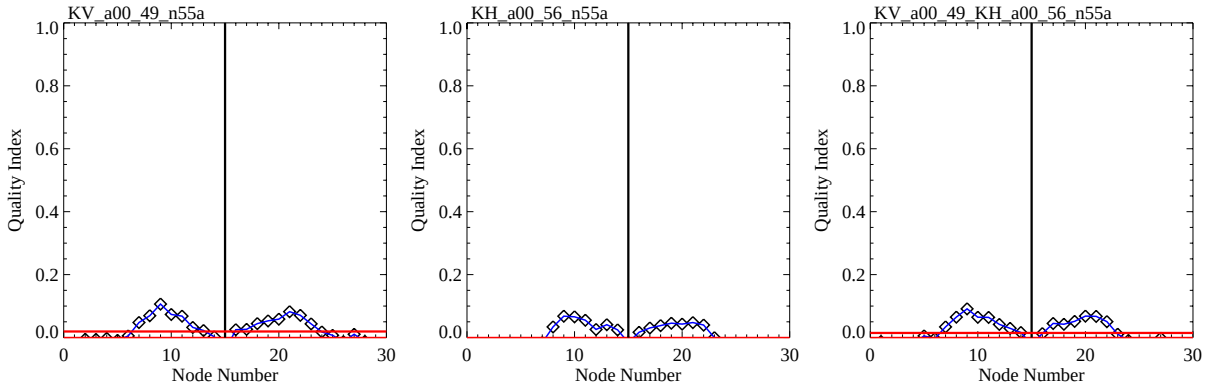


**78 W**

## 24. Annex R – Combination of C-Band VV-Pol and Ku-Band VV Pol

The following table summarizes the graphs of the quality index versus node number for a dual radar band vertically polarized system. The pulse peak power decrease from 80 KW to 78 W in steps of 3 dB. For the wind retrieval only C-band and only Ku-band data as well as both data together was used.

Orbit height - 725 km
Swath width - 1500 km
Resolution - 50 km

| C-VV | Ku-VV | C-VV & Ku-VV |
|---|---|---|
| CV_a00_81_n55a | KV_a00_63_n55a | CV_a00_81_KV_63_n55a |
| **80 KW** | | |
| CV_a00_82_n55a | KV_a00_62_n55a | CV_a00_82_KV_62_n55a |
| **40 KW** | | |
| CV_a00_84_n55a | KV_a00_61_n55a | CV_a00_84_KV_61_n55a |
| **20 KW** | | |

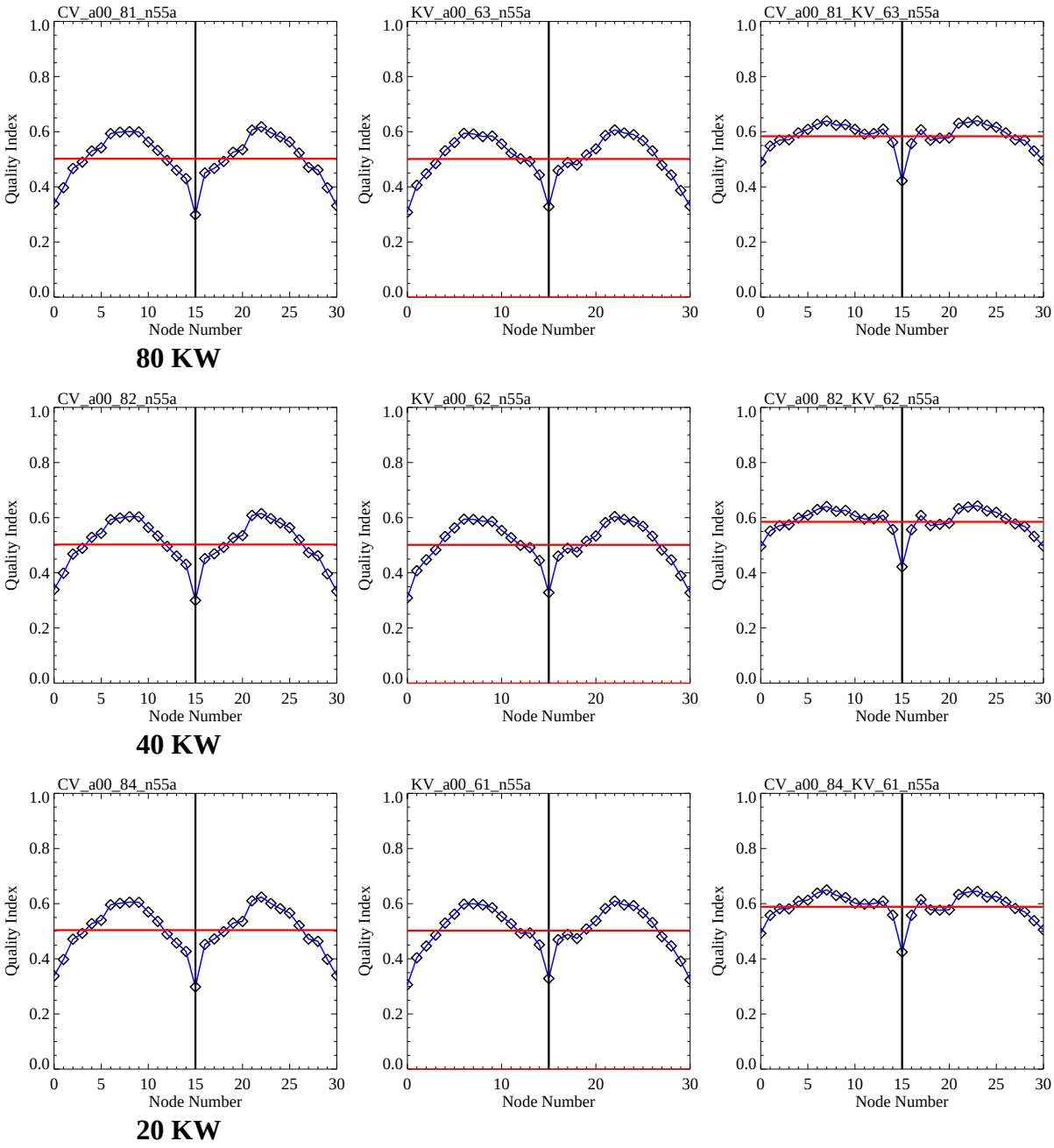

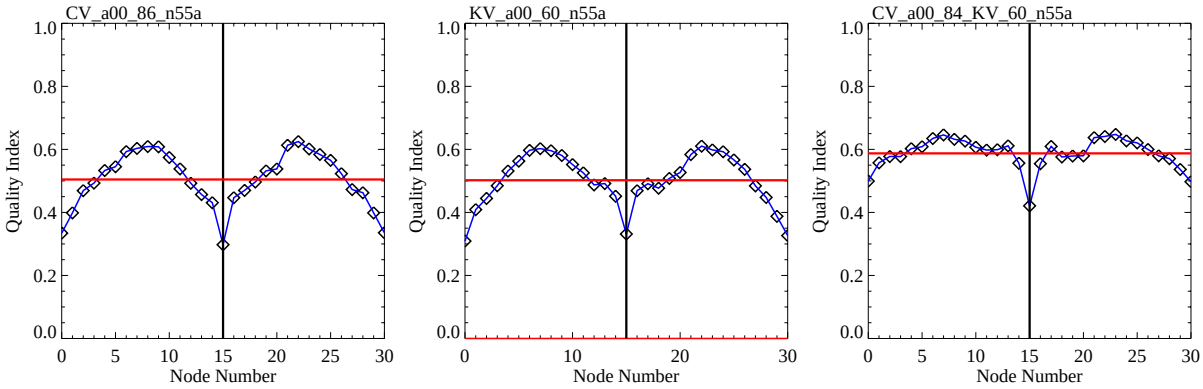


**10 KW**


**5000 W**

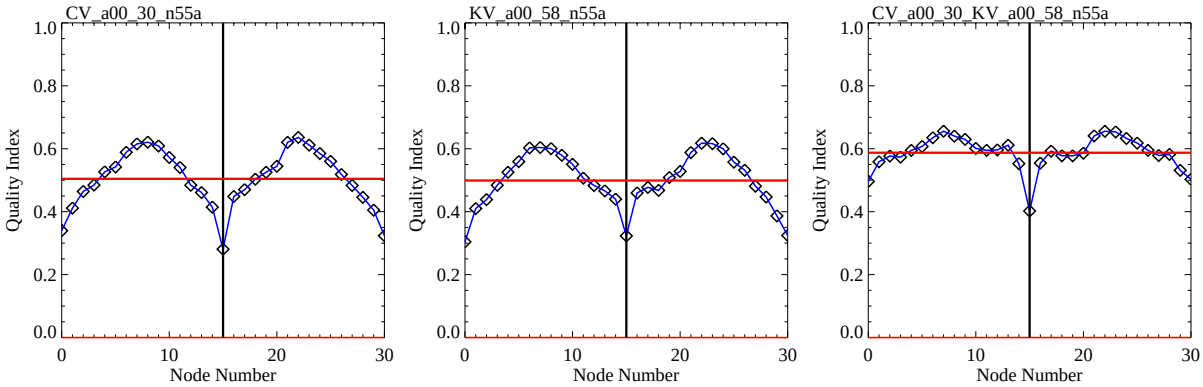


**2500 W**

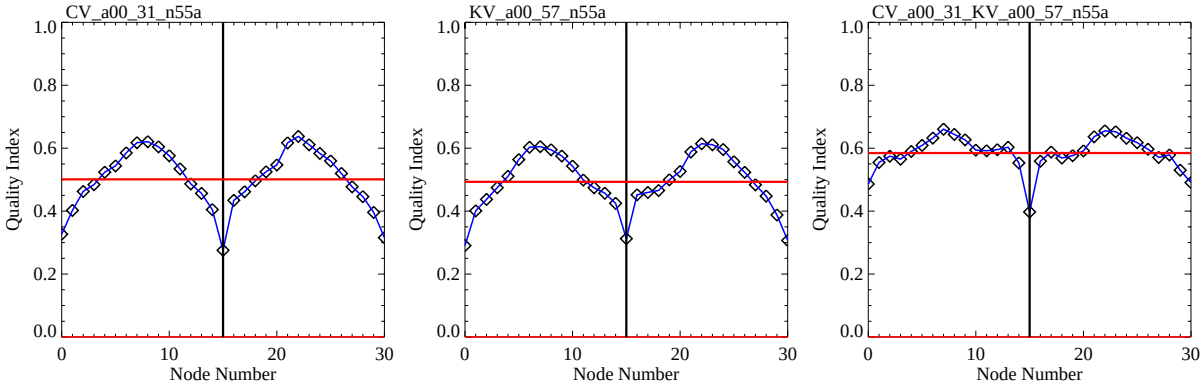


**1250 W**

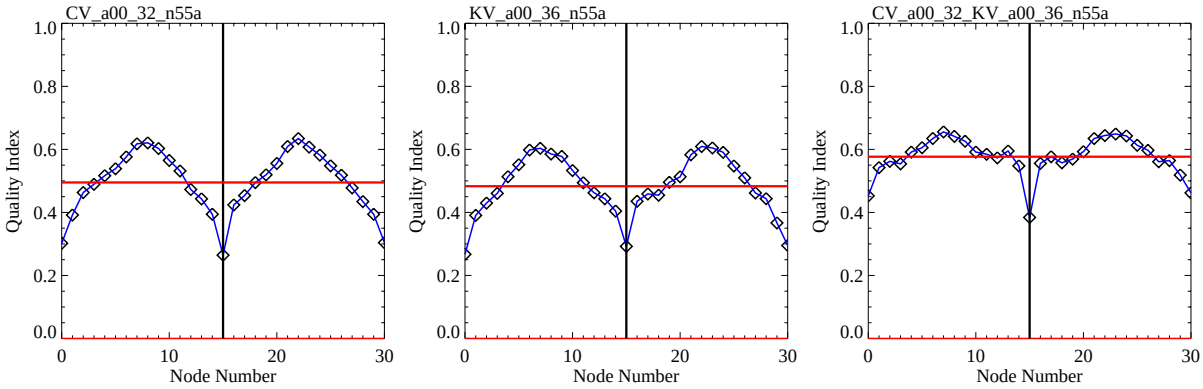


**625 W**

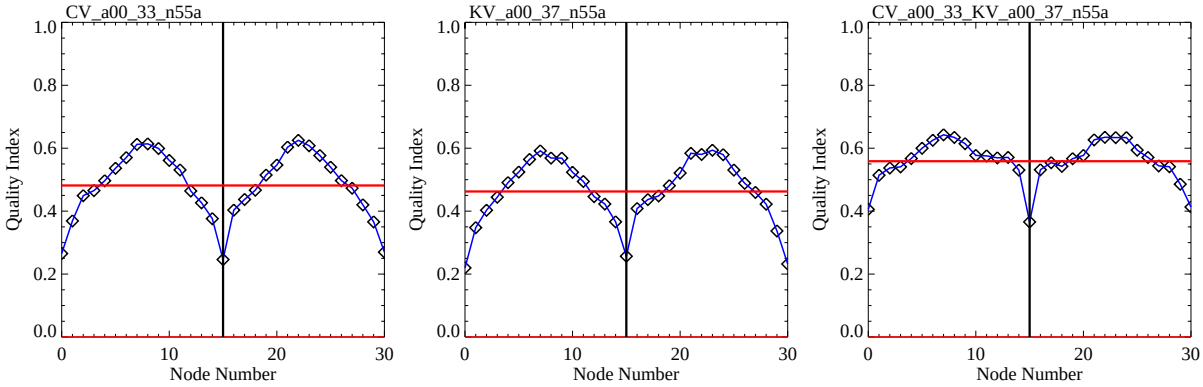


**312 W**

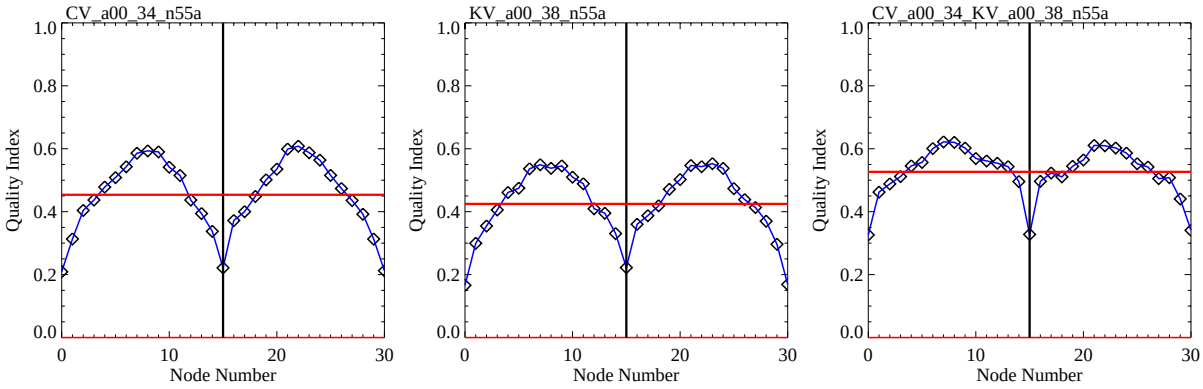


**156 W**

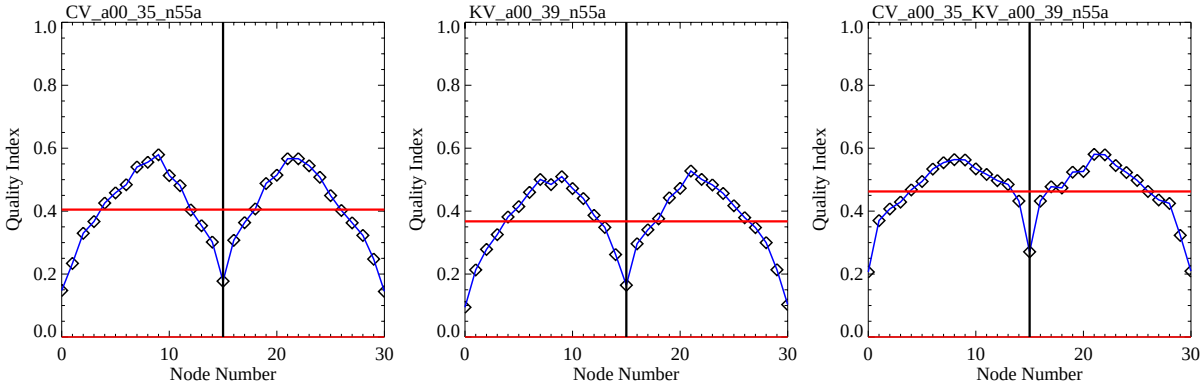


**78 W**